

## University of Southampton Research Repository ePrints Soton

Copyright © and Moral Rights for this thesis are retained by the author and/or other copyright owners. A copy can be downloaded for personal non-commercial research or study, without prior permission or charge. This thesis cannot be reproduced or quoted extensively from without first obtaining permission in writing from the copyright holder/s. The content must not be changed in any way or sold commercially in any format or medium without the formal permission of the copyright holders.

When referring to this work, full bibliographic details including the author, title, awarding institution and date of the thesis must be given e.g.

AUTHOR (year of submission) "Full thesis title", University of Southampton, name of the University School or Department, PhD Thesis, pagination

**UNIVERSITY OF SOUTHAMPTON**

**FACULTY OF NATURAL AND ENVIRONMENTAL SCIENCES**

**Institute for Life Sciences**

**Centre for Biological Sciences**

**The Effects of Ageing on Microglial  
Phenotypes and the Central Nervous System  
Response to Systemic Inflammation**

by

**Adam David Hart, BSc**

Thesis for the degree of Doctor of Philosophy

October 2013



UNIVERSITY OF SOUTHAMPTON

## **ABSTRACT**

FACULTY OF NATURAL AND ENVIRONMENTAL SCIENCES, INSTITUTE FOR LIFE SCIENCES, CENTRE FOR BIOLOGICAL SCIENCES  
Doctor of Philosophy

### **The Effects of Ageing on Microglial Phenotypes and the Central Nervous System Response to Systemic Inflammation**

By Adam David Hart, BSc

Microglial cells are resident immune cells of the central nervous system (CNS) that participate in the CNS response to systemic inflammation by producing inflammatory mediators, which subsequently contribute to the behavioural and metabolic adaptations to systemic infections collectively termed sickness behaviour. Ageing leads to changes in microglial phenotype and a maladaptive, exaggerated CNS inflammatory and behavioural response to systemic infection has been described in aged rodents, which could have a negative impact on CNS health. However, most studies examining the effects of ageing on microglia have focused on a single region of the brain (the hippocampus) and have used a single model of infection, the bacterial mimetic lipopolysaccharide (LPS). This raises two important questions – are microglia in different parts of the brain equally effected by ageing, and do different models of systemic infections have different effects on sickness behaviour and on microglia? To address these questions we used immunohistochemistry, quantitative PCR and behavioural assays to investigate the effects of region on age related changes in microglial phenotype along a rostral to caudal axis and the CNS inflammatory and behavioural response elicited by LPS was compared to that elicited during a live infection with *Salmonella typhimurium*.

We detected significant differences in the effects of ageing on microglia of different regions of the CNS, with microglia of white matter areas and the cerebellum demonstrating significantly greater changes in expression of activation markers than those of rostral grey matter areas. Co-ordination and balance was impaired in aged mice at baseline and some sickness behaviours were exaggerated in aged mice in response to LPS injection, whereas *Salmonella typhimurium* infection induced long-lasting reductions in exploratory activity of equal size in young and aged mice and, in aged mice, co-ordination and balance deficits and prolonged weight loss. A low grade, prolonged inflammatory response was detected in the hippocampus which was accompanied by increased expression of microglial activation markers throughout the young and aged CNS, particularly in the spinal cord, where increased axonal stress and changes in the organisation of the paranodal junction were also observed. These changes in cytokine levels and microglial phenotype were mostly of similar magnitude in young and aged mice, contrasting to the effects of LPS.

These results highlight regional differences in the sensitivity of microglia to systemic infection and ageing and show extensive differences between the effects of the bacterial mimetic LPS and a live bacterial infection on microglia and on sickness behaviour in young and aged mice. They also have important implications for the study of ageing microglia regarding the selection of the infection models and in deciding which CNS regions to examine.

# Contents

<b>ABSTRACT</b> .....	<b>i</b>
<b>Contents</b> .....	<b>ii</b>
<b>List of tables</b> .....	<b>ix</b>
<b>List of figures</b> .....	<b>xi</b>
<b>DECLARATION OF AUTHORSHIP</b> .....	<b>xvii</b>
<b>Acknowledgements</b> .....	<b>xix</b>
<b>List of Abbreviations</b> .....	<b>xx</b>
<b>1. Introduction</b> .....	<b>1</b>
1.1    Physiology of the immune response, the brain and their communication .....	2
1.1.1    Introduction to the Innate Immune System (for references, see Paul (2008)) .....	2
1.1.2    The immune response to a peripheral bacterial infection: focus on <i>Salmonella typhimurium</i> . .....	5
1.1.3    Introduction to the central nervous system (for references, see (Purves et al., 2008)) .....	9
1.1.4    Oligodendrocyte-neuron interactions: focus on the paranodal junction. 12	
1.1.5    Immune to brain communication .....	16
1.1.5.1    Immune to brain communication via the vagus nerve.....	17
1.1.5.2    Circumventricular organs .....	19
1.1.5.3    De novo production of inflammatory mediators within the CNS 19	
1.1.5.4    An integrated view of sickness behaviour and its application to real infections .....	23
1.1.5.5    Summary .....	25
1.2    Microglia .....	26
1.2.1    Resting microglia.....	27
1.2.2    Pro-inflammatory activation of microglia .....	28
1.2.3    Alternative activation of microglia .....	33
1.2.4    Priming vs tolerance .....	35
1.3    Ageing .....	36
1.3.1    Mechanisms of ageing .....	36
1.3.1.1    ROS and Ageing.....	36

1.3.1.2	mTOR, calorie restriction and ageing .....	37
1.3.1.3	Developmental drift.....	39
1.3.2	Ageing, the CNS and neurodegenerative disease.....	39
1.3.3	Ageing and white matter.....	40
1.3.4	Ageing and the peripheral immune system.....	41
1.4	Microglial Priming.....	43
1.4.1	Microglial Priming in the neurodegenerative brain .....	43
1.4.2	Microglial Priming in the ageing brain .....	45
1.5	Causes of Microglial Priming .....	47
1.5.1	The CNS microenvironment – immune regulating molecules of the CNS	48
1.5.1.1	CD200 & CD200R.....	48
1.5.1.2	SIRP $\alpha$ & CD47.....	49
1.5.1.3	TREM receptors.....	51
1.5.1.4	AGE and RAGE.....	51
1.5.1.5	Fractalkine .....	53
1.5.1.6	Immune regulating molecules of the CNS – summary.....	54
1.5.1.7	Blood Brain Barrier Integrity.....	55
1.5.2	Increased innate immune stimulation .....	56
1.5.3	Intrinsic changes.....	56
1.6	Summary .....	57
1.7	Project aims.....	58
<b>2.</b>	<b>Materials &amp; Methods.....</b>	<b>59</b>
2.1	Animals.....	59
2.1.1	Animal housing.....	59
2.1.2	Tissue harvesting.....	59
2.1.3	LPS/saline injection.....	60
2.1.4	Salmonella typhimurium infection.....	60
2.2	Behavioural assays.....	60
2.2.1	Inverted screen – test of muscle strength.....	60
2.2.2	Rod climbing assay – test of forelimb strength.....	61
2.2.3	Multiple Static Rod test – test of balance/co-ordination .....	62
2.2.4	Rotarod test – test of co-ordination. ....	63
2.2.5	Automated open field test – an assay of spontaneous locomotor activity .....	63
2.2.6	Manual open field test - an assay of spontaneous locomotor activity .....	63
2.2.7	Glucose water consumption test .....	64
2.2.8	Burrowing .....	64

2.2.9	Novel Object Recognition test .....	65
2.2.10	Body weight measurement.....	66
2.3	Immunohistochemistry .....	66
2.3.1	Fresh frozen Sections – DAB staining.....	66
2.3.2	Fresh frozen sections – fluorescent immunohistochemistry .....	70
2.3.3	PFA fixed sections. ....	70
2.4	Quantitative PCR.....	71
2.4.1	RNA extraction.....	71
2.4.2	Reverse transcription .....	72
2.4.3	Quantitative polymerase chain reaction (qPCR).....	73
2.4.4	qPCR data analysis – Delta Delta Ct method .....	75
2.4.5	Agarose gel for PCR products.....	76
2.5	Enzyme-linked immunosorbent assay (ELISA) .....	76
2.6	Meso Scale Discovery multiplex cytokine measurements.....	77
2.7	Statistical analysis .....	78
<b>3.</b>	<b>Characterisation of the behavioural response to LPS in young, middle-aged and aged mice.....</b>	<b>79</b>
3.1	Introduction .....	79
3.2	Materials and Methods .....	80
3.2.1	Animals .....	80
3.2.2	Procedures .....	80
3.2.3	Behavioural assays.....	80
3.3	Results.....	83
3.3.1	Sickness behaviours .....	83
3.3.2	Co-ordination and motor function assays.....	92
3.4	Discussion.....	102
3.4.1	Sickness behaviours .....	102
3.4.2	Co-ordination and balance deficits.....	104
3.4.3	Summary .....	106
<b>4.</b>	<b>Histological and molecular analysis of the microglial response to LPS and ageing.....</b>	<b>107</b>
4.1	Introduction .....	107
4.2	Materials and Methods .....	108
4.2.1	Animals .....	108
4.2.2	Immunohistochemistry .....	109
4.2.3	Quantification of immunohistochemistry staining .....	110
4.2.4	Quantitative PCR.....	111

4.2.5	Statistical analysis .....	111
4.3	Results .....	111
4.3.1	Immunohistochemical investigations into microglial phenotype and morphology .....	111
4.3.2	Quantification of inflammatory molecule expression in the young and aged brain by qPCR.....	129
4.4	Discussion .....	134
4.4.1	Microglial phenotype changes in response to injury along the rostral-caudal axis .....	135
4.4.2	Pronounced white matter related changes.....	136
4.4.3	Pronounced changes in CD11c expression.....	136
4.4.4	Neurodegeneration in the ageing brain .....	138
4.4.5	Impact of systemic inflammation on aged-related microglia phenotype .....	139
4.4.6	Summary .....	140
<b>5.</b>	<b>Characterisation of the behavioural response to salmonella typhimurium infection in young and aged mice. ....</b>	<b>141</b>
5.1	Introduction .....	141
5.2	Materials and Methods .....	142
5.2.1	Animals.....	142
5.2.2	Salmonella typhimurium infection.....	143
5.2.3	Food intake measurement.....	143
5.2.4	Behavioural testing regime .....	143
5.2.5	Novel Object Recognition Test.....	145
5.2.6	Static rod test.....	146
5.2.7	Manual Open field test .....	146
5.3	Results .....	147
5.3.1	Pilot experiments .....	147
5.3.2	Experiment 1 (main experiment).....	151
5.3.3	Experiment 2.....	161
5.4	Discussion .....	165
5.4.1	Preliminary experiments .....	165
5.4.2	Anorexic weight loss .....	167
5.4.3	Static rod test performance.....	168
5.4.4	Open field and novel object recognition test.....	169
5.4.5	Summary .....	172
<b>6.</b>	<b>A longitudinal study of the effects of Salmonella infection and ageing on microglial phenotype and function.....</b>	<b>175</b>

6.1	Introduction .....	175
6.2	Methods .....	176
6.2.1	Animals .....	176
6.2.2	Tissue collection.....	176
6.2.3	Cytokine measurements .....	177
6.2.4	Immunohistochemistry .....	177
6.2.5	Quantification of immunohistochemistry .....	177
6.2.6	qPCR .....	178
6.3	Results.....	178
6.3.1	The effect of <i>S. typhimurium</i> infection on circulating cytokine levels in young and aged mice .....	178
6.3.2	An immunohistological assessment of microglial phenotype in different regions of the young and aged CNS after <i>S. typhimurium</i> infection .....	180
6.3.3	The effect of <i>S. typhimurium</i> infection on production of pro-inflammatory molecules in the young and aged CNS .....	208
6.4	Discussion.....	215
6.4.1	The peripheral cytokine response to <i>S. typhimurium</i> .....	215
6.4.2	Regional differences in the effects of ageing on microglial phenotype.....	215
6.4.3	The effects of <i>S. typhimurium</i> infection on microglial phenotype in the young and aged CNS.....	216
6.4.4	The CNS inflammatory response to <i>S. typhimurium</i> infection. .	218
6.4.5	Summary .....	220
<b>7.</b>	<b>The effect of systemic inflammation on the organisation of the paranodal junction in the spinal cord.....</b>	<b>221</b>
7.1	Introduction .....	221
7.2	Materials and Methods .....	222
7.2.1	Complete Freund's adjuvant (CFA) experiment.....	222
7.2.2	EAE experiment .....	223
7.2.3	<i>S. typhimurium</i> experiment.....	223
7.2.4	Immunofluorescence.....	223
7.2.5	Microscopy.....	224
7.2.6	Quantitative analysis .....	225
7.3	Results.....	226
7.3.1	EAE experiment .....	226
7.3.2	CFA experiment.....	230
7.3.3	<i>S. typhimurium</i> experiment.....	232
7.4	Discussion.....	239
7.4.1	The effects of EAE on paranodal organisation.....	239

7.4.2	Selection of spinal cord as site of study.....	239
7.4.3	The effect of CFA on paranodal organisation .....	240
7.4.4	The effect of <i>S. typhimurium</i> and ageing on paranodal organisation .....	241
7.4.5	Summary .....	243
<b>8.</b>	<b>General discussion .....</b>	<b>244</b>
8.1	Changes in microglia.....	244
8.2	Sickness behaviour after LPS injection or <i>S. typhimurium</i> infection .....	247
8.3	Implications.....	254
8.4	Future experiments .....	255
8.5	Summary .....	258
	<b>Appendices .....</b>	<b>261</b>
	Appendix 1: Preparation of buffers and solutions.....	261
A1.1	Fixatives .....	261
A1.2	Mouse food pellets composition.....	261
A1.3	Immunohistochemistry reagents .....	261
A1.4	Buffers .....	262
	<b>List of References .....</b>	<b>263</b>



# List of tables

Table 1.1. Types of glia resident in the CNS.....	11
Table 1.2. The TLR family of receptors and their ligands and functions. ..	32
Table 2.1. Inverted screen scoring system.....	61
Table 2.2. Scoring system for the climbing rod assay.....	62
Table 2.3. A table of all primary antibodies used. ....	68
Table 2.4. A table of all secondary antibodies used. ....	70
Table 2.5. The reverse transcription master mix components.....	72
Table 2.6. Reagents used for qPCR when using iTaq SYBR green supermix.73	
Table 2.7. Reagents used for qPCR whe using iQ SYBR green supermix....	73
Table 2.8. A list of all primers used throughout this thesis.....	75
Table 4.1. A brief description of all the molecules investigated in this chapter.....	110
Table 4.2. Statistical results of analysis of qPCR data from young or aged cerebellum or hippocampus/cortex tissue 24h after saline/LPS injection.....	131
Table 4.3. Statistical results of analysis of qPCR data from young or aged cerebellum or hippocampus/cortex tissue 24h after saline/LPS injection.....	134
Table 6.1. Statistical analysis of the effects of <i>S. typhimurium</i> infection and ageing on circulating levels of IL-1 $\beta$ , IL-6, TNF $\alpha$ , IFN $\gamma$ , IL- 12 and IL-10. ....	180
Table 6.2. Statistical analysis of the effects of <i>S. typhimurium</i> infection and ageing on expression of CD11b.....	185

<b>Table 6.3. Statistical analysis of the effects of <i>S. typhimurium</i> infection and ageing on expression of CD68.....</b>	<b>192</b>
<b>Table 6.4. Statistical analysis of the effects of <i>S. typhimurium</i> infection time-point and ageing on expression of F4/80.....</b>	<b>198</b>
<b>Table 6.5. Statistical analysis of the effects of <i>S. typhimurium</i> infection and ageing on expression of Fc<math>\gamma</math>RI. ....</b>	<b>202</b>
<b>Table 6.6. Statistical analysis of the effects of <i>S. typhimurium</i> infection and ageing on expression of CD11c.....</b>	<b>206</b>
<b>Table 6.7. Statistical results of analysis of qPCR data from young or aged cerebellum or hippocampus after <i>S. typhimurium</i> infection (experiment 1).....</b>	<b>212</b>
<b>Table 6.8. Statistical results of analysis of qPCR data from young or aged cerebellum or hippocampus after <i>S. typhimurium</i> infection (experiment 2).....</b>	<b>215</b>
<b>Table 8.1. A summary table listing the key observations made during this thesis.....</b>	<b>259</b>

# List of figures

Figure 1.1. The complement system.....	4
Figure 1.2. Early events of <i>Salmonella enterica</i> infection.....	7
Figure 1.3. The structure of the blood brain barrier.....	10
Figure 1.4. An electron micrograph of a tranverse section of the anterior commissure of a monkey. ....	13
Figure 1.5. A simplified diagram showing some of the key components of the node of ranvier, the paranodal junction and the juxtaparanode and how they are organised in a healthy axon.....	15
Figure 1.6. A modified version of figure 1.5 demonstrating how a “disrupted” paranode may be organised. ....	16
Figure 1.7. The main pathways of immune brain communication.....	26
Figure 1.8. Morphological activation of microglial cells. ....	30
Figure 1.9. Control of microglial phenotype by extracellular signals.....	54
Figure 2.1. An example of a burrowing tube.....	65
Figure 3.1. A timeline illustrating the sequence of behavioural tests performed. ....	82
Figure 3.2. The effect of LPS or saline injection on body weight.....	83
Figure 3.3. 2h Burrowing performance after injection of LPS or saline. ....	84
Figure 3.4. Overnight burrowing performance after injection of LPS or saline. ....	85
Figure 3.5. The effect of ageing on baseline burrowing activity. ....	87
Figure 3.6. The effect of LPS or saline injection on glucose water consumption.....	88

<b>Figure 3.7 The effect of LPS and saline on open field locomotor activity...</b>	<b>90</b>
<b>Figure 3.8. The effects of LPS or saline injection on open field rearing activity.....</b>	<b>91</b>
<b>Figure 3.9. Average body weight at baseline.....</b>	<b>92</b>
<b>Figure 3.10. The effect of LPS or saline injection on rotarod performance.</b>	<b>94</b>
<b>Figure 3.11. The influence of age and LPS injection on 9mm static rod test performance. ....</b>	<b>96</b>
<b>Figure 3.12. The influence of age on 9mm static rod transit time. ....</b>	<b>97</b>
<b>Figure 3.13. Baseline inverted screen performance.....</b>	<b>98</b>
<b>Figure 3.14. Baseline climbing rod performance and its correlation with static rod test performance. ....</b>	<b>100</b>
<b>Figure 3.15. The influence of weight on climbing rod performance.....</b>	<b>101</b>
<b>Figure 4.1. An illustration of the distribution of the CNS regions selected for study. ....</b>	<b>112</b>
<b>Figure 4.2. The effect of age and LPS on CD11b expression.....</b>	<b>114</b>
<b>Figure 4.3. The effect of age and LPS on CD68 expression. ....</b>	<b>115</b>
<b>Figure 4.4. Expression of microglial activation markers in the aged brain.</b>	<b>117</b>
<b>Figure 4.5. Expression of a panel of myeloid cell markers in the young spleen of saline injected mice. ....</b>	<b>118</b>
<b>Figure 4.6. Age related changes in microglial phenotype in different brain regions. ....</b>	<b>121</b>
<b>Figure 4.7. Age related changes in CD11c and FcγRI expression in different brain regions.....</b>	<b>122</b>
<b>Figure 4.8. Dectin 1 marker expression increases with age, but not LPS..</b>	<b>124</b>
<b>Figure 4.9. FcγR II/III expression in the ageing brain following a systemic challenge LPS.....</b>	<b>125</b>

Figure 4.10. MHC class II expression does not change with age or LPS. . .	126
Figure 4.11. Expression of Dectin 1, MHC class II, Dec205 and FcγRII/III in the young spleen. ....	127
Figure 4.12. The effect of LPS on expression of IL-1β, IL-6 and F4/80 mRNA levels in young and aged cerebellum and hippocampus/cortex tissue 24h after saline/LPS injection.	130
Figure 4.13. The effect of LPS on expression of expression of inflammatory molecules in young and aged cerebellum 3h after saline/LPS injection.....	132
Figure 4.14. The effect of LPS on expression of IL-1β, IL-6, TNFα and COX-2 mRNA levels in young and aged hippocampus 3h after saline/LPS injection. ....	133
Figure 5.1. Experimental design for behavioural testing in experiment 1.	144
Figure 5.2 The overall experimental design for experiment 1.....	145
Figure 5.3. Optimisation of <i>S. typhimurium</i> doses for aged mice.....	148
Figure 5.4. Optimisation of the novel object recognition test. ....	149
Figure 5.5. Changes in body weight of young or aged mice followed infection with 3 x 10 <sup>5</sup> CFU <i>S. typhimurium</i> .....	153
Figure 5.6 Changes in body weight of young or aged mice followed infection with 3 x 10 <sup>5</sup> CFU <i>S. typhimurium</i> over a prolonged period of time (55 days). ....	154
Figure 5.7. The effect of <i>S. typhimurium</i> infection on novel object recognition test performance in young or aged mice.....	156
Figure 5.8. The effects of <i>S. typhimurium</i> infection on static rod test performance in young and aged mice. ....	158
Figure 5.9. The effect of <i>S. typhimurium</i> infection on open field test performance in young and aged mice. ....	160

Figure 5.10. Changes in body weight of young or aged mice followed infection with $3 \times 10^5$ CFU <i>S. typhimurium</i> – experiment 2.	163
Figure 5.11 Changes in daily food intake of young or aged mice followed infection with $3 \times 10^5$ CFU <i>S. typhimurium</i> – experiment 2.	164
Figure 6.1. The effect of <i>S. typhimurium</i> infection on serum cytokine levels in young and aged mice..	179
Figure 6.2. The effect of ageing on expression of microglia markers in various regions of the aged CNS.....	182
Figure 6.3. The effect of <i>S. typhimurium</i> infection on CD11b expression in various regions of the young and aged CNS.....	184
Figure 6.4. Representative images of CD11b expression in the hippocampus of young or aged mice following <i>S. typhimurium</i> infection.....	187
Figure 6.5. Representative images of CD11b expression in spinal cord white matter tracts of young or aged mice following <i>S. typhimurium</i> infection.....	188
Figure 6.6. Representative images of CD11b expression in the cerebellar white matter tracts of young or aged mice following <i>S. typhimurium</i> infection.....	190
Figure 6.7. The effect of <i>S. typhimurium</i> infection on CD68 expression in various regions of the young and aged CNS.....	191
Figure 6.8. Representative images of CD68 expression in the hippocampus of young or aged mice following <i>S. typhimurium</i> infection..	192
Figure 6.9. Representative images of CD68 expression in spinal cord white matter tracts of young or aged mice following <i>S. typhimurium</i> infection.....	194
Figure 6.10. Representative images of CD68 expression in the cerebellar white matter tracts of young or aged mice following <i>S. typhimurium</i> infection.....	196

Figure 6.11. The effect of <i>S. typhimurium</i> infection on F4/80 expression in various regions of the young and aged CNS. ....	197
Figure 6.12. Representative images of F4/80 expression in the CNS of young or aged mice following <i>S. typhimurium</i> infection. ..	199
Figure 6.13. The effect of <i>S. typhimurium</i> infection on FcγRI expression in various regions of the young and aged CNS. ....	201
Figure 6.14. Representative images of FcγRI expression in the CNS of young or aged mice following <i>S. typhimurium</i> infection. ..	203
Figure 6.15. The effect of <i>S. typhimurium</i> infection on CD11c expression in various regions of the young and aged CNS. ....	205
Figure 6.16. Representative images of CD11c expression in the CNS of young or aged mice following <i>S. typhimurium</i> infection. ..	207
Figure 6.17. Characterisation of PGK1 as a reference gene for qPCR. ....	210
Figure 6.18. The effect of <i>S. typhimurium</i> infection on expression of pro-inflammatory molecules in the young and aged hippocampus. ....	211
Figure 6.19. The effect of <i>S. typhimurium</i> infection on expression of pro-inflammatory molecules in the young and aged hippocampus. ....	213
Figure 6.20. The effect of <i>S. typhimurium</i> infection on expression of pro-inflammatory molecules in the young and aged cerebellum. ....	214
Figure 7.1. A schematic showing the schedule for the CFA experiment. ..	223
Figure 7.2. An example demonstrating how skeletal lengths are obtained using Volocity software. ....	225
Figure 7.3. The effect of EAE on paranodal integrity. ....	228
Figure 7.4. The effect of EAE on paranodal length and SMI-32 reactivity. ....	229
Figure 7.5. The effects of CFA and PTX injection on paranodal length and paranodal/juxtaparanodal compartmentalisation. ....	231

Figure 7.6. The effect of <i>S. typhimurium</i> infection on paranodal integrity in SMI-32 negative and positive axons of young and aged mice.	233
Figure 7.7. Quantification of paranodal (Nfasc155) length on SMI-32 negative or positive axons.	235
Figure 7.8. Quantification of SMI-32 immunoreactivity in <i>S. typhimurium</i> infected young and aged mice.	236
Figure 7.9. The effect of <i>S. typhimurium</i> infection on paranodal/ juxtapanodal compartmentalisation in young and aged mice.	237
Figure 7.10. The effect of <i>S. typhimurium</i> infection on caspr and Nfasc155 co-localisation in young and aged mice.	238
Figure 8.1. A summary figure showing the changes induced by <i>S. typhimurium</i> infection in the young and aged CNS.	253
Figure 8.2. A summary figure showing the changes induced by systemic LPS injection in young and aged mice.	253

# DECLARATION OF AUTHORSHIP

I, Adam Hart

declare that the thesis entitled

The Effects of Ageing on Microglial Phenotypes and the Central Nervous System Response to Systemic Inflammation

and the work presented in the thesis are both my own, and have been generated by me as the result of my own original research. I confirm that:

- this work was done wholly or mainly while in candidature for a research degree at this University;
- where any part of this thesis has previously been submitted for a degree or any other qualification at this University or any other institution, this has been clearly stated;
- where I have consulted the published work of others, this is always clearly attributed;
- where I have quoted from the work of others, the source is always given. With the exception of such quotations, this thesis is entirely my own work;
- I have acknowledged all main sources of help;
- where the thesis is based on work done by myself jointly with others, I have made clear exactly what was done by others and what I have contributed myself;
- parts of this work have been published as: (Hart et al., 2012)

Signed: ...ADAM HART.....

Date: ...21/01/2014.....



# Acknowledgements

Firstly I would like to thank my supervisors past and present, Jessica Teeling, Hugh Perry and Andreas Wyttenbach, whose guidance and support have been invaluable during the last four years. I have learnt a huge amount since arriving in Southampton four years ago, and the three of you have all played a big part in that process.

I have to say a big thank you to Steven Booth and Ursula Püntener, who I have worked very closely with in all my Salmonella experiments – I couldn't have done it without either of you and it's been a lot of fun working with the two of you. My fellow PhD students Olivia Larsson, Salomé Murinello and James Fuller also deserve credit for always being a willing ear when I needed to vent some frustration, test out some ideas or just go to the pub. I'd also like to thank all the other former and current members of the Teeling and Perry lab I have worked with for their help and advice at various points.

I would like to thank the staff at the Biomedical Research Facility for all their assistance with my in vivo work, especially Lesley Lawes, who has always gone the extra mile to help us with our Salmonella experiments. Thank you to Felino Cagampang and Kim Bruce for providing the high fat diet mice, Su Wu and Feng Liu from Peking University, China for their help with RNA extractions and David Johnson for all his help capturing confocal images. I'd also like to thank Professor Peter Brophy and Dr Barbara Zonta from the University of Edinburgh for providing the neurofascin antibodies and their advice on using them, Dr Karl Goodyear from the University of Glasgow for providing the EAE tissue for chapter 7 and Professor Martin Glennie from the University of Southampton for providing the CD11c antibody. I extend my thanks to the Biotechnology and Biological Sciences Research Council and Wellcome Trust for their financial support during my PhD.

Thanks also to all my family and friends, especially my parents, for your support and understanding and for helping me let off steam when I've needed to. Finally I'd like to reserve the biggest thank you for my wife Nic. Even when we haven't been able to be together you've been the one who has kept me sane when things have gone wrong and who has supported me every inch of the way in getting through my PhD, despite all the late nights and weekends at work.

# List of Abbreviations

5-HT	5-hydroxytryptophan (serotonin)
Ab	antibody
ABC	avidin biotin complex
AD	Alzheimer's disease
A $\beta$	amyloid beta
AGE	advanced glycation end product
ANOVA	analysis of variance
APES	3-aminopropyltriethoxysilane
ATP	adenosine triphosphate
BBB	blood brain barrier
BDNF	brain derived neurotrophic factor
BSA	bovine serum albumin
Ca <sup>2+</sup>	calcium ion
Caspr	contactin associated protein
CB	cerebellum
CFA	complete Freund's adjuvant
CFU	colony forming units
Cm	centimeter
CR	caloric restriction
CD	cluster of differentiation
CNS	central nervous system
COX	cyclooxygenase
Ct	cycle threshold
CVO	circumventricular organ
D	day
DAB	3,3'-Diaminobenzidine
DAMP	danger-associated molecular pattern
DAPI	4',6-diamidino-2-phenylindole
DG	dentate gyrus
Dia-1	diaphorase 1
DNA	deoxyribonucleic acid
EAE	experimental autoimmune encephalomyelitis

<i>E. Coli</i>	Escherichia coli
ELISA	enzyme-linked immunosorbent assay
EP receptor	prostaglandin E receptor
Fc $\gamma$ R	Fc gamma receptor
G	grams
gm	grey matter
GAPDH	glyceraldehyde 3-phosphate dehydrogenase
GFAP	glial acidic fibrillary protein
GM-CSF	granulocyte macrophage colony-stimulating factor
h	hour
H <sub>2</sub> O <sub>2</sub>	hydrogen peroxide
H <sub>2</sub> SO <sub>4</sub>	Sulphuric acid
HIV	human immunodeficiency virus
HPA	hypothalamic pituitary axis
HRP	horseradish peroxidase
i.c.	intracortical
i.c.v.	intracerebroventricular
IDO 2,3	indoleamine-pyrrole 2,3-dioxygenase
IFA	incomplete Freund's adjuvant
IFN	interferon
IgG	immunoglobulin G
IHC	immunohistochemistry
IL	interleukin
iNOS	inducible nitric oxide synthase
i.p.	intraperitoneal
IRAK	interleukin 1 receptor-associated kinase
IRF	interferon regulatory factor
ITAM	immunoreceptor tyrosine-based activation motif
ITIM	immunoreceptor tyrosine-based inhibitory motif
i.v.	intravenous
JNK	c-Jun N-terminal kinases
K <sup>+</sup>	potassium ion
KO	knockout
Kv1.2	potassium voltage-gated channel subfamily A member 2
LDL	low density lipoprotein
LPS	lipopolysaccharide

LTP	long term potentiation
m	months old
M.O.M.	mouse on mouse
MAPK	mitogen-activated protein kinase
MBH	mediobasal hypothalamus
MCP-1	monocyte chemoattractant protein-1
mg	milligram
MHC	major histocompatibility complex
ml	millilitre
mm	millimeter
mM	millimolar
mPGES	membrane associated prostaglandin E synthase
mRNA	messenger ribose nucleic acid
ms	milliseconds
MAPK	mitogen-associated protein kinase
MS	multiple sclerosis
mTOR	mammalian target of rapamycin
n	sample number
Na <sup>+</sup>	sodium ions
Nav1.6	voltage gated sodium channel type VIII
NADPH	nicotinamide adenine dinucleotide phosphate-oxidase
Nfasc155	neurofascin 155
NFκB	nuclear factor kappa B
nm	nanometer
NO	nitric oxide
NOD	nucleotide-binding oligomerization
NOR	novel object recognition
NOS	nitric oxide synthase
p-	phosphorylated form of...
PAMP	pathogen-associated molecular pattern
PBS	phosphate buffered saline
PD	Parkinson's disease
PFA	paraformaldehyde
pg	picogram
PGE	prostaglandin E
PGK1	phosphoglycerate kinase 1

PI3K	phosphatidylinositol 3-kinase
Poly I:C	polyinosinic:polycytidylic acid
PPRs	pattern recognition receptors
PTX	pertussis toxin
qPCR	quantitative real time-polymerase chain reaction
RAGE	receptor for advanced glycation endproducts
RNA	ribonucleic acid
RNS	reactive nitrogen species
ROS	reactive oxygen species
RPM	rotations per minute
RT	room temperature
s	seconds
<i>S. typhimurium</i>	Salmonella typhimurium
SEM	standard error of the mean
Sirp	signal regulatory protein
SOD	superoxide dismutase
Spc	spinal cord
sRAGE	soluble RAGE
TGF	tumour growth factor
Th1	T helper cell subtype 1
Th2	T helper cell subtype 2
TLR	toll-like receptor
TNF	tumour necrosis factor
TREM	triggering receptor expressed on myeloid cells
V	volts
v/v	volume per volume
wm	white matter
w/v	weight per volume
µl	microlitres
µm	micrometres



# 1. Introduction

The central nervous system (CNS) is a uniquely specialised anatomical compartment. Functionally it co-ordinates and regulates organismal function and behaviour on almost every level, from control of metabolism and basic homeostatic processes such as breathing through to complex direction of behaviours directed through multiple neuronal circuits and their afferent projections. The brain is also an immune privileged organ, with a tightly regulated population of perivascular macrophages, microglia and a small number of T cells transiently entering the parenchyma of the brain providing the basis of the brain's immune system. This immune privilege is in part maintained by the blood brain barrier, a tightly regulated structure principally consisting of endothelial cells which are supported by pericytes, astrocytes and perivascular macrophages.

Despite this separation from the rest of the body, the brain communicates bi-directionally with the peripheral immune system through multiple routes to direct adaptive behavioural and metabolic responses which function to assist the immune system's attempts to eliminate infections from the body. These responses are critical for the resolution of infection, but in some circumstances may become maladaptive, for example in the damaged or ageing brain where microglia respond in an exaggerated manner to peripheral inflammatory stimuli and, through their excessive inflammatory responses, may precipitate or accelerate the progression of pathology in the brain and drive maladaptive behavioural responses to infection (Cunningham et al., 2009; Godbout et al., 2008). The causes and consequences of these exaggerated responses are not fully understood at present. This thesis aims to characterise the response of the ageing CNS to peripheral inflammation and infection on a cellular and behavioural level and to investigate regional differences within the CNS in these responses.

## **1.1 Physiology of the immune response, the brain and their communication**

### **1.1.1 Introduction to the Innate Immune System (for references, see Paul (2008))**

The mammalian immune system is divided into two branches; the adaptive and the innate immune system. The innate immune system presents a rapid and robust response to insult that develops within hours; the adaptive response takes longer to develop and eliminates pathogens in a specific manner via the production of antibodies and T cell responses. The innate immune system initially reacts to infection via pathogen recognising pattern recognition receptors (PRRs) such as mannose receptors, scavenger receptors, nucleotide-binding oligomerisation receptors and toll like receptors. Each of these receptors recognise different structural motifs associated with pathogens and initiate distinct signalling cascades upon their activation; for a more complete discussion see section 1.2.3. This initial identification of a pathogen is normally performed by resident tissue macrophages and dendritic cells (DCs). PRR activation triggers the beginning of the innate immune response, leading to phagocytosis of micro-organisms/virus infected cells by macrophages and dendritic cells, lysosomal degradation of the phagocytosed material and subsequent presentation of antigens in MHC complexes. Macrophages and DCs also produce cytokines and chemokines after PRR stimulation, which attract other immune cells to the site of insult, activates immune cells, increases vascular permeability and increases expression of MHC and co-stimulatory molecules. The subsequent infiltrating immune cells include neutrophils and natural killer (NK) cells, which phagocytose or lyse bacteria or virus infected cells and form an important part of the innate immune response in the direct elimination of pathogens. These cells are not normally present in healthy tissue, but are present in the circulation and upon activation migrate via chemotaxis to the site of inflammation. The cytokine profiles elicited by PRR activation differ according to the type of immune challenge encountered and can influence the immune response through initiation of a Th1 or Th2 (or Th17/Th9) dominant response. These different responses are adapted to the clearance of different types of pathogens. For example, Th2 responses are initiated in response to helminths (Hoffmann et al., 2000), while Th1 responses

are elicited by bacterial stimuli such as *E. coli* lipopolysaccharide (Re and Strominger, 2001).

Phagocytosis of extracellular material by antigen presenting cells such as macrophages or dendritic cells results in the display of antigen fragments via MHCII. Dendritic cells constitutively express MHC molecules and co-stimulatory molecules and one of their principle roles is to migrate via lymph vessels to a lymph node where they can activate naïve CD4+ T cells, triggering the adaptive arm of the immune system. Dendritic cells thus act as a bridge between the innate and the adaptive immune response. B cells can bind soluble antigens via their unique B cell receptor (an immunoglobulin specific to one particular epitope) and, if co-stimulated by T cells, clonally expand and begin producing antibodies against the antigen they recognise. Long lived B memory cells are also formed during this clonal expansion, which express the antibody produced during expansion on the outer cell membrane to allow rapid pathogen recognition and clonal expansion following future encounters with that particular antigen.

Complement also plays an important role in both the innate and the adaptive immune response. The complement system is a range of small proteins that are produced primarily by the liver which can be found circulating in the blood of healthy individuals in inactivated conformations. They can also be produced on a local basis by epithelium, endothelium and lymphocytes, including in the brain (Godbout et al., 2005b). They play a role in innate immunity via the alternative complement pathway and in the adaptive immune response via the classical and the lectin complement pathways. Complement opsonises membranes for phagocytosis and forms membrane attack complexes to help lyse targeted cells such as bacteria. The classical pathway is mediated by IgG/IgM interactions with C1q and along with the lectin pathway (which acts on repetitive microbial patterns e.g. via MBL) triggers C4 and C2 metabolism to form C4b and C2a, which together make up the classical pathway C3 convertase. This C3 convertase then cleaves a thioester bond in C3 to form C3b (Martinez-Barricarte et al., 2010). The classical pathway also plays an important role in the opsonisation of apoptotic cells (Nauta et al., 2002). The alternative pathway relies on C3b generated from spontaneous hydrolysis of the thioester bond of inactive C3 by H<sub>2</sub>O or C3b derived from the other two pathways, which both bind to “activator” surfaces such as bacterial

lipopolysaccharide sequences (Pangburn et al., 1980). Factor B and D bind to membrane bound C3b and form a C3 convertase, subsequently cleaving further C3 and leading to further C3b binding, forming a positive feedback loop. Unbound C3b and C3b on non-activator surfaces is rapidly inactivated by Factor H in plasma to control C3b levels. When C3 convertase is covalently linked to an additional C3b molecule it forms C5 convertase and initiates the terminal pathway, provided sufficient concentrations of terminal pathway factors are present. The terminal pathway eventually results in the assembly of the lysis inducing membrane attack complex consisting of C5b-C9, which disrupts membrane integrity and will, if there are sufficient numbers of complexes bound, result in death of the bound cell. Sublytic concentrations of membrane attack complexes can also effect the target cell, such as by increasing intracellular calcium concentrations (Seeger et al., 1986), and thereby a number of calcium sensitive molecules such as protein kinase C. C3b labelling also opsonises the cell, enhancing phagocytosis via binding to the complement receptors CD11b and CD11c (see figure 1.1 for an illustration of the complement system).

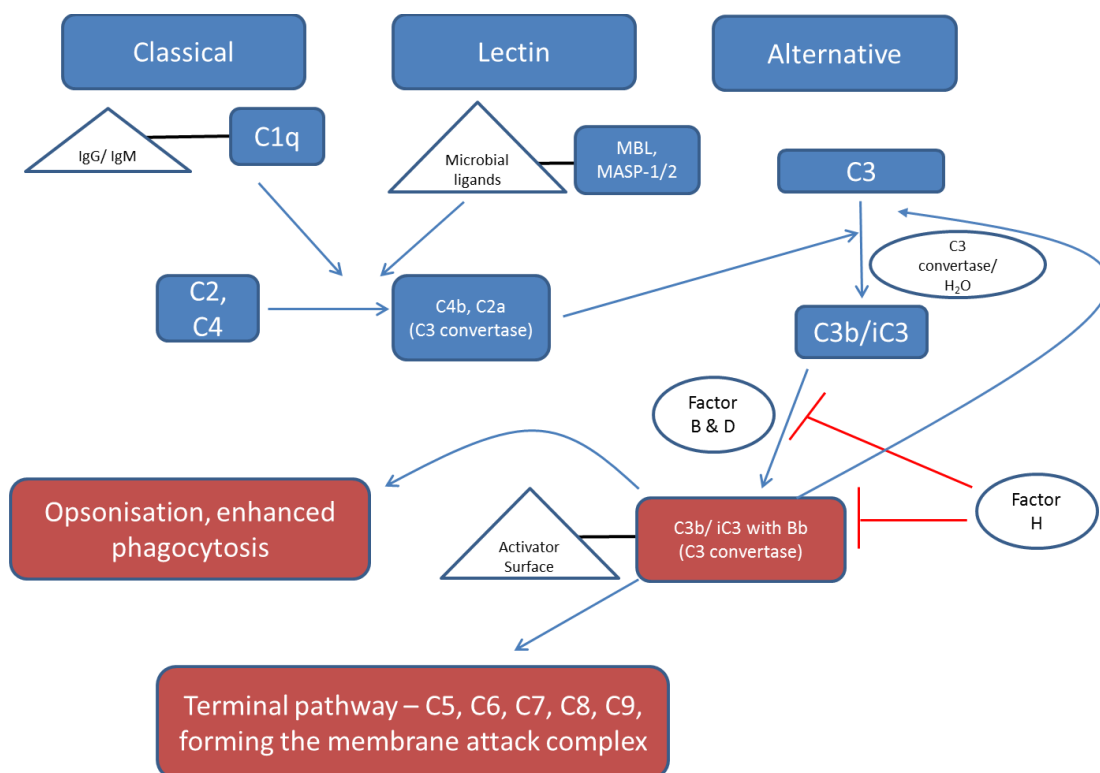


**Figure 1.1. The complement system.**

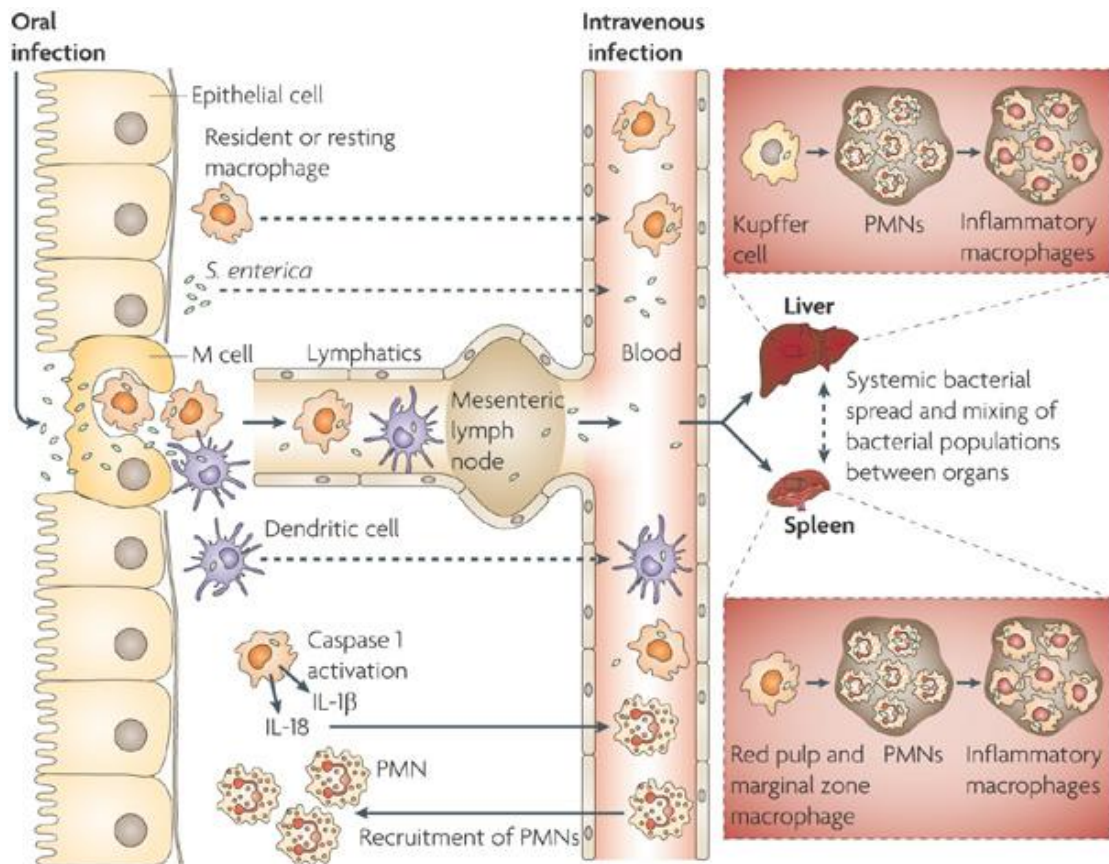
The three activating pathways all converge on C3 and subsequently the terminal pathway, marked in red boxes, provided there are sufficient concentrations of terminal pathway components.

### 1.1.2 The immune response to a peripheral bacterial infection: focus on *Salmonella typhimurium*.

Pathogenic infectious bacteria are responsible for a wide variety of highly prevalent diseases, such as whooping cough (*Bordetella pertussis*), typhoid fever (*Salmonella typhi*) or cholera (*Vibrio cholerae*). There is a huge diversity in types of pathogenic bacteria, their methods of infection and subsequently the strength and profile of an organism's immune responses to them. Some of the most common serious bacterial infections that affect humans are intracellular bacteria, such as *Salmonella typhi* or *Mycobacterium tuberculosis*. Often intracellular bacteria infect phagocytic cells, such as macrophages, and inhabit the phagosome until they break out and proliferate within the cytosol (Peterson, 1996).

Typhoid fever is a serious and very prevalent disease worldwide with an estimated 16-31 million cases and over 200,000 deaths a year (Crump et al., 2004), with most of these cases occurring in the developing world. The first symptoms to present are often diarrhoea caused by gastroenteritis, and after an incubation period of 10-14 days from infection other symptoms appear including fever, headache, abdominal pain, anorexia and vomiting (Bhutta, 2006; Giannella, 1996). Typhoid fever is usually caused by the consumption of food or water contaminated with *Salmonella typhi*, *paratyphi* or *schottmuelleri* (Giannella, 1996), leading to invasion through the intestinal cell wall by the bacteria and subsequent colonisation of liver, spleen, peyer's patches and lymph nodes (Dougan et al., 2011). *Salmonella typhimurium* (*S. typhimurium*) is a serovar from the same species as *Salmonella typhi*, but in humans ingestion of *S. typhimurium* usually only induces enteritis (Santos et al., 2001). However, in mice *S. typhimurium* ingestion leads to symptoms similar to those seen in human typhoid fever (Santos et al., 2001). As a result of these similarities, murine infection with *S. typhimurium* has been used to model human typhoid fever since the early 20<sup>th</sup> century (Santos et al., 2001).

Genetically modified strains with attenuated virulence are frequently used when studying *S. typhimurium* to model vaccination against typhoid Salmonella infections (Mittrucker et al., 2000) or because strains with decreased virulence produce a milder disease course that is less likely to cause death of infected mice and are less likely to infect researchers working with the bacterium. SL3261 is an example of a genetically modified strain of *S. typhimurium* which has attenuated virulence as a result of the insertion of a transposon in the AroA gene (Hoiseth and Stocker, 1981), which prevents synthesis of p-amino-benzoic acid from chorismate. *S. typhimurium* cannot assimilate exogenous folate and instead synthesises folate from precursors such as p-amino-benzoic acid, which is not present in vertebrate tissue in significant quantities (Hoiseth and Stocker, 1981). Blocking production of p-amino-benzoic acid from chorismate prevents folate production by *S. typhimurium* during vertebrate infection, which restricts DNA synthesis (Reichard, 1988) and therefore bacterial proliferation. Inoculation of C57/BL6 mice with SL3261 led to substantially less colonisation of the liver and spleen compared to its wild-type parent strain, SL1344 (Benjamin et al., 1990), demonstrating the reduced virulence of this strain of *S. typhimurium*.



Nature Reviews | Microbiology

**Figure 1.2. Early events of *Salmonella enterica* infection.**

*Salmonella enterica* reaches the intestine and invades microfold cells, which are specialised epithelial cells that transcytose antigens from the intestinal lumen to the abluminal side (Mastroeni et al., 2009). *Salmonella enterica* bacteria then invade phagocytic cells such as macrophages and dendritic cells which enter the circulation in systemic salmonellosis (typhoid fever). Free circulating salmonella that have escaped from apoptosing phagocytes populate tissue with large resident populations of phagocytic cells, such as the liver, spleen, mesenteric lymph nodes, bone and gall bladder. This figure is taken from Mastroeni et al, 2009.

The initial events that lead to colonisation of multiple organs by *S. typhimurium* are outlined in figure 1.2. If *S. typhimurium* is injected intraperitoneally instead of being administered orally then free bacteria enter the blood stream without having to invade through the gut mucosa, but infection via both routes leads to colonisation of organs with large phagocyte populations e.g. spleen, liver (Dougan et al., 2011). During the first few days

after infection bacteria multiply in numbers (Grant et al., 2008) and the innate immune system is activated (Sebastiani et al., 2002). The innate immune response is characterised by local production of a range of pro-inflammatory cytokines, including IFN $\gamma$ , IL-1 $\beta$ , IL-6, IL-12, IL-18 and TNF $\alpha$  (Mittrucker and Kaufmann, 2000) and induction of iNOS activity and macrophage migration inhibitor factor release (Koebernick et al., 2002; Schwacha et al., 1998). These cytokines recruit cells such as natural killer cells, polarise T cells and mediate and potentiate the bactericidal response of infected phagocytic cells. IFN $\gamma$ , TNF $\alpha$  and IL-12 are particularly important in controlling *S. typhimurium* infection, as demonstrated by studies which used antibodies to block these cytokines (Mastroeni et al., 1998). Multicellular lesions consisting of recruited and infected cells called granulomas form around sites of infection and attempt to prevent the spread of the infection to other cells (Mastroeni et al., 1992).

Although T cells do not contribute much to the initial response to *S. typhimurium* infection (Hess et al., 1996), they play an important role in achieving elimination of bacteria rather than merely controlling infection (Hess et al., 1996). CD4 T cell responses contribute to the elimination of infected cells by production of large amounts of IFN $\gamma$  and by stimulating B cell maturation and antibody production (Hess et al., 1996). The role of CD8 cells in primary *S. typhimurium* infection is less well established, with some reports claiming that elimination of CD8 T cells has no impact in attenuated salmonella infection (Hess et al., 1996) while others show decreased survival in CD8 depleted mice following infection with attenuated *S. typhimurium* (Lo et al., 1999).

The extent of B cell participation in primary salmonella infection seems to depend on the virulence of the *S. typhimurium* strain used. Resistance to oral infection with unattenuated, virulent *S. typhimurium* was impaired in B cell deficient mice (Mittrucker et al., 2000; O'Brien et al., 1979), but unimpaired in mice infected with an attenuated strain of *S. typhimurium* (McSorley and Jenkins, 2000; Mittrucker et al., 2000). Another study showed that bacterial counts in the spleen were similar between B cell deficient and wild type mice 7, 28 or 42 days after infection with an attenuated strain, but that B cell deficient mice had a higher bacterial load in the blood, suggesting that the antibody

response may be important in preventing the systemic spread of infection but not in clearance of bacteria (Cunningham et al., 2007a).

By approximately 40 days after infection most studies find that *S. typhimurium* is no longer detectable in spleen or liver of infected mice (Cunningham et al., 2007a; McSorley and Jenkins, 2000; Mittrucker et al., 2000). In summary, *S. typhimurium* challenge produces a systemic infection that lasts several weeks and invokes an immune response that encompasses many different cell types at different stages of the disease, with critical roles for both the innate and adaptive arms of the immune system.

### **1.1.3 Introduction to the central nervous system (for references, see (Purves et al., 2008))**

The mammalian CNS is separated from the rest of the body by the blood brain barrier (BBB), which is present at all the blood vessels of the CNS (apart from the circumventricular organs) and consists primarily of endothelial cells, their tight junctions and a basement membrane which restrict the entry of cells and transmembrane diffusion of large or lipophobic macromolecules above ~8kDa under normal physiological conditions (Banks, 2009), but allows simple molecules such as glucose to pass through. Astrocytes associate closely with the endothelial cells of the BBB, influencing their function via soluble factors such as growth factors (Popescu et al., 2009). Other cells that participate in BBB function include perivascular macrophages, which play an important role in transducing immune responses from the periphery into central responses (Serrats et al., 2010), and pericytes, which contribute to the regulation of BBB tightness and perform contractile functions to regulate CNS blood flow (Winkler et al., 2011). Ageing, neurodegenerative disease and systemic infection have all been proposed to increase the permeability of the BBB (Bake et al., 2009; McQuaid et al., 2009), but in the absence of these conditions it excludes undesired blood components, actively transports those which are required into the brain and contributes to the immune privilege of the brain by restricting infiltration of non-resident immune cells (Popescu et al., 2009).

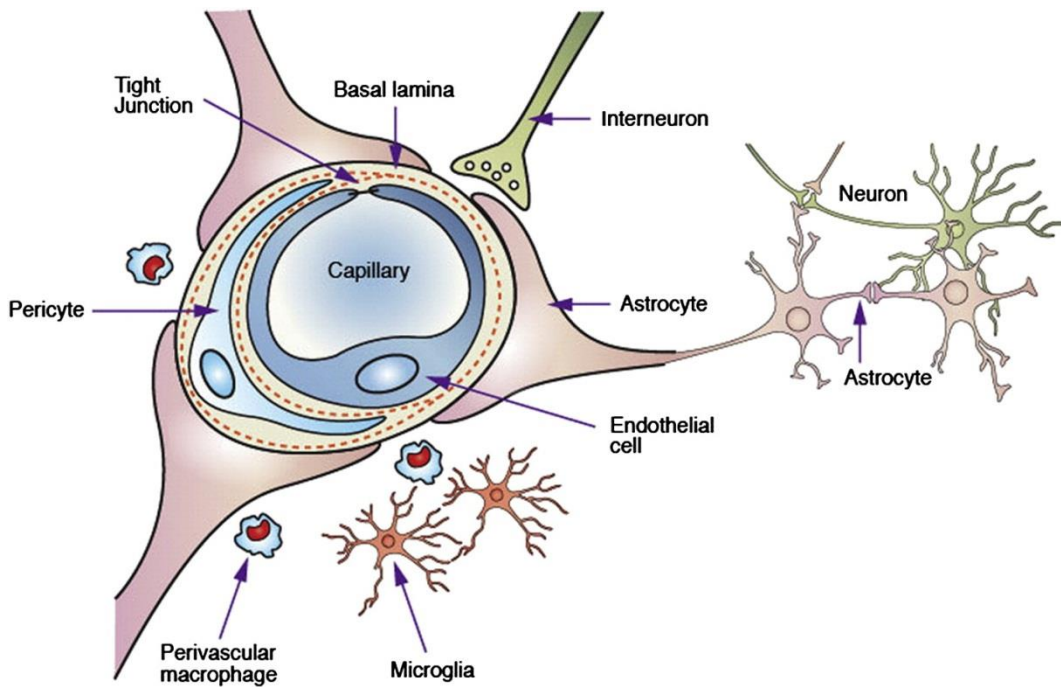


**Figure 1.3. The structure of the blood brain barrier.**

This diagram is taken from Chen and Liu (2012).

The brain itself is a heterogeneous organ. The simplest division is between grey and white matter – grey being made up of neuronal cell bodies and neuropil, white matter of myelinated axons. Both grey and white matter contain a wide range of glial cells, including astrocytes, microglia, oligodendrocytes and pericytes. Table 1.1 outlines their roles. The brain is organised into distinct areas of grey and white matter and is functionally organised into circuits, with neurons receiving and projecting neuronal inputs and outputs to and from specific brain regions, with a range of neurotransmitters employed to transfer these signals. These circuits are the mechanism by which information processing, comprehension, memory and generation of physiological outputs occurs. While a detailed description of brain anatomy is not the focus of this introduction, it is important to note that these spatially and functionally distinct regions may differentially influence microglial function, for example through microglial neurotransmitter receptors (Kettenmann et al., 2011), and that different brain regions are selectively vulnerable to cell loss in neurodegenerative disease and ageing – see section 1.3.2 for discussion. These factors may contribute to the variations in microglial phenotype described across the CNS (De Haas et al., 2008).

Cell type	Origin	Functions
Microglia	Yolk sac origin (Ginhoux et al., 2010), post embryonic proliferation within the CNS, infiltration from periphery in BBB breakdown (Ajami et al., 2007).	Myeloid cells of the CNS; repair, surveillance, microbial defence, trophic support of neurons (Kettenmann et al., 2011).
Astrocyte	Post embryonic mitotic proliferation, radial glia, neural stem cells (Kriegstein and Alvarez-Buylla, 2009)	Structural and metabolic support, BBB control, neurotransmitter uptake and release, ion concentration regulation, repair.
Oligodendrocyte	Neural stem cells (Kriegstein and Alvarez-Buylla, 2009)	Myelination of axons, trophic support of neurons (Wilkins et al., 2001).
Oligodendrocyte precursor cells	Neural stem cells (Trotter et al., 2010)	Generation of oligodendrocytes and astrocytes, trophic support of neurons (Trotter et al., 2010)
Pericyte	Mesoderm and neuroectoderm (Winkler et al., 2011)	Blood brain barrier maintenance, vascular constriction (Winkler et al., 2011).

**Table 1.1. Types of glia resident in the CNS.**

Descriptions taken from Purves et al, 2008, or referenced in text.

#### **1.1.4 Oligodendrocyte-neuron interactions: focus on the paranodal junction.**

Oligodendrocytes are cells that populate the “white matter” of the CNS. They extend processes to axons and ensheath them, wrapping layers of cell membrane around an axon to form a structure called a myelin sheath (Figure 1.4). The myelin sheath provides insulation to axons to prevent transmembrane ionic flux at areas other than the nodes of Ranvier. This myelin sheath leads to the polarisation of ion channels into spatially restricted domains, termed nodes of Ranvier, that in combination with the tight ensheathment of internodal spaces with myelin allow the rapid conduction of action potentials via saltatory conduction (Salzer, 2003). The oligodendrocyte attaches to the axon on either side of the node of Ranvier forming structures known as paranodal junctions.



**Figure 1.4. An electron micrograph of a transverse section of the anterior commissure of a monkey.**

The thick dark layers surrounding axonal cytoplasm are internodal myelin sheaths, indicated by red arrows. The black arrows point out transverse profiles through paranodes, where the myelin sheaths open into loop shaped endings and attach to the axon at paranodal junctions - hence the layer of

cytoplasm between the myelin sheath and the axon. Adapted from (Peters and Sethares, 2013).

Paranodal junctions are structures with an important role in facilitating saltatory conduction in myelinated neurons through the efficient segregation of  $\text{Na}_v1.6$  and  $\text{K}_v1.2$  channels. They accomplish this by the formation of tight junctions between the axon and oligodendrocyte, forming a barrier between the two populations of ion channels (Salzer, 2003) (Figure 1.5). The paranodal junction principally comprises of three proteins – neurofascin 155 (Nfasc155), contactin and caspr. Nfasc155 is anchored in the cell membrane of oligodendrocyte processes and forms a tight junction with contactin, which in turn is tightly bound to contactin associated protein (caspr), which anchors the complex to the axon. These complexes cluster together in structures known as transverse bands. Caspr associates with ankyrin B and various spectrins to anchor the paranodal junction to the axon's cytoskeleton. The  $\text{Nav}1.6$  channels are segregated to the node of Ranvier, where they are anchored in place by neurofascin 186, NrCAM and ankyrin G.  $\text{Kv}1.2$  channels are located in the juxtaparanode. A full, detailed description of the structure of the node of Ranvier, paranode and juxtaparanode is provided by Salzer, 2003. This architecture, illustrated in figure 1.5, separates the two populations of ion channels and concentrates depolarisation and repolarisation of the axon into a smaller area, allowing for quicker action potential generation and propagation.

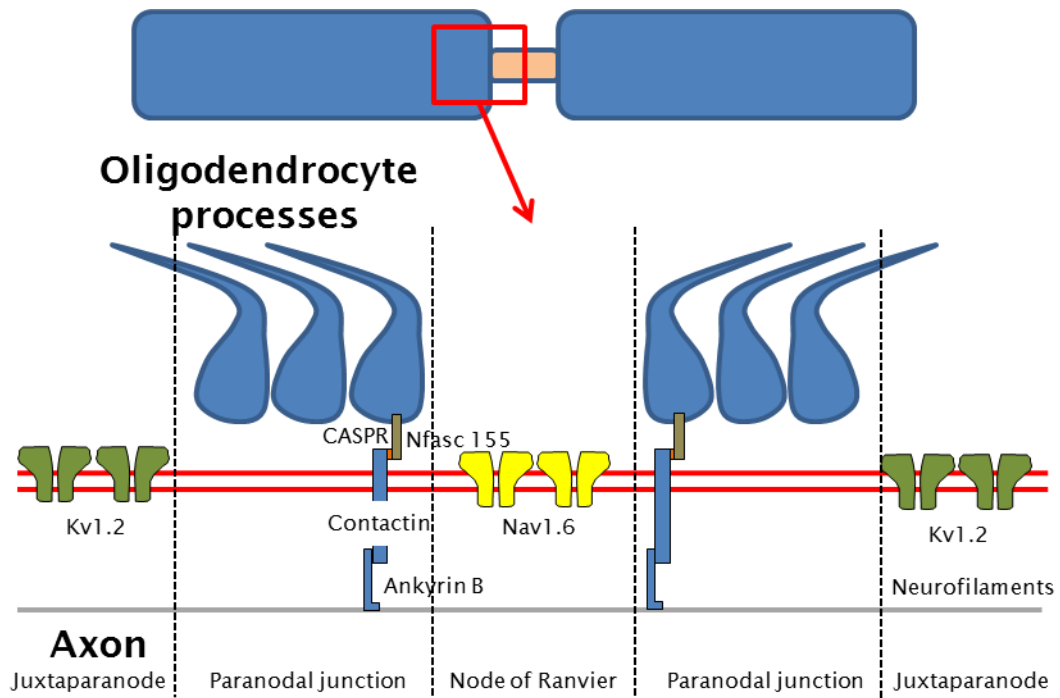


**Figure 1.5. A simplified diagram showing some of the key components of the node of ranvier, the paranodal junction and the juxtaparanode and how they are organised in a healthy axon.**

The paranodal junction is formed of the three proteins Nfasc155, contactin and caspr, which segregate Nav1.6 channels in the node of ranvier from Kv1.2 channels in the juxtaparanode.

The consequences of paranodal junction disruption are well characterised through mutant models. In mouse knock out models of either Nfasc155, contactin or caspr the mice develop ataxia, tremor, reduced conduction velocity of white matter tracts, axonal transport deficits and, in the case of Nfasc155 knockouts, sudden early death (Bhat et al., 2001; Boyle et al., 2001; Sherman et al., 2005). On a molecular level Kv1.2 channels are no longer strictly segregated to the juxtaparanodal region in these knockouts, but instead mislocalise to the paranodal and nodal region, as illustrated in figure 1.6. Detachment of paranodal loops also occurs in these knockout models, demonstrating the importance of these proteins in maintaining nodal architecture.

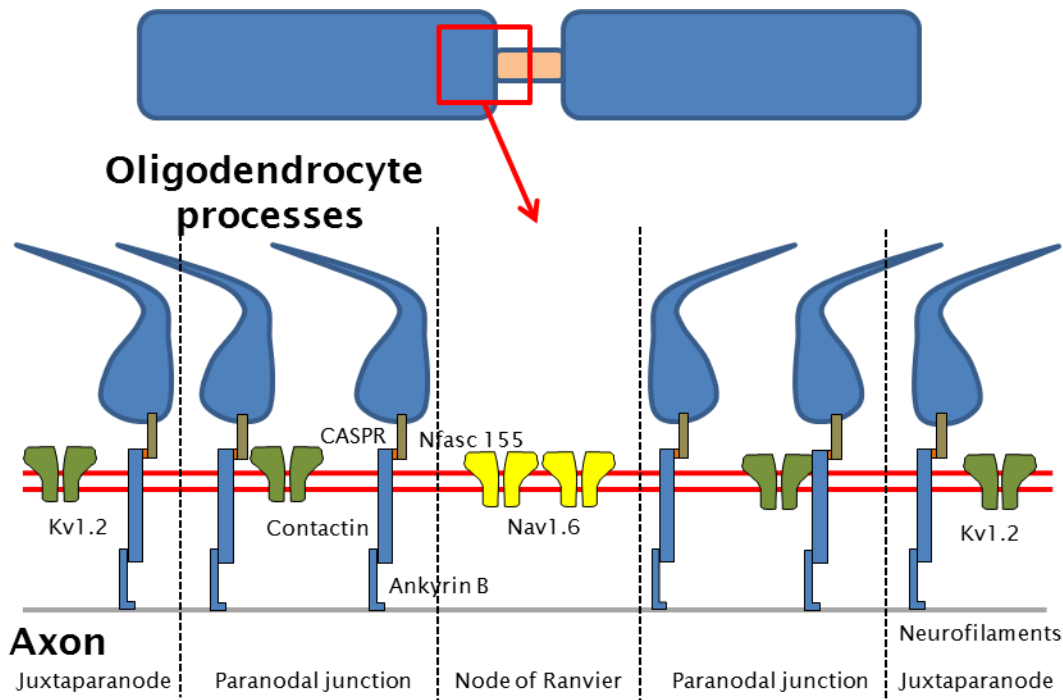


**Figure 1.6. A modified version of figure 1.5 demonstrating how a “disrupted” paranode may be organised.**

Kv1.2 channels are no longer segregated to the juxtaparanodal regions, but are now also present in the paranodal regions.

### 1.1.5 Immune to brain communication

Immune brain communication is a critical component of a host organism’s response to infection or peripheral inflammation. A collection of behavioural and metabolic adaptations are initiated over the course of an infection with the purpose of restricting the spread of a pathogen within an organism, optimising conditions for a successful immune response and preventing the spread of infection to other organisms (Hart, 1988). Collectively these behaviours have been termed “sickness behaviours”. Some of the more common sickness behaviours induced in infection include depression, reduced appetite, anhedonia, social withdrawal, reduced locomotor activity, hyperalgesia, reduced motivation, cognitive impairment and impairments in memory encoding and recall (Dantzer, 2004). Metabolic adaptations to infection include fever, altered dietary intake and reductions in the bioavailability of nutrients that may facilitate the growth of pathogens such as iron or zinc (Hart, 1988). These behavioural and metabolic adaptations also occur in humans (Bucks et al., 2008; Smith, 2012; Smith, 2013).

Exactly how the immune system initiates and maintains these behaviours depends on the locality, type and severity of inflammatory stimulus. The three principle routes of immune brain communication are described below.

#### **1.1.5.1 Immune to brain communication via the vagus nerve**

The vagus nerve is a cranial nerve that predominately innervates the viscera and blood vessels of the thorax and abdomen. Vagal afferent fibres innervate the liver, lungs, heart, aorta, gastrointestinal tract and numerous other organs and project to the nucleus of the solitary tract (NTS), area postrema (AP) (together known as the dorsal vagal complex (DVC)) and the dorsal motor nucleus of the vagus (Berthoud and Neuhuber, 2000). Neurons project from these regions to a wide range of areas including medullary motor nuclei such as the vagal dorsal motor nucleus and nucleus ambiguus, to the dorsolateral pons (including the locus coeruleus), and to forebrain regions including the hypothalamus, bed nucleus of the stria terminalis (BST) and the amygdala (Berthoud and Neuhuber, 2000). These vagal afferents are sensory neurons, containing (depending on the area innervated) baroreceptors, mechanoreceptors, osmoreceptors, chemoreceptors and thermoreceptors (Berthoud and Neuhuber, 2000). They can also detect local inflammation through expression of IL-1, TNF $\alpha$  and prostaglandin receptors on the paraganglia and ganglia (Ek et al., 1998; Goehler et al., 1997; Rogers and Hermann, 2012). The vagus nerve also contains efferent fibres which project from the dorsal motor nucleus of the vagus (Berthoud and Neuhuber, 2000). These fibres modulate local immune responses via the cholinergic anti-inflammatory pathway (Borovikova et al., 2000) and motor functions such as gut motility (Chang et al., 2003).

Several studies have attempted to identify the precise role of the vagus nerve in immune brain communication using subdiaphragmic vagotomy followed by intraperitoneal (i.p.) injection of LPS or pro-inflammatory cytokines. Two studies in mice showed a lack of influence of vagotomy on sickness behaviour (burrowing, locomotor activity, sweetened milk intake) in mice following i.p. injection of 100 $\mu$ g/kg or 1 $\mu$ g/mouse LPS (Teeling et al., 2007; Wiczorek et al., 2005), whereas in contrast other authors demonstrated the necessity of the vagus nerve for social interaction deficits following an intraperitoneal injection of either 250 $\mu$ g/kg LPS or 25 $\mu$ g IL-1 $\beta$  (Konsman et al., 2000a) in rats, induction

of fever by i.p. injection of low levels of human IL-1 $\beta$  (1  $\mu$ g/kg) in rats (Watkins et al., 1995), conditioned taste aversion in rats following i.p. injection of human IL-1 $\beta$  or TNF $\alpha$  (Goehler et al., 1995) and food seeking behaviour in mice following i.p. injection of 400  $\mu$ g/kg of LPS or 1.5  $\mu$ g of human IL-1 $\beta$  (Bretz et al., 1995). At higher doses of rat IL-1 $\beta$  (25  $\mu$ g/rat, injected i.p.) subdiaphragmatic vagotomy did not attenuate fever (Konsman et al., 2000a), demonstrating that the importance of vagal signalling may depend on the degree of inflammation present.

Some studies have inactivated or lesioned the dorsal vagal complex instead of performing subdiaphragmatic vagotomy to block vagal signalling. The caveat of this approach is that it also prevents one of the circumventricular organs, the area postrema (AP), from signalling in response to circulating inflammatory mediators, presenting a confounding factor when trying to attribute specific immune responses to vagus nerve mediated signalling. However, this approach still retains some value when investigating BBB independent routes of immune to brain communication. Inactivation of the dorsal vagal complex with bupivacaine blocked social withdrawal (Marvel et al., 2004) and LPS-induced reductions in locomotor activity (Gaykema and Goehler, 2011) in response to an i.p. injection of 100  $\mu$ g/kg LPS and prevented c-fos activation of several forebrain regions including the amygdala, bed nucleus of the stria terminalis and periventricular nucleus of the hypothalamus (Marvel et al., 2004).

These studies together demonstrate that vagal signalling contributes to some aspects of sickness behaviour, such as social withdrawal or fever, but not to other aspects such as reduced sweetened milk intake (a measure of anhedonia) or locomotor activity. Some of these effects may be mediated through activation of the hypothalamic-pituitary-adrenal axis (Wieczorek et al., 2005), particularly the metabolic effects, while projections to forebrain structures such as the amygdala likely mediate many of the vagus dependent behavioural effects (Gaykema et al., 2007b). Hansen et al showed that vagotomy did not influence brain levels of IL-1 $\beta$  in response to i.p. 10-100  $\mu$ g/kg LPS (Hansen et al., 2000b), suggesting that the effects of vagal afferent stimulation are not mediated by induction of IL-1 $\beta$  synthesis within the CNS.

### **1.1.5.2 Circumventricular organs**

The sensory circumventricular organs (CVOs) are areas of the brain which are highly vascularised and not fully protected by the BBB (Fry and Ferguson, 2007), allowing exposure of neurons to blood components and circulating inflammatory mediators such as cytokines. These areas include the AP, subfornical organ and organum vasculosum of lamina terminalis (OVLT) (Fry and Ferguson, 2007). A tanycytic barrier limits diffusion of small molecular weight tracers such as Evans blue and prevents diffusion of larger molecular weight tracers such as horse radish peroxidase and 70kDa dextran beads from the CVOs into neighbouring CNS parenchyma (Morita and Miyata, 2012; Peruzzo et al., 2000), demonstrating the presence of an effective barrier against diffusion of complex molecules such as cytokines. The CVOs have been shown using c-fos staining shown to be activated following systemic LPS (Gaykema et al., 2007a) and are known to project to the amygdala, hypothalamus and hippocampus (Quan, 2008), converging with central vagal pathways at some points (Gaykema et al., 2007b). Cells in these regions have been shown to express high levels of a variety of receptors for immune mediators including TLR4 and CD14 (Laflamme and Rivest, 2001), IL-1 receptor (Ericsson et al., 1995) and prostaglandin E (EP) receptors (Ek et al., 2000; Zhang and Rivest, 1999). The precise role of CVOs in sickness behaviour are not well defined, but ablation of the AP has been shown to attenuate HPA axis activation following an i.v. injection of LPS (Lee et al., 1998), and inhibition of inflammation in the OVLT before i.v. injection of LPS attenuated fever (Lin and Lin, 1996). CVO activation may contribute to other cytokine behaviours via its projections to other brain regions that are important in sickness behaviour e.g. the amygdala, but this has not been investigated in detail to date.

### **1.1.5.3 De novo production of inflammatory mediators within the CNS**

Systemic inflammation results in production of IL-1 $\beta$ , IL-6, TNF $\alpha$  and PGE<sub>2</sub> within the CNS (Lacroix and Rivest, 1998; Teeling et al., 2010). Glia and neurons throughout the brain express receptors for these inflammatory mediators (Bette et al., 2003; Frost et al., 2001; Nakamura et al., 2000; Oka et al., 2000; Vallieres and Rivest, 1997) with neuronal expression of these receptors more pronounced in brain areas thought to play roles in sickness behaviour such as the hippocampus, hypothalamus, circumventricular organs,

NTS and the amygdala (Bette et al., 2003; Ek et al., 2000; Ericsson et al., 1995; Vallieres and Rivest, 1997).

This increased production of inflammatory mediators in the brain is initiated at the blood brain barrier by circulating cytokines and ligands for pathogen recognition receptors (PRRs) such as LPS, which act on TLRs and cytokine receptors expressed on endothelial cells and perivascular macrophages to initiate de novo synthesis of inflammatory mediators such as IL-1 $\beta$  and PGE<sub>2</sub> (Laflamme and Rivest, 2001; Laflamme et al., 2001; Serrats et al., 2010; Skelly et al., 2013). These inflammatory mediators diffuse through the parenchyma to activate cells such as microglia and astrocytes (Konsman et al., 2000b), which themselves contribute to the inflammatory milieu produced in the CNS following systemic inflammation (Henry et al., 2009). The induction of this inflammatory response at the BBB and subsequent behavioural responses can be achieved by a variety of peripheral inflammatory mediators. Abrogation of peripheral IL-6, TNF $\alpha$  and IL-1 $\beta$  either separately or simultaneously with blocking antibodies has been shown to only partially attenuate sickness behaviours and not to affect central cytokine production in response to i.p. LPS injection (Swiergiel and Dunn, 1999; Teeling et al., 2007), suggesting that LPS can directly activate brain endothelium to mediate some behavioural effects. Some sickness behaviour e.g. anhedonia (measured by sweetened milk intake) was however attenuated by simultaneous blocking of IL-1 $\beta$ , TNF $\alpha$  and IL-6 before i.p. LPS injection (Swiergiel and Dunn, 1999). Intraperitoneal injection of mouse IL-1 $\beta$  (50 $\mu$ g/kg) or TNF $\alpha$  (250 $\mu$ g/kg) individually can induce changes in open field activity, body temperature, central production of IL-1 $\beta$  and TNF $\alpha$  and endothelial COX-2 production in a dose dependent manner (Skelly et al., 2013), demonstrating that in the absence of circulating LPS these cytokines are capable of inducing central cytokine responses and sickness behaviour, with the possible exception of IL-6. Engagement of other PRRs on endothelial cells such as TLR3 by polyinosinic:polycytidylic acid (poly I:C) can also induce central cytokine production and behavioural changes (Cunningham et al., 2007b).

One of the cytokines produced in the CNS following a peripheral LPS challenge is IL-1 $\beta$  (Godbout et al., 2005b), which is produced by endothelial cells/perivascular macrophages and microglial cells (Cunningham et al., 2005; Henry et al., 2009) and has been suggested to play a role in potentiating the

central cytokine response to LPS (Laye et al., 2000). Expression of IL-1 $\beta$  within the CNS is involved in the control of multiple sickness behaviours, including social interaction (Kent et al., 1992) (Bluthe et al., 2000a), depressive behaviour (Kent et al., 1992), anxiety (Connor et al., 1998), fever (Luheshi et al., 1997), anorexia (Laye et al., 2000) food seeking behaviour (Kent et al., 1992; Pecchi et al., 2006) and locomotor activity (Bluthe et al., 2000a). Some of these roles may be exerted through downstream induction of PGE<sub>2</sub> synthesis within the CNS (Hein et al., 2007; Pecchi et al., 2006).

PGE<sub>2</sub> is one of the key mediators of immune to brain communication across the BBB. PGE<sub>2</sub> is produced by PGE synthase from PGH<sub>2</sub>, which is produced from arachadonic acid by COX-1 (the constitutively active isoenzyme) and COX-2 (the inducible isoenzyme) (Hopkins, 2007). Both COX-1 and COX-2 have been proposed to have important roles in mediating sickness behaviour and fever. COX-2 is strongly induced in the cerebral microvasculature after peripheral immune challenge (Serrats et al., 2010; Skelly et al., 2013). COX-1 mRNA on the other hand is not upregulated by peripheral immune challenge, but inhibition using COX-1 specific inhibitors such as piroxicam has suggested that it has a role in mediating early response behavioural responses to systemic inflammation (Swiergiel and Dunn, 2002; Teeling et al., 2010).

Non-specific systemic COX inhibition using indomethacin has been shown to prevent LPS induced fever, burrowing deficits (Teeling et al., 2007) (a species typical murine spontaneous behaviour (Deacon et al., 2002)) and social interaction deficits (Bluthe et al., 1992), although the relative contribution of peripheral (i.e. vagal) and central prostaglandin signalling is not distinguishable in these studies. Intracerebroventricular injection of PGE<sub>2</sub> reduces performance in tests of memory function (Hein et al., 2007), and microsomal PGE synthase-1, an enzyme downstream of COX-2 involved in PGE<sub>2</sub> production, has been shown to be necessary for the induction of anorexia by i.p. injection of IL-1 $\beta$  (Pecchi et al., 2006) or fever by i.p. injection of LPS (Engblom et al., 2003). EP3 receptor knockout mice, but not EP1, 2 or 4 receptor knock outs, do not develop fever in response to i.c.v. injection of PGE<sub>2</sub> (Ushikubi et al., 1998), suggesting that central PGE<sub>2</sub> signalling via EP3 receptors is sufficient to evoke fever. Together these data suggest a role for central PGE<sub>2</sub> in anorexia, fever and some behavioural changes e.g. impaired memory function, reduced burrowing activity and social interaction deficits.

Central TNF $\alpha$  is also capable of mediating some sickness behaviours such as depressive behaviour, food intake and locomotor activity (Bluthe et al., 2000a), anxiety (Connor et al., 1998) with some redundancy between IL-1 $\beta$  and TNF $\alpha$  in their behavioural effects having been suggested (Bluthe et al., 2000a). Central IL-6 expression has been shown to have a role in fever and activation of the HPA axis (Harden et al., 2008; Lenczowski et al., 1999), but does not appear to play a direct role in inducing sickness behaviour (Connor et al., 1998; Lenczowski et al., 1999), although it does potentiate responses to IL-1 $\beta$  (Lenczowski et al., 1999) or LPS (Bluthe et al., 2000b).

Some of the depressive components of sickness behaviour are mediated by indoleamine 2,3-dioxygenase activity (IDO 2,3). IDO 2,3 is an enzyme that degrades tryptophan, which is a precursor for the neurotransmitter serotonin. IDO 2,3 activation is thought to exert depressive effects either through restricting the precursors for serotonin production (Moreau et al., 2005) or through the metabolites produced from tryptophan breakdown such as quinolic acid, which is neurotoxic and an NDMA receptor agonist (Stone, 1993), or L-kynurenine, which when injected intraperitoneally induced depressive behaviour in mice in a dose dependent manner (O'Connor et al., 2009d). Inhibition of IDO 2,3 has been shown to abrogate depressive like behaviour in acute (O'Connor et al., 2009d), and chronic inflammation (O'Connor et al., 2009c). IDO 2,3 can be induced by IFN $\gamma$  and TNF $\alpha$  (O'Connor et al., 2009a) and possibly by type 1 interferons (Capuron et al., 2003; Jansen and Reinhard, 1999).

Type 1 interferons are a separate class of immune mediators that also play a role in immune to brain communication. The best known members of the type 1 interferon family are interferon alpha and beta. Peripheral administration of interferon alpha in treatment of diseases such as cancer has been associated with depression and "flu like symptoms" in humans (Loftis and Hauser, 2004). These depressive symptoms may be mediated by changes in tryptophan/kynurenine metabolism (Capuron et al., 2003; Jansen and Reinhard, 1999), possibly mediated by IDO 2,3. Interferon alpha and beta expression in the CNS can be induced by activation of TLR3 by i.p. injection of poly I:C (Cunningham et al., 2007b) or for interferon beta via i.p. LPS injection, but not by circulating cytokines such as IL-1 $\beta$  (Skelly et al., 2013).

Pharmacological studies have suggested that opioid receptors play an

important role in mediating interferon alpha induced depressive behaviour (Makino et al., 2000).

#### **1.1.5.4 An integrated view of sickness behaviour and its application to real infections**

The different routes of immune to brain communication described here are often studied in isolation from one another, but systemic inflammation has been shown to signal to the brain via all three of the routes described above. The CNS response to peripheral inflammation integrates inputs from these different pathways, with certain pathways being more salient depending on the type, locality and severity of the inflammation. Much of the research described above has used sterile mimetics of infection e.g. LPS to investigate sickness behaviour, but this does not fully recapitulate the nature of a systemic infection. Inflammatory reactions during infection usually have longer kinetics than those induced by sterile mimetics and may engage a variety of different PRRs rather than only one or two. The site of infection is often also limited to a few particular sites in the body, such as the upper respiratory tract or the GI tract, and therefore PRRs on the brain endothelium may not be exposed to ligands such as LPS for much of the infection period. In contrast, i.p. injection of 10µg/kg or more of LPS leads to detectable levels of LPS in serum (Hansen et al., 2000a) and therefore direct binding of LPS to TLRs on brain endothelium, which is sufficient to induce transcription of several inflammatory molecules within the brain (Chakravarty and Herkenham, 2005). LPS can be found in circulation in the initial, but not the later stages of *S. typhimurium* infection induced by i.p. injection (Püntener et al., 2012) and therefore LPS injection can be considered to only model the early part of these infections.

The literature on the immune to brain communication of live infections is limited, as most authors prefer to work with sterile models of inflammation, presumably due to their relative ease and safety of use and increased reproducibility. The principle models of live infection that have been used to investigate immune to brain communication in the literature to date are *Mycobacterium bovis* strain Bacillus Calmette-Guérin (BCG), *E. Coli*, *Campylobacter jejuni* and influenza.

BCG (an attenuated strain of *Mycobacterium bovis*) is a mycobacterium that is used in humans as a vaccine against tuberculosis, which is caused by the

closely related *Mycobacterium tuberculosis* (McMurray, 1996). Intraperitoneal injection of BCG causes an acute (<48h) reduction in body weight and open field locomotor and rearing activity and an elevation in core body temperature that lasted 5 days (Moreau et al., 2008). Longer lasting effects in measures of depressive behaviour (the forced swim test, sucrose consumption and the tail suspension test) were observed up to 21 days after infection (Moreau et al., 2008). The depressive symptoms observed in BCG infection are mediated by induction of IDO 2,3 (O'Connor et al., 2009c), probably via induction of peripheral IFN $\gamma$  and TNF $\alpha$  (O'Connor et al., 2009b), and the subsequent activity of IDO 2,3 metabolites in the CNS (O'Connor, Lawson et al. 2009).

*E. coli* is a bacteria that in humans usually infects the lower GI tract and is a common cause of enteritis (Evans and Evans, 1996). The infection of rats with live *E. coli* (Campisi et al., 2003) leads to acutely detectable levels of LPS in circulation, as well as elevation of serum IL-1 $\beta$ , TNF $\alpha$  and IL-6 levels (Campisi et al., 2003) and PGE $_2$  (Tian and Baracos, 1989). Rats infected with *E. coli* exhibit an acute increase in core body temperature, and reduced open field activity (Barrientos et al., 2009b). *E. coli* infection also leads to impaired memory function in aged rats (Barrientos et al., 2006), but not young rats, which the authors propose is mediated by increases in hippocampal IL-1 $\beta$  levels and reduced brain derived neurotrophic factor (BDNF) expression (Barrientos et al., 2009a; Cortese et al., 2011).

*Campylobacter jejuni* localises to the GI tract and causes gastroenteritis (Perez-Perez and Blaser, 1996) and has been used to investigate infection induced sickness behaviour. *Campylobacter jejuni* infection acutely increases anxiety behaviour in the holeboard test (Goehler et al., 2008), and Goehler et al suggested that the activation of pathways associated with vagal afferent signalling are responsible for these behavioural changes. A role for the vagus nerve in mediating *Campylobacter jejuni* induced anxiety is supported by c-fos activation of vagal ganglia, the NTS and several forebrain areas in the absence of elevated circulating cytokine levels (Goehler et al., 2005). Similar results were obtained by Lyte et al when using *Citrobacter rodentium*, an animal model of inflammatory bowel disease (Lyte et al., 2006).

Influenza is a virus that infects the upper respiratory tract of hosts (Dasaraju and Liu, 1996). Infection with influenza leads to pronounced weight loss

accompanied by anorexia, decreased sweetened milk take, which is indicative of decreased fluid intake and/or anhedonia, decreased open field locomotor and rearing activity, and impaired reversal in the Morris water maze, which is indicative of impaired hippocampus dependent learning (Jurgens et al., 2012; Swiergiel and Dunn, 1999; Swiergiel et al., 1997). Simultaneous abrogation of IL-1 $\beta$ , IL-6 and TNF $\alpha$  only slightly attenuated the effects of influenza on weight loss and sweetened milk intake, suggesting that influenza elicits immune to brain communication through an alternative route, possibly through increased levels of circulating interferons or through vagally mediated immune to brain communication. There is a neuroinflammatory reaction during influenza infection, with an 1.5-3 fold increase in expression of IL-1 $\beta$ , IL-6, TNF $\alpha$  and IFN- $\alpha$  in the hippocampus 7 days after infection (Jurgens et al., 2012), accompanied by a decreased in expression of neurotrophins and immunoregulatory molecules such as BDNF and CD200. It should be noted however that this dose of influenza did cause a very large decrease in body weight (30%) which led to the authors of this study culling the mice after 7 days of infection (Jurgens et al., 2012).

#### **1.1.5.5 Summary**

Immune to brain communication operates on multiple levels through different pathways to alter the behavioural and metabolic state of an organism. The relative contribution of these pathways depends on the type of immune challenge faced by the organism and the phase of the immune challenge. During the course of most real infections it is likely that all these immune to brain communication routes play a role, either simultaneously or individually at different points during the disease. The differences between the acute phase of infection modelled by bacterial or viral mimetics are marked compared to live infection, where sickness behaviour is experienced over a more prolonged period of time and is often of a more subtle nature. A summary of the principle components of immune to brain communication is provided in figure 1.7.

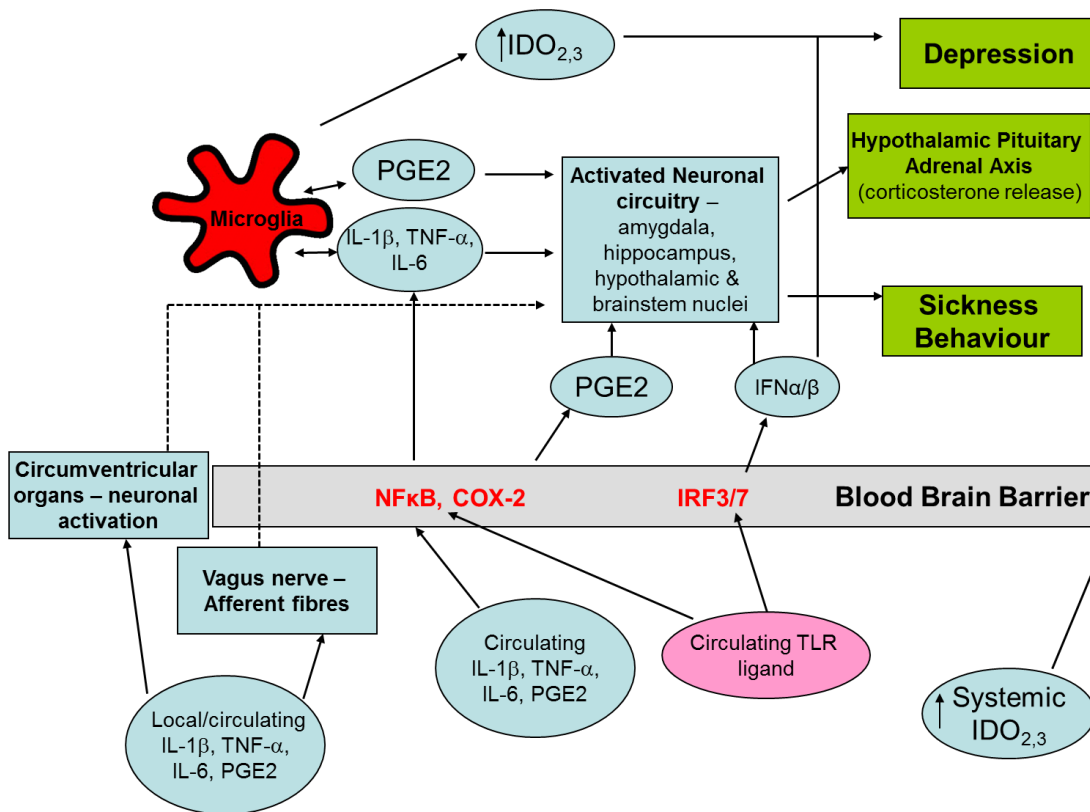


**Figure 1.7. The main pathways of immune brain communication.**

The red text represents activated transcription factors and enzymes in cells at the BBB. The green boxes represent the end products of immune brain communication.

## 1.2 Microglia

Microglia are myeloid-derived cells originating from the yolk sac that populate the CNS during early development (Ginhoux et al., 2010). Recent work has established that in the adult mouse microglia are renewed by local proliferation within the CNS and are not replenished by myeloid cells from outside the CNS, even in the presence of CNS pathology (Ajami et al., 2007; Mildner et al., 2007), although peripheral macrophages are recruited to the CNS parenchyma in a transgenic mouse model of Alzheimer's disease (AD) probably due to the well characterised vascular pathology associated with increased amyloid beta levels in AD (Mildner et al., 2011). Lawson and Perry's study in 1992 demonstrated that over 24h only 0.19% of F4/80 expressing cells with resident microglial morphology in the adult mouse brain had undergone proliferation, suggesting that adult murine microglia are long lived cells, perhaps only

proliferating 1-2 times across a murine lifespan (Lawson et al., 1992). It remains unknown if macrophage recruitment from the periphery is altered in the ageing brain.

The shared origins of microglia and macrophages means that, especially upon activation of microglia, the two cell types can be very hard to distinguish – macrophages can adopt a microglia-like morphology after infiltration of the CNS (Ajami et al., 2007) and microglia when activated can morphologically resemble macrophages (Karperien et al., 2013). On a molecular basis the two cell types can be almost impossible to separate if exposed to the same environment and stimuli (Guillemin and Brew, 2004).

### **1.2.1 Resting microglia**

The CNS environment promotes a unique phenotype in resident myeloid cells of the healthy CNS that has been termed “resting” or “surveillant” microglia. In the absence of inflammatory stimuli microglia constantly monitor their environment (Wake et al., 2009), performing a range of housekeeping functions within the CNS, for example phagocytosis of apoptotic cells, promoting repair of localised disruption to the BBB (Nimmerjahn et al., 2005) and providing trophic support for neurons and glial cells (Kettenmann et al., 2011). The study by Wake et al. (2009) showed regular transient contacts between microglia and synapses, suggesting a role in checking the health and activity of synapses. This hypothesis is supported by the presence of neurotransmitter receptors on microglia (Pocock and Kettenmann, 2007). The processes of resting microglia are highly motile, but the cell body remains static under resting conditions, suggesting that each microglia has a geographically restricted domain that it resides in (Davalos et al., 2005). Basal release of cytokines such as IL-1 $\beta$  and TNF $\alpha$  also plays a role in supporting neuronal plasticity and learning (del Rey et al., 2013; Yirmiya et al., 2002).

A variety of stimuli can activate these cells – it is important however to specify that the term ‘activated’ microglia, often defined by morphological characteristics, encompasses a diverse and impressively plastic range of phenotypes, from an anti-inflammatory, regulatory state to the classically activated pro-inflammatory microglia. These differing states of activation can influence the cells reaction to different stimuli e.g. LPS and influence how

active/efficient the cell is in performing functions such as phagocytosis. Identifying if there is a shift towards a certain phenotype in the aged or diseased brain would subsequently give greater understanding of how one may expect microglia to behave. The principle states are outlined below. Some of the characteristics outlined below regarding alternative activation states have been described in peripheral macrophages rather than microglia; as discussed previously they share a number of common features, particularly upon stimulation. Hence studying peripheral macrophages can inform our ideas about how microglia might behave.

### **1.2.2 Pro-inflammatory activation of microglia**

Exposure to IL-1 $\beta$ /TNF $\alpha$  or TLR activating pathogen-associated molecular patterns (PAMPs) such as LPS and some danger-associated molecular patterns (DAMPs) induces an activated, pro-inflammatory phenotype in microglia. In vitro studies have shown that microglia can respond to a variety of pro-inflammatory stimuli such as LPS challenge, pro-inflammatory cytokines (e.g. IL-1 $\beta$ ) or DAMPs such as amyloid beta by increasing production of some or all of IL-6, IL-1 $\beta$ , IL-12, TNF $\alpha$ , PGE<sub>2</sub>, reactive oxygen and nitrogen species and interferons (Henry et al., 2008; Li et al., 2007; Neher et al., 2011; Wang et al., 2004). Production of these molecules is mostly transduced through branches of the MAPK and NF- $\kappa$ B signalling pathways (Koistinaho and Koistinaho, 2002).

In vivo, one would not expect direct contact between LPS and TLR4 within the parenchyma of the CNS due to the presence of the BBB; activation of TLR4 via DAMPs however is a plausible scenario, especially in the aged or diseased brain where cell damage and misfolded proteins are more likely to be present.

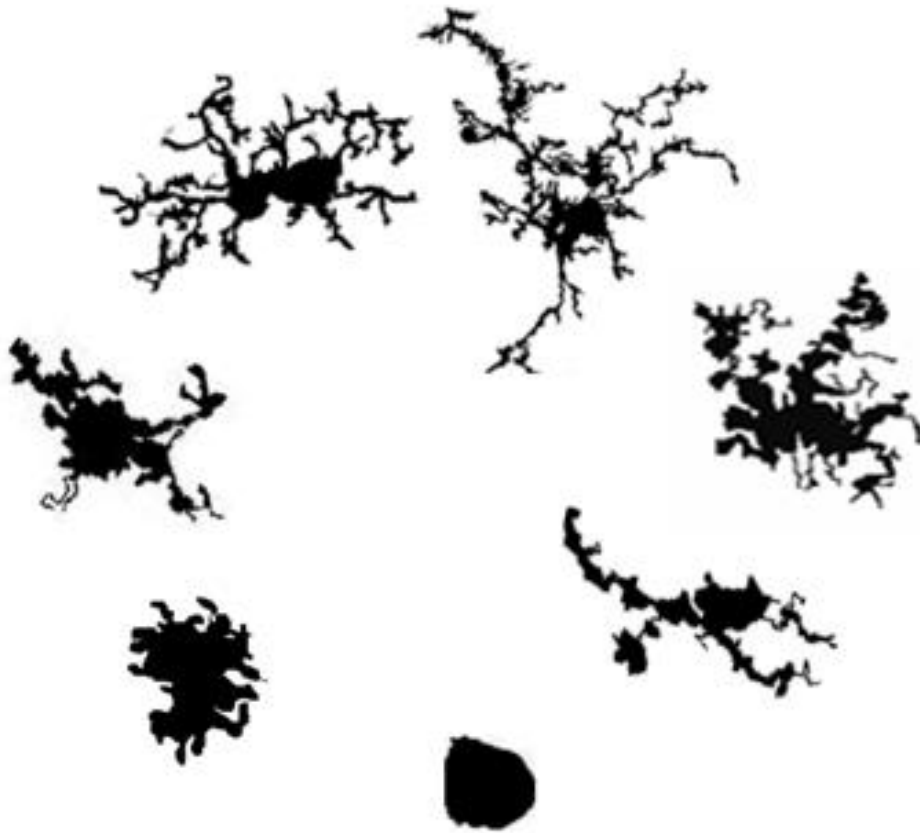
Microglia are also activated during systemic inflammation by the inflammatory mediators produced at the BBB. Peripheral immune challenges cause microglia to increase mRNA levels of pro-inflammatory molecules such as TNF $\alpha$ , IDO 2,3, IL-1 $\beta$  and iNOS (Corona et al., 2010; Wohleb et al., 2012) and expression of activation markers such as CD11b and MHC II (Corona et al., 2010; Henry et al., 2009; Laflamme et al., 2001).

Activation of microglia by pro-inflammatory molecules is often accompanied by morphological changes in the microglia as they adopt a more amoeboid shape,

defined by deramified processes and hypertrophy of the cell body (Karperien et al., 2013; Qin et al., 2007), as illustrated in figure 1.8.

Pro-inflammatory activation of microglia can be neurotoxic, either directly through release of ROS, NO and peroxynitrate or via chemokine secretion to recruit further cells to the site of injury or into the wider CNS from the periphery (Ambrosini and Aloisi, 2004; Arimoto and Bing, 2003; Gibbons and Draganow, 2006; Neher et al., 2011). Exposure of neurons to lower levels of peroxynitrate (5 $\mu$ M) or ROS (25 $\mu$ M H<sub>2</sub>O<sub>2</sub>) leads to the reversible exposure of phosphatidylserine on the outer membrane, the “eat me” signal of phagocytosis, and subsequent phagocytosis of the neuron, without the neuron committing to apoptosis (Neher et al., 2011). Higher doses of peroxynitrate (10, 20 $\mu$ M) lead directly to increases in apoptosis or necrosis of neurons (Neher et al., 2011).

## RAMIFIED



## UNRAMIFIED/AMOEBOID/ACTIVATED

**Figure 1.8. Morphological activation of microglial cells.**

Resting or “surveying” microglia are highly ramified, with extensive primary, secondary and tertiary branching from the soma. Microglia can change in morphology when activated, where they become progressively less ramified until eventually becoming fully amoeboid, resembling peripheral macrophages. Image taken from Karperien et al. (2013).

Heterogeneity of the innate immune response is mediated by the wide diversity of PAMP and DAMP sensing pathways expressed in the peripheral immune system and on microglia. Toll like receptors are an important family of PRRs that recognise a variety of different ligands in conjunction with their cognate co-receptors. Table 1.2 summarises the characteristics of the different TLRs.

TLR	Location of TLR	PAMPs recognized by TLR	Signalling adaptor	Transcription factor(s)
TLR1/2	Plasma membrane (cell surface)	Triacyl lipopeptides (Bacteria and Mycobacteria)	TIRAP, MyD88	NFκB
TLR2	Plasma membrane (cell surface)	Peptidoglycan (Gram-positive bacteria), LAM (Mycobacteria), Hemagglutinin (Measles virus), phospholipomannan ( <i>Candida</i> ), Glycosylphosphatidylinositol mucin ( <i>Trypanosoma</i> )	TIRAP, MyD88	NFκB
TLR3	Endosome	ssRNA virus (WNV), dsRNA virus (Reovirus), RSV, MCMV	TRIF	NFκB, IRF3,7
TLR4	Plasma membrane (cell surface)	LPS (Gram-negative bacteria), Mannan ( <i>Candida</i> ), Glycoinositolphospholipids ( <i>Trypanosoma</i> ), Envelope proteins (RSV and MMTV)	TIRAP, MyD88, TRAM and TRIF	NFκB, IRF3,7
TLR5	Plasma membrane (cell surface)	Flagellin (Flagellated bacteria)	MyD88	NFκB
TLR6/2	Plasma membrane (cell surface)	Diacyl lipopeptides (Mycoplasma), LTA (Streptococcus), Zymosan ( <i>Saccharomyces</i> )	TIRAP, MyD88	NFκB

TLR7	Endosome	ssRNA viruses (VSV, Influenza virus)	MyD88	NFκB, IRF7
TLR8	Endosome	ssRNA from RNA virus	MyD88	NFκB, IRF7
TLR9	Endosome	dsDNA viruses (HSV, MCMV), CpG motifs from bacteria and viruses, Hemozoin (Plasmodium)	MyD88	NFκB, IRF7
TLR1 1	Plasma membrane (cell surface)	Uropathogenic bacteria, profillin-like molecule ( <i>Toxoplasma gondii</i> )	MyD88	NFκB

**Table 1.2. The TLR family of receptors and their ligands and functions.**

This table is adapted from Kumar et al. (2009b).

Inflammatory stimuli can act at more than one receptor during an immune reaction. A gram-negative bacteria endowed with flagella will for instance activate both TLR4 and TLR5. Examples of DAMP activation of TLRs include heat shock protein 60 (TLR4) (Ohashi et al., 2000), the blood component fibrinogen (TLR4) (Smiley et al., 2001) and amyloid beta (TLR2, 4 and 6) (Reed-Geaghan et al., 2009; Stewart et al., 2010). DAMPs can also activate cells via RAGE receptors, which are discussed further in section 1.5.1.5. Although all TLR populations signal via branches of the MAPK and NF-κB signalling pathways, TLRs 3, 4, 7, 8 and 9 also signal via IRF3 and IRF7 to induce type 1 interferon signalling (Kumar et al., 2009b).

Examples of other receptors capable of inducing pro-inflammatory macrophage/microglial activation include C-type lectins (Geijtenbeek and Gringhuis, 2009), the Rig-I like receptor family (RLRs) and Nucleotide-binding domain and Leucine-Rich repeat containing proteins (NLRs) (Kumar et al., 2009a). Pro-inflammatory cytokines such as TNFα and IL-1β can also evoke pro-inflammatory activation of microglia by activation of NFκB and MAPK pathways via IRAK-2 or TRAF2 mediated pathways, leading to production of pro-inflammatory cytokines such as IL-1β and morphological changes in microglia (Hinkerohe et al., 2005; Janssens and Beyaert, 2003; Wajant and Scheurich,

2011). Intracellular ROS can also contribute to enhanced iNOS activity and cytokine release (Pawate et al., 2004; Qin et al., 2004).

### 1.2.3 Alternative activation of microglia

Microglia and macrophages exhibit a range of phenotypes beyond simply “resting” and “activated”. Regulatory macrophages are proposed to be induced by cells undergoing apoptosis, immune complexes (when cell is co-stimulated with other ligands e.g. LPS) (Edwards et al., 2006; Gerber and Mosser, 2001) and the cytokines IL-10 and TGF- $\beta$ . Characteristics of this macrophage population include enhanced production of IL-10 and TGF- $\beta$ , while the pro-inflammatory cytokine response to LPS is attenuated, as demonstrated by reduced IL-12, IL-1 $\beta$  and TNF $\alpha$  production (Edwards et al., 2006; Fadok et al., 1998; Gerber and Mosser, 2001; Voll et al., 1997). A population of regulatory macrophages may therefore be expected in areas of damaged, diseased or degenerating tissue where apoptosis and/or antibody opsonised tissue may be present.

Elevated TGF- $\beta$  levels have been reported in the CNS of a murine prion model, reduction of which led to widespread neuronal apoptosis, suggesting a protective role for TGF- $\beta$  and a role in maintaining a neuroprotective regulatory microglial phenotype (Boche et al., 2006). Work in an optic nerve crush model showed elevated TGF- $\beta$  levels 3 days after crush and increased scavenger receptor expression, indicating an injury dependent induction of TGF- $\beta$  (Palin et al., 2008), which presumably polarises microglia to a more regulatory phenotype.

Interestingly, LPS induced greater levels of pro-inflammatory cytokine in animals that had undergone optic nerve crush 28 days previously compared to sham operated animals (Palin et al., 2008), suggesting that these microglia were primed for a greater inflammatory reaction despite the presence of TGF $\beta$ , which has been described in vitro as attenuating LPS induced cytokine production. Prion infected mice, which have elevated TGF- $\beta$  levels, demonstrate greater IL-1 $\beta$ , IL-6, iNOS and TNF $\alpha$  induction in the brain and an accelerated progression of neurodegeneration following i.p. or i.c. injection of LPS than mice injected with saline (Cunningham et al., 2005). The in vivo injured brain is a complex environment and it is likely that these cells are not differentiated

purely towards a “regulatory” phenotype, but instead exist somewhere in a continuum between different states of activation.

Alternatively activated macrophages have been described following treatment with IL-4 or IL-13, cytokines typically associated with a Th2 type immune response (Abbas et al., 1996; Ramirez-Icaza et al., 2004). IL-4/IL-13 induced macrophages typically express increased levels of mannose receptor, Ym1 and Fizz1 at the cell surface (Colton et al., 2006; Edwards et al., 2006; Stein et al., 1992), increased arginase activity (Sandler et al., 2003), an attenuated antigen presenting capacity (Edwards et al., 2006) and an attenuated pro-inflammatory cytokine response to LPS compared to classically activated macrophages (Colton, 2009). IL-4 has been shown to evoke a similar profile in microglia (Colton et al., 2006; Ponomarev et al., 2007), while both IL-4 and IL-13 have been shown to evoke apoptosis of classically activated (but not resting) microglia (Yang et al., 2002). Changes in the expression of phagocytosis receptors also occur following exposure of macrophages to IL-4, which causes increases in expression of mannose receptor, complement receptor 3 and dectin 1, while expression of Fc $\gamma$ RI, Fc $\gamma$ RII and CD163 decreases following exposure to IL-4 (Gordon, 2003; Nimmerjahn and Ravetch, 2006; Schaer et al., 2002; Willment et al., 2003). This suggests a more complex role for these cells than simple clearance of post injury debris. Atorvastatin, a drug that stimulates IL-4 release within the CNS, has been shown to ameliorate the effects of systemic LPS on LTP and IL-1 $\beta$ /IFN $\gamma$  release (Clarke et al., 2008), suggesting an *in vivo* anti-inflammatory action of IL-4 in the brain, a concept further supported by work suggesting that IL-4 upregulates CD200 expression (Lyons et al., 2009b).

IL-4 and IL-13 release in the CNS have not been widely reported *in vivo*. IL-4 mRNA has been detected in the brain in the absence of immune challenge (Loane et al., 2009), but IL-4 (and IL-13) protein was absent from mouse scrapie infected brains (Tribouillard-Tanvier et al., 2009). Interestingly, a role has been described for microglial release of IL-13 in exacerbation of microglial respiratory burst following hippocampal exposure to the blood component thrombin (Park et al., 2009). Induction of IL-13 release in activated microglia was also demonstrated following *i.c.* injection of LPS, where IL-13 knockdown exacerbated LPS induced neuronal cell death and microglial survival (Shin et al., 2004).

#### 1.2.4 Priming vs tolerance

Microglia and macrophages are plastic in phenotype, switching between activation states depending on the stimuli they are exposed to, as discussed above. This also applies to their responsiveness to pro-inflammatory stimuli. Priming is a concept originally described in macrophages treated with IFN $\gamma$ . IFN $\gamma$  treated macrophages have an enhanced response to LPS, producing larger amounts of inflammatory cytokines than macrophages stimulated with LPS without being exposed to IFN $\gamma$  (Schroder et al., 2006). This enhanced response is mediated by increased expression of TLRs, downstream TLR signalling apparatus e.g. TRAF6 and the synergistic action of IFN $\gamma$  receptor and TLR signalling on transcription factors (Schroder et al., 2006). Granulocyte macrophage-colony stimulating factor (GM-CSF) has also been shown in vitro to prime microglia to stimulation with LPS through increased expression of TLR4 and CD14 (Parajuli et al., 2012). The absence of monocyte chemoattractant protein-1 (MCP-1) attenuates microglial production of cytokines in response to intrastriatal injection of LPS, suggesting a role in potentiating microglial responses to LPS (Rankine et al., 2006).

Enhanced reactivity to inflammatory stimuli has been described in microglia in vivo in injured, diseased or aged brains (Cunningham et al., 2005; Henry et al., 2009; Palin et al., 2008). The mechanisms underlying these changes are not well understood at present and are discussed in section 1.4. Stress can also prime microglia to systemic inflammation via a glucocorticoid dependent mechanism, causing enhanced production of IL-1 $\beta$  and enhanced NF $\kappa$ B signalling in response to an i.p. LPS injection (Frank et al., 2012). In vivo exposure of microglia to a different set of molecules associated with stress, beta adrenergic receptor agonists, also sensitises microglia to ex vivo stimulation with LPS, leading to increased IL-1 $\beta$  and IL-6 production (Johnson et al., 2013).

Tolerance is a phenomenon in which exposure of a cell or animal to endotoxin (LPS) blunts its response to a latter re-exposure of that stimulus. This allows homeostasis to be maintained in areas of the body where cells might be constantly exposed to LPS, such as in the mouth to periodontal bacteria (Biswas and Lopez-Collazo, 2009). Tolerance can be seen to occur in the systemic immune system following consecutive i.p. injections of LPS (Püntener

et al., 2012) and in the CNS after consecutive i.c.v. injections of LPS (Faggioni et al., 1995), but not in the CNS after systemic i.p. injection of LPS, suggesting the need for direct ligation of TLRs on microglia for the induction of tolerance (Püntener et al., 2012). To what extent tolerance occurs in response to chronic cytokine signalling is not known.

## **1.3 Ageing**

### **1.3.1 Mechanisms of ageing**

At first, defining ageing appears easy: “To age – to grow old,” according to the Oxford dictionary. In biological terms however this definition is insufficient. A more comprehensive definition is that ageing after the onset of adulthood is the progressive dysfunction of an organism and its biological processes. Alternative definitions describe ageing as a progressive accumulation of damage in an organism, but whether this is a cause or a consequence of ageing and the biological impact of this damage is currently under debate. Three of the most prominent theories of ageing are oxidative stress mediated ageing, developmental drift and TOR-centric ageing. There are many more theories of ageing – a review in 1990 by Medvedev counted over 300 (Medvedev, 1990) - but this introduction will focus on these three concepts. Ageing affect cells throughout the body, and understanding the general concepts underlying the ageing process is useful for understanding how and why certain cells and systems become dysfunctional during ageing.

#### **1.3.1.1 ROS and Ageing**

Reactive oxygen species (ROS) damage accumulates over the lifetime of an organism in the form of lipid peroxidation and protein oxidation (Droge and Schipper, 2007). The stochastic nature of ROS means that any macromolecule in the organism can be oxidised. The oxidative damage theory of ageing hypothesises that oxidative damage of macromolecules accumulates and progressively impairs cellular function. Damage in particular to mitochondria and DNA have been implicated as potential mechanisms for age-related impairment of cellular function (Chan, 2006; Sinclair and Oberdoerffer, 2009).

A large number of studies have attempted to increase lifespan by manipulating the oxidative state of mice. However the majority have shown that

modifications to antioxidant expression, both positively and negatively, failed to alter lifespan (Salmon et al., 2010). What has subsequently been proposed is that accumulated ROS damage or increased ROS levels in an organism may affect the health span rather than life span of an organism. Evidence from mouse models implicates reduced expression of the antioxidant enzymes Superoxide Dismutase 1 (SOD1), SOD2, glutathione peroxidase 1 and methionine sulfoxide reductase A in an accelerated progression of/earlier onset of hearing loss, macular degeneration, cataract formation, muscle atrophy, tumour formation, insulin resistance and hippocampal degeneration (Salmon et al., 2010). In mouse models of neurodegenerative disease, knock out or transgenic overexpression of antioxidant enzymes accelerated or slowed respectively progression of AD, Parkinson's Disease, ALS, atherosclerosis and insulin resistance models (Salmon et al., 2010).

Notably, however, these studies were all in mice. Numerous clinical human trials with a total of half a million participants have failed to show any protective effect of antioxidants against cardiovascular disease, cancer incidence, stroke incidence or mortality (Howes, 2006). A clinical antioxidant trial for AD (Tabet et al., 2000) was similarly disappointing. Some of these trials lasted a number of years (>5) and some were stopped early due to increased mortality/disease incidence. One is forced to conclude that there is insufficient evidence to support the idea that progressive stochastic molecular damage is the major driving force of ageing. ROS is an important signalling molecule in numerous cell types (D'Autreaux and Toledano, 2007), and also amplifies pro-inflammatory signalling in microglia (Pawate et al., 2004; Qin et al., 2004; Wang et al., 2004) through increased NF $\kappa$ B signalling (Gloire et al., 2006) which gives rise to the notion that increased ROS may participate in certain aspects of age related changes, such as microglial priming.

### **1.3.1.2 mTOR, calorie restriction and ageing**

The mTOR pathway offers an attractively linear explanation of the life extending effects of caloric restriction (CR) and reduced insulin signalling via nutrient sensing and Phosphatidylinositide 3-kinase (PI3K) mediated insulin signalling pathways. There are two mTOR complexes, mTORC1 and mTORC2, and it is mTORC1 where most studies have identified a role in the attenuation of the ageing process via mTOR inhibition. mTORC1 activation promotes cell

growth (but not proliferation), and negatively regulates autophagy, apoptosis and protein ubiquitination via 4E-binding protein 1, MAF-1 and S6 kinase (Hall, 2008; Michels et al., 2010). mTOR signalling is required for life extension via caloric restriction in *Drosophila* (Zid et al., 2009) and autophagy, which is promoted by mTOR inhibition, is required for CR life extension in *C. Elegans* (Hansen et al., 2008). Expression of S6 kinase, one of mTOR's downstream targets, in 24m old CR treated mice was reduced 13 fold compared to 24m old non-treated mice, indicating that caloric restriction in aged mice has a powerful effect on the downstream components of the mTOR pathway. Sirtuins are proteins which are involved in epigenetic regulation of gene expression and have also been shown in yeast to be essential for life extension via mTOR and CR (Medvedik et al., 2007).

Studies in *C. Elegans* and *Drosophila* suggest that the life extending effects of mTOR inhibition is at least partly mediated by promotion of autophagy (Hansen et al., 2008; Simonsen et al., 2008; Toth et al., 2008), which is impaired in ageing (Simonsen et al., 2008; Szweda et al., 2003). Autophagy, literally "self eating", is the process of delivering cellular components to the lysosome and has two principle purposes: the generation of energy in times of low nutrient availability and the removal of proteins and organelles from the cytoplasm. The mechanism of age-related decreases in autophagy is not clear; accumulation of lipofuscin has however been suggested as one potential cause of reduced lysosomal efficiency (Szweda et al., 2003). Blocking autophagy in mice causes severe neurodegeneration in the CNS and eventual death at 28 weeks of age, demonstrating the importance of autophagy in maintaining homeostasis within cells, particularly in the CNS (Komatsu et al., 2006).

There is not much literature that has actually shown increased mTOR signalling in aged cells. Increased mTOR signalling has been described in aged haematopoietic stem cells (Chen et al., 2009), hypothalamic proopiomelanocortin neurons (Yang et al., 2012) and muscle cells (Paturi et al., 2010), but the state of mTOR signalling in most cell types in aged organisms remains undefined. Manipulation of mTOR signalling certainly extends lifespan, even in complex vertebrates (Harrison et al., 2009), but how prevalent increased mTOR signalling in different cell types aged organisms remains to be determined.

### **1.3.1.3 Developmental drift**

Developmental drift theory postulates that epigenetic regulation of genes becomes progressively more dysfunctional with age. The principle idea is that the regulation of genetic programming by organisms is only optimised for the period of life where an organism is alive and reproducing – without reproduction there is no evolutionary pressure to shape genetic programming. Expression of a gene may play a beneficial role early in an organism's life but be detrimental to the organism in later life, but the detrimental effects in later life have no evolutionary pressure on the genome. This concept is known as antagonistic pleiotropy (Williams, 1957). Epigenetic regulation of gene expression controls patterns of gene expression between different cell types and during development through changes in DNA methylation or histone modification. Ageing leads to drastic changes in the epigenetic landscape of an organism (Li et al., 2011) which may underlie some of the changes observed in ageing organisms. Variations in gene methylation have been proposed to contribute to late onset AD (Wang et al., 2008) and manipulation of the epigenetic landscape has been shown to reverse some of the effects of ageing and age related diseases (Sung et al., 2013; Zeng et al., 2011).

### **1.3.2 Ageing, the CNS and neurodegenerative disease**

For many years it was assumed that the cognitive decline that occurs with ageing was a result of a global, age related neuronal loss throughout the brain (Long et al., 1999). The application of stereological counting techniques has subsequently shown however that neuronal loss does not occur globally across the brain and varies between CNS regions and between species. For example, neuronal numbers in the rodent hippocampus have been reported to be stable (Calhoun et al., 1998; Rasmussen et al., 1996), whereas in humans neuronal loss in some, but not all hippocampal subregions (such as the hilus of the dentate gyrus) has been reported (West, 1993). Other brain regions reported to retain the same number of neurons across human ageing include the putamen (Pesce and Reale, 1987) and locus coeruleus (Ohm et al., 1997), and a range of nuclei in the mouse (Sturrock, 1991, 1992). A modest (10%) loss of neurons has been reported with age in the human neocortex (Pakkenberg and Gundersen, 1997), while approximately half of all neurons in the Purkinje layer and substantia nigra of mice (Mouton et al., 2012; Woodruff-Pak et al., 2010),

humans (Sjobeck et al., 1999) or monkeys (Emborg et al., 1998) are lost over the ageing process. Clearly age related neuronal loss varies significantly between populations, but the causes for these variations remain to be identified. Reduction of dendritic tree size and spine numbers have also been reported (Dickstein et al., 2007), suggesting loss of synapses occurs during ageing.

Increasing age in humans is also associated with increasing frequency of neurodegenerative disorders. Environmental and genetic risk factors do influence the probability of an individual developing AD or PD, but the biggest risk factor is age. Indeed, many cognitively healthy aged individuals display at autopsy a range of the molecular markers typically used to confirm diagnosis of AD or PD, namely amyloid beta plaques, neurofibrillary tangles and Lewy bodies (Gibb and Lees, 1988; Knopman et al., 2003; Rowe et al., 2007), which may be indicative of subclinical disease. While the proteins which are involved in formation of these aggregates are well described, the underlying causes of these disease states remain unknown. AD and PD are both characterised by neuronal dysfunction and (later) death of specific groups of neurons, elevated cytokine levels, movement/memory problems (in PD and AD respectively) and behavioural changes (Beal et al., 2005) which are not characteristic of healthy ageing. What remains to be determined is what triggers the transition from healthy ageing to neurodegenerative disease, particularly in sporadic disease such as late onset AD. Systemic inflammation could potentially play a role in precipitating pathology in aged individuals and accelerating disease progression (Cunningham et al., 2009; Holmes et al., 2009; Krstic et al., 2012).

### **1.3.3 Ageing and white matter**

Significant changes also occur within the white matter of ageing animals, with the majority of investigations being conducted in aged rhesus monkeys. Abnormalities in myelin sheath thickness and morphology and a loss in the total number of myelinated fibres has been reported in a range of brain areas, including the rhesus monkey anterior commissure (Sandell and Peters, 2003), cingulate bundle (Bowley et al., 2010), fornix (Peters et al., 2010) and optic nerve (Sandell and Peters, 2002). A 45% reduction in the total length of white matter tracts has been estimated using stereology in humans between 20 and 80 years old (Marner et al., 2003). Increased myelin turnover in mice (Ando et

al., 2003) and the appearance of white matter lesions in humans have also been reported with age (Fernando et al., 2006). These decreases in myelinated fibre numbers seem to occur across the brain, but there are variations between white matter tracts in the extent to which they undergo age related changes, with the optic nerve for example losing more myelinated nerve fibres with age (Sandell and Peters, 2002) than the corpus callosum (Bowley et al., 2010). Myelin has been reported to be present inside microglia in aged white matter tracts, suggesting that microglia may play a role in either driving white matter loss during ageing or in clearing myelin debris (Peters et al., 2010; Sandell and Peters, 2002).

There is some evidence to suggest disruption to paranodal junctions in normal ageing. The number of transverse bands present at paranodal regions has been reported to decrease in the spinal cord of aged mice (Shepherd et al., 2010). The same study reported detection of caspr in juxtaparanodal regions, although Kv1.2 channels were still restricted to the juxtaparanodal region. In the aged rhesus monkey optic nerve Kv1.2 was detectable in the paranodal region more often than in young monkeys (Hinman et al., 2006). This study also showed examples of abnormal caspr distribution in aged monkeys and caspr/Kv1.2 overlap in aged rat optic nerve. Both of these papers also demonstrated paranodal loop “piling” in ageing mice through electron microscopy, suggesting previous withdrawal of paranodal loops and subsequent reattachment of new paranodal loops. Reduced conduction velocity has been reported in aged white matter tracts of cats and rats (Aston-Jones et al., 1985; Morales et al., 1987), and disruption of paranodal junctions could contribute to this reduced conduction velocity. Various studies have shown axonal swellings in aged white matter tracts (Baurle and Grussercornehl, 1994; Munari et al., 1989; Nishimura et al., 1998), which could be symptomatic of disrupted axonal transport as a result of paranodal disruption (Garcia-Fresco et al., 2006).

#### **1.3.4 Ageing and the peripheral immune system**

Other areas of the body are affected by ageing apart from the CNS, including the immune system. Increased susceptibility to infection is characteristic of the elderly population (Gardner, 1980). Age related changes to the adaptive immune system include clonal expansion of CD4/8<sup>+</sup> memory T cells (Schwab et

al., 1997), deficits in the formation of new T memory cells (Haynes and Maue, 2009) and declining efficacy of antigen presentation (Donnini et al., 2002). Aged B cell populations have a reduced antibody repertoire and an increase in experienced B cells and a decrease in naïve B cells, compromising the antibody response to novel antigens (Mehr and Melamed, 2011). The innate immune system also exhibits age dependent changes characterised by a systemic, chronic, asymptomatic, low grade increase in expression of inflammatory mediators, including cytokines such as IL-1 $\beta$ , TNF $\alpha$  and IL-6 and other molecules associated with the Th1 inflammatory response such as NO and PGE<sub>2</sub> (Franceschi et al., 2007; Goto, 2008). This age dependent change in the immune system has been termed “inflammageing” and has mostly been described in humans rather than experimental animals. This may reflect the difference in environment between “clean” animal houses and the environment that humans inhabit, which contains many pathogens (Franceschi et al., 2007).

In contrast to the reported chronic activation of the aged innate immune system, there is some evidence to suggest that acute responses to inflammatory stimuli are blunted in aged organisms. The IL-1 $\beta$  and TNF $\alpha$  response to LPS was attenuated in ex vivo blood culture from elderly humans compared to young humans (IL-6 release was unaffected) (Bruunsgaard et al., 1999; van den Biggelaar et al., 2004), suggesting a decreased responsiveness to TLR4 stimulation in blood macrophages stimulated in vitro. Similar results were obtained in macrophages derived from mice (Chelvarajan et al., 2005). Aged monocytes have been shown to express reduced levels of TLR1 and TLR4 in the absence of infection (Chelvarajan et al., 2005; van Duin et al., 2007), which may explain the blunted responses of macrophages from aged humans and mice.

In vivo studies of cytokine responsiveness to TLR ligands have produced mixed results. The effect of age on the acute phase response to LPS at levels that do not induce septic shock levels remains understudied, but those studies that have been carried out show an attenuated or unchanged IL-1 $\beta$  and TNF $\alpha$  response but an enhanced IL-6 response to intraperitoneal injection of LPS or live *E. coli* (Barrientos et al., 2009a; Chorinchath et al., 1996; Godbout et al., 2005b; Henry et al., 2009). The increased IL-6 levels have been associated with enhanced adipocyte production of IL-6 in response to LPS, which may explain why induction of IL-6 by LPS is enhanced in ageing whereas IL-1 $\beta$  and TNF $\alpha$  are

not (Starr et al., 2009). Injection of significantly higher concentrations of LPS to model sepsis induce exaggerated inflammatory responses in aged mice (Chorinchath et al., 1996; Tateda et al., 1996). Other aspects of innate immune senescence include the reduced induction of MHCII in response to IFN $\gamma$  evident in aged macrophages (Herrero et al., 2001) and a decreased phagocytic capacity of aged macrophages and neutrophils (Plowden et al., 2004), both of which may impair the immune system's capacity to resist infection.

## **1.4 Microglial Priming**

### **1.4.1 Microglial Priming in the neurodegenerative brain**

The descriptions of the CNS immune system in this introduction so far have mostly referred to transient, acute influences so far; the influence of chronic, neurodegenerative changes to the CNS can alter microglial phenotypes and their responses to immunogenic stimuli (such as DAMPs and PAMPs), potentially exacerbating their release of pro-inflammatory cytokines, PGE $_2$ , ROS and NO. Increased levels of pro-inflammatory cytokines and NO/ROS has been reported in the post-mortem brains and cerebrospinal fluid of dementia patients compared to age-matched control subjects (BlumDegen et al., 1995; McGeer et al., 1988; Müller et al., 1998), suggesting a possible role for inflammation in the pathogenesis of dementia. Genome wide association studies have also associated several genes linked to inflammation with AD susceptibility (Naj et al., 2011). One study drew a correlation between circulating basal TNF $\alpha$  levels or systemic inflammatory events and the progression of cognitive decline in Alzheimer's disease (Holmes et al., 2009), demonstrating that systemic inflammation accelerated cognitive decline in AD patients. A similar, smaller study pointed to a possible association between accelerated cognitive decline and elevated circulating IL-1 $\beta$  levels (Holmes et al., 2003). Systemic infections and elevated cytokines may accelerate cognitive decline via endothelial and microglial activation and subsequent increase in inflammatory mediators within the brain parenchyma, which could cause sickness behaviour like symptoms and memory deficits (Dantzer, 2004) and, if produced in sufficient quantities, could induce neuronal loss (Neher et al., 2011) and drive increased amyloid precursor protein secretion (Buxbaum et al., 1992). A study using prenatal poly I:C challenges has also provided evidence

that early life inflammatory events may increase the susceptibility of an organism to the development of AD-like pathology in later life following a second immune challenge (Krstic et al., 2012).

Neurodegeneration also seems to potentiate microglial inflammatory responses to systemic inflammation. In a murine model of prion disease intraperitoneal LPS administration induced exaggerated sickness behaviour and increased induction of central  $\text{TNF}\alpha$ ,  $\text{IL-1}\beta$  and  $\text{IFN}\beta$  mRNA compared to normal brain homogenate (NBH) treated controls (Cunningham et al., 2009). In the same study prion infected mice demonstrated accelerated decline in motor performance through the course of the disease if treated once with i.p. injected LPS in the early disease stages, showing that a single dose of LPS induces sufficiently profound changes within the CNS to accelerate the pathology of prion disease. This accelerated disease progression is likely driven by neuronal damage and loss incurred during the acute inflammatory challenge (Cunningham et al., 2005). Microglia in the prion infected brain in the absence of LPS robustly express markers of microglial activation (Williams et al., 1994), but lack the cytokine profile that is normally associated with pro-inflammatory activation of microglia (Cunningham et al., 2009). These microglia have been proposed to exist in a 'primed' state; ready to produce a larger than normal inflammation response, but only when an inflammatory cue is present. Further studies from the same group show exaggerated sickness behaviour and CNS cytokine release in the prion infected mouse in response to the TLR3 agonist poly I:C (Field et al., 2010). A similar accelerating effect of i.p. injected LPS (albeit administered in multiple acute challenges rather than a single dose) on disease progression was seen in a mouse model of familial ALS (Nguyen et al., 2004).

It has been proposed that the microglia described in the above studies are primed by changes in their microenvironment that occur during neurodegenerative disease, explaining the exaggerated release of cytokines that occurs in these conditions following systemically or centrally administered LPS challenge. Corresponding exaggerated sickness behaviour has not been investigated in a wide range of models; work in prion mice forms the largest base of evidence for microglial priming exacerbating sickness behaviour in the context of chronic neurodegenerative conditions.

#### 1.4.2 Microglial Priming in the ageing brain

Microglial priming also occurs in the normally ageing brain. Various authors have demonstrated that aged rodents exhibit exaggerated sickness behaviour and a prolonged/enhanced cytokine release in the CNS in response to systemic inflammation, as well as showing that aged microglia bear typical markers of activation including CD11b, CD68 and F4/80 (Deng et al., 2006; Godbout et al., 2005b; McLinden et al., 2012). A role for systemic inflammation in delirium in elderly humans has been suggested too (Cerejeira et al., 2010; de Rooij et al., 2007) providing further evidence of aberrant behavioural responses to systemic inflammation in the aged brain. It has been established for some time that there is increased expression of microglial activation markers such as CD11b in the aged rodent brain (Perry et al., 1993) and subsequent work has built on those observations, making frequent use of rodent models.

Comprehensive studies of microglial priming in ageing have primarily come from Dr Johnson's group at the University of Illinois. Data from their group has shown two fold greater induction of IL-1 $\beta$  and IL-6 mRNA in the brain 4 hours after i.p. injection of 330 $\mu$ g/kg LPS in aged (20-24 month) vs young adult (3-6 month) BALB/C mice (Godbout et al., 2005b). Prolonged elevation (24h post injection) of IL-6 mRNA was also present in the brains of the aged (but not young) mice. Preceding injection of LPS, aged mice expressed increased levels of CD68, a marker of microglial activation, and iC3b complement receptor 3, aka CD11b (Godbout et al., 2005b), also a microglial activation marker (Graber et al., 2010). Aged mice exhibited more severe and prolonged deficits in social behaviour, open field exploration and food intake following LPS challenge (Godbout et al., 2005b). A later study recapitulated some of these earlier behaviour deficits and showed prolonged depressive behaviour in aged (20-24m) mice injected i.p. with 330 $\mu$ g/kg LPS vs young mice (3-6m), as measured by the duration of immobility in the forced swim test 72 hours post injection (Godbout et al., 2008). This corresponded with prolonged elevation of IDO 2,3 activity - 24 hours after LPS injection in the young adult brain IDO 2,3 levels had returned to saline levels, while they remained elevated in the aged animals (Godbout et al., 2008). These authors demonstrated that this enhanced cytokine response to systemic inflammation is mediated, at least in part, by microglia by isolating microglia from LPS injected young or aged mice and measuring cytokine transcripts in the purified microglia transcripts, reporting

increased induction of IL-1 $\beta$ , TNF $\alpha$ , iNOS and IDO 2,3 transcript in aged microglia compared to young microglia (Corona et al., 2010; Henry et al., 2009; Wohleb et al., 2012).

A similar profile of exaggerated sickness behaviour and cytokine response to inflammation in aged mice was generated by i.c.v. injection of the HIV envelope protein HIV-gp120 (Abraham et al., 2008) or LPS (Huang et al., 2008), showing that an enhanced central immune response is not limited to systemic immune challenges – HIV-gp120 activates microglia by binding to CXCR5 (Rottman et al., 1997), a receptor which has not been implicated in mediating peripheral to brain immune communication to date. Huang's 2008 study also showed that exaggerated responses to inflammation in ageing are not restricted to the hippocampus, as IL-1 $\beta$ , IL-6 and TNF $\alpha$  release was also enhanced in the aged cerebellum. In a separate study elevated IL-1 $\beta$  levels 24h after LPS injection in the aged (22-24m) but not the young adult (3-6m) brain were attenuated with centrally administered IL-1ra, which correlated with attenuated deficits in social and locomotor behaviour following LPS injection, suggesting a role for IL-1 $\beta$  in mediating the exaggerated inflammatory response in aged mice (Abraham and Johnson, 2009a). Induction of IL-10, the anti-inflammatory cytokine, was also greater and more prolonged following systemic LPS injection in aged vs young brain, demonstrating that it is not only the pro-inflammatory arm of the microglial response that is primed in the aged brain (Henry et al., 2009). A study using an i.p. injection of 3-6mg/kg poly I:C demonstrated exaggerated sickness behaviour in aged mice by measuring overnight burrowing activity, although expression of the cytokines measured (IL-1 $\beta$  and IL-6) was not enhanced in aged (18-19m) C57/BL6 mice (McLinden et al., 2012). Injection of IFN $\gamma$  and TNF $\alpha$  i.c.v. in aged and middle aged mice (Deng et al., 2006) caused a greater induction of microglial activation markers CD11b and F4/80 in old (18-21m) than in middle aged (10-11m) and young (2-3.5m) brains, adding weight to the idea of enhanced microglial responses to inflammatory stimuli and suggesting that microglial priming may begin in middle age rather than old age.

Data from rat studies offers additional support for microglial priming with ageing. Elderly rats (24 month old) experienced prolonged weight loss and core body temperature drop in response to injection of live *E. coli* compared to young rats (3 month) (Barrientos et al., 2009b). The same group also

demonstrated that live *E. coli* infection induced memory deficits and elevation of IL-1 $\beta$  in the hippocampus of aged (24 month old) rats compared to 3 month old rats (Barrientos et al., 2009a). These memory deficits may have been induced by changes in BDNF expression that occur following *E. coli* infection (Cortese et al., 2011). Intrapallidial injection of LPS into rats induced prolonged expression of TNF $\alpha$  (which was still elevated 4 weeks post injection) and elevated expression of IL-6 2 days after injection in elderly vs young adult rats (Choi et al., 2008). Increased expression and induction of CD11b and MHC II has been reported in aged rat brain before and after LPS injection vs young rat brain (Bilbo, 2010). Increased DNA binding of NF $\kappa$ B subunit p65 has been reported in aged (30m) rat brain vs 3m rat brain, suggesting constitutive upregulation of the pro-inflammatory response (ToliverKinsky et al., 1997).

Further work is required to clarify the consequences of these exaggerated microglial reactions. While a co-incidence of systemic inflammatory events with accelerated progression of AD in humans has been demonstrated (Holmes et al., 2009), the effects of systemic inflammatory events on the neuronal health of ageing humans and whether these events are capable of precipitating neurodegenerative disease remains unstudied. The studies in mice and rats discussed above do not focus on the effect of these inflammatory events on neuronal survival and cellular function, e.g. synaptic density – this is a critical question relating to how pathologically significant microglial priming is to systemic inflammation in humans. The literature describes in depth the altered phenotype of microglia in the aged brain, their enhanced reactions to inflammatory challenge and in further studies (Abraham and Johnson, 2009b) has begun to investigate ways of attenuating this enhanced response to systemic inflammatory challenge.

## **1.5 Causes of Microglial Priming**

Microglial priming and macrophage priming are both characterised by an exaggerated reaction to inflammatory stimuli. However, levels of molecules such as GM-CSF, IFN $\gamma$  and MCP-1 which have been linked to macrophage and microglial priming previously have not been described as changed in the aged brain to date (Godbout et al., 2005b). Furthermore, isolated macrophages from aged organisms are less responsive to stimulation than those from young

organisms (Chelvarajan et al., 2005), which contrasts to what has been observed in aged microglia. Therefore changes in the microenvironment surrounding microglia or differences in the life cycle of macrophages and microglia e.g. longevity may account for microglial priming in the ageing CNS.

### **1.5.1 The CNS microenvironment – immune regulating molecules of the CNS**

There is a multitude of signals within the CNS that can affect the activation state of microglia, causing alterations in phagocytic activity, release of pro/anti-inflammatory cytokines, membrane protein and receptor expression levels, nitric oxide release and cell survival. These interactions allow the microglia to monitor their local environment and react to changes within it. Some of these signals (for example CD200) act in a tonic manner to influence microglial phenotype, keeping the microglia in a constrained, resting phenotype, and perturbations in this tonic signalling could contribute to microglial priming. In an aged brain exhibiting region-specific neuronal loss (e.g. Purkinje neurons – (Woodruff-Pak et al., 2010)) or compromised neuronal function (Erickson and Barnes, 2003), the microglial microenvironment may be altered to some degree – thus chronic changes to the microglial microenvironment represent a potential cause of priming.

#### **1.5.1.1 CD200 & CD200R**

CD200-CD200R interactions are one example of neuronal-glia contact interactions that exert a tonic inhibitory influence on microglial activation state (Meuth et al., 2008). CD200 is expressed on neurons and oligodendrocytes, but not microglia or astrocytes (Koning et al., 2009), while expression of CD200 receptor (CD200R) is limited to microglia and perivascular macrophages in the context of the CNS (Koning et al., 2009; Wright et al., 2000). CD200R has multiple isoforms, but only the inhibitory receptor CD200R1 binds CD200 (Hatherley et al., 2005). CD200R1 has been shown to exert its inhibitory effects on pro-inflammatory activation of macrophages and microglia by docking protein 2 (Dok2) and RasGAP (the inactivator of Ras) signalling (Mihirshahi et al., 2009; Zhang et al., 2004). Within this discussion CD200R1 will be referred to as CD200R.

Administration of anti-CD200R blocking antibody exacerbates the severity of a guinea pig model of EAE, suggesting that disruption of CD200-CD200R interaction exacerbates microglial inflammatory activity (Wright et al., 2000). Another study offered supporting evidence for this conclusion using neuronal-macrophage co-culture studies, showing that pre-treatment with blockading anti-CD200R antibody enhanced IFN $\gamma$  mediated IL-6 release in peritoneal macrophages extracted from rats suffering from MOG-induced EAE (Meuth et al., 2008). CD200 knockout mice exhibit increased expression of microglial activation markers CD11b, MHCII and F4/80, fusion of microglia to form multinucleated giant/aggregated cells, increased basal expression of TNF $\alpha$  and IL-6 in the hippocampus and expressed greater levels of inflammatory markers following facial nerve transection or EAE induction (Denieffe et al., 2013; Hoek et al., 2000), suggesting that CD200 is the necessary partner for the CD200R protein to mediate CD200R's constitutive anti-inflammatory effects.

The CD200-CD200R interaction represents an influential constitutive, anti-inflammatory, contact mediated signal within the CNS; age related changes in neuronal expression levels of this protein could drive an exaggerated inflammatory response similar to that seen in primed microglia. An age related decline in CD200 expression has indeed been reported in the hippocampus (Frank et al., 2006) and the substantia nigra (Wang et al., 2011), although CD200R levels remained unchanged (Frank et al., 2006). Loss of neurons could have the same effect as reductions in neuronal CD200 expression - the levels of CD200 within the CNS would decline with neuronal loss, which would hold true for other contact dependent anti-inflammatory mechanisms within the CNS too. One should bear in mind however that the CD200-CD200R interaction is contact dependent and the resting microglia are dynamic in monitoring their environment - if the microglial cell is still able to find sufficient neurons to interact with then perhaps there would be no significant decline in the quantity of CD200-CD200R interactions.

#### **1.5.1.2 SIRP $\alpha$ & CD47**

Signal regulatory protein alpha (SIRP $\alpha$ ) is a transmembrane glycoprotein belonging to the SIRP family (part of the immunoglobulin superfamily) that is paired with CD47, also of the immunoglobulin superfamily. Both are expressed within the CNS and when SIRP $\alpha$  is ligated it exerts an anti-inflammatory

influence on microglia. CD47 is widely expressed within the CNS by a variety of cell types including microglia, neurons, oligodendrocytes and astrocytes, whereas SIRP $\alpha$  is expressed in neurons and microglia (Gitik et al., 2011b; Han et al., 2012; Matozaki et al., 2009). CD47-SIRP $\alpha$  signalling is also present in cells outside the CNS and one of the cell types that expresses SIRP $\alpha$  is macrophages (Matozaki et al., 2009). When ligated by CD47, SIRP $\alpha$  is phosphorylated at its tyrosine residues and SIRP $\alpha$  subsequently recruits and activates SHP-1 and SHP-2 (Matozaki et al., 2009), which are negative regulators of phagocytosis and cytokine release (Neel et al., 2003; Okazawa et al., 2005; Zhao et al., 2006). This inhibition of phagocytosis has led to SIRP $\alpha$ -CD47 signalling being described as a “don’t eat me” signal. SIRP $\alpha$ -CD47 interactions have been shown to downregulate myelin phagocytosis in microglia (Gitik et al., 2011a; Han et al., 2012) and disruption of CD47-SIRP $\alpha$  signalling during EAE worsens the symptoms of the disease and increases cytokine production (Han et al., 2012).

Evidence for a role of these interactions in regulation of macrophage activation comes from several studies. Knockdown of SIRP $\alpha$  enhanced LPS induced NF $\kappa$ B, activator protein 1 (AP-1), extracellular signal-regulated kinase (ERK) and c-Jun N-terminal kinases (JNK) signalling and enhanced LPS induced pro-inflammatory cytokine production (IFN $\beta$ , TNF $\alpha$ , IL-6) and nitric oxide production in a RAW264-7 macrophage cell line (Kong et al., 2007). Another study found similar effects in RAW264-7 cells in response to TLR3 stimulation via poly I:C (Dong et al., 2008). Smith et al (Smith et al., 2003) described an attenuated TNF $\alpha$  response to LPS and zymosan in human peripheral blood mononuclear cells (PBMCs) following ligation of SIRP $\alpha$ . One study using rat peritoneal macrophages surprisingly showed induction of nitric oxide production (but not pro-inflammatory cytokine production) following ligation of macrophage SIRP $\alpha$  with a SIRP $\alpha$  specific mAb (Alblas et al., 2005). However, the use of an anti-SIRP $\alpha$  antibody to ligate SIRP $\alpha$  rather than its normal binding partner CD47 was proposed by the authors not to have the same effects on NO production as the binding of membrane bound CD47, suggesting this interaction is mimicking a different ligand interaction with SIRP $\alpha$ , possibly surfactant A or D or soluble CD47. Inhibition of phagocytic activity in macrophages via CD47 mediated SIRP $\alpha$  ligation has also been demonstrated in

haematopoietic stem cells and erythrocytes (Jaiswal et al., 2009; Okazawa et al., 2005).

#### **1.5.1.3 TREM receptors**

The TREM2 receptor is a DAP12 signalling receptor (Hamerman et al., 2005) that are expressed on myeloid cells, including microglia. TREM2 ligation attenuates cytokine production (Hamerman et al., 2006; Turnbull et al., 2006), despite signalling via DAP-12, which contains an ITAM motif (Hamerman et al., 2005). These studies support the surprising conclusion that ITAMs can also exert inhibitory signalling, and that the ITAM motif is necessary for attenuation of cytokine production by TREM2 ligation. The mechanisms underlying inhibitory ITAM activity have not yet been fully elucidated, but may be associated with the strength of ligation of the receptor (Blank et al., 2009). TREM2 is ligated by gram-negative and positive bacteria and by expression of Hsp60 on astrocytes (Daws et al., 2003; Quan et al., 2008; Stefano et al., 2009). This ligation by resident CNS cells suggests a possible basal role in maintenance of a down regulated microglial inflammatory phenotype. A decrease in TREM2 receptor/ligand expression or increase in soluble TREM2 would amplify inflammatory responses and therefore represents a further potential contributor to microglial priming. Loss of function mutations lead to a chronic neurodegenerative disease known as Nasu-Hakola disease, suggesting that TREM2 signalling plays an important role in maintaining homeostasis within the CNS (Neumann and Takahashi, 2007). Polymorphisms in the TREM2 gene have also been associated with Alzheimer's disease (Guerreiro et al., 2013). TREM2 also exists in a soluble, non-signalling form which is believed to be generated by metalloproteinases (Gomez-Pina et al., 2007; Piccio et al., 2008), which is hypothesised to be antagonistic to the membrane bound receptor through binding of free TREM2 ligands (i.e. acting as a decoy receptor).

#### **1.5.1.4 AGE and RAGE**

Advanced Glycation End products (AGEs) are modifications to proteins caused by derivatives of glycation pathway components (Grillo and Colombatto, 2008). AGEs have been shown to accumulate in aged organisms (usually due to their longevity on long lived proteins) (Hallam et al., 2010), including in the brain, albeit in a region specific manner (Dei et al., 2002; Luth et al., 2005;

Thangthaeng et al., 2008). These AGEs are normally removed from proteins via deglycating enzymes (Grillo and Colombatto, 2008) or the AGE-modified proteins are degraded by the lysosome (Grimm et al., 2010) or the proteasome (Schmid et al., 2008).

The principle membrane receptor for AGEs is RAGE (Guglielmotto et al., 2012), although AGEs can signal via TLR2 and TLR4 as well (Hodgkinson et al., 2008). RAGE is expressed by neurons, astrocytes and microglia (Schmitt et al., 2006), and can also be ligated by amyloid beta (Fang et al., 2010), S100B (Bianchi et al., 2007) and High Mobility Group protein B1 (HMGB1) (Qin et al., 2009). Studies using mice expressing a dominant negative mutation of RAGE have suggested that the microglial activation seen in mouse AD models requires RAGE signalling acting via MAPK p38 and ERK1/2 (Fang et al., 2010).

The signalling transducer between RAGE and activation of NF $\kappa$ B via MAPK, Rac/Cdc42 and JAK/STAT kinases remains unknown (Zong et al., 2010). Work in a yeast two-hybrid system has pointed to Diaphanous-1 (Dia-1), a member of the formin family, as a potential mediator of interaction between RAGE and Rac/Cdc42 (Hudson et al., 2008). However, the association of the human homologue gene, DFNA1 (Lynch et al., 1997), with RAGE has not yet been investigated. One study has however showed that RAGE induction of early growth response gene-1 (egr-1) (a hypoxia response gene involved in fibrin deposition) by hypoxia required Dia-1 in primary mouse macrophages and in a human macrophage cell line (Xu et al., 2010), suggesting a potential role for Dia-1 in RAGE signalling in mammalian cells too.

AGEs have been shown to induce TNF $\alpha$  and NO release in a microglial cell line (Gasic-Milenkovic et al., 2003) and IL-6, IL-1 $\alpha$  and TNF $\alpha$  in J774 macrophages (Neumann et al., 1999). A RAGE-dependent activation of NF $\kappa$ B signalling via AGEs was also shown in vitro using SK-N-BE neuroblastoma cells (Guglielmotto et al., 2012), while Li et al, 1997 in their original characterisation of the RAGE protein showed the presence of NF $\kappa$ B promoter regions (Li and Schmidt, 1997). RAGE activation also increases levels of ROS release in microglia, neurons, astrocytes and endothelial cells (Nitti et al., 2007; Schmitt et al., 2006; Wautier et al., 2001).

A soluble form of the RAGE receptor (sRAGE) also exists - sRAGE is formed by proteolytic cleavage of the membrane bound form and acts as a decoy

receptor, competing for RAGE binding ligands (Raucci et al., 2008). sRAGE is capable of attenuating inflammatory responses (Hofmann et al., 1999) and is released in response to endotoxin challenge (Soop et al., 2009). Perturbations to sRAGE levels with age could mediate exaggerated reactions to inflammatory challenge.

Although increased AGE levels are present in the aged brain, there have not been any studies examining the effect of elevated AGE levels on the microglial or macrophage response to a systemic innate immune challenge. An interesting study using an alternative RAGE agonist, HGBM1, showed that pre-incubation of ex vivo bone marrow derived macrophages with HGBM1 induced tolerance to LPS (Aneja et al., 2008). This tolerance was not induced in RAGE deficient macrophages, suggesting that this tolerance is RAGE mediated. Pre-conditioning of mice with HGBM1 in vivo 1 h before injection also reduced the TNF $\alpha$  response to i.p. administration of a large dose of LPS (10mg/ml) (Aneja et al., 2008). This study suggests that the pro-inflammatory presence of AGEs, if they signal in the same manner as HGBM1, will not be additive to the pro-inflammatory effects of LPS. A study supporting this conclusion showed that while AGE tagged protein did induce IL-6 release from CD14+ monocytes, this effect of AGE tagged protein was not additive to that of LPS (Hodgkinson et al., 2008). The effects of RAGE signalling on cytokine mediated activation of macrophages/microglia has not yet been determined.

#### **1.5.1.5 Fractalkine**

Fractalkine (CX3CL1) is a chemokine produced by neurons (Harrison et al., 1998) that binds in either a soluble or membrane bound conformation to the CX3CR1 receptor, which is expressed on microglia (Wynne et al., 2010). CX3CR1 ligation by fractalkine leads to PI3K induced protein kinase B (Akt) signalling and calcium influx, which in turn activates MAPK signalling (Re and Przedborski, 2006). Studies have been published suggesting both a pro-inflammatory (Denes et al., 2008; Shan et al., 2009; Soriano et al., 2002) and anti-inflammatory (Cardona et al., 2006; Mizuno et al., 2003; Zujovic et al., 2000) influence of fractalkine on microglia. Soluble fractalkine injection has been shown to attenuate age related changes microglia in vivo (Lyons et al., 2009a), and there are decreases in fractalkine expression in the aged hippocampus and forebrain of rodents (Bachstetter et al., 2011; Lyons et al.,

2009a; Wynne et al., 2010), suggesting that fractalkine may exert an anti-inflammatory role in the aged CNS. Decreased fractalkine expression has also been reported in the aged human brain (Cribbs et al., 2012).

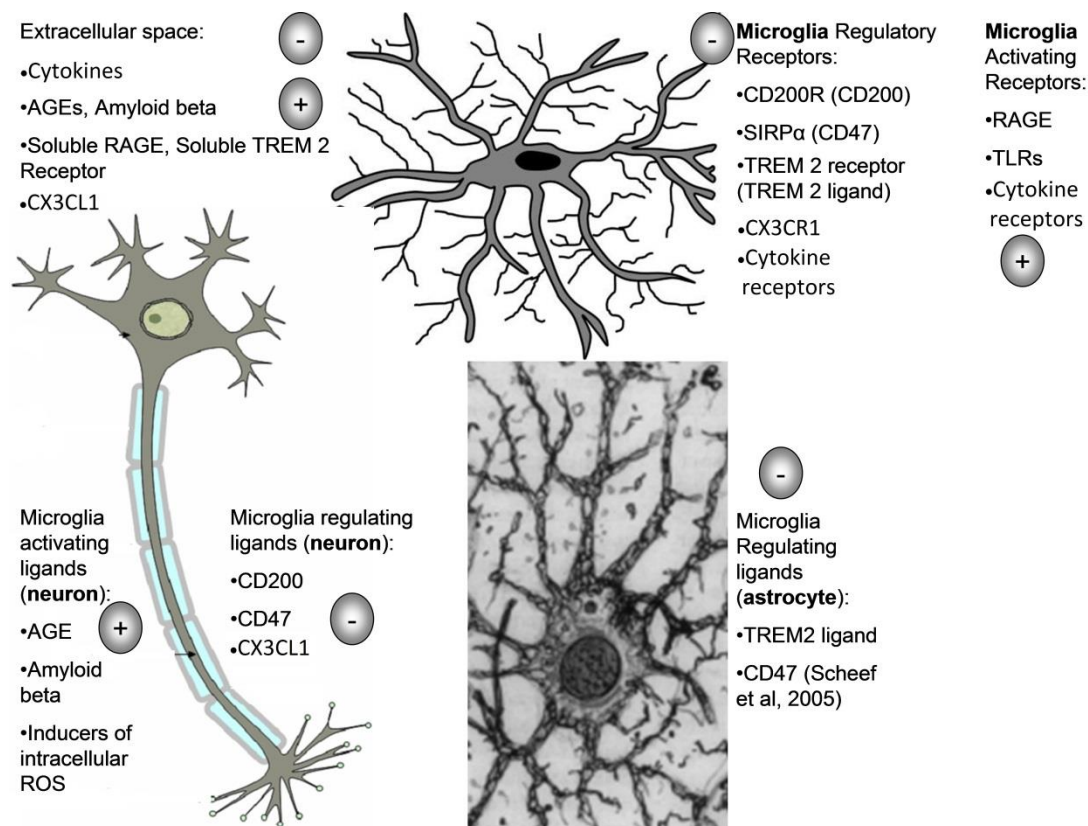


**Figure 1.9. Control of microglial phenotype by extracellular signals.**

A diagram illustrating some of the extracellular modifiers of microglial phenotype.

### 1.5.1.6 Immune regulating molecules of the CNS – summary

The above section describes the known constitutive pro and anti-inflammatory regulators of microglial phenotype that are well defined at present; others may yet emerge, while further research may more precisely define the functions of molecules such as Semaphorin 3A and 4D, neurotransmitters and CD22, which have all been suggested to play immunomodulatory roles within the CNS (Majed et al., 2006; Mott et al., 2004; Pocock and Kettenmann, 2007; Toguchi et al., 2009). Decreased contacts between microglia and neurons because of decreased motility of microglial processes, which has been reported to occur with ageing (Hefendehl et al., 2013), or loss of neurons could cause reduced neuron-microglia signalling and therefore reduced suppression of microglial

inflammatory status. One significant change that seems to occur with ageing is increased blood brain permeability, which is described below.

#### **1.5.1.7 Blood Brain Barrier Integrity**

The blood brain barrier (BBB) acts as the gatekeeper of the CNS that controls what enters and leaves the parenchyma from the circulation. Peripheral immune challenges with LPS have been shown to increase BBB permeability, as shown using Evans blue after i.p. injection of 100µg/kg of LPS in rats, while still excluding larger molecules such as LPS or cytokines (Lu et al., 2009). In ageing it appears that BBB permeability may be increased in the absence of immune challenge. Increased IgG levels around blood vessels has been observed in senescence accelerated prone mouse (SAMP8) mice, a model for accelerated murine senescence, at 12 months of age (Pelegri et al., 2007). Another study looked at IgG deposition within the CNS of middle aged rats and found that by 10-11 months IgG levels around blood vessels were significantly greater than in younger mice (Bake et al., 2009). A meta-analysis of studies into BBB permeability in humans using a variety of techniques found that BBB permeability is consistently reported to increase during healthy ageing and further increase during dementia, particularly vascular dementia (Farrall and Wardlaw, 2009). Increased IgG deposition has also been reported in AD brains and age matched control brains, suggesting a disruption in BBB integrity (D'Andrea, 2003), and the majority of IgG opsonised neurons in control brains were apoptotic, suggesting that labelling of these neurons is specific and targeted.

Increased infiltration of blood components to the CNS would represent a significant change to the microglial microenvironment. IgG could influence microglia reaction to immune stimulation in a variety of ways, depending on the nature of deposition e.g. monomeric IgG vs immune complexes, while other blood components such as thrombin are neurotoxic (Xue et al., 2006). Increased BBB permeability in ageing could lead therefore to sustained infiltration of blood components that may change microglial phenotypes and potentially contribute to priming.

### 1.5.2 Increased innate immune stimulation

One may hypothesise that a lifetime of minor infections and exposure of microglial cells to DAMPs in an aged animal may lead to a ramped up microglial phenotype with heightened responsiveness to pathogens. Several studies have shown that the prenatal environment can affect adult immune responses in the periphery and in the brain (Bilbo and Tsang, 2010; Diz-Chaves et al., 2012; Krstic et al., 2012; Williams et al., 2011). Changes in epigenetic regulation of inflammatory genes in immune cells likely underlie at least some of these changes in the phenotype of these cells, as they do for other phenomena such as endotoxin tolerance (Biswas and Lopez-Collazo, 2009).

Microglia are slowly proliferating, long lived cells (Lawson et al., 1992) and over the course of an organisms lifetime it is not known how the epigenetic regulation of their signalling changes. Persistent immune signalling to microglia could alter microglial phenotypes through changes in epigenetic regulation of inflammatory genes. Manipulation of histone deacetylation using histone deacetylase (HDAC) inhibitors does cause changes in microglial cytokine release, but the published data has been contradictory on the influence of HDAC inhibition thus far (Faraco et al., 2009; Suuronen et al., 2003). Expression of IFN $\gamma$ , GM-CSF and MCP-1 has not been reported to be increased in the aged brain (Godbout et al., 2005b) and is not normally induced in the brain after an i.p. injection of LPS or during *S. typhimurium* infection (Püntener et al., 2012), suggesting that other mechanisms than those that typically drive macrophage priming are at work in the aged brain.

### 1.5.3 Intrinsic changes

Microglia are long lived cells (Lawson et al., 1992). This longevity of microglia means that, like neurons, they senesce and may develop age related cellular dysfunction leading to microglial priming. Increased levels of ROS occur in aged organisms, including in the aged brain (Hayashi et al., 2008), and it has been suggested that elevated ROS levels may also be found in aged microglia. Only one study so far has directly demonstrated reduced antioxidant enzyme activity in aged microglia, which reported a 21% reduction in total glutathione (an antioxidant enzyme) levels in ex vivo microglia from 14-16m mice vs 1-2m old mice, although this was not statistically significant (Njie et al., 2010).

Decreased ROS production via knockout of NADPH oxidase have been shown to attenuate TNF $\alpha$  release following LPS stimulation of microglia in vivo (Qin et al., 2004) and reduction of ROS levels via addition of antioxidant enzyme catalase or the phosphate-oxidase (PHOX) inhibitor 4-(2-aminoethyl) benzenesulfonylfluoride attenuated iNOS activity and NF $\kappa$ B activation (Pawate et al., 2004), so one may hypothesise that increased levels of intracellular microglial ROS may contribute to microglial priming. Reduction of glutathione levels in vitro was recently reported to induce IL-6 and TNF $\alpha$  release from microglia and astrocytes (Lee et al., 2010).

Other studies have reported systemic use of antioxidants reducing the brain cytokine and sickness behaviour response to LPS (Abraham and Johnson, 2009b; Godbout et al., 2005a). However, the antioxidants used, Resveratrol and  $\alpha$ -tocopherol, are known to also effect the sirtuin pathway (Gracia-Sancho et al., 2010) and to have more general, non-ROS mediated anti-inflammatory effects (Reiter et al., 2007). Further investigation into age related changes in expression of antioxidant enzymes in aged microglia and of ROS levels is required to unravel the contribution of intracellular ROS to microglial priming.

mTOR signalling has been proposed to potentially underlie many of the effects of ageing, as discussed in section 1.3. The effects of mTOR inhibition on cytokine release in the absence of stimulation and after application of LPS have been investigated in macrophages and microglia in vitro, but the data is complex and contradictory, with no clear answer on whether mTOR inhibition potentiates or attenuates inflammatory responses (Dello Russo et al., 2009; Schmitz et al., 2008; Weichhart et al., 2008). What role mTOR plays in age induced changes to microglia has not been investigated. Changes to the epigenetic landscape of microglia could also significantly alter the phenotype of microglia in the aged brain, but this has also not been investigated to date.

## **1.6 Summary**

The evidence for priming of microglia in the ageing brain now forms a robust body of literature. The relevance of microglial priming in accelerating the progression of neurodegenerative disease has been demonstrated using murine models of prion disease (Cunningham et al., 2009) and it remains unknown whether microglia also play a role in the cognitive changes seen over

the course of normal ageing, particularly regarding the loss of myelinated fibres from white matter tracts. What is not well defined is what role microglial priming plays during real infections in aged animals, whether the exaggerated behavioural reactions observed following LPS injection are also present during live infections and how real infections affect microglial phenotypes. There is also little work assessing regional differences in microglial phenotypes and priming in the ageing brain. This thesis aims to shed some light on these questions using intraperitoneal LPS injections and *Salmonella typhimurium* infections in young and aged mice.

## 1.7 Project aims

The specific aims of this project were to:

1. Investigate regional differences in age-associated changes in microglial phenotype.
2. Investigate regional differences in the effects of LPS and *S. typhimurium* infection on microglial phenotype and CNS cytokine production.
3. Characterise and compare the behavioural responses of young and aged mice injected systemically with LPS or infected with *S. typhimurium*.
4. To investigate the effects of *S. typhimurium* infection on paranodal junctions.

## 2. Materials & Methods

### 2.1 Animals

#### 2.1.1 Animal housing

C57BL/6 mice were used in all experiments and were either bred in house or obtained from Charles River (Margate, UK). Mice were housed in groups of 5-10 in plastic cages with sawdust bedding and standard chow diet and water available *ad libitum*. The holding room temperature was kept between 19-23°C with a 12:12 hour light-dark cycle (light on at 0700h). All procedures were performed under the authority of a UK Home Office License in accordance with the UK animals (Scientific Procedures) Act 1986 and after obtaining local ethical approval by the University of Southampton.

#### 2.1.2 Tissue harvesting

Mice were terminally anaesthetized via intraperitoneal injection of either 300-400µl rat avertin ((2,2,2) tribromoethanol in tertiary amyl alcohol) or 150-200µl pentobarbital (5-(1-methylbutyl)-2,4,6(1*H*,3*H*,5*H*)-pyrimidinetrione). Blood samples were collected by cardiac puncture after which the mouse was transcardially perfused with chilled 0.9% saline with heparin (1:1000) (5000 units/ml, CP Pharmaceuticals, Wrexham, UK). For perfusion fixation the mouse was first perfused with heparinised saline, followed by ice-cold 4% paraformaldehyde (PFA) (Fisher Scientific, Loughborough, UK) until the mouse became completely rigid (typically 1-2 minutes). Tissues taken for immunohistochemistry were embedded in optical cutting temperature medium (OCT, Sakura Finetek, Thatcham, UK) and rapidly frozen using isopentane placed on dry ice. Samples were stored at -80°C until required. Tissue taken for post fixation were placed in ice-cold 4% PFA for 4-6 hours and then transferred to 30% sucrose for 24-48 hours, after which tissue was embedded in OCT. Tissue taken for qPCR analysis was placed in an eppendorf tube and snap frozen in liquid nitrogen, then stored at -80°C. The blood sample was kept at RT for a maximum of 4 hours before being centrifuged at 5000RPM for 5 minutes and the serum transferred to a clean eppendorf tube and frozen at -80°C.

### **2.1.3 LPS/saline injection**

Mice received lipopolysaccharide (LPS) derived from *Salmonella abortus equi* (lot 91K4143, Sigma, Poole, UK) at a dose of 100µg/kg via intraperitoneal injection. A 10µg/ml LPS solution was diluted in 0.9% saline from a stock solution of 10 mg/ml for injection. Following injection mice were monitored for the next 6 hours.

### **2.1.4 *Salmonella typhimurium* infection**

Mice were injected intraperitoneally with  $1 \times 10^5$ ,  $3 \times 10^5$  or  $1 \times 10^6$  CFU of attenuated *Salmonella typhimurium* strain SL3261, depending on the experiment (cultured in house by Dr Ursula Püntener; original vial provided by Dr. H Atkins, DSTL, Salisbury, UK). Body weight was monitored daily post infection and mice were culled if their body weight fell to less than 85% of their original pre-infection body weight. In vivo experiments using *S. typhimurium* infected mice were carried out in the category 2 lab within the Southampton University biomedical research facility.

## **2.2 Behavioural assays.**

Behavioural assays were either performed in the category 2 lab or the behaviour rooms of the biomedical research facility, depending whether mice were infected with *S. typhimurium* or injected with LPS. Prior to all tests in the behavioural room, mice were brought into the behavioural room and allowed to habituate to their new environment for at least 20 minutes. In the category 2 lab mice were moved from the incubator to the safety cabinet and left to habituate for at least 20 minutes before commencing behavioural tests.

### **2.2.1 Inverted screen – test of muscle strength.**

The mouse was placed in the middle of a wire mesh screen. The screen was then inverted and suspended approximately half a meter above a bed of soft foam. If the mouse remained inverted for 1 minute the score was recorded as a maximal score of 60 seconds. Otherwise the time of the mouse's fall was recorded. Performance on the inverted screen was rated as described in table 2.1.

Inverted screen latency to fall (s)	Score
1-10	1
11-25	2
26-59	3
>60	4

**Table 2.1. Inverted screen scoring system.**

### 2.2.2 Rod climbing assay – test of forelimb strength.

An L shaped metal rod of 2mm diameter, 28cm in length and with a 2.5cm protrusion at the bottom of the rod was suspended from a wire mesh screen via a hook at the top of the rod. The rod was suspended half a meter above a bed of foam. In this test, the mouse was placed onto the bottom of the rod from where it climbs upwards using its two forepaws, wrapping its hind legs around the rod. The mouse is then given a maximum of 60 seconds to climb the rod and reach the above inverted screen. The time taken to reach the screen is recorded and marked “escape”. If the mouse stays on the rod for 60 seconds but fails to reach the screen a maximal time of 60 seconds is recorded. If the mouse falls the time the mouse fell at is recorded and marked “fall”.

Climbing rod performance	Score
Fell within 1-10s	1
Fell within 11-25s	2
Fell within 26-59s	3
Fell at 60 or more seconds	4
Escaped within 26-59s	5
Escaped within 11-25s	6

Escaped within 1-10s	7
----------------------	---

**Table 2.2. Scoring system for the climbing rod assay.**

### **2.2.3 Multiple Static Rod test – test of balance/co-ordination**

Three rods of varying diameter (experiments using LPS - 35, 22 and 9 mm diameter, experiments using *S. typhimurium* - 15, 12, 9mm diameter), each 60 cm long were fixed on one end to a bench. To attenuate any anxiety of the mice caused by handling the operator positioned their hand in the cage for at least two minutes before beginning the assay. Mice were trained on each of the three rods 24 hours prior to testing.

During testing a mouse was placed at the exposed end of the largest diameter rod with its nose facing away from the bench. The time taken to orientate 180 degrees from the starting position (“orientation”) and the time taken to travel to the bench following orientation (“transit time”) were noted. If the mouse fell or did not reach the platform within 180s it was not tested on the smaller rods. If the mouse turned upside down or slipped and held on with only two paws during the test the result was recorded as “fail”. If the mouse successfully orientated itself and transited from the end of the rod to the bench then the test result was recorded as “pass”. If the mouse failed the test within less than 5s of being placed on the rod it was replaced on the rod and another attempt allowed, for a maximum of three trials. Mice were allowed to recover for at least two minutes between test sessions.

In experiments using LPS, testing was stopped if the mouse turned or fell off a rod after being on it for more than 5s. In experiments using *S. typhimurium*, testing was paused if the mouse turned or fell off a rod after being on it for more than 5s and they were replaced on the rod in the same location. Recording of orientation or transit time resumed once the mouse resumed movement. These transit times were then included in calculation of the mean transit time for that group. The differences between protocols were adaptations to increase the amount of data collected in experiments using *S. typhimurium*.

#### **2.2.4 Rotarod test – test of co-ordination.**

The Ugo Basile 7650 accelerating mouse Rotarod (Ugo Basile, Comerio, Italy) was used to assess balance and co-ordination. The mouse was placed on the rod when rotating at a constant speed of 4 RPM, the lowest speed setting. A total of up to 5 mice were tested simultaneously in parallel bays. Once all mice were on the rod the pressure pads used to detect the fall of a mouse were reset and the rod set to accelerating mode. Latency to fall was recorded, up to a maximal value of 300 seconds. Mice were habituated to the test on two occasions prior to the day of the experiment. Mice that fell within the first 90 seconds of accelerating were replaced on the rod. If the mouse did not fall again within a further 60 seconds then the first sub-90 seconds fall was disregarded. Mice in the first 90 seconds frequently turn around on the rod and attempt to explore their environment rather than running forwards and their falls are often deliberate jumps to another location rather than co-ordination faults, hence the replacement of a mouse if it fell within 90s.

#### **2.2.5 Automated open field test – an assay of spontaneous locomotor activity**

Open-field activity in mice was assessed using a Med Associates Activity Monitor (Med Associates Inc., Vermont). The open field consisted of an aluminium base (27x27 cm) enclosed on four sides with 0.7cm thick acrylic sheet, surrounded by an opaque screen. Each mouse was placed in the middle of the open field and observed for 3 min. During this period the total distance travelled (cm) and the total number of rears was recorded. Mice were not habituated to the open field box prior to use.

#### **2.2.6 Manual open field test - an assay of spontaneous locomotor activity**

For experiments in the category 2 lab it was necessary to perform open field testing manually, due to the absence of automated behavioural equipment within the category 2 lab. To assess open field activity manually a dark blue plastic box measuring 30cm height x 36cm width x 30cm length was used. The floor of the box was divided into 12 quadrants measuring 9 x 10cm,. The mice were habituated to the box for 14 minutes 24h prior to the open field

test. Before any habituation or testing phase the box was cleaned with 70% ethanol. The testing phase starts with the mouse being placed in the proximal right hand corner facing the corner of the box with the operator watching from the proximal right hand corner of the box. The number of rears (where the mouse raises itself on its hind legs) and the number of quadrant entries (defined as when the whole body of the mouse crosses over a line or two intersecting lines i.e. a diagonal) were counted over the course of a 5 minute testing period.

### **2.2.7 Glucose water consumption test**

5% (weight/volume) glucose water was made up on the day of the experiment by dissolving glucose (Sigma, Poole, UK) in tap water. Mice were left overnight with at least 100ml of glucose water and the subsequent change in glucose water bottle weight was measured. Mice were habituated to glucose water overnight in two separate overnight sessions at least 24 hours before performing assay. The glucose water replaced the normal glucose free water as the only fluid source in the cage. The glucose water assay was performed at the same time as the overnight burrowing assay. The mean weight loss from a water bottle which is inverted on two separate occasions with no mouse in the cage was 3 grams (n = 7).

### **2.2.8 Burrowing**

Burrowing tubes (see figure 2.1 for an example) were filled with 190g of food pellets. The burrowing tubes and mice were placed in individual cages lacking any environmental enrichment other than sawdust. Mice were left to burrow for 2 hours and the remaining pellets after 2 hours were weighed. Pellets that have been displaced were then replaced into the tube which was weighed again the following morning, approximately 18 hours since the pellets were replaced. Mice were habituated twice in a group cage with one full burrowing tube and three times in individual cages with a full burrowing tube. A baseline measurement of burrowing performance was recorded 24h prior to the experiment.



**Figure 2.1. An example of a burrowing tube.**

Image taken from (Deacon, 2009).

### **2.2.9 Novel Object Recognition test**

The protocol used for this assay was adapted from Mazarati et al, 2011(Mazarati et al., 2011). The metal box used for testing measured 28cm height x 33cm width x 50cm length and was placed on top of a bench. The box and bench were cleaned with 70% ethanol before and after each test/habituation session, with the box always placed in the same orientation and location on the bench. The mice were habituated to the box during two 5 minute sessions at 24h intervals, which is sufficient to stabilise exploratory locomotor activity (Oliveira et al., 2010) before beginning the familiarisation phase 24h later. During habituation the mice were also handled for one minute each to habituate them to handling. The familiarisation phase consisted of placing two identical objects in opposite corners of the box for either 10 minutes or until the mouse spent 30 seconds investigating each object, depending on the protocol used. The amount of time spent investigating the object was timed using a stopwatch. All objects were cleaned with 70% ethanol before each test.

The testing phase consisted of replacing one of the two identical “familiarised” objects with a novel object and then allowing the mouse to explore the two objects for 5 minutes. To prevent positional bias the position of the novel

object was alternated between the two locations used during the familiarisation phase. Investigation of the object was defined by orientation of the nose towards the object at a distance of no more than 1 cm, including when the mouse was climbing on the object. If the mouse was climbing on the object but orientating its nose away from the object, for example if it was rearing while standing on the object, then this was not included in the time spent investigating the object. All objects were cleaned with 70% ethanol before each test. Testing was performed 90 minutes or 24h after the end of the familiarisation phase.

The two objects in the box were placed approximately 3cm from the corner of the box in opposite corners. They were always placed in the same orientation within the box and relative to each other. After the test the novel object preference ratio was determined using the calculation below:

$$\frac{\text{time spent investigating novel object}}{\text{time spent investigating novel object} + \text{time spent investigating familiar object}}$$

time spent investigating novel object + time spent investigating familiar object

A novel object preference ratio of above 0.5 indicates a preference for the novel object over the familiar object.

#### **2.2.10 Body weight measurement**

Body weight was recorded by taring the weight of a beaker on a weighing scale, placing the mouse inside the beaker and replacing the beaker on the weighing scale. Body weights during *S. typhimurium* infection were always taken at the same time of day (8-10AM).

### **2.3 Immunohistochemistry**

#### **2.3.1 Fresh frozen Sections - DAB staining**

Sections were cut at 10µm thickness on a cryostat, mounted onto 3-aminopropyltriethoxysilane (APES) coated glass slides and stored at -20°C. Sections were dried at 37°C for 30 minutes and then fixed in 100% ethanol at +4°C. After being fixed slides were placed in PBS (appendix 1) to dissolve the remaining OCT. Sections were encircled using a wax pen (DAKO, Ely, UK) and

quenched with 3% H<sub>2</sub>O<sub>2</sub>, (Sigma, Poole, UK) in PBS for 10 minutes followed by 3 x 3 minute PBS washes on an orbital stirrer. Sections were then blocked with 60µl of 1% normal animal serum (Vector Labs, Peterborough, UK) of the same animal as the secondary antibody and 1% Bovine Serum Albumin (BSA) (Sigma, Poole, UK) for 45 minutes at RT in a humidified chamber. The blocking solution was tapped off and replaced with 60µl of primary antibody diluted to desired concentration in PBS. For negative controls the primary antibody was omitted. Sections were incubated with primary antibody in a humidified chamber at 4°C overnight. A list of all primary antibodies used in this thesis is provided in table 2.3.

Following primary antibody incubation slides were washed in PBS 3 x 10 minutes each on an orbital stirrer. 60µl of biotinylated secondary antibody (see table 2.4 for details) was added to each section and incubated at room temperature for 45 minutes. Slides were washed 3 x 3 minutes in PBS.

Sections were then incubated with pre-prepared avidin biotin complex (prepared at least 30 minutes before use) (Vector Laboratories, Peterborough, UK) for 45 minutes at RT in a humidified chamber. Slides were washed 3 x 3 minutes in PBS and during the wash the DAB (3,3'-Diaminobenzidine) solution (Appendix 1) was prepared. Slides were placed in DAB solution for a minimum of 30s, normally 1-2 minutes, depending on the antibody tested. Slides were then placed in PBS, counterstained in Harris Hematoxylin (Sigma, Poole, UK) for 1-4s, washed in tap water, differentiated in acid alcohol (Appendix 1) for 20s, washed in tap water and placed in tap water for 2-3 minutes. Slides were then dehydrated as follows:

Dehydration:

70% alcohol – 60s, 80% alcohol – 60 sec, 95% alcohol – 60 sec, absolute alcohol – 60 sec, absolute alcohol II– 2 min, Xylene I – 5 min, Xylene II – 10 min.

Following dehydration slides were cover-slipped using DPX mounting medium (VWR, Poole, UK) and dried for at least 48h before viewing under a microscope.

Antibody target	Clone	Animal of origin	Source	Dilution
CD11b	5C6	Rat	Serotec (Oxford, UK)	1:500

CD11c	N148	Hamster	Kind gift from Prof. M. Glennie (University of Southampton, UK)	1:500
CD68	FA-11	Rat	Serotec (Oxford, UK)	1:500
F4/80	Cl:A-1	Rat	Serotec (Oxford, UK)	1:250
FcγRI	290322	Rat	R&D Systems (Abingdon, UK)	1:500
MHCII	M5/114.15.2	Rat	Abcam (Cambridge, UK)	1:500
CD16/32	FCR4G8	Rat	Serotec (Oxford, UK)	1:500
Dectin-1	218820	Rat	R&D Systems (Abingdon, UK)	1:500
Ki67	Polyclonal	Rabbit	Abcam (Cambridge, UK)	1:500
DEC-205	NLDC-145	Rat	Serotec (Oxford, UK)	1:500
Collagen IV	Polyclonal	Rabbit	Serotec (Oxford, UK)	1:1000
Neurofascin 155 (Nfasc155)	Polyclonal	Rabbit	Kind gift from Professor Peter Brophy (University of Edinburgh, UK)	1:500
Caspr	S65-35	Mouse	Novus Biologicals (Cambridge, UK)	1:500
Kv1.2	S14-16	Mouse	Novus Biologicals (Cambridge, UK)	1:500
Non-phosphorylated neurofilament H	SMI-32	Mouse	Merck (Nottingham, UK)	1:500

**Table 2.3. A table of all primary antibodies used.**

Antibody (ab)/ Streptavidin	Code & manufacturer	Notes
--------------------------------	------------------------	-------

Goat anti-Hamster ab	BA9100, Vector Laboratories, Peterborough, UK	Affinity purified, biotinylated, used at 1:200 dilution
Rabbit anti-Rat ab	BA4001, Vector Laboratories, Peterborough, UK	Affinity purified, adsorbed, biotinylated, used at 1:100 dilution
Goat anti-Rat ab	BA-9400, Vector Laboratories, Peterborough, UK	Affinity purified, biotinylated, used at 1:200 dilution
Goat anti-Rat ab, 568nm fluorophore tagged	A11077, Invitrogen, Paisley, UK	Used at 1:500 dilution
Donkey anti-Goat ab, 568nm fluorophore tagged	A11057, Invitrogen, Paisley, UK	Used at 1:500 dilution
Donkey anti-Rat ab, 488nm fluorophore tagged	A21208, Invitrogen, Paisley, UK	Used at 1:500 dilution
Donkey anti-Rabbit ab, 568nm fluorophore tagged	A21206, Invitrogen, Paisley, UK	Used at 1:500 dilution
Goat anti-Rabbit ab 568nm fluorophore tagged	A11011, Invitrogen, Paisley, UK	Used at 1:500 dilution
Goat anti-Rabbit ab 488nm fluorophore tagged	A11008, Invitrogen, Paisley, UK	Used at 1:500 dilution
Goat anti-Mouse ab 568nm fluorophore tagged	A11004, Invitrogen, Paisley, UK	Used at 1:500 dilution

Goat anti-Mouse ab 488nm fluorophore tagged	A11029, Invitrogen, Paisley, UK	Used at 1:500 dilution
Streptavidin, 488nm fluorophore tagged	S-11223, Invitrogen, Paisley, UK	Used at 1:500 dilution
Streptavidin, 568nm fluorophore tagged	S-11226, Invitrogen, Paisley, UK	Used at 1:500 dilution

**Table 2.4. A table of all secondary antibodies used.**

### **2.3.2 Fresh frozen sections – fluorescent immunohistochemistry**

Fluorescent immunohistochemistry was performed using the same method as DAB staining up to the secondary antibody step. All staining steps were performed in a dark chamber using fluorescently conjugated antibodies, or streptavidin in the case of biotinylated antibodies. A list of all fluorescently labeled secondary antibodies used is provided in table 2.4. Slides were also incubated with secondary antibodies for a shorter time (30 minutes) at RT. Slides were washed 3 x 3 minutes and then mounted and cover-slipped using DAPI containing Prolong Gold antifade mounting medium (Invitrogen, Paisley, UK) or were counterstained for 10 minutes with Hoechst (Sigma, Poole, UK) or DAPI (Invitrogen, Paisley, UK) nuclear counterstain (1:1000) for 10 minutes, washed 3 x 3 minutes and mounted using Mowiol mounting medium (appendix 1).

### **2.3.3 PFA fixed sections.**

PFA fixed and frozen sections were cut at 10µm thickness and mounted on gelatinised slides (Appendix 1) and stored at -20°C. Sections were dried at 37°C and then placed directly into PBS. Post fixed fresh frozen sections were air dried at 37°C, immersed in 4°C 4% PFA for 10-20 minutes and then washed 3 x 3 minutes in PBS. The slides were then processed as described in 2.3.1 and 2.3.2 after the ethanol fixation step.

## 2.4 Quantitative PCR

### 2.4.1 RNA extraction

RNA was extracted using RNeasy mini kits (Qiagen, Crawley, UK) and treated with a DNase I enzyme to remove any contaminating genomic DNA. Samples were kept on dry ice until use.

Pestles for homogenisation were autoclaved, treated with RNase away (Sigma, Poole, UK) and rinsed with RNase free water before use. RNA was isolated according to manufacturers instructions, with minor modifications. Samples were then homogenised in RLT buffer and beta mercaptoethanol (1:100) using an electronic tissue homogeniser. The homogenised sample was pipetted onto a Qias shredder column and centrifuged at 13000RPM for 6 minutes. 450µL of the homogenised lysate was pipetted from the collection tube into a volume of 450µL of 70% ethanol and triturated until a precipitate formed, at which point 450µL of the sample was transferred to a RNeasy column and centrifuged at 13000RPM for 15 seconds. The liquid that flowed through the RNeasy column and accumulated in the collection tube (the “flow through”) was discarded and the remaining 450µL of sample added to the column and centrifuged at 13000RPM for 15 seconds. The column was then washed by adding 350µL of RW1 buffer to the column and centrifuging at 13000RPM for 15 seconds and discarding the flow through. The RNeasy column was treated with DNase I enzyme (Qiagen, Crawley, UK) for 15 minutes at RT and washed twice with 350µL of RW1 buffer. 500µL of RPE buffer was then added to the RNeasy column and centrifuged for 15 seconds at 13000RPM, after which the flow through was discarded and another 500µL of RPE buffer added to the column and centrifuged for 2 minutes at 13000RPM and the flow through discarded. The RNeasy column was then transferred to a clean collection tube and 30µL of RNase free water added to the column membrane to elute the RNA. 1 minute after adding the water the column was centrifuged at 13000RPM for 1 minute and the eluted RNA/water transferred from the collection tube to a RNase free PCR tube.

RNA yield and quality was assessed using a Nanodrop ND-1000 spectrophotometer (Fisher Scientific, Loughborough, UK). Before use and between samples the Nanodrop was cleaned with a fine tissue dampened with

RNAse free water. 2µL of sample was loaded onto the Nanodrop and the RNA concentration, 260/280 ratio and 260/230 ratio measured. RNA has an absorbance of 260nm, and by using the 260/280 ratio one can obtain some indication of the purity of the sample, with a ratio of less than 2.0 indicating a degree of protein, phenol or ethanol contamination. The 260/230 ratio is also a measure of RNA sample purity, with a ratio of less than 1.8 indicative of contamination with phenol, salts or proteins.

## 2.4.2 Reverse transcription

cDNA was synthesised from RNA using reverse transcription reagents from Applied Biosystems, Warrington, UK. The components of the reverse transcription master mix are listed below in table 2.5:

Reagent	Volume per sample (µL)
10x RT buffer	2
25mm MgCl <sub>2</sub>	4.4
dNTPs mix (stock concentration = 10mM)	4
Random hexamers/dT16s	1
RNAse inhibitor	0.4
Multiscribe RT	0.5
RNA in RNAse free water	400ng in 7.7µL
Total volume	20

**Table 2.5. The reverse transcription master mix components.**

All reagents and RNA were kept on ice until use. The master mix was prepared first, then the required volume of RNAse free water was added to a RNAse free PCR tube and the required volume of RNA was added to bring the total RNA content in the tube to 400ng. The PCR tubes were then placed in a PTC240 tetrad 2 peltier thermal cycler (MJ Research, St Bruno, Canada) and heated to 25°C for 10 minutes, 48°C for 30 minutes, 95°C for 5 minutes and then cooled

to 4°C until removed from the machine. cDNA was then stored at -20°C until required.

### 2.4.3 Quantitative polymerase chain reaction (qPCR)

Either iQ SYBR green supermix or iTaq SYBR green supermix (BioRad, Hemel Hempstead, UK) were used to detect amplification of primer products. The two master mixes are below in tables 2.6 and 2.7.

Reagent	Volume (µL)
iTaq SYBR green supermix	10
DNase free water	4.92
Fwd primer (stock 100µM)	0.04
Rev primer (stock 100µM)	0.04
5µL DNA (1:5 diluted)	5
Final volume	20

**Table 2.6. Reagents used for qPCR when using iTaq SYBR green supermix.**

Reagent	Volume (µL)
iQ SYBR green supermix	6.5
DNase free water	13.4
Fwd primer (stock 100µM)	0.05
Rev primer (stock 100µM)	0.05
5µL DNA (1:5 diluted)	5
Final volume	25

**Table 2.7. Reagents used for qPCR when using iQ SYBR green supermix.**

The master mix was pipetted into a 96 well non-skirted low profile plate (Starlab, Milton Keynes, UK), followed by the cDNA. The plate was covered with clear optical caps and centrifuged for 2 minutes at 3000RPM. The plate was then loaded into a PTC-200 peltier thermal cycler (MJ Research, St Bruno, Canada) and the following cycle started:

1. Incubate at 95°C for 5 minutes
2. Incubate at 95°C for 30 seconds
3. Incubate at 60°C for 1 minute
4. Plate read
5. Incubate at 72°C for 1 minute
6. Return to step 2, repeat 44 more times
7. Construct a melting curve from 55°C to 90°C at intervals of 0.2°C
8. Incubate at 4°C until cycle is terminated.

All samples were pipetted onto the plate in duplicate. A negative control (master mix and DNase free water) and a positive control (master mix and cDNA from a sample with robust expression of the target gene) were included in duplicate on each plate.

Data was recorded using MJ Opticon Monitor 3.1.32 software (BioRad, Hemel Hempstead, UK). This software measures the change in fluorescence in each well after each cycle. A threshold was set on a graph plotting cycle number against fluorescence to determine the cycle number when the fluorescence begins to increase exponentially in each well. This threshold is referred to as the Ct value and provides a relative measure of the quantity of cDNA that the primers have bound to at the beginning of the PCR reaction, and thereby an estimation of the abundance of the transcript of interest within the sample. The threshold was set at 1 x the standard deviation over cycle range after subtracting the average baseline over cycle range. A list of all the primers used during this thesis is provided in table 2.8.

Gene	Primer	Sequence 5' to 3'
ATP5b	Forward	CACGGTCAGAACTATTGCTATG
	Reverse	TCCTTTAATGGTCTCCTTCAA
GAPDH	Forward	TCCACCACCCTGTTGCTGTA

	Reverse	TGAACGGGAAGCTCACTGG
Beta actin	Forward	ATGGATGACGATATCGCT
	Reverse	ATGAGGTAGTCTGTCAGGT
IL-1 $\beta$ (24h time-point LPS)	Forward	CTCCAGGCGGTGCCTATG
	Reverse	ACCGTTTTTCCATCTTCTTCT
IL-1 $\beta$ (3h time-point LPS, <i>S. typhimurium</i> experiments)	Forward	TGTGTTTTCTCCTTGCCTC
	Reverse	CTGCCTAATGTCCCCTTGAA
TNF $\alpha$	Forward	CGAGGACAGCAAGGGACTA
	Reverse	GCCACAAGCAGGAATGAGA
IL-6	Forward	GGATACTACTCCCAACAGACC
	Reverse	GCACAACCTTTTTCTCATTTC
COX-1	Forward	CCAGAACCAGGGTGTCTGTGT
	Reverse	GTAGCCCGTGCGAGTACAATC
COX-2	Forward	GGGTGTCCCTTCACTTCTTTCA
	Reverse	TGGGAGGCACTTGCATTGA
F4/80	Forward	TTACGATGGAATTCTCCTTGTATATCAT
	Reverse	CACAGCAGGAAGGTGGCTATG
PGK1	Forward	GTCGTGATGAGGGTGGACT
	Reverse	TTTGATGCTTGGAACAGCAG
BDNF	Forward	TTCACAGGAGACATAGCAA
	Reverse	CCAACAAGAGACCACAGCA
IFN $\beta$	Forward	CCATCATGAACAACAGGTGGA
	Reverse	GAGAGGGCTGTGGTGGAGAA

**Table 2.8. A list of all primers used throughout this thesis.**

#### 2.4.4 qPCR data analysis – Delta Delta Ct method

This method compares the mean Ct values of the gene of interest against those of a reference gene using the following equation:

$$2^{-\Delta\Delta Ct} = [(Ct \text{ gene of interest} - Ct \text{ internal control}) \text{ sample A} - (Ct \text{ gene of interest} - Ct \text{ internal control}) \text{ sample B}]$$

Sample A was always the treated sample e.g. *S. typhimurium* infection, Sample B was the control sample e.g. saline injected. Changes in the delta delta Ct were always expressed as fold change from young, saline treated samples.

#### **2.4.5 Agarose gel for PCR products**

To check the specificity of the products of new primers, the amplification product of a positive control sample was loaded on an agarose gel. The gel was made by adding 1.8g of agarose to 100ml 1 x TAE buffer (Appendix 1), heating in a 800W microwave at high power for 1 ½ minutes to dissolve the agarose and then adding 3µL of ethidium bromide (Fisher Scientific, Loughborough, UK). This solution was mixed and then poured into a cast with a 20 well comb at one end and left to set for 30 minutes. Once the gel had set it was placed in an electrophoresis tank with the comb at the negative end and covered with 1x TAE buffer. The comb was removed and the wells filled with a mixture of 10µL of loading buffer (Appendix 1) and 12.5µL of sample. 4µL of a 1kb ladder (Fisher Scientific, Loughborough, UK) was loaded onto one end of the gel with 10µL of loading buffer. The gel was run at 85V for 15-30 minutes and pictures taken using a High Performance Ultraviolet Transilluminator (UVP, Cambridge, UK). Primers were deemed specific if there was a single clear band on the gel at the anticipated molecular weight for the primers' product.

## **2.5 Enzyme-linked immunosorbent assay (ELISA)**

Serum samples were collected upon exsanguination as described in section 2.1.2. IL-6 levels were measured by ELISA (R&D Systems, Abingdon, UK, mouse IL-6 kit) according to the manufacturer's instructions with minor adaptations. The mouse IL-6 kit provided the substrate solution, capture antibody, detection antibody and standard for the ELISA.

First the capture antibody was diluted to a working concentration of 2.0µg/mL in PBS. A 96-well Maxisorp microplate (Nunc, Fisher Scientific, Loughborough, UK) was coated with 100µL per well of the diluted capture antibody. The plate was sealed and incubated overnight at RT. The following morning each well was aspirated and washed with wash buffer, repeating the process two times for a total of three washes. Each well was washed by filling with 400µL of wash

buffer (0.05% PBS-tween). Any remaining wash buffer was removed by inverting the plate and blotting it against clean paper towels. Plates were then blocked by adding 300 $\mu$ L of reagent diluent (1% BSA in PBS) to each well and incubating at room temperature for a minimum of 1 hour. The wells were then washed as previously described.

100 $\mu$ L of undiluted sample or standards (1000pg/ml IL-6 diluted in reagent diluent, 7x1:2 serial dilutions, 1 dilution per well) were added per well. The plate was covered with an adhesive strip and incubated for 2h at RT. Following incubation the wells were washed with wash buffer and 100 $\mu$ L of the detection antibody (diluted to 200ng/ml in reagent diluent) added. The plate was then covered with a new adhesive strip, incubated for 1h at RT and shaken vigorously.

After one hour the wells were washed again as previously described and 100 $\mu$ L of poly-Streptavidin-HRP (Sanquin, Amsterdam, Netherlands) diluted 1:10000 in reagent diluent to each well. The plate was covered with a new adhesive strip and incubated for 30 minutes at RT and covered with tin foil. After another wash 100 $\mu$ L of Substrate Solution (1:1 mix of H<sub>2</sub>O<sub>2</sub> and tetramethylbenzidine) was added to each well and the plate incubated for 20 minutes at room temperature covered in tin foil. After 20 minutes 50 $\mu$ L of 2M H<sub>2</sub>SO<sub>4</sub> was added to each well and the plate gently tapped to ensure thorough mixing. After the addition of H<sub>2</sub>SO<sub>4</sub> the optical density of each well was determined as using a microplate reader set to 450nm with wavelength correction.

## **2.6 Meso Scale Discovery multiplex cytokine measurements**

Serum cytokine measurements were obtained using a MSD multiplex kit ((K15012B) Meso Scale Discovery, Gaithersburg, MD, USA) following the manufacturer's instructions.

First the plate calibrator was prepared through serial dilution of the stock solution in diluent 4. The detection antibody and read buffer were diluted from their stock vials 1:50 in diluent 5 and 1:2 in distilled water respectively. 25 $\mu$ L of diluent 4 was added to each well and the plate was covered with an adhesive strip before incubating for 30 minutes at RT while being shaken at

500 RPM. 25µL of sample or calibrator were then added to the diluent 4 in each well and triturated before re-covering the plate and incubating for 2 hours at room temperature while being shaken at 500RPM. The plate was washed 3 times with 0.05% PBS-tween and 25µL of detection antibody solution added to each well before sealing and incubating at RT for 2 hours while being shaken at 500RPM in the dark. The plate was then washed 3 times in 0.05% PBS-tween and 150µL of read buffer added to each well before reading the plate using a Sector Imager 2400 (MesoScale Discovery, Gaithersburg, MD, USA). After reading data was analysed using MSD Discovery Workbench software (MesoScale Discovery, Gaithersburg, MD, USA) to fit standard curves using the calibrator samples and the sample values obtained by comparing their values to the standard curve.

## **2.7 Statistical analysis**

Normality of data was tested using the D'Agostino-Pearson omnibus test on either individual groups or on the residuals (sample value - group mean) of all the data points within an analysis. All tests were performed in either Sigmaplot 11.0 or 12.0 or GraphPad Prism 5.0 or 6.0. Normally distributed data was analysed using student's t-tests, one, two or three way ANOVAs and Holm-Sidak post tests. Data that was not normally distributed was logarithmically transformed to achieve normality. If after logarithmic transformation the data was still not normally distributed then data was analysed using non-parametric tests, such as then Kruskal-Wallis test with Dunnet's post hoc tests or Mann-Whitney U tests. Data arranged in frequency tables were analysed using a partitioned Chi squared test (Kimball, 1954).

### **3. Characterisation of the behavioural response to LPS in young, middle-aged and aged mice**

#### **3.1 Introduction**

There is a growing literature that suggests ageing causes exaggerated and prolonged behavioural reactions to systemic inflammation (Barrientos et al., 2009b; Chen et al., 2008; Godbout et al., 2005b). Intraperitoneal injection of 333-500µg/kg of LPS in aged mice causes prolonged reductions in locomotor activity, exaggerated and prolonged deficits in social interaction, exaggerated reductions in weight loss and food intake (Godbout et al., 2005b), prolonged depressive behaviour (Godbout et al., 2008) and working memory deficits (Chen et al., 2008). Many of these effects have been associated with increased hippocampal neuroinflammation (Chen et al., 2008; Godbout et al., 2005b).

In contrast there have been fewer investigations into the effects of systemic inflammation on performance of aged mice behaviours that are dependent on the function of other brain regions, such as the cerebellum. Ageing causes a decline in performance in the eye blink conditioning test (Woodruff-Pak et al., 2010), a cerebellum dependent assay, and there is a progressive loss of Purkinje neurons in the aged brain (Woodruff-Pak et al., 2010), loss of which can cause deficits in tasks which assess co-ordination and balance (Chen et al., 1996; Kyuhou et al., 2006). A rostral-caudal gradient of age-related increases in microglial expression of CD11b and CD68 has been shown previously (Kullberg et al., 2001), suggesting that the microglia of caudal brain areas such as the cerebellum may be affected by ageing differently to those in brain areas such as the hippocampus. To test this hypothesis, cerebellar dependent behaviours were assessed following LPS-mediated systemic inflammation as well as sickness behaviours in which the hippocampus plays a role, such as burrowing (Deacon et al., 2002; Teeling et al., 2007). Young, middle-aged and aged mice were injected with 100µg/kg of LPS and behavioural assays were performed over the next 24 hours.

## **3.2 Materials and Methods**

### **3.2.1 Animals**

C57/Bl6 mice (Harlan, UK, bred in house) were used in this experiment. Young mice were 4 months old, middle-aged mice were 11-13 months old and aged mice were 20-21 months old. Young and aged mice were female, middle-aged mice were male. An additional group of young mice fed on a high fat diet were used to control for the effect of weight differences on performance in the static rod test and rotarod assay. High fat diet mice were given chow diet supplemented with 18% (w/w) animal lard and additional vitamins, minerals, protein and choline (Special Diet Services, Witham, UK) (Lanham S.A. et al., 2010) (Appendix 1). High fat diet mice were kindly provided by Felino Cagampang and Kim Bruce (University of Southampton). All procedures were performed under the authority of a UK Home Office License in accordance with the UK animals (Scientific Procedures) Act 1986, and after obtaining local ethical approval by the University of Southampton.

### **3.2.2 Procedures**

Mice were injected intraperitoneally with either 100µg/kg of LPS (batch 91K4143, Sigma, Poole, UK) or 200µL of saline. Mice were culled 24 hours after injection. Mice were terminally anaesthetised and perfused with heparinised saline as described in Chapter 2.

### **3.2.3 Behavioural assays**

Behavioural assays were performed as described in Chapter 2. Assistance was received while performing behavioural assays from Steven Booth (University of Southampton). Figure 3.1 is a schematic illustrating the timing of different behavioural tests during the experiment. All baseline measurements were taken 24 hours before injection of LPS or saline, except for the inverted screen test and climbing rod test, which were tested 48 hours before injection. The amount of training mice underwent for each test is outlined below:

Burrowing: the week before the experiment commenced mice were presented with a full tube of food pellets in their home cages overnight on two consecutive days. In the next three consecutive days mice were placed in

individual cages overnight with a full tube of food pellets. Mice were then rested from burrowing for the next two days before baseline readings were taken.

Open field test: mice were not trained in the open field test before commencing testing.

Glucose water consumption: during individual training for burrowing mice were left with a bottle of glucose water overnight on two separate occasions.

Rotarod test: mice were trained on the rotarod on two separate occasions in the two days preceding baseline measurements.

Static rod test: mice were trained on each of the static rods on one occasion the day before baseline recordings.

Inverted screen test: mice were not trained for this assay.

Climbing rod test: mice were not trained for this assay.

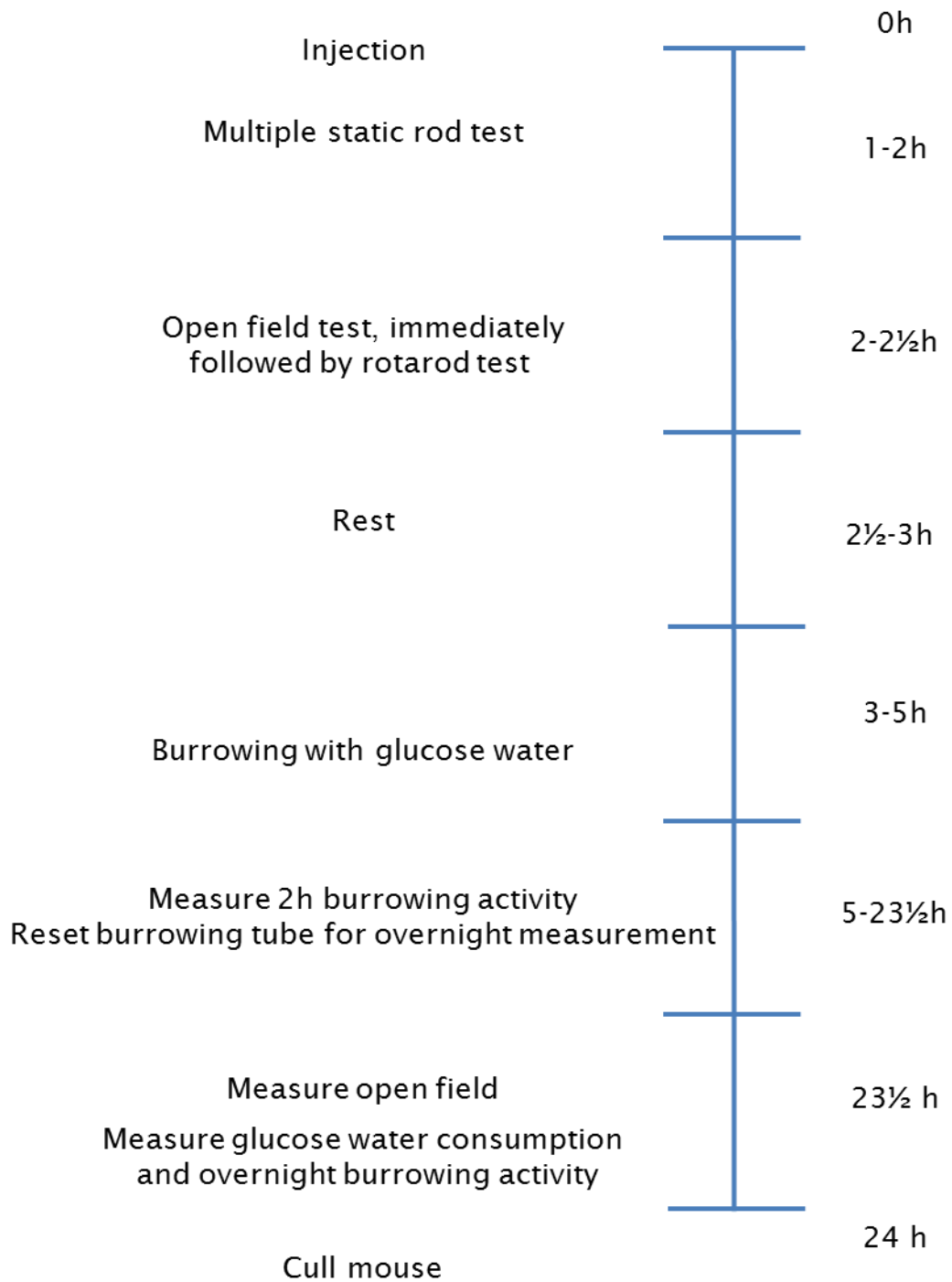


**Figure 3.1. A timeline illustrating the sequence of behavioural tests performed.**

LPS injections were carried out at 9am, saline injections were carried out at 11am.

### 3.3 Results

#### 3.3.1 Sickness behaviours

LPS injection induced a greater weight change than saline (2 way ANOVA: LPS:  $F_{1,75} = 35.47$ ;  $p < 0.0001$ ) (Figure 3.2), but there was no significant interaction between age and LPS (LPS x age interaction:  $F_{2,75} = 1.498$ ;  $p = 0.232$ ). Age alone exerted a significant effect on body weight (age: two way ANOVA  $F_{2,75} = 3.964$ ;  $p = 0.0231$ ). The statistically significant effect of age rather than an age x LPS interaction is probably due to the small decline in body weight in saline injected mice that occurs in saline injected mice. Holm-Sidak post tests only showed a significant effect of LPS in the middle-aged and aged groups.

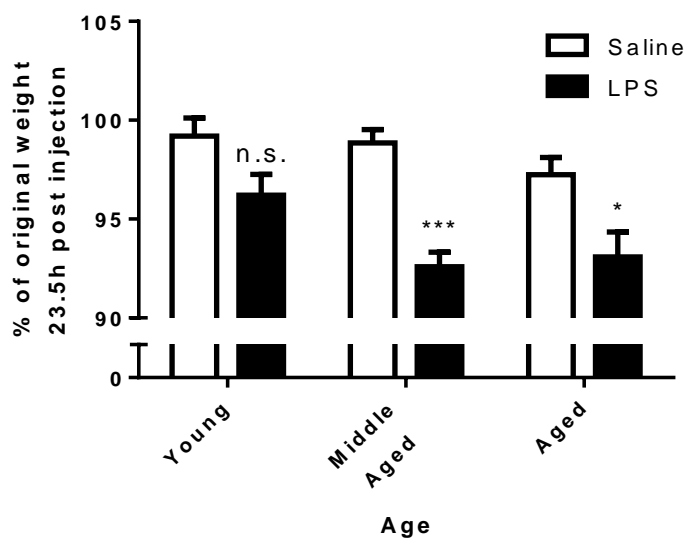


**Figure 3.2. The effect of LPS or saline injection on body weight.**

Weight was measured 24h before injection and 23.5h after injection and the percentage change in weight calculated for aged, middle-aged and young mice. LPS injection elicits a greater change in body weight than saline injection, and this decrease was more pronounced in middle-aged and aged mice than young mice. Bars represent means  $\pm$  SEM.  $n = 11$  for aged saline injected mice,  $n = 14$  for middle-aged and aged LPS injected mice,  $n = 12$  for middle-aged saline injected mice,  $n = 15$  for young saline/LPS injected mice. Stars indicate a

significant difference saline and LPS group (Holm-Sidak post test). \* =  $p < 0.05$ , \*\*\* =  $p < 0.001$ .

Between 3-5 hours after LPS injection all mice showed a decline in burrowing, with a greater decline in burrowing activity in both middle-aged and aged mice compared to young mice (Figure 3.3) (Kruskal-Wallis test: LPS group:  $\chi^2 = 19.38$ , d.f. = 2, effect of age  $p < 0.0001$ ). Data was not normally distributed and was therefore analysed non-parametrically using separate Kruskal-Wallis tests on the LPS and saline groups. Most LPS injected aged mice failed to show any burrowing activity between 3-5 hours (median = 0%), and the activity in middle-aged mice was negligible (median = 1.6%). In comparison, most young mice retained a degree of burrowing activity (median = 12.1%). There was no age related effect of injection on burrowing within the saline treated group ( $\chi^2 = 1.574$ , d.f. = 2,  $p = 0.455$ ). Analysis by Dunnett's post hoc tests showed that LPS has a greater effect on middle-aged and aged mice compared to young mice ( $p < 0.05$ ).

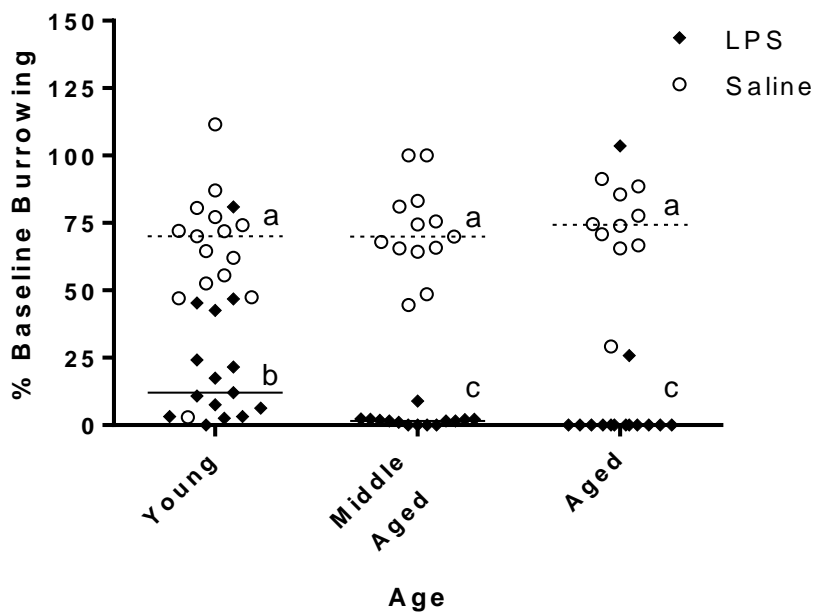


**Figure 3.3. 2h Burrowing performance after injection of LPS or saline.**

Burrowing performance is represented as percentage of baseline burrowing activity over 2 hours between 3-5 hours after injection. Baseline burrowing activity was represented as percentage of 190g of food pellets displaced. Bars represent medians +/- SEM.  $n = 10$  for aged saline injected mice,  $n = 14$  for

aged LPS injected mice, n = 13-14 for middle-aged saline/LPS injected mice and n = 15 for young saline/LPS injected mice. Medians with different letters are significantly different ( $p < 0.05$ ) from each other (Dunnett's post hoc tests).

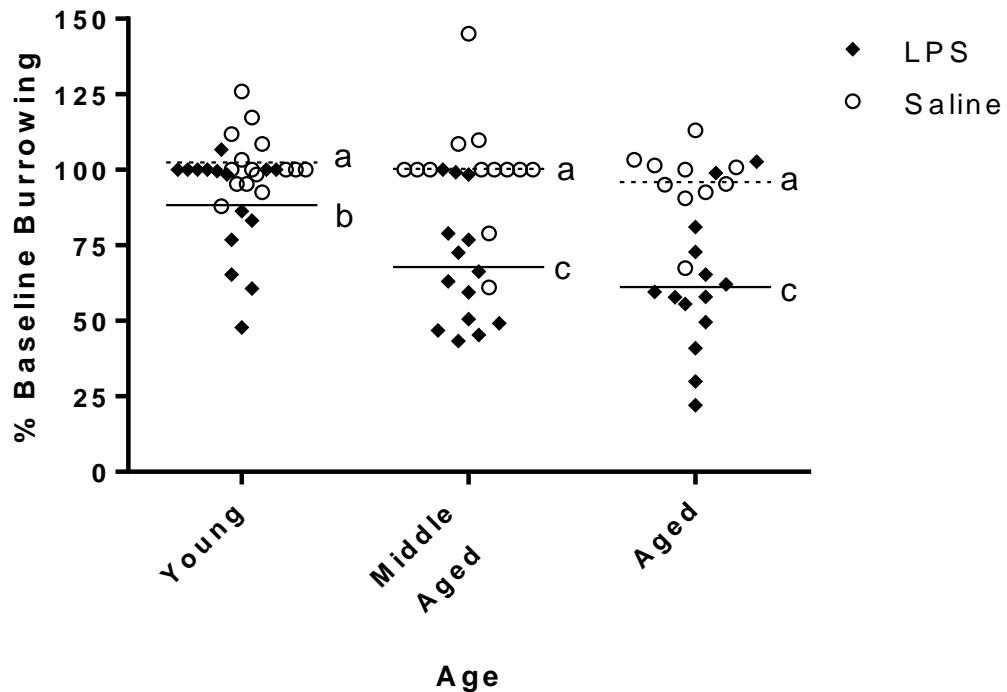


**Figure 3.4. Overnight burrowing performance after injection of LPS or saline.**

Burrowing performance is represented as percentage of baseline burrowing activity over 18 hours between 5.5-23.5 hours after i.p. injection. Baseline burrowing activity was represented as percentage of 190g of food pellets displaced. Bars represent means  $\pm$  SEM. n = 10 for aged saline injected mice, n = 14 for aged LPS injected mice, n = 13-14 for middle-aged saline/LPS injected mice and n = 15 for young saline/LPS injected mice. Means with different letters are significantly different ( $p < 0.05$ ) from each other (Holm Sidak post tests).

After measuring the pellets displaced within 2h, the food pellets were returned to the tube and mice were allowed to burrow overnight between 5.5-23.5 hours after LPS or saline injection. LPS challenged mice partially recovered their burrowing activity overnight (Figure 3.4), but this recovery was attenuated in middle-aged and aged mice compared to young mice (young vs middle-

aged/aged group  $p < 0.001$ ,  $n = 14-15$ ). Age and LPS both had a significant effect on overnight burrowing (Two way ANOVA: Age:  $F_{2, 75} = 6.362$ ,  $p < 0.01$ . LPS:  $F_{1, 75} = 46.52$ ,  $P < 0.0001$ ). In addition a strong trend towards an interaction between the two factors was detectable (Age  $\times$  LPS:  $F_{2, 75} = 2.852$ ,  $p = 0.064$ ). Taken together, these data show that the effects of LPS are more pronounced and prolonged in middle-aged and aged mice than in young mice.

There was also an effect of age alone on baseline burrowing activity (Figure 3.5). Age significantly affected burrowing activity over two hours (Kruskal-Wallis test:  $\chi^2 = 19.36$ , d.f. = 2,  $p < 0.0001$ ) or overnight ( $\chi^2 = 13.04$ , d.f. = 2,  $p = 0.0015$ ). Only aged mice demonstrated this decrease in burrowing activity, which was significantly reduced compared to either young or middle-aged mice (Dunnet's post test,  $P < 0.01$ ).

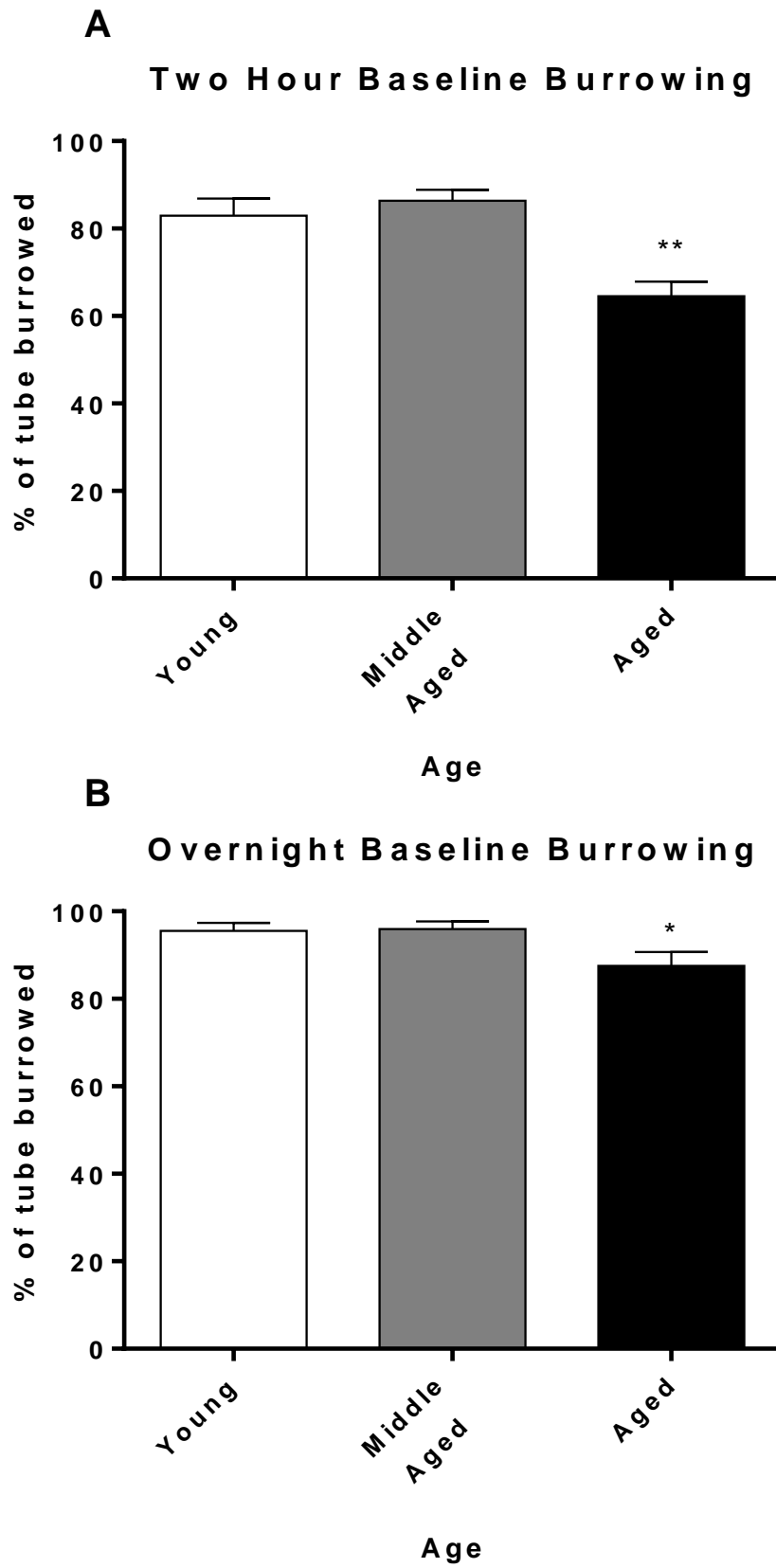


Figure 3.5. The effect of ageing on baseline burrowing activity.

Aged mice burrowed less than young or middle-aged mice over two hours ( $p < 0.001$ ) (A) or overnight (B) ( $p < 0.01$ ). Bars represent means  $\pm$  SEM.  $n = 24$  for aged mice,  $n = 27$  for middle-aged mice and  $n = 30$  for young mice.

Glucose water consumption was assessed between 3-23.5 hours after injection with LPS. Analysis of glucose water consumption as percentage of baseline consumption showed a significant reduction after injection of LPS compared to saline (two way ANOVA:  $F_{1,73} = 27.02$ ;  $p < 0.0001$ ) (Figure 3.6). Age also had a significant effect on glucose water consumption, with both saline and LPS treatment leading a greater decrease in glucose water consumption in middle-aged or aged than young mice (age:  $F_{2,73} = 5.812$ ;  $p < 0.01$ ). There was no interaction between age and LPS treatment on glucose water consumption (age  $\times$  LPS:  $F_{2,73} = 0.643$ ;  $p = 0.529$ ). Holm-Sidak post tests showed that all age groups consumed significantly less glucose water following injection with LPS compared to saline injected mice ( $p < 0.05$ ).

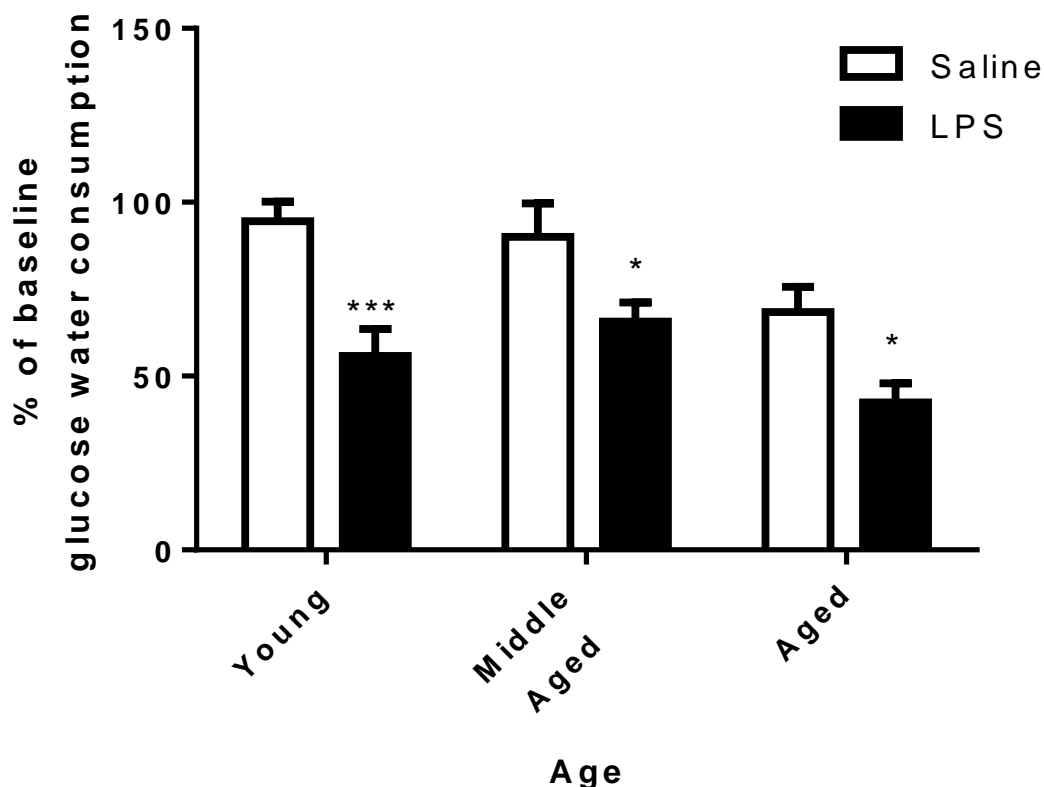
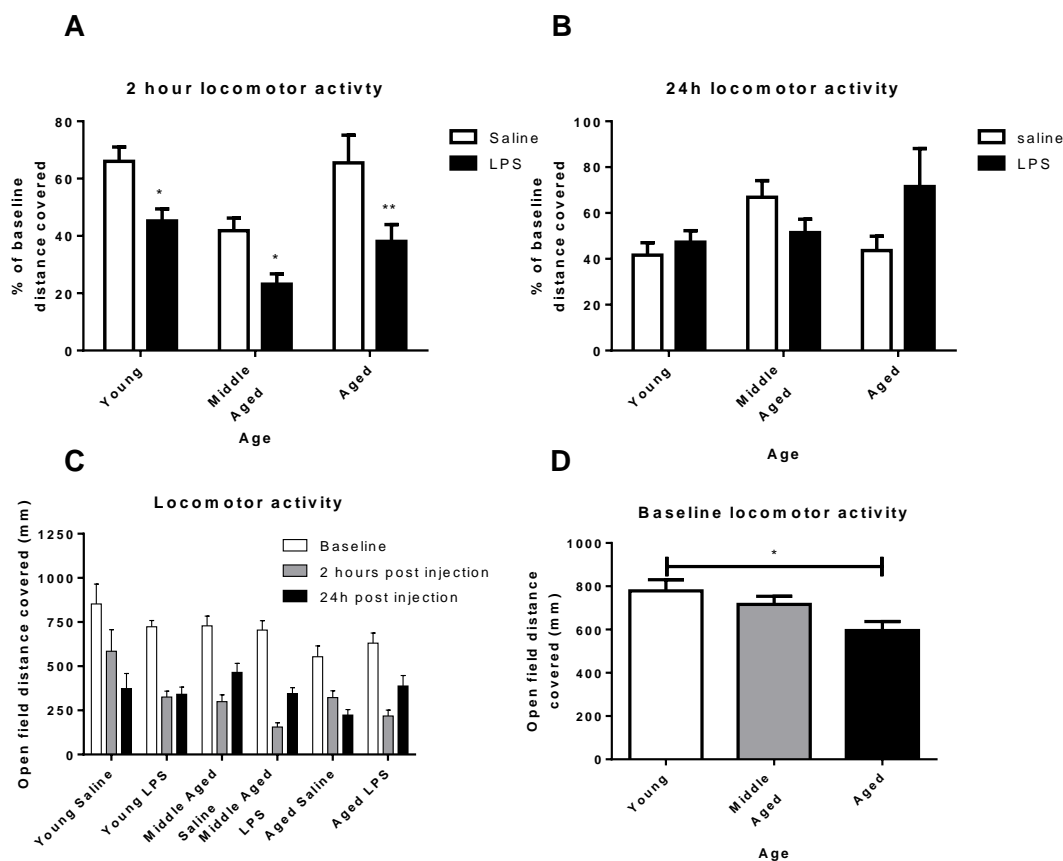


Figure 3.6. The effect of LPS or saline injection on glucose water consumption.

LPS and age had a significant effect on glucose water consumption vs saline ( $p < 0.01$ ), but there was no interaction between the two groups. Bars represent means  $\pm$  SEM.  $n = 11$  for aged saline injected mice,  $n = 13$  for aged injected mice,  $n = 13$  for middle-aged saline injected mice,  $n = 14$  for middle-aged LPS injected mice,  $n = 14$  for young saline/LPS injected mice. Stars indicate a significant difference saline and LPS group. \* =  $p < 0.05$ , \*\*\* =  $p < 0.001$ .

Open field activity was assessed at baseline, 2 hours after injection and 24 hours after injection. Mice were not habituated to the open field box prior to baseline measurement. Two hours after injection all groups had reduced locomotor activity (Figure 3.7 A), but this reduction was more pronounced in LPS injected mice than saline injected mice (two way ANOVA on logarithmically transformed values: LPS:  $F_{1,71} = 24.46$ ,  $P < 0.0001$ ). There was also a significant effect of age (age:  $F_{2,71} = 10.48$ ,  $p = 0.0001$ ), but there was no interaction between age and LPS (age  $\times$  LPS:  $F_{2,71} = 0.332$ ,  $p = 0.719$ ). LPS injected mice had significantly lower locomotor activity than saline injected mice at each age group (Holm-Sidak post tests,  $p < 0.05$ ). 24 hours after injection (Figure 3.7 B) there was no longer any significant effect of LPS injection (two way ANOVA on logarithmically transformed values: LPS:  $F_{1,71} = 0.705$ ,  $p = 0.404$ ) or age (age:  $F_{2,71} = 1.693$ ,  $p = 0.191$ ). There was no interaction between the two factors (age  $\times$  LPS:  $F_{2,71} = 3.016$ ,  $p = 0.0553$ ). Baseline locomotor activity was affected by ageing (Kruskal-Wallis test: d.f.= 2,  $\chi^2 = 8.225$ ,  $p < 0.0164$ ) and was significantly reduced in aged mice compared to young mice ( $p < 0.05$ ).



**Figure 3.7 The effect of LPS and saline on open field locomotor activity.**

(A) Locomotor activity 2h after injection expressed as percentage of baseline. (B) Locomotor activity 24h after injection expressed as percentage of baseline. (C) - Open field locomotor activity at all time-points expressed as total distance covered. (D) - Baseline locomotor activity. Bars represent means +/- SEM. n = 11 for aged saline injected mice, n = 14 for aged LPS injected mice, n = 13-14 for middle-aged saline/LPS injected mice and n = 15 for young saline/LPS injected mice. \* = p<0.05, \*\*\* = p<0.001.

Rearing activity was also measured during the open field assay. Similarly to locomotor activity, two hours after injection all groups had reduced rearing activity (Figure 3.8 A), but this reduction was more pronounced in LPS injected mice than saline injected mice (two way ANOVA on logarithmically transformed values: LPS:  $F_{1,72} = 20.97$ ,  $P < 0.0001$ ). There was also a significant effect of age (age:  $F_{2,72} = 20.94$ ,  $p = 0.0001$ ), but there was no interaction between age and LPS (age x LPS:  $F_{2,72} = 0.36$ ,  $p = 0.700$ ). LPS injected mice had significantly lower locomotor activity than saline injected mice in the middle-aged and aged

groups, but not the young group (Holm-Sidak post tests,  $p < 0.05$ ). 24 hours after injection (Figure 3.8 B) there was no longer any significant effect of LPS injection (two way ANOVA on logarithmically transformed values:  $F_{1,72} = 0.169$ ,  $p = 0.845$ ) or age ( $F_{2,72} = 0.382$ ,  $p = 0.538$ ). There was no interaction between the two factors (age x LPS:  $F_{2,72} = 0.843$ ,  $p = 0.435$ ). Baseline rearing activity was affected by ageing (one way ANOVA:  $F_{2,75} = 15.75$ ,  $p < 0.0001$ ) and was significantly reduced in aged mice compared to young or middle-aged mice ( $p < 0.001$ ).

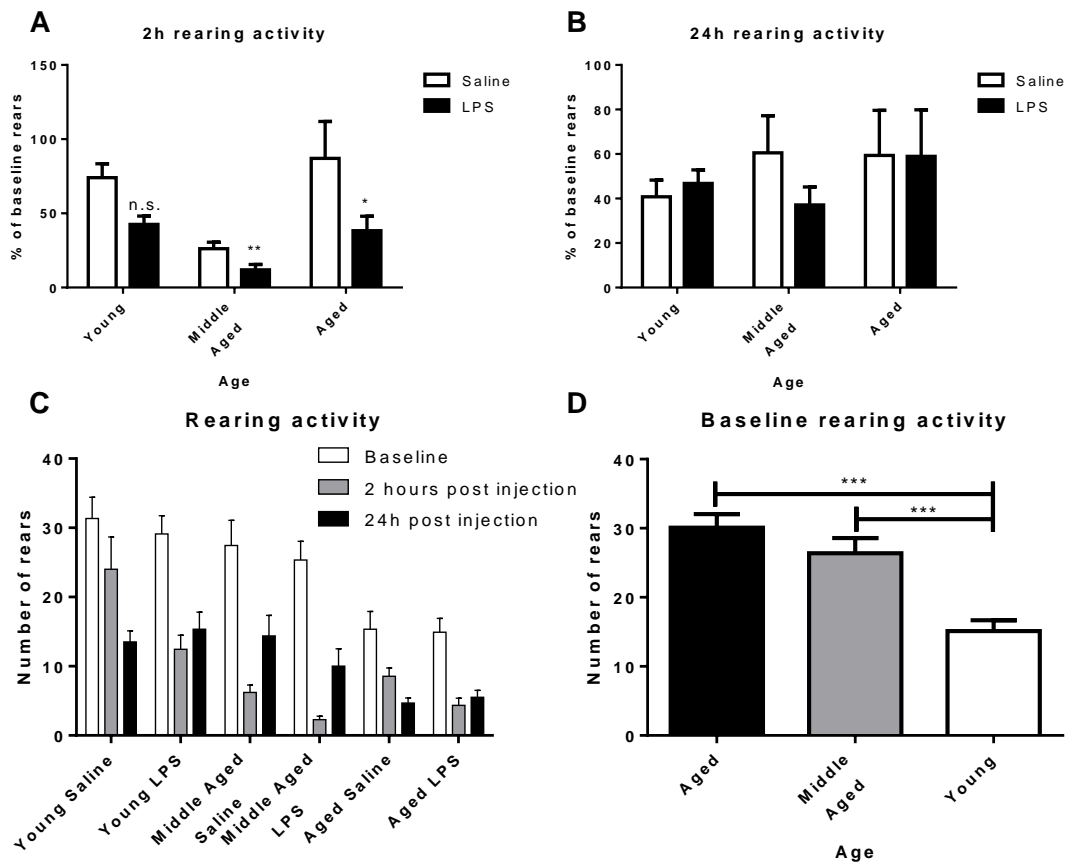


**Figure 3.8. The effects of LPS or saline injection on open field rearing activity.**

(A) Rearing activity 2h after injection expressed as percentage of baseline. (B) Rearing activity 24h after injection expressed as percentage of baseline. (C) Open field rearing activity at all time-points expressed as total number of rears. (D) Baseline rearing activity. Bars represent means  $\pm$  SEM.  $n = 11$  for aged saline injected mice,  $n = 14$  for aged LPS injected mice,  $n = 13-14$  for

middle-aged saline/LPS injected mice and n = 15 for young saline/LPS injected mice.

### 3.3.2 Co-ordination and motor function assays

When taking baseline measurements of these mice body weight differences were observed between the groups (Kruskal Wallis test:  $\chi^2 = 65.60$ , d.f. = 2,  $p < 0.0001$ ) (Figure 3.9). All three age groups were significantly different from each other in weight (Dunnett's post test,  $p < 0.01$ ), with middle-aged males heaviest (mean weight = 34g), then aged females (mean weight = 28.5g) followed by young females (mean weight = 22.9g). These differences in weight were deemed a potentially confounding factor in assays where a degree of balance is required e.g. the static rod test. To determine if body weight affects performance in tests of co-ordination and balance, data was gathered from young mice that were fed a high fat diet and/or were the offspring of a mother fed a high fat diet, and therefore weighed more than age matched mice fed on a standard diet. These mice are labelled as "HF" in all figures in this chapter. Mice between 30-40g were selected (mean weight = 34.8g) for inclusion in this control group.

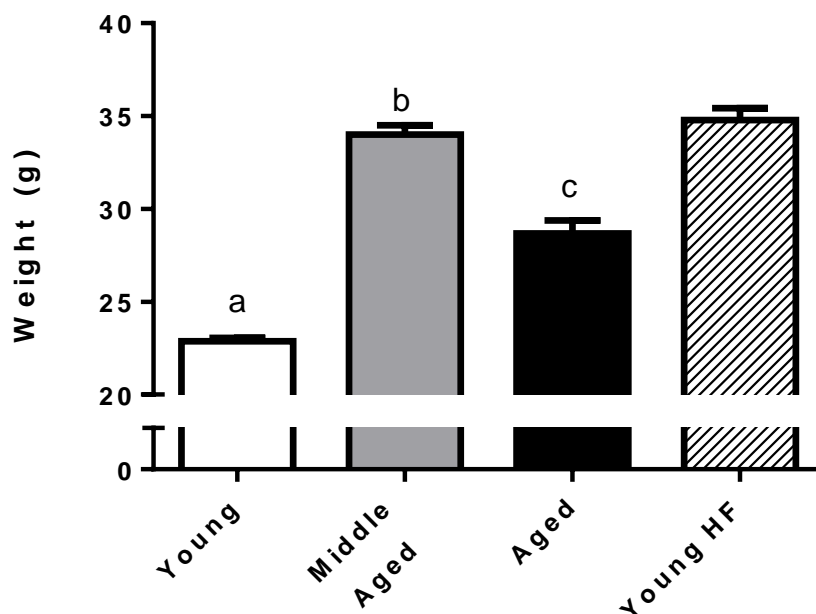
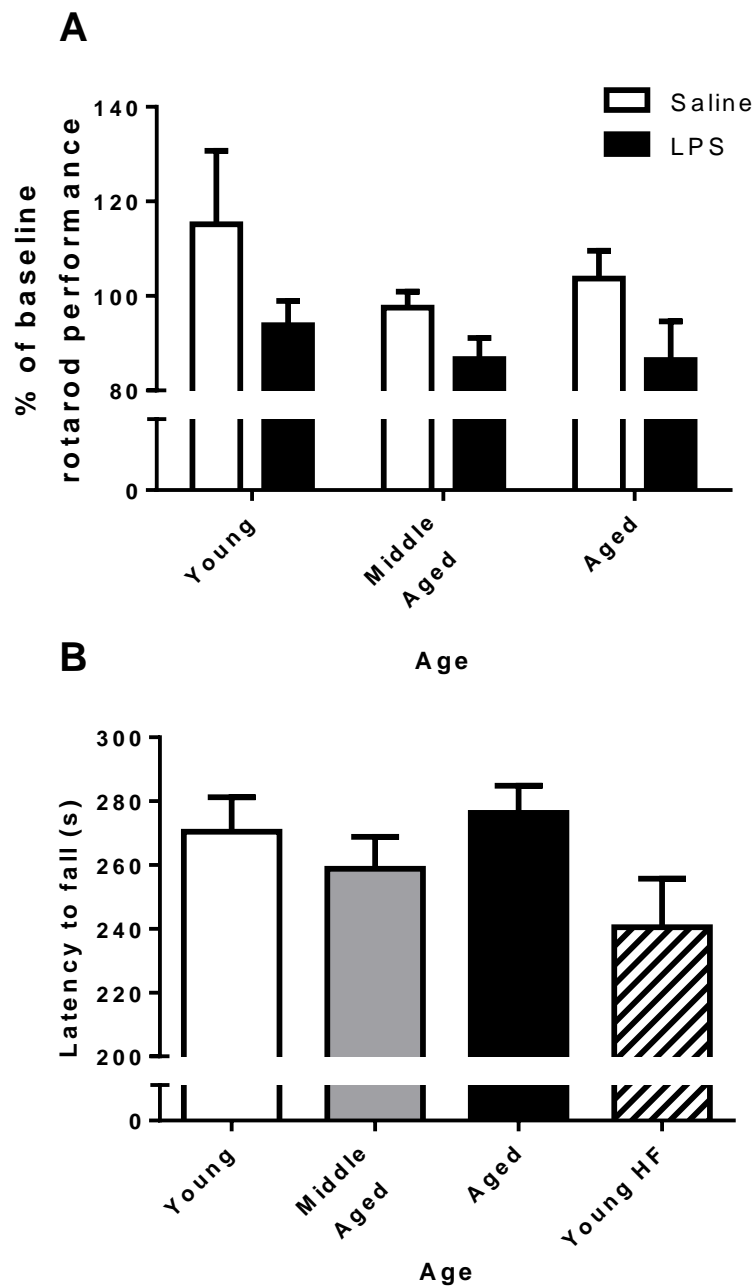


Figure 3.9. Average body weight at baseline.

Aged, middle aged and young mice all have significantly different weights to each other. Bars represent means +/- SEM. n = 25 for aged mice, n = 27 for middle-aged mice, n = 30 for young standard diet mice, n = 23 for young high fat diet mice. Means with different letters are significantly different ( $p < 0.01$ ) from each other (Kruskal-Wallis test and Dunnett's post tests).

Mice were tested on a rotarod at baseline and 2-2.5 hours after injection of LPS or saline. The groups did not differ significantly in their performance at baseline (Figure 3.10 B) (Kruskal-Wallis test;  $\chi^2 = 6.815$ , d.f. = 3,  $p = 0.0780$ ). Mice injected with LPS performed worse in the rotarod test than mice injected with saline (two way ANOVA: LPS:  $F_{1,75} = 6749$ ;  $p = 0.0113$ ) (Figure 3.10), but age had no effect (age:  $F_{2,75} = 1.702$ ;  $p = 0.189$ ) and no interaction with LPS treatment was observed (age x LPS  $F_{2,75} = 0.697$ ;  $p = 0.363$ ). As some groups were not normally distributed, non-parametric analysis of the effect of age within the LPS or saline groups was also performed. There was no effect of age within the LPS (Kruskal-Wallis test:  $\chi^2 = 0.9149$ , d.f. = 2,  $p = 0.633$ ) or saline ( $\chi^2 = 2.971$ , d.f. = 2,  $p = 0.226$ ) group.



**Figure 3.10. The effect of LPS or saline injection on rotarod performance.**

**(A)** LPS causes a decrease in rotarod performance compared to saline injection. Data is expressed as percentage of baseline performance. **(B)** Baseline rotarod performance. Data is expressed as latency to fall. Bars represent means  $\pm$  SEM.  $n = 11$  for aged saline injected mice,  $n = 14$  for aged LPS injected mice,  $n = 13-14$  for middle-aged saline/LPS injected mice and  $n = 17-18$  for young saline/LPS injected standard diet mice,  $n = 23$  for young high fat diet mice. Baseline data is pooled from saline and LPS groups of the same age.

Mice were tested in the multiple static rod test at baseline and between 1-2h after injection. Mice from all groups successfully traversed the 35mm and 22mm diameter rods at baseline and after injection. On the 9mm rod performance at baseline varied, with some mice failing to successfully traverse the rod (Figure 3.11). These attempts were marked as pass/fail. Data was analysed by Chi-squared analysis and partitioned for comparison between individual groups as described by Kimball (Kimball, 1954). Initial Chi-squared analysis of baseline static rod performance showed a significant difference between age groups in pass/fail ratios on the 9mm static rod ( $\chi^2 = 65.09$ , d.f. = 9,  $p < 0.0001$ ) (Figure 3.11). There was a significant difference in fail rates between aged (68%,  $\chi^2 = 24.08$ ,  $n = 25$ ) and middle-aged mice (46%,  $\chi^2 = 10.19$ ,  $n = 26$ ) when compared to young mice (7%,  $n = 30$ ). Analysis of baseline transit times was performed using a one way ANOVA of logarithmically transformed data followed by Holm-Sidak post tests. Baseline transit times also showed a significant effect of age ( $F_{3,55} = 23.75$ ,  $p < 0.0001$ ) and a significant difference between all three age groups ( $p < 0.05$ ) (Figure 3.12). Injection of LPS or saline did not have a significant effect on pass/fail rates at any age and there were not sufficient successful completions of the test in the aged mice to test for differences in transit times after injection.

To control for variations in weight between different groups of mice high fat diet mice were also tested on the 9mm static rod. The high fat diet group's performance was equivalent to the middle-aged mice in terms of pass/fail ratio and transit time, but worse in both measures than the young mice raised on a standard diet ( $p < 0.01$ ). However, aged mice performed worse than the high fat diet group in both transit time ( $p < 0.05$ ) and pass/fail ratio ( $\chi^2 = 7.32$ ,  $p < 0.01$ ), despite having a lower body weight.

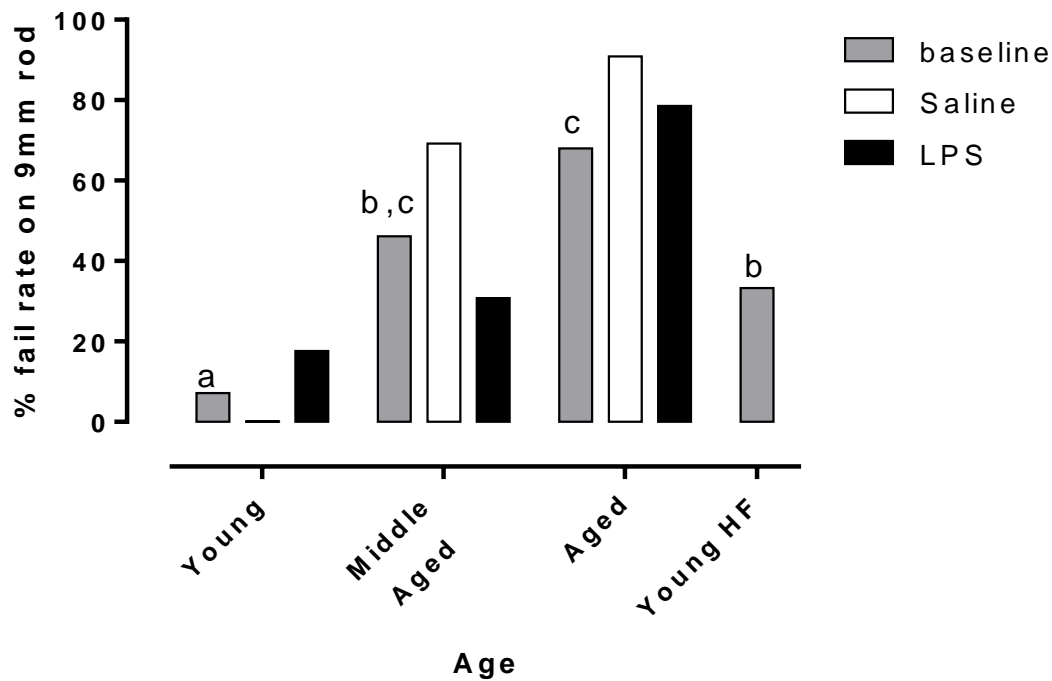


**Figure 3.11. The influence of age and LPS injection on 9mm static rod test performance.**

Aged mice performed significantly worse than both young groups but not middle-aged mice. Middle-aged mice demonstrated no deficit in performance vs weight matched young mice. n = 24 for aged mice, n = 27 for middle-aged mice, n = 30 for young standard diet mice and n = 23 for the young high fat diet mice at baseline. n = 11 for aged saline injected mice, n = 14 for aged LPS injected mice, n = 13-14 for middle-aged saline/LPS injected mice and n = 15 for young saline/LPS injected mice. Bars represent percentage of cohort failing to complete the 9mm rod. Bars with different letters are baseline data that differ significantly ( $p < 0.01$ ) from each other.

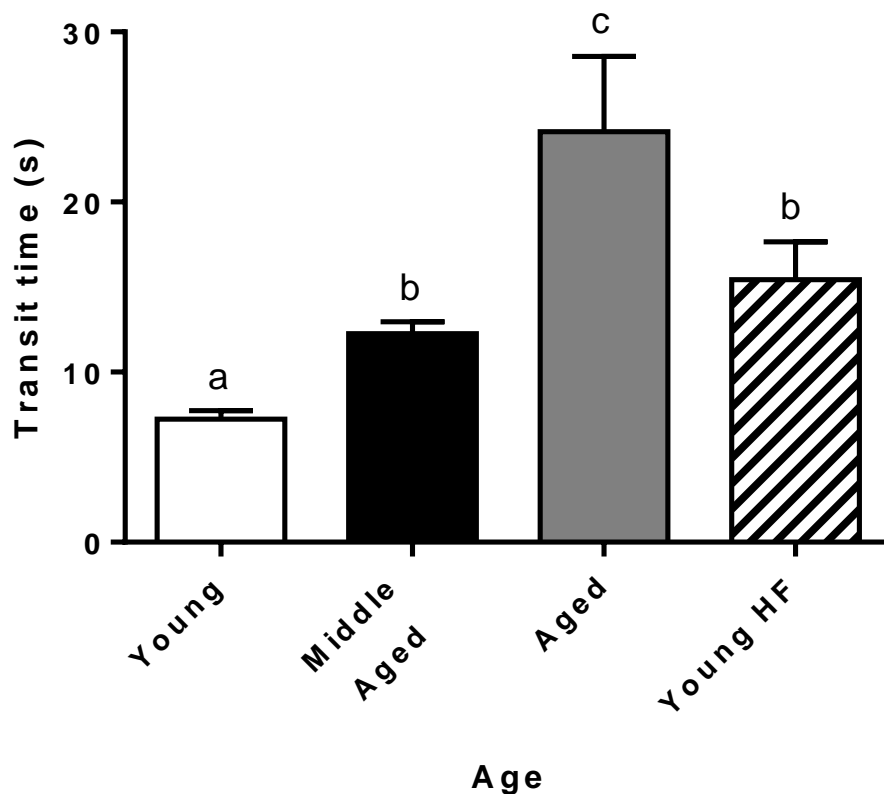


**Figure 3.12. The influence of age on 9mm static rod transit time.**

All groups were significantly different to each other except middle-aged mice vs young high fat diet mice.  $n = 7$  for aged mice,  $n = 15$  for middle-aged mice,  $n = 30$  for young standard diet mice and  $n = 7$  for the young high fat diet mice. Bars represent means  $\pm$  SEM. Bars with different letters are significantly different ( $p < 0.01$ ) from each other.

Mouse performance on the inverted screen was assessed the day before baseline readings of other tasks were taken. No post-injection sampling was undertaken using the inverted screen. Due to the large percentage of maximal scores obtained, sampling in the aged mice cohort was stopped at only 9 of the cohort. Full data sets were collected from the other cohorts. For weight matched controls all mice with a weight between 30-40g (mean sample weight = 34.8g) were pooled together. Analysis by Kruskal-Wallis test found differences between the groups (Kruskal-Wallis test;  $\chi^2 = 12.74$ , d.f.=3,  $p = 0.0052$ ) (Figure 3.13), but following analysis by Dunn's multiple comparison test differences were only found between middle-aged mice and young standard diet mice and young standard diet mice vs young weight matched high fat diet mice (Dunn's

multiple comparison test,  $p < 0.05$ ). There was no difference between both aged or middle-aged mice vs weight matched young mice ( $p > 0.05$ ). This lack of an effect of age on muscle strength assay performance led to the decision to use the climbing rod assay as an alternative measure of muscular strength.

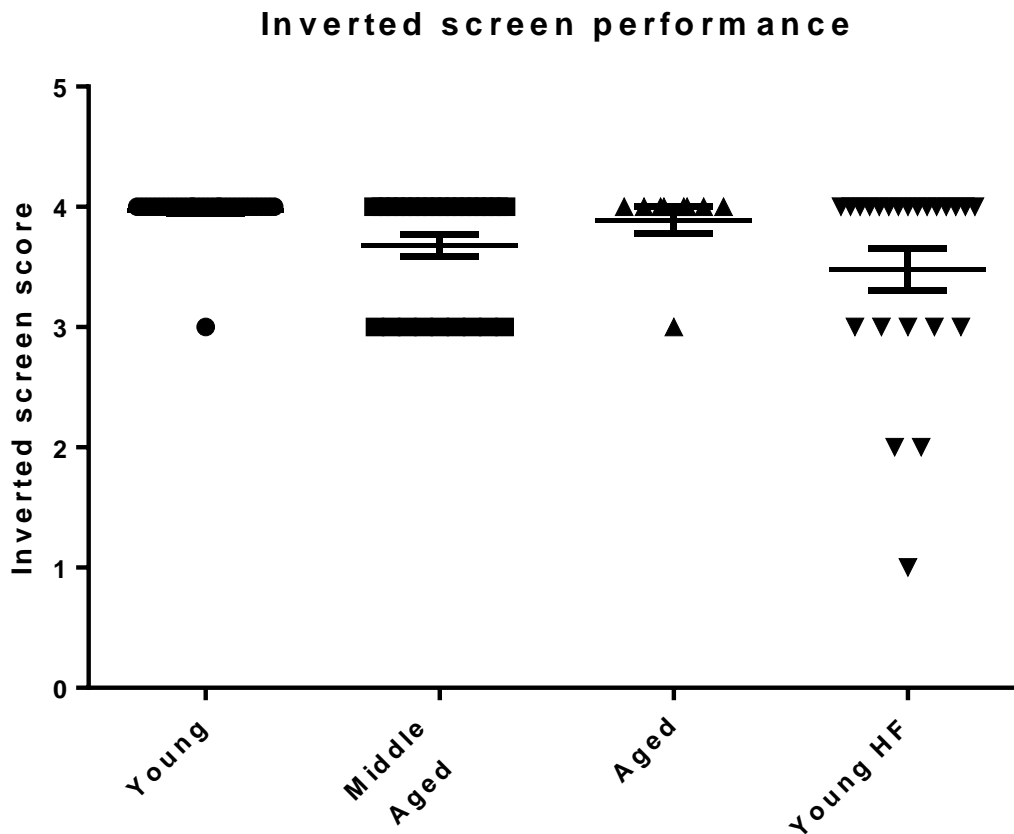


**Figure 3.13. Baseline inverted screen performance.**

The only significant differences ( $p < 0.05$ ) between individual groups were between young standard diet and middle-aged mice and young weight matched high fat diet mice vs young standard diet mice.  $n = 9$  for aged mice,  $n = 27$  for middle-aged mice,  $n = 30$  for young standard diet mice and  $n = 23$  for the high fat diet young mice. Bars represent means  $\pm$  SEM.

Immediately following inverted screen assessment climbing rod performance was assessed. Analysis by Kruskal-Wallis test found significant differences in median score between the groups ( $\chi^2 = 59.69$ , d.f. = 2,  $p < 0.0001$ ) (Figure 3.14 A). Dunn's multiple comparison test found statistically significant differences between all groups ( $p < 0.05$ ) except aged vs middle-aged ( $p > 0.05$ ), showing that climbing rod performance is affected by both weight and by age.

Figure 3.14 E suggests that poorer climbing rod performance did not correlate with increased likelihood to fail the 9mm static rod test within the two young cohorts. Comparison of medians by Mann Whitney test revealed no significant difference between medians (Mann Whitney test;  $U = 162.0$ ,  $p = 0.086$ ) (Figure 3.14 D) and this weak trend may be explained by the negative correlation between climbing rod score and weight ( $R^2 = 0.371$ ,  $n = 75$ ,  $p < 0.0001$ ) in mice fed either a standard or a high fat diet (Figure 3.15). Plotting 9mm rod transit time vs climbing rod score from the pooled young cohorts also showed no correlation between the two variables ( $R^2 = 0.054$ ,  $n = 55$ ,  $p = 0.325$ ) (Figure 3.14 E). This lack of a relationship between climbing rod score and static rod performance was mirrored in the middle-aged and aged groups, in which the median climbing score was not different between mice that either passed or failed the static rod test (Figure 3.14 B & C). These data suggest that the impaired static rod performance of aged mice is not caused by loss of strength or increasing weight.

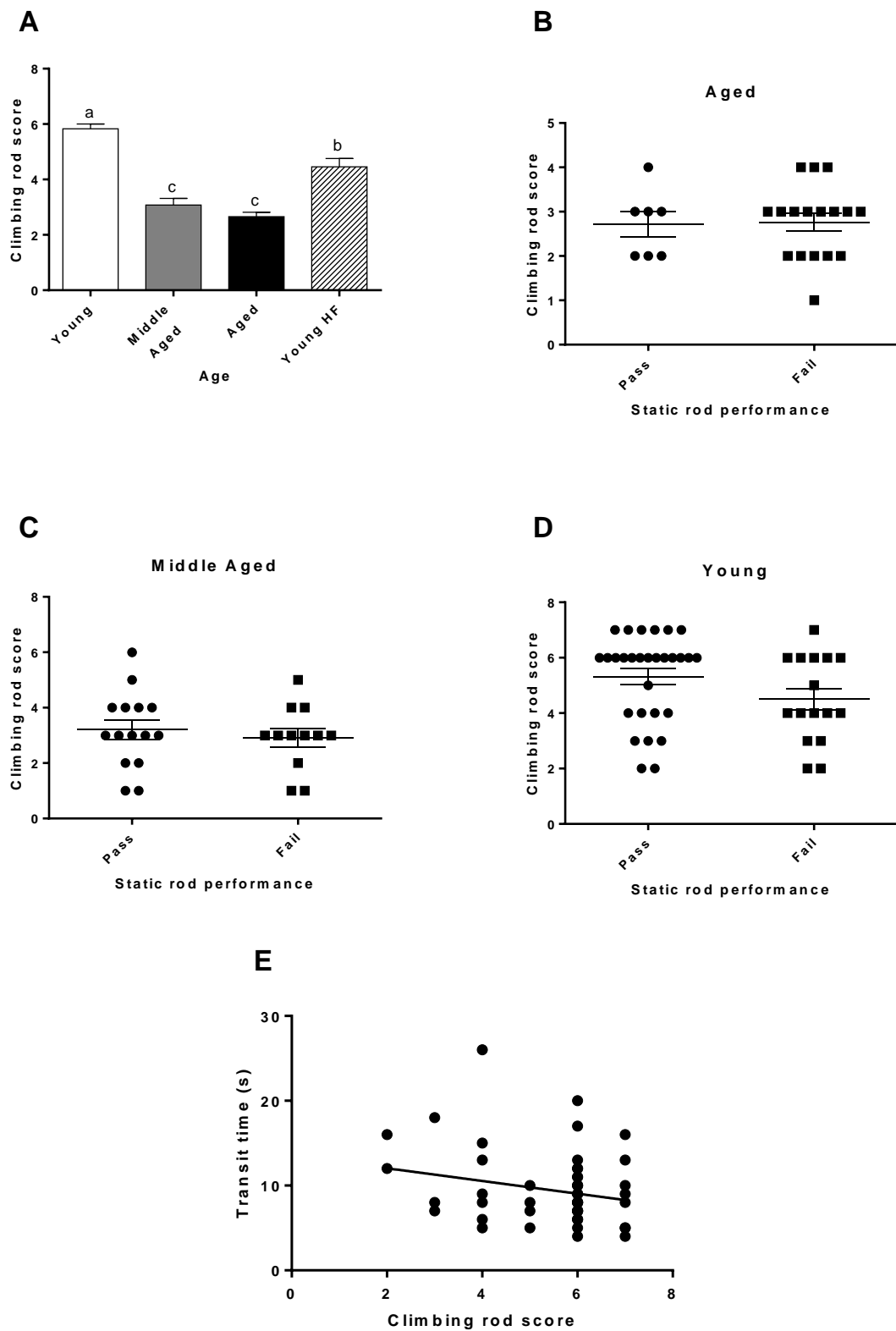
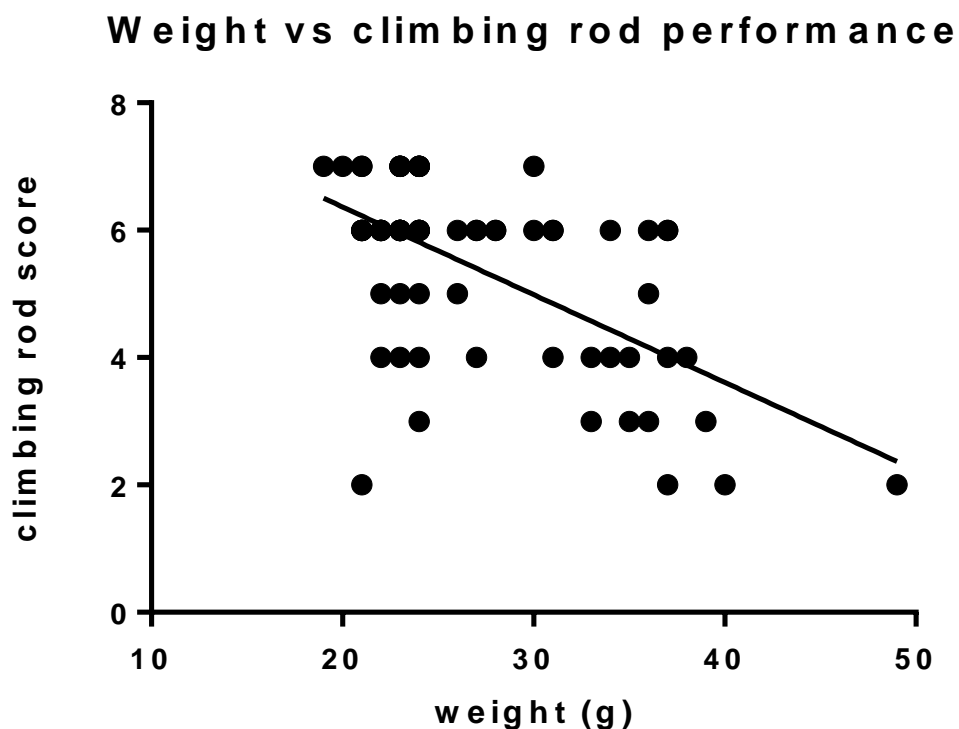


Figure 3.14. Baseline climbing rod performance and its correlation with static rod test performance.

There was a significant effect of age on climbing rod test performance ( $p < 0.001$ ) (A), suggesting that muscle strength declines with age. Letters denote a significant difference between groups ( $p < 0.05$ ). Data is shown as mean  $\pm$  SEM. There was no significant difference in median climbing rod test score between aged (B), middle-aged (C) or young (D) mice that passed or failed the static rod test. D includes mice fed on a standard diet and those fed on a high fat diet. There was also no significant correlation between climbing rod score and transit time within the young mice fed either a standard or high fat diet (E).  $n = 26$  for aged,  $n = 27$  for middle-aged,  $n = 30$  for young and  $n = 24$  for the high fat diet young mice.



**Figure 3.15. The influence of weight on climbing rod performance.**

Young mice fed a high fat diet and/or whose mother was fed a high fat diet were pooled with young mice fed a normal chow diet both to assess the influence of weight on climbing rod performance ( $n = 45$  HF diet,  $n = 30$  standard diet; total  $n = 75$ ). Linear regression analysis showed a significant relationship between the two variables ( $R^2 = 0.371$ ,  $n = 75$ ,  $p < 0.0001$ ).

## 3.4 Discussion

LPS injection negatively affected the performance of mice in burrowing (2h and overnight), glucose water consumption, open field activity, rotarod performance and induced weight loss. Age exacerbated the effects of LPS on burrowing, but no other behaviour was prolonged or exacerbated by LPS treatment in aged mice. LPS injection also induced enhanced weight loss in aged mice. Age decreased 9mm rod performance independently of weight and muscle strength, but rotarod performance was unaffected by age. The effect of LPS in the static rod test could not be accurately determined due to the limited sample size, but rotarod performance was impaired in LPS injected mice. LPS induced deficits in rotarod performance were not significantly different between young, middle-aged or aged mice. The differences in data collected from these two different tasks may reflect differences in the sensitivity of these assays.

### 3.4.1 Sickness behaviours

LPS injection induced a change in performance of mice in all the assays of sickness behaviour measured in this experiment. However, burrowing was the only behavioural assay where the response to LPS was more pronounced in aged mice than young mice. Burrowing is a hippocampus dependent (Deacon et al., 2002), species typical behaviour that is sensitive to systemic inflammatory challenge (Teeling et al., 2007). Aged and middle-aged mice injected with LPS exhibited an exaggerated reduction in burrowing between 3-5 hours after injection and a delayed recovery when burrowing activity was assessed overnight. Exaggerated sickness behaviour in aged animals in response to systemic inflammatory challenge has been previously reported (Barrientos et al., 2006; Godbout et al., 2005b; Godbout et al., 2008; McLinden et al., 2012), but this is the first study to use burrowing in response to systemic LPS treatment in an ageing context. A delayed recovery of burrowing activity has been previously reported in response to poly I:C injection in aged mice (McLinden et al., 2012), which the authors attributed to elevated hippocampal cytokine expression.

Burrowing activity was also affected by ageing at baseline, with aged mice burrowing less food pellets than middle-aged or young mice in 2 hour or

overnight burrowing. This may be attributable to general changes in the activity levels of aged mice. Baseline rearing and locomotor activity of aged mice was reduced in the open field test compared to young mice. Decreases in spontaneous locomotor activity have been described as a component of ageing in a variety of models, including invertebrates, simple vertebrates, rodents and humans (Adamson et al., 2004; Godbout et al., 2005b; Lebourg and Lints, 1984; Valenzano et al., 2006), and is likely driven by multiple processes.

Exaggerated sickness behaviour has not been reported previously in middle-aged (12 month old) mice. The reductions in burrowing activity of middle-aged mice over two hours or overnight were comparable to those observed in aged mice, showing that the increased behavioural sensitivity to immune challenge observed in aged mice begins at an earlier time-point than previously observed. These mice were male instead of female however, which may have impacted on the sensitivity of the mice to ageing (Cribbs et al., 2012) or LPS (Pitychoutis et al., 2009). Conversely there are other studies that show no difference between aged microglia from a male or female brain (Sierra et al., 2007). An experiment with matched genders would be necessary to confirm that exaggerated sensitivity of burrowing to LPS injection is present in middle-aged mice.

LPS injection had a negative effect on both open field activity and glucose water consumption, but this effect was not exacerbated in aged mice. The mice were not habituated to the open field box prior to baseline, so there was a large decline in locomotor and rearing activity in both saline and LPS injected mice when they were tested 2 hours after injection, but this decline was significantly more pronounced in LPS injected mice. 24 hours after injection there was no difference in open field locomotor or rearing activity between saline or LPS injected mice, suggesting mice had recovered in this aspect of their behaviour. Other studies have previously shown exaggerated and prolonged reductions in open field activity in aged mice injected with LPS (Godbout et al., 2005b; Godbout et al., 2008), but these studies used a higher dose of LPS (333µg/kg vs 100µg/kg) in 22-24 month old male BALB/C mice, whereas 20-21 month old female C57/Bl6 mice were used in this study. Any of these differences between the two studies could have contributed to the lack of differences in the effects of LPS on open field activity between young,

middle-aged or aged mice, as could have the lack of habituation to the open field arena before commencing the experiment.

The glucose water consumption assay is frequently used as a measure of anhedonia and depressive behaviour. LPS induced a larger decrease in glucose water consumption than saline in all age groups, but the size of this decrease was not different between groups. Depressive behaviour has previously been shown to be of similar severity in young and aged mice following a systemic inflammatory challenge, but the depressive behaviour persists for a longer period of time in aged mice (Godbout et al., 2008; Kelley et al., 2013). This may explain the lack of age differences observed in this study – prolonged deficits in glucose water consumption may have been observed if the experiment had been continued until a later time-point.

Aged mice also lost more weight in response to LPS than young mice. Increased weight loss due to reduced food intake has been a widely reported consequence of systemic inflammation in aged rodents (Barrientos et al., 2009b; Godbout et al., 2005b) and these data support those observations.

### **3.4.2 Co-ordination and balance deficits**

In this study a significant age-related deficit in static rod test performance was observed that was not dependent on weight gain or muscle strength loss. There is a progressive loss of Purkinje neurons with age (Woodruff-Pak et al., 2010) and Purkinje neuron specific degeneration has previously been shown to compromise the performance of mice in tasks assessing co-ordination and balance (Chen et al., 1996; Kyuhou et al., 2006). A correlation of conditioned eye blink response with Purkinje neuron numbers has also been previously shown, suggesting that Purkinje cell loss is a critical component of age related cerebellar dysfunction (Woodruff-Pak, 2006). LPS injection did not appear to exacerbate deficits in performance in the static rod test task at any age, suggesting the cerebellar circuitry controlling static rod performance is not sensitive to systemic LPS at this time-point (1-2h) after injection and/or to this dose of LPS (100 µg/kg). Alternatively this study may have been insufficiently powered to detect LPS induced changes in static rod performance. Many aged mice failed to traverse 9mm static rod successfully and therefore only a few transit times were successfully recorded from this test group. The percentage

failure rate on the static rod did slightly increase following injection of saline or LPS, but this measure requires high sample numbers to see significant differences and there may have been a ceiling effect in this measure of static rod performance, as so many mice were already failing the task at baseline. All mice still successfully traversed the 22 and 35mm static rods following LPS or saline injection. Further testing at different time-points after LPS injection and with a slightly larger diameter rod, e.g. 12mm, would provide a more conclusive answer to whether LPS injection affects static rod performance.

The lack of any effect of age on rotarod performance is contrary to the conclusion that cerebellar performance is impaired with age. One explanation may be a lack of sensitivity of the rotarod assay, particularly given that the mice were trained extensively before acquiring measurements and they frequently attained maximal scores in this assay. There are variations in the literature in the level of training mice receive prior to rotarod testing (Barreto et al., 2010), but for the experiment described in this chapter it was necessary for the mice to adopt a stable baseline performance to allow comparison after LPS injection. Recording of other measures such as foot faults or percentage of time spent gripping the rod as it rotates instead of walking on top of it may give more sensitive data about co-ordination and balance deficits in this task. A recent review (Kennard and Woodruff-Pak, 2011) points out that there have been mixed reports on the effects of age on rotarod performance.

The lack of sensitivity of the rotarod to age related co-ordination and balance deficits makes the interpretation of LPS induced deficits in rotarod performance challenging. The decreased rotarod performance following LPS may represent co-ordination and balance deficits, but supportive data from other assays of co-ordination and balance would be helpful in interpreting these data. Decreased rotarod performance following LPS injection may also be a result of increased fatigue rather than co-ordination deficits as the rotarod is a physically demanding task that requires stamina from the mice. Fatigue, or an altered motivational state where an organism prioritises conserving energy, is considered a key component of the sickness behaviour syndrome (Dantzer, 2004; Gaykema and Goehler, 2011; Miller, 1964), and may induce mice to give up and allow themselves to fall off the rod at an earlier time-point than saline injected mice would.

### 3.4.3 Summary

These data show that aged mice demonstrate enhanced sickness behaviour in response to an i.p. injection of 100µg/kg LPS, as demonstrated by their reduced burrowing activity and enhanced weight loss. However, not all LPS sensitive behaviours are exacerbated by ageing at this dose of LPS – open field activity, rotarod performance and glucose water consumption were equally affected by LPS injection in mice of all age groups. Aged mice performed much worse than young mice in the cerebellum dependent multiple static rod test, but not the rotarod test. LPS injection did not affect performance in the static rod task, suggesting that this dose and time-point after LPS injection do not compromise co-ordination and balance.

## 4. Histological and molecular analysis of the microglial response to LPS and ageing.

### 4.1 Introduction

Microglia share a common developmental origin (Ginhoux et al., 2010), but their morphology and density is region specific and can range from 5 up to 12% of total cells per region, with higher densities found in the grey matter in mice (Lawson et al., 1990). The density and phenotype of microglia also differs between regions in the human brain (Mittelbronn et al., 2001). To gain more insight into the cellular functions of microglia in the adult mouse brain, De Haas et al compared the cellular expression level of a number of functional surface molecules in different brain regions and found distinct regional differences (De Haas et al., 2008). For example, the expression levels of CD11b and CD40 per cell in the cerebral cortex were significantly lower than the levels in the spinal cord. The different regional expression of some immune molecules on microglia may reflect different aspects of microglial activation, which is of interest in the context of the rostro-caudal gradient of reactivity to injury and inflammatory stimuli in the CNS. Mechanical lesions to spinal cord, the most caudal region of the CNS, promote more extensive leucocyte recruitment and blood-brain barrier breakdown than comparable lesions to cortex (Schnell et al., 1999a). The rostro-caudal gradient is also observed following focal cytokine injections with more overt induction of MHCII expression and leucocyte recruitment in the caudal than forebrain regions (Phillips and Lampson, 1999; Phillips et al., 1999; Schnell et al., 1999b).

With age the number and density of microglia changes little, if at all (Deng et al., 2006; Long et al., 1998; Ogura et al., 1994). In contrast, age-related changes in phenotype and functional properties of microglial cells have been widely reported. In the healthy adult brain, microglia display a down-regulated phenotype characterized by low expression of functionally relevant molecules such as CD45, CD68 and MHC class II (Aloisi, 2001; Perry et al.,

2007) and low phagocytic activity, but the expression levels of these molecules increase after acute CNS injury or ageing (Conde and Streit, 2006; DiPatre and Gelman, 1997; Ogura et al., 1994; Perry et al., 1993; Rogers et al., 1988; Streit, 1996). These changes have been associated with an increased sensitivity to systemic inflammatory challenge with increased cytokine production and altered behavioural responses (Barrientos et al., 2006; Chen et al., 2008; Henry et al., 2009; Wynne et al., 2010).

Many studies on age-related changes in microglia phenotype and function during ageing have focussed on single regions and have not addressed possible regional differences within the CNS. Microglia activation is evident in the white matter of the cerebral hemispheres of old rats (Ogura et al., 1994), old monkeys (Sheffield and Berman, 1998; Sloane et al., 1999) and elderly humans (Simpson et al., 2007), and it has been reported that the extent of microglial cell activation in white matter as measured by increased expression of MHCII and iNOS is related to the degree of cognitive impairment (Sloane et al., 1999). The aim of the experiments described in this chapter was to compare the phenotype and morphology of microglia in various regions of the young (4 months) and aged (20-21 months) mouse brain using a large range of functional surface markers and to assess changes in their phenotype following a systemic inflammatory challenge.

## **4.2 Materials and Methods**

### **4.2.1 Animals**

Tissue used for immunohistochemical and qPCR analysis at 24 hours after LPS injection was obtained from the 4 (young) and 20-21 (aged) month old C57/BL6 mice described in chapter 3. For analysis of inflammatory cytokines at 3 hours after LPS injection, a separate cohort of female C57/BL6J mice (3 and 18 months old, Charles River, Margate, UK) was used.

Mice were injected i.p. with saline or LPS at a dose of 100 µg/kg (lot 91K4143, Salmonella abortus equi, Sigma, Poole, UK). After perfusion with heparinised saline the brain was rapidly dissected and tissue was either embedded directly in OCT for immunohistochemistry or flash frozen in liquid

nitrogen for qPCR. Cerebellar tissue collected for qPCR consisted of one half of the hemisphere cut sagittally. For the 24h post LPS injection experiment the hippocampus and surrounding cortex were flash frozen together. For the 3h post LPS injection a hippocampal punch was obtained using a sterile RNase free pipette tip to capture hippocampus enriched tissue. Serum was collected as described in chapter 2. Assistance was received during tissue collection from Ursula Püntener and Olivia Larsson (University of Southampton).

#### 4.2.2 Immunohistochemistry

Immunohistochemistry was performed as described in chapter 2. A brief description of the function of each molecule investigated in this chapter is provided in table 4.1.

Molecule	Description
CD11b - complement receptor 3	An integrin that is upregulated on microglia following classical or alternative activation. Involved in phagocytosis and cell migration. (Kettenmann et al., 2011)
CD68 - macrosialin	A lysosomal glycoprotein that is highly expressed in macrophages/microglia. Expression is upregulated following phagocytosis and classical activation (Kettenmann et al., 2011).
F4/80	A transmembrane protein, the function of which is unknown in microglia but contributes to induction of T cell tolerance by peripheral myeloid cells (Lin et al., 2005). F4/80 is frequently used as a marker of microglia (Kettenmann et al., 2011).
CD11c - complement receptor 4	An integrin that is expressed endogenously in dendritic cells and upon induction in macrophages/microglia. Involved in phagocytosis and migration (Kettenmann et al., 2011).
Fc gamma receptor I	Transmembrane receptor for monomeric IgG, contains an activating ITAM motif. Expressed by myeloid cells, including microglia (Aderem and Underhill, 1999;

	Lunnon et al., 2011).
Fc gamma receptor II/III	Transmembrane receptors for IgG with high sequence homology between Fc $\gamma$ RII and III. Fc $\gamma$ RII contains an inhibitory ITIM motif, while Fc $\gamma$ RIII contains an activating ITAM motif. Expressed by myeloid cells and B cells (Aderem and Underhill, 1999; Lunnon et al., 2011).
MHC Class II	Presents antigen fragments at the cell surface, expressed by activated microglia and is constitutively expressed on dendritic cells (Kettenmann et al., 2011).
Dectin-1	A transmembrane lectin that recognises sugar residues from fungi and plants that is associated with alternative activation of microglia/macrophages (Shah et al., 2008).
Dec-205	An endocytic receptor involved in antigen presentation that is expressed on dendritic cells (Jiang et al., 1995).

**Table 4.1. A brief description of all the molecules investigated in this chapter.**

#### **4.2.3 Quantification of immunohistochemistry staining**

Images were analysed and quantified using ImageJ (Schneider et al., 2012). The DAB and haematoxylin channels were isolated using a plugin and a threshold was determined for quantification. Thresholds were determined for each molecule to control for variation in DAB staining intensity between molecules. Background or excessively dark haematoxylin staining was removed using the “despeckle” setting and, when required, by superimposing a mask of the haematoxylin channel onto the image. The region of interest was traced “freehand” from the image and the average pixel density within the selected area was calculated. For each animal (n=4-5 per treatment group), two images per region of interest were captured at x20 magnification for quantification, using a brain atlas (Franklin and Paxinos, 2008) to identify matching regions of interest in each hemisphere. The average of the two images was calculated and data expressed as fold increase over young saline treated expression levels in the same region. Fc $\gamma$ RI expression in the striatum was excluded from analysis due to non-specific nuclear binding in this particular region.

#### **4.2.4 Quantitative PCR**

All data was quantified using the Delta Delta Ct method described in chapter 2. GAPDH was used as the housekeeping gene in all experiments. Assistance was received from Su Wu and Feng Liu (Peking University, Beijing, China) in performing some of the RNA extractions for the 24h time-point hippocampus samples.

#### **4.2.5 Statistical analysis**

Data sets were tested for a normal distribution using the D'Agostino-Pearson omnibus test. All tests were performed in either Sigmaplot 11.0 or GraphPad Prism 6.0. Quantification of the immunohistochemical analysis was performed by expressing data as fold increase from the mean of the young saline values from the same brain region, logarithmically transforming data to obtain a normal distribution and using a three way ANOVA with Holm-Sidak post tests to analyse data. Quantitative PCR data was logarithmically transformed and analysed by two way ANOVA and Holm-Sidak post tests.

### **4.3 Results**

#### **4.3.1 Immunohistochemical investigations into microglial phenotype and morphology**

Microglial activation was assessed by analysing both morphology and differential expression of functionally relevant molecules within eight distinct regions of grey or white matter distributed along a rostral-caudal axis in young or aged mice 24h after an intraperitoneal injection of either saline or LPS. The regions selected were: striatum, corpus callosum, fimbria, dentate gyrus, substantia nigra, cerebellar nuclei, molecular layer of the cerebellar cortex and the inferior cerebellar peduncle (Figure 4.1). The striatum is a mixed white/grey matter region – the most caudal segment of the putamen, an area that is mostly grey matter, was used in this study. The corpus callosum and fimbria are rostral white matter areas, while the dentate gyrus is a grey matter region in the hippocampus. The substantia nigra is a grey matter area caudal to the hippocampus with a particularly high microglial density (Lawson et al., 1990). Within the cerebellum the white matter tracts

of the inferior cerebellar peduncle, the deep cerebellar nuclei, which represent a mixture of white and grey matter, and the molecular layer, which is grey matter neuropil representative of the cerebellar cortex, were selected for analysis.

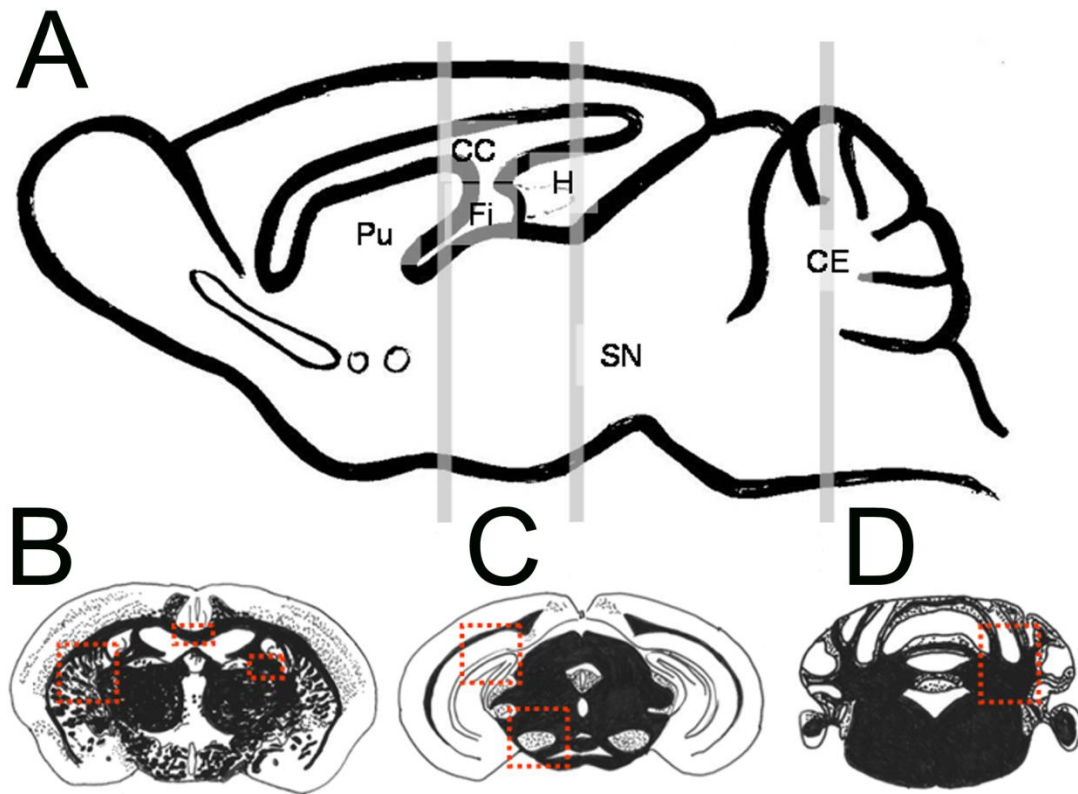


**Figure 4.1. An illustration of the distribution of the CNS regions selected for study.**

**A** – A sagittal section through the brain illustrating the rostral-caudal distribution of areas studied. Letters indicate the following regions: Pu – putamen, CC – corpus callosum, Fi – fimbria, H – hippocampus, SN – substantia nigra, CE – cerebellum. Grey bars represent the location of the coronal sections collected. **B-D** – the three coronal sections investigated in this study. Myelin rich areas are coloured black. The red boxes highlight the specific areas studied. **B** – Bregma -1.0. The boxes from left to right illustrate the striatum, corpus callosum and fimbria. **C** – Bregma -3.0. The left box is the dentate gyrus of the hippocampus, the right box is the substantia nigra. **D** – Bregma -6.0. The box indicates the area studied, which includes the cerebellar nuclei, inferior peduncle and molecular layer.

Many, but not all, microglia exhibited a change in morphology in the aged brain (Figure 4.2), including a thickening and de-ramification of processes and hypertrophy of the cell body (Figure 4.2 E and G). Morphological changes were observed in all regions studied, and microglia broadly retained the morphology that has previously been reported in grey versus white matter (Lawson et al., 1990), with longitudinal processes that run parallel to the axonal tracts in the white matter and radially branched microglia in the grey matter. The aged mice also exhibited cell aggregates of approximately 20-30 $\mu$ m in diameter, containing multiple nuclei and fewer, shorter, highly thickened processes. Some aggregates contained as many as 6 or 7 nuclei. These aggregates were predominantly found in the white matter, particularly in the cerebellum (Figure 4.2 G). Systemic LPS challenge did not appear to change the morphology of the microglia or the number of multinucleate aggregates observed in aged mice (Figure 4.2 H).

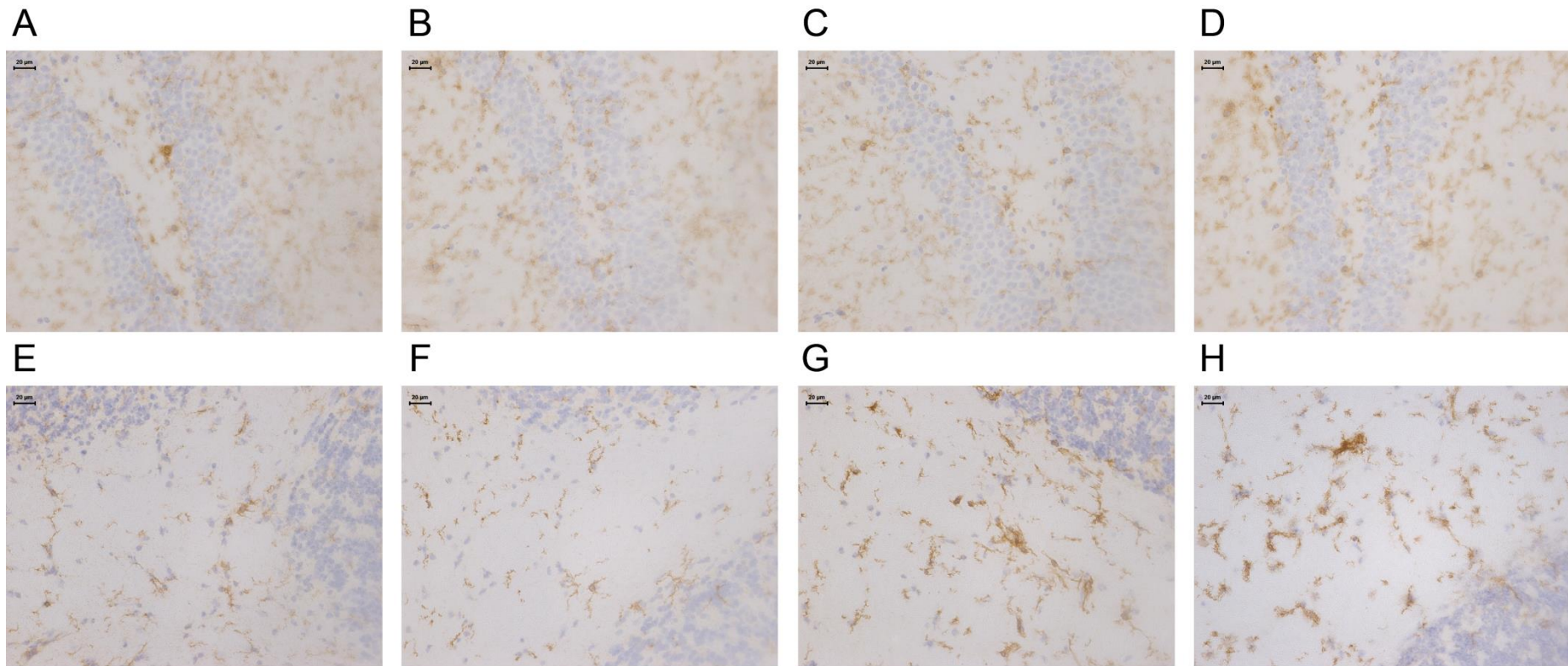


**Figure 4.2. The effect of age and LPS on CD11b expression.**

A-D Hippocampus. A - young saline, B - young LPS, C - aged saline, D - aged LPS. E-G Cerebellum. E - young saline, F - young LPS, G - aged saline, H - aged LPS. Scale bar represents 20μm.

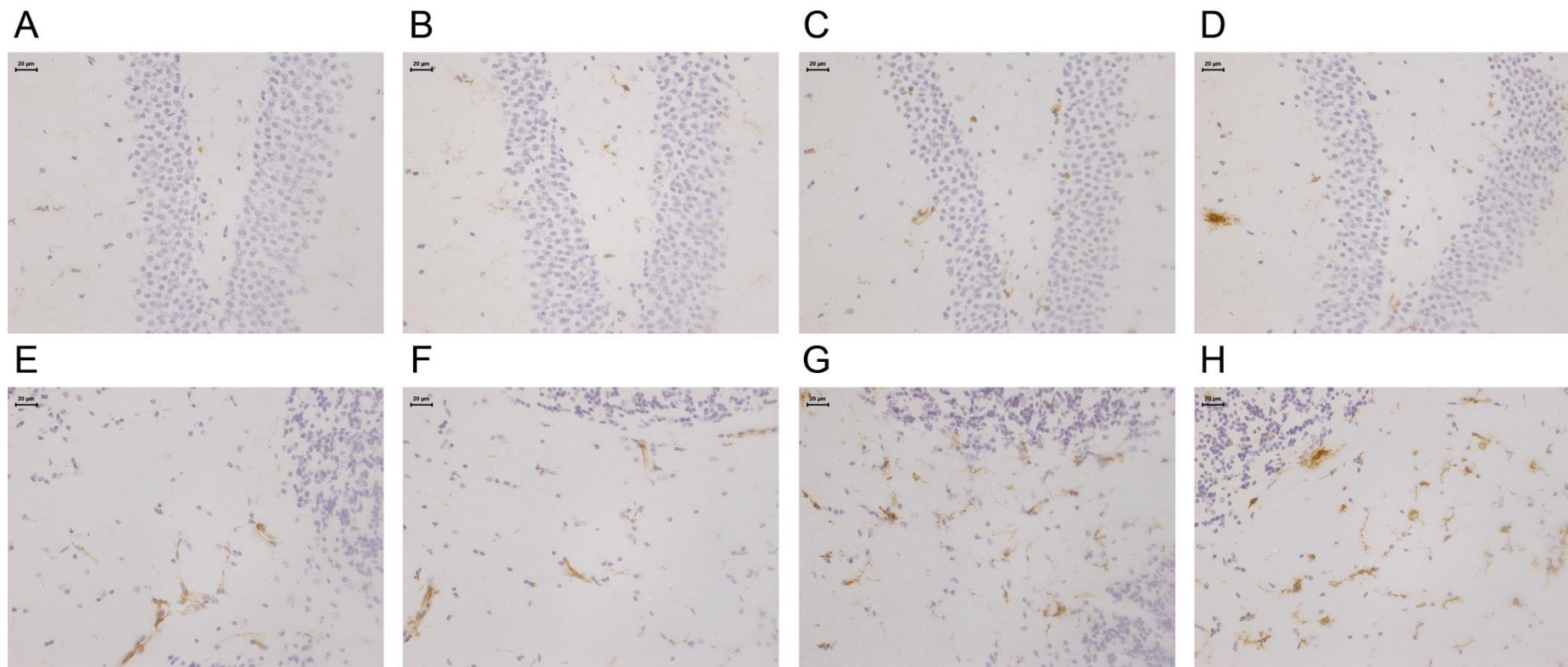


**Figure 4.3. The effect of age and LPS on CD68 expression.**

A-D Hippocampus. A - young saline, B - young LPS, C - aged saline, D - aged LPS. E-G Cerebellum. E - young saline, F - young LPS, G - aged saline, H - aged LPS. Scale bar represents 20μm.

In addition to morphological changes distinct phenotypic changes in the aged brain were noted, including increased expression of CD11b (Figure 4.2), CD68 (Figure 4.3), CD11c, F4/80, and Fc $\gamma$ RI (Figure 4.4). Spleen tissue from a saline injected young mouse was stained for these five markers to provide a positive control for these antibodies (Figure 4.5), with each of the markers being found in the zones of the spleen expected given their expression by specific immune cells. CD11b and CD68 are strongly expressed in macrophages and dendritic cells (Holness et al., 1993; Pack et al., 2008; Pickl et al., 1996), and were both strongly expressed in the marginal zone and the red pulp (Figure 4.5 A & B). F4/80 and Fc $\gamma$ RI expression, which should both be restricted to myeloid derived cells in the naïve spleen (Austyn and Gordon, 1981; Heijnen and Van de Winkel, 1995; Tuijnman et al., 1993), was largely restricted to the red pulp (Figure 4.5 C & D) while CD11c positive dendritic cells (Pack et al., 2008) were present in the marginal zone (Figure 4.5 E).

Changes in microglial phenotype were more pronounced in the cerebellum compared to the hippocampus. Increased levels of CD68 were found on microglia in the white matter regions of the cerebellum of aged brain, while in the young brain immunoreactivity for this marker was predominantly associated with perivascular macrophages (Figure 4.3 A and B). Double immunofluorescence showed that cell aggregates in the aged brain are activated microglia as CD11b positive aggregates were not associated with blood vessels and were mainly found in the parenchyma, and are therefore not components of the perivascular macrophage population (Figure 4.4 A and B). Some aggregates extended processes that made contact with vasculature, but most did not. These aggregates were not groups of proliferating cells as assessed by double staining for CD11c and Ki67, a marker of cell proliferation (Schluter et al., 1993) (Figure 4.4 C). Expression of CD11c, Fc $\gamma$ RI and F4/80 was very weak or not detectable in the young brain, but all three markers were robustly expressed in aged cerebellar white matter (Figure 4.4 D-I). In summary, age dependent changes in morphology and phenotype appear to arise in a region dependent manner, with a specific white matter phenotype present in the aged brain, in particular in the cerebellum.

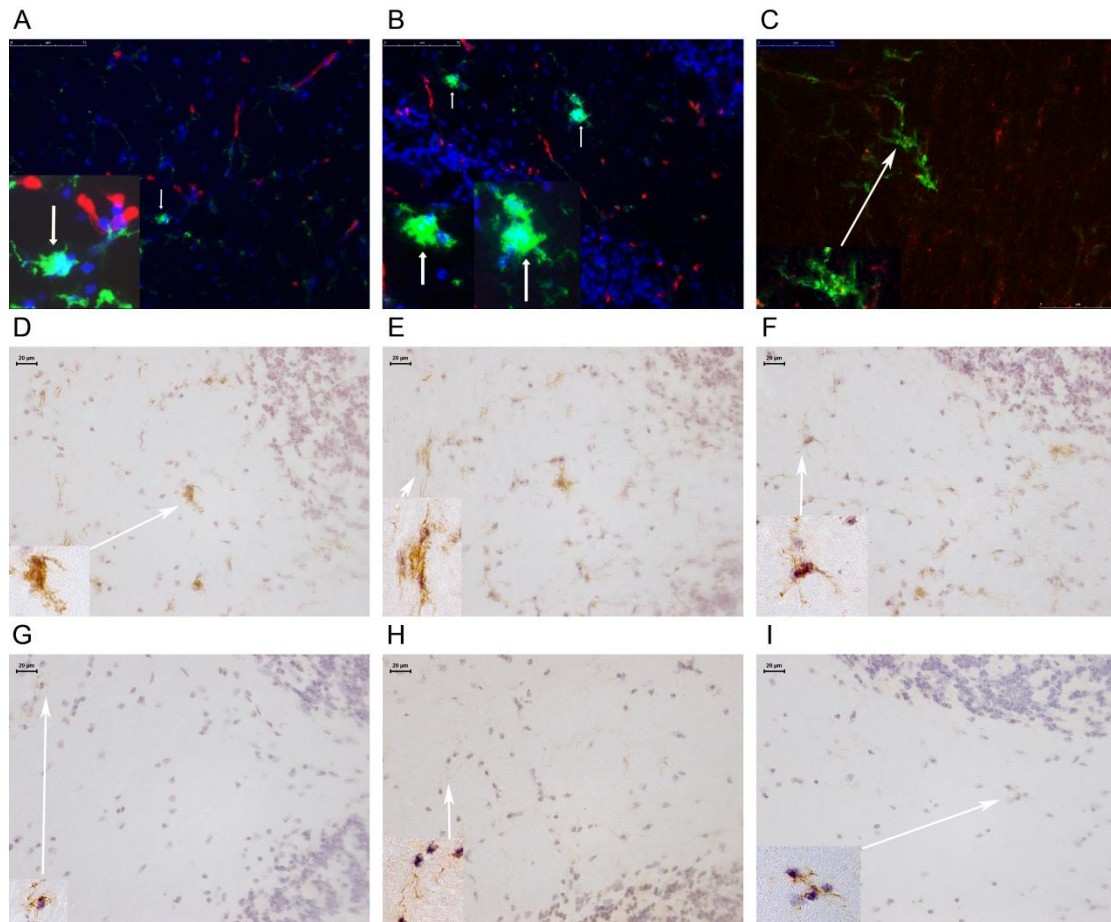


**Figure 4.4. Expression of microglial activation markers in the aged brain.**

**A-B** Double immunofluorescence staining for CD11b (green) and collagen IV (red) in the fimbria (**A**) and cerebellar inferior peduncle (**B**) of an aged mouse. CD11b positive cell aggregates are indicated by white arrows. The aggregates contain multiple nuclei and are not situated directly adjacent to blood vessels, as indicated by collagen IV positive basement membranes. Nuclei are blue after DAPI staining. **C** - Double immunofluorescence staining for CD11c (green) and Ki67 (red), a marker of proliferation, in the cerebellar inferior peduncle. CD11c positive aggregates do not co-localise with Ki67 positive nuclei. **D&G** - CD11c staining in the cerebellar inferior peduncle of an aged (**D**) and young (**G**) mouse. **E&H** - FcγRI staining in the cerebellar inferior peduncle of an aged (**E**) and young (**H**) mouse. **F&I** - F4/80 staining in the cerebellar inferior peduncle of an aged (**F**) and young (**I**) mouse. Insets show magnified, contrast enhanced areas of images indicated by arrows. **A-C**

scale bar represents 75  $\mu\text{m}$ . D-I Scale bar represents 20 $\mu\text{m}$ .

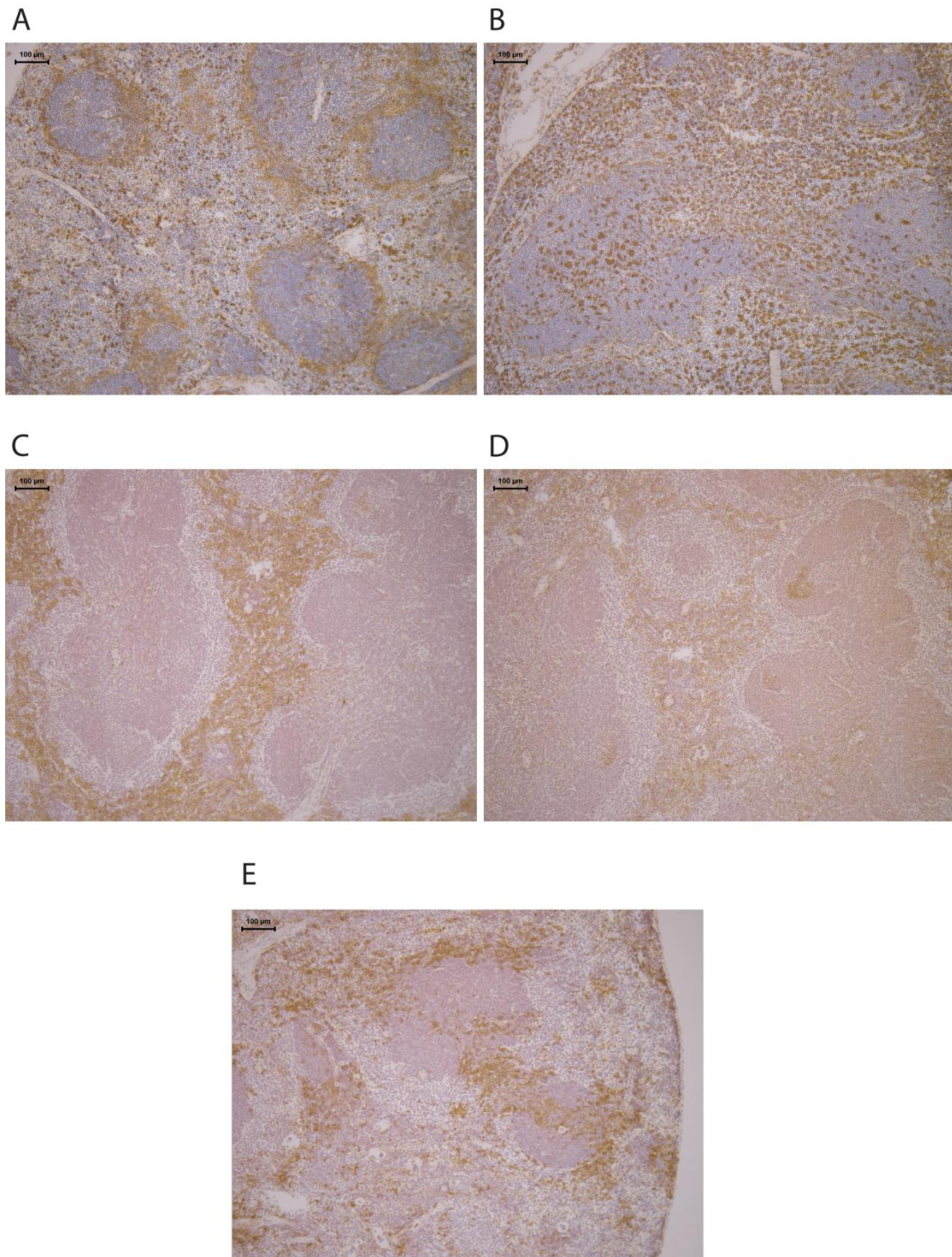


**Figure 4.5. Expression of a panel of myeloid cell markers in the young spleen of saline injected mice.**

Spleens from young, saline injected mice were stained for CD11b (A), CD68 (B), F4/80 (C), Fc $\gamma$ RI (D) or CD11c (E). Scale bar represents 100 $\mu$ m. Representative of n = 5.

The expression levels of functional microglial markers in the different regions studied was quantified by measuring the percentage of an image positively stained above a threshold. In the ageing brain increased expression of CD11b, CD68 and F4/80 was detected (Figure 4.6, n = 5 per group). For all three markers there was a strong effect of age on expression level (CD11b:  $F_{(1,111)} = 38.35$ ,  $p < 0.001$ ; CD68:  $F_{(1,108)} = 271.36$ ,  $p < 0.001$ ; F4/80:  $F_{(1,109)} = 75.86$ ,  $p < 0.001$ ). The expression of these markers was not significantly affected by systemic LPS 24h after injection. Region had a strong effect on expression of all three markers, (CD11b:  $F_{(7,111)} = 2.45$ ,  $p = 0.022$ ; CD68:  $F_{(7,108)} = 7.90$ ,  $p < 0.001$ ; F4/80:  $F_{(7,109)} = 4.64$ ,  $p < 0.001$ ). We detected an interaction between age and region for expression of all three markers (CD11b:  $F_{(7,111)} = 2.12$ ,  $p = 0.047$ ; CD68:  $F_{(7,108)} = 7.789$ ,  $p < 0.001$ ; F4/80:  $F_{(7,109)} = 4.64$ ,  $p < 0.001$ ), suggesting that microglial activation is differentially affected by age in different brain regions. The increases in expression of CD11b, CD68 and F4/80 were greatest in the cerebellum and in particular in the cerebellar inferior peduncles. Microglial expression of all three markers in the fimbria and for CD11b and CD68 the corpus callosum was also strongly increased in aged animals (Figure 4.6 A-B). Changes in the expression of these molecules in the white matter were greater than those in the grey matter. The dentate gyrus did not exhibit any changes in expression with ageing for any of these three markers.

The expression levels of CD11c (Figure 4.7 A) and Fc $\gamma$ RI (Figure 4.7 B) were also quantified and expression of both was significantly increased by age (CD11c:  $F_{(1,128)} = 63.08$ ,  $p < 0.001$ ; Fc $\gamma$ RI:  $F_{(1,92)} = 61.37$ ,  $p < 0.001$ ), region (CD11c:  $F_{(7,128)} = 15.76$ ,  $p < 0.001$ ; Fc $\gamma$ RI:  $F_{(6,92)} = 4.84$ ,  $p < 0.001$ ) and, for Fc $\gamma$ RI, LPS injection ( $F_{(1,92)} = 5.97$ ,  $p < 0.05$ ). An interaction between age and region was detected for CD11c expression ( $F_{(7,128)} = 11.72$ ,  $p < 0.001$ ), but not Fc $\gamma$ RI. Strikingly, CD11c expression was up-regulated exclusively in white matter regions during ageing. All four white matter regions examined demonstrated a significant increase in CD11c expression with age (Figure 4.7 A) and the most caudal area of white matter studied, the inferior cerebellar peduncle,

exhibited the greatest increase in expression, but CD11c expression was not further influenced by systemic LPS. Although expression of Fc $\gamma$ RI was increased in all regions of the aged brain, changes in Fc $\gamma$ RI expression were more pronounced in white matter areas and the cerebellum than in the hippocampus of aged mice (Figure 4.7 B). Fc $\gamma$ RI expression after LPS injection was also highest in the three cerebellar regions investigated.

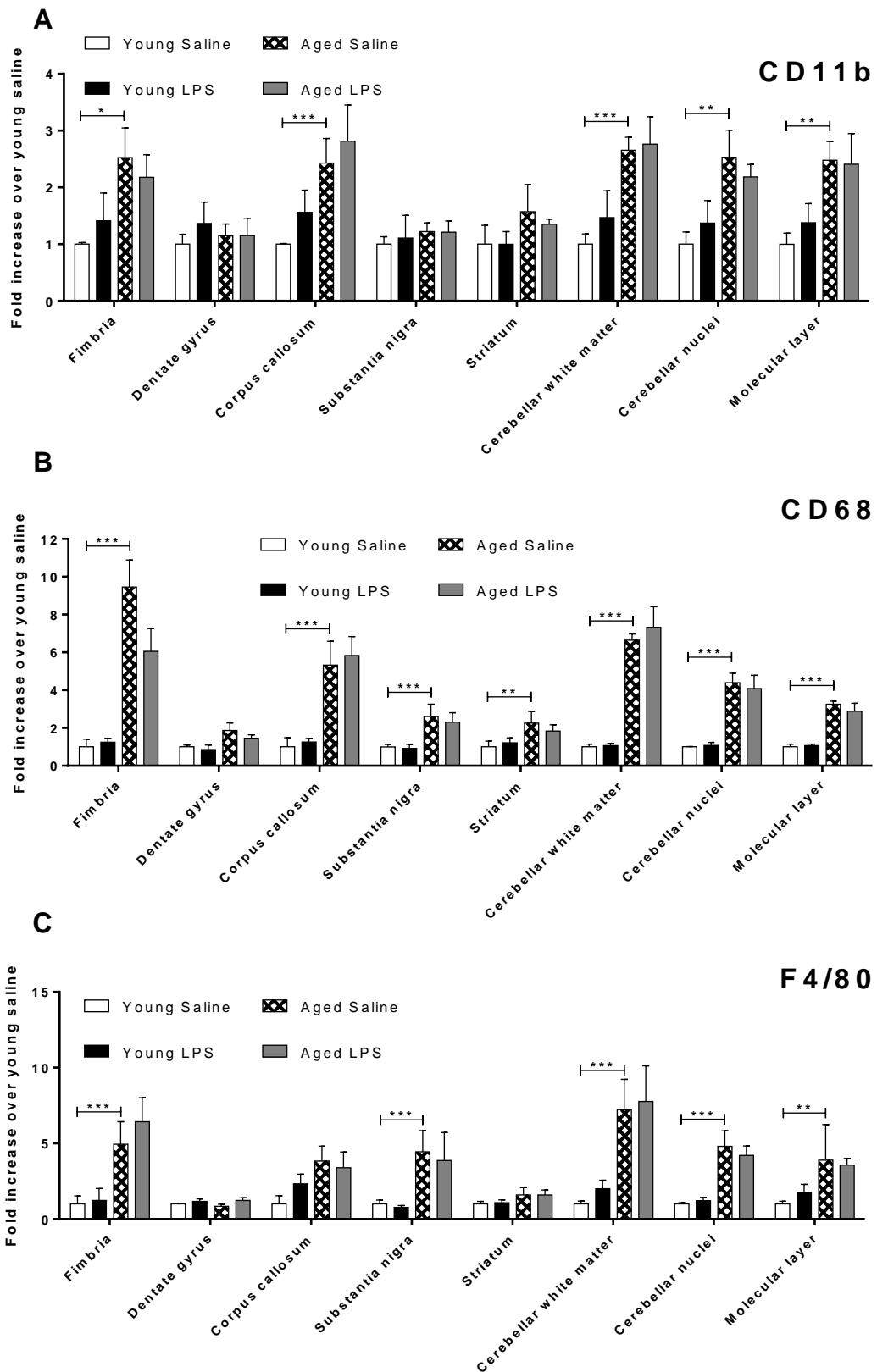
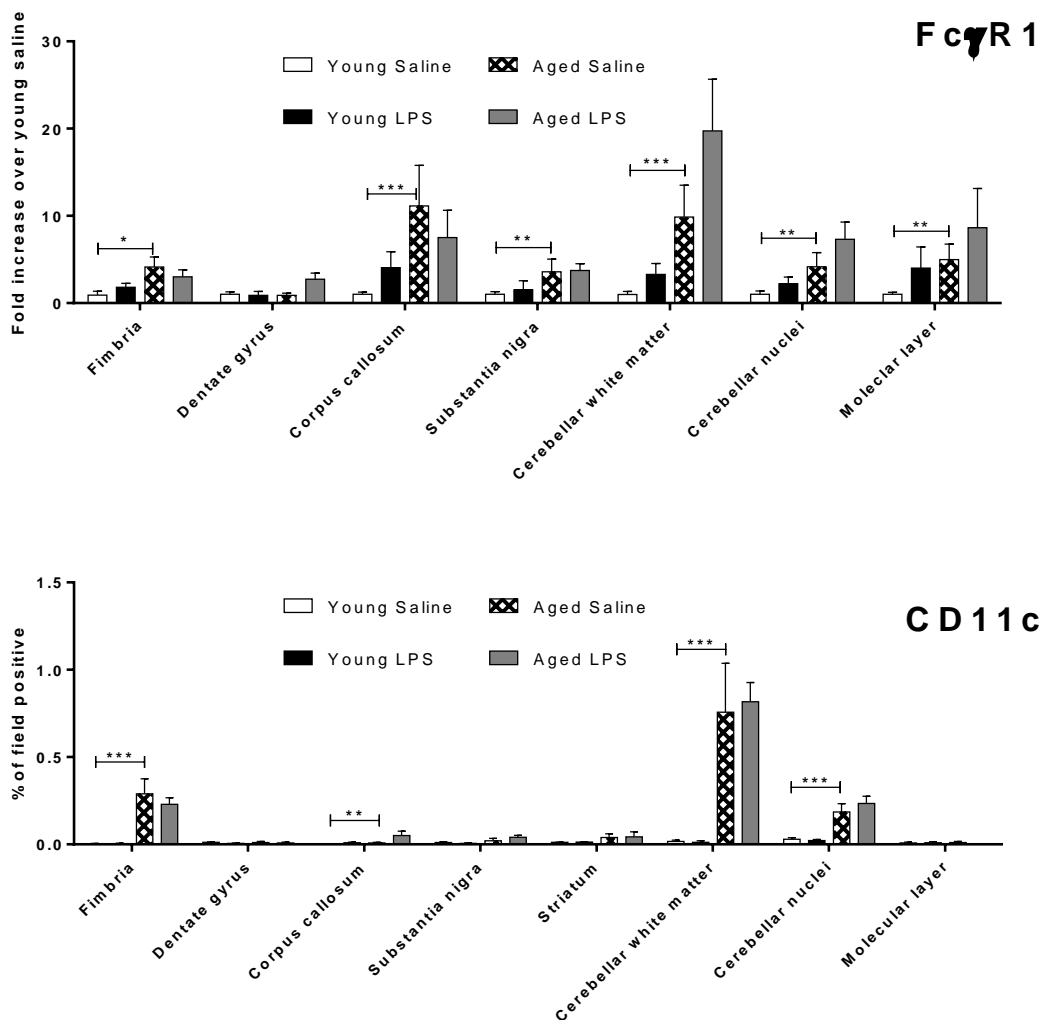


Figure 4.6. Age related changes in microglial phenotype in different brain regions.

(A) CD11b expression in selected regions of the CNS. n = 4-5 per region. (B) CD68 expression in selected regions of the CNS. n = 4-5 per region. (C) F4/80 expression in selected regions of the CNS. n = 4-5 per region. Horizontal bars denote a significant effect of age (4m saline to 21m saline) or LPS (21m saline to 21m LPS) within that region. Data is shown as mean  $\pm$  SEM. \* denotes  $p < 0.05$ ; \*\* denotes  $p < 0.01$ ; \*\*\* denotes  $p < 0.001$  in Holm-Sidak post tests.



**Figure 4.7. Age related changes in CD11c and FcγRI expression in different brain regions.**

(A) CD11c expression in selected regions of the CNS. n = 5 per region. (B) FcγRI expression in selected regions of the CNS. n = 4-5 mice per region. Horizontal bars denote a significant effect of age (4m saline to 21m saline) or

LPS (21 m saline to 21 m LPS) within that region. Data is shown as mean  $\pm$  SEM. \* denotes  $p < 0.05$ ; \*\* denotes  $p < 0.01$ ; \*\*\* denotes  $p < 0.001$  in Holm-Sidak post tests.

Changes in additional molecules expressed by microglia during ageing and after systemic LPS injection were investigated in a qualitative manner using immunohistochemistry. A small number of Dectin-1 positive cells were detected in the white matter tracts of aged animals (3-4 cells per  $\times 20$  field of cerebellum), but not in aged grey matter or young white matter (Figure 4.8). Dectin-1 positive cells were present in white matter throughout the aged brain, but were most frequently seen in the cerebellum. The expression levels of Dectin-1 did not appear to be influenced by systemic LPS. Some of these Dectin-1 positive cells were aggregates, with multiple nuclei visible within the stained area (Figure 4.8 C-D). Dectin-1 positive cells were present in the white pulp of the spleen, as has been previously reported (Reid et al., 2004) (Figure 4.11 A). DEC-205 positive cells were not observed in any region of either the young or aged brain, despite the detection of positive staining in the marginal zone and white pulp of the spleen (Figure 4.11 D), where DEC-205 positive cells are expected to be present (Pack et al., 2008). Expression levels of Fc $\gamma$ RII/III and MHCII were also investigated and the majority of positive cells for these two markers in the brain were associated with blood vessels. Some faintly Fc $\gamma$ RII/III positive cells with a microglial morphology were however present in aged white matter tracts (Figure 4.9 C-D). There was no detectable change in microglial MHCII expression dependent on age or LPS (Figure 4.10), despite the presence of strong staining throughout the spleen (Figure 4.11 C). Fc $\gamma$ RII/III was restricted to the red pulp and marginal zone of the spleen (Figure 4.11 B), as was expected given its myeloid cell specific expression (Tuijnman et al., 1993).

In summary, age related changes in expression of microglial activation markers varied greatly between different brain regions, with the cerebellum and the white matter showing the most pronounced changes, while the effect of systemic LPS on microglia associated molecule expression was limited to Fc $\gamma$ RI.

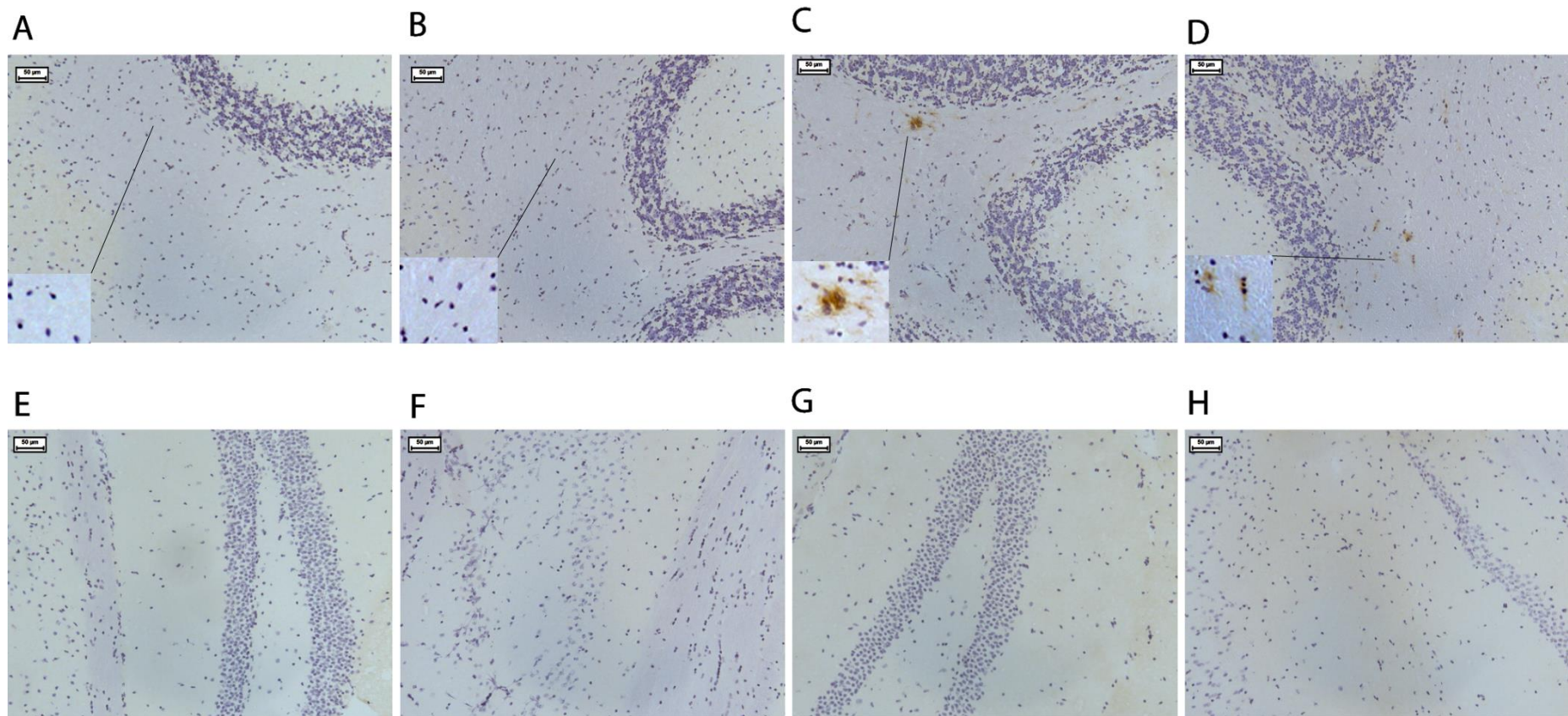


**Figure 4.8. Dectin 1 marker expression increases with age, but not LPS.**

A-D Cerebellum. A – young saline, B – young LPS, C – aged saline, D – aged LPS. E-G Hippocampus. E – young saline, F – young LPS, G – aged saline, H – aged LPS. Insets show magnified, contrast enhanced areas of images indicated by lines. Representative of n = 5. Scale bar represents 50 $\mu$ m.

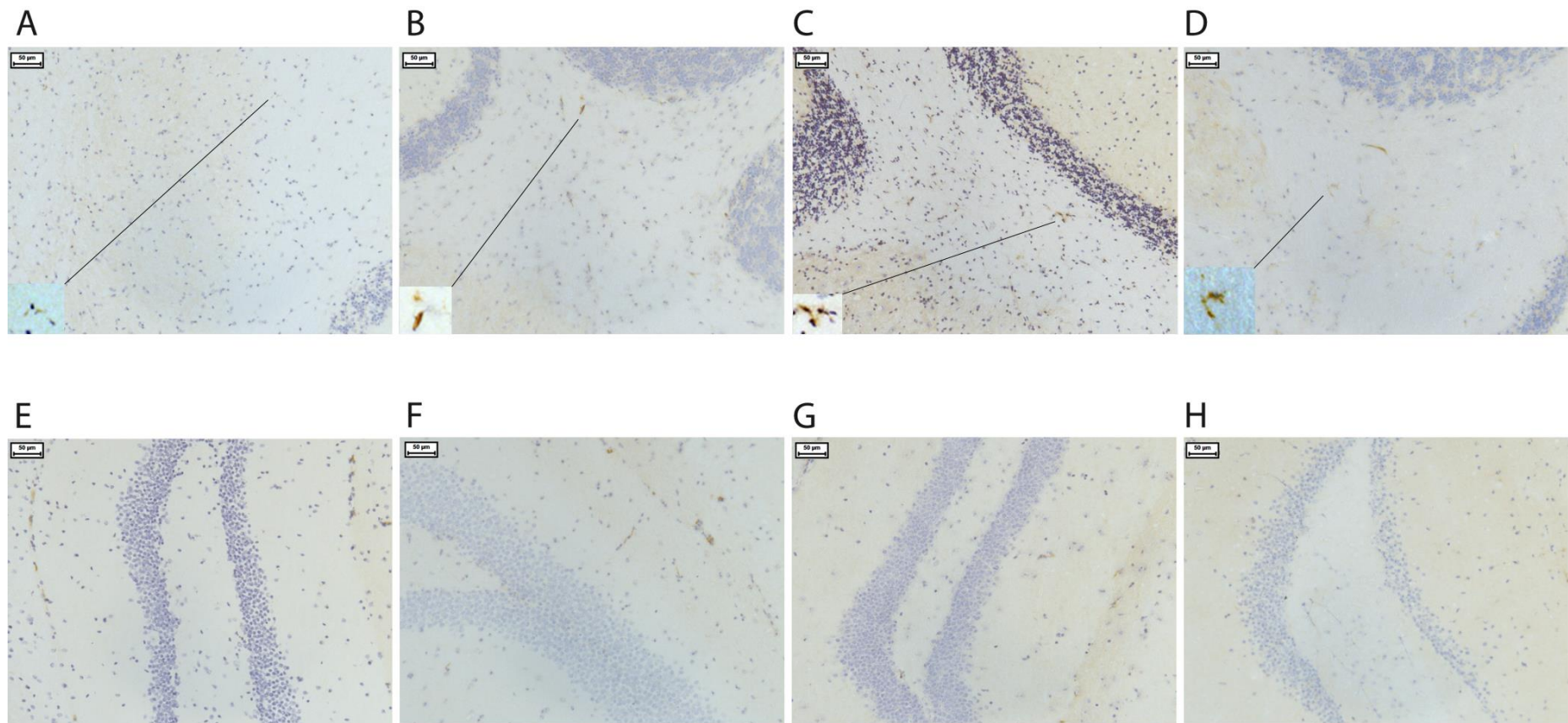


**Figure 4.9. Fc $\gamma$ R II/III expression in the ageing brain following a systemic challenge LPS.**

A-D Cerebellum. A - young saline, B - young LPS, C - aged saline, D - aged LPS. E-G Hippocampus. E - young saline, F - young LPS, G - aged saline, H - aged LPS. Insets show magnified, contrast enhanced areas of images indicated by lines. Representative of n = 5. Scale bar represents 50 $\mu$ m.

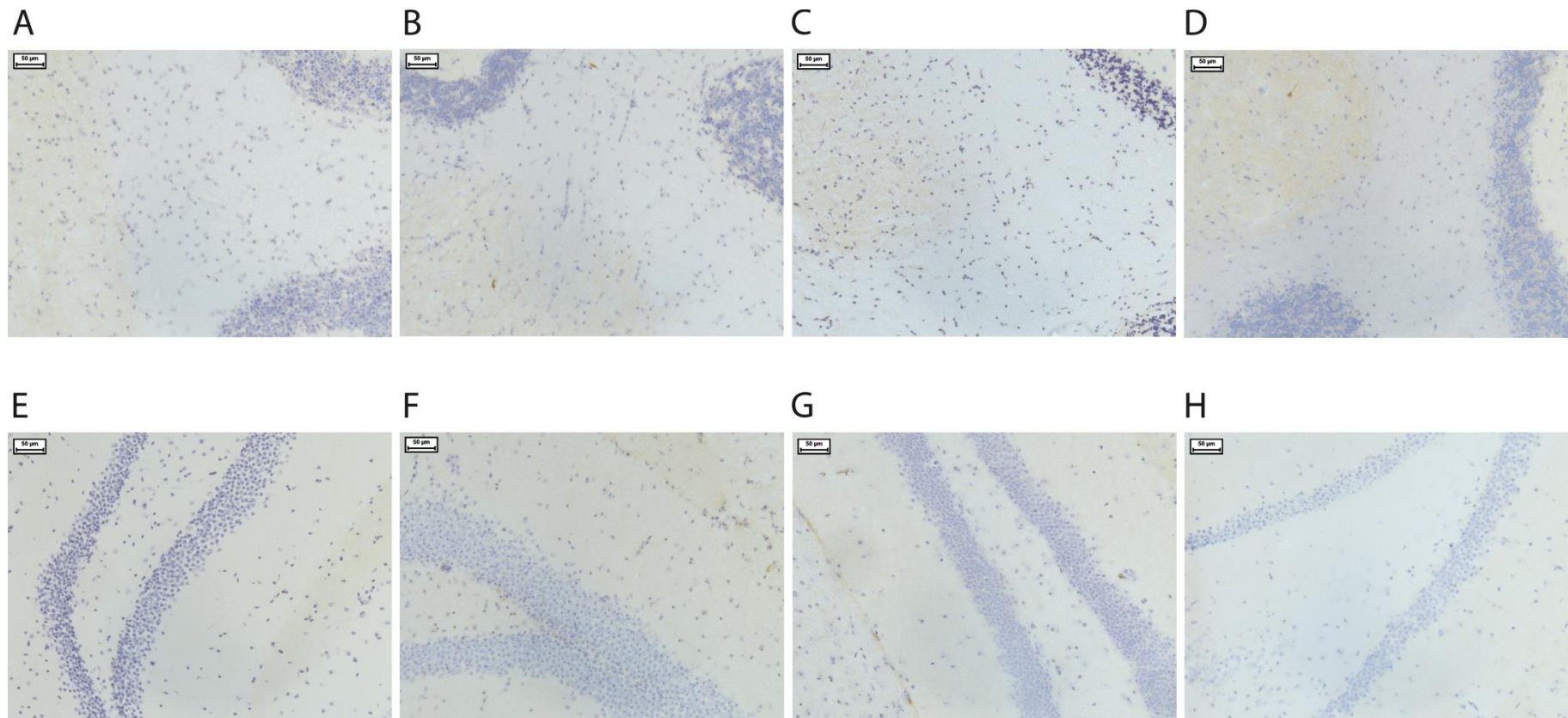


**Figure 4.10. MHC class II expression does not change with age or LPS.**

**A-D Cerebellum. A - young saline, B - young LPS, C - aged saline, D - aged LPS. E-G Hippocampus. E - young saline, F - young LPS, G - aged saline, H - aged LPS. Scale bar represents 50μm.**

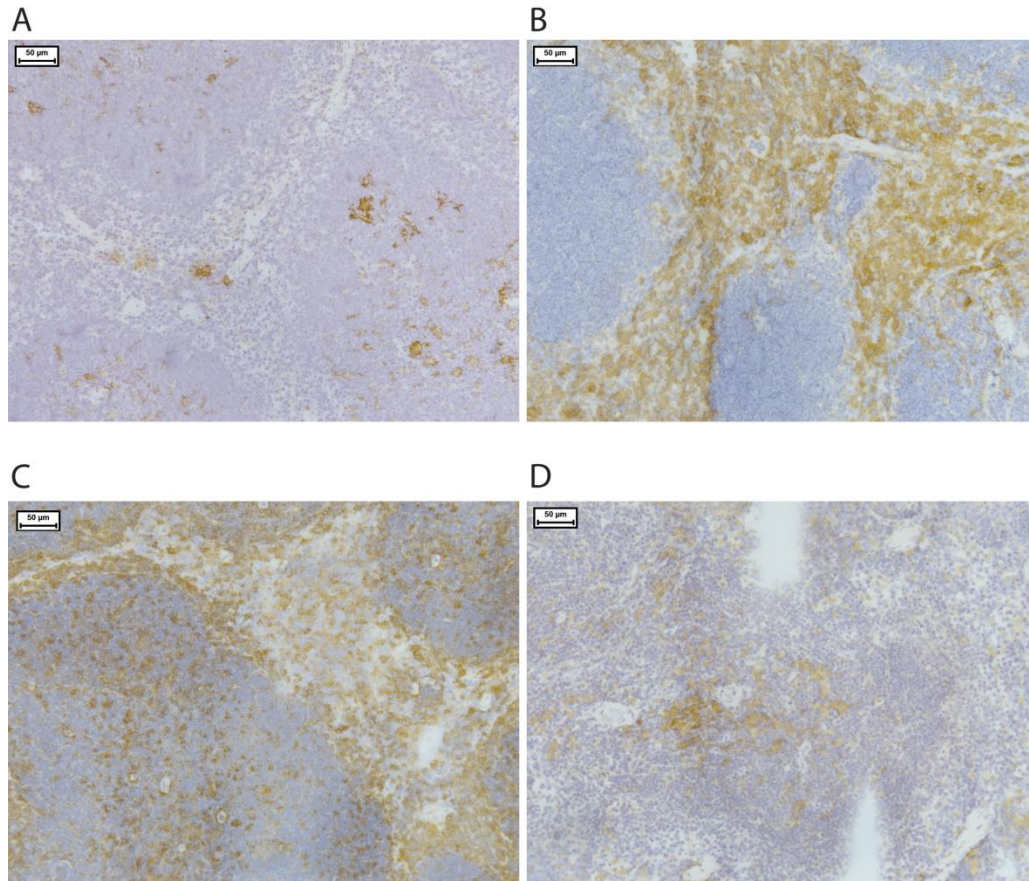


**Figure 4.11. Expression of Dectin 1, MHC class II, Dec205 and Fc $\gamma$ RII/III in the young spleen.**

**(A)** Dectin 1 staining is localised to the white pulp of the spleen of a saline injected 11 month old mouse. **(B)** CD16/32 expression is limited to the red pulp and marginal zone of the spleen of a saline injected young mouse. **(C)** MHCII expression is present on cells throughout the spleen of a saline injected young mouse, but is most abundant in the marginal zone and white pulp. **(D)** Dec205 expression is present in the marginal zone and white pulp of the spleen saline injected aged mouse. Representative of n = 5. Scale bar represents 50 $\mu$ m.



### 4.3.2 Quantification of inflammatory molecule expression in the young and aged brain by qPCR

Expression of pro-inflammatory molecules in the CNS which have possible roles in sickness behaviour were investigated using quantitative PCR. GAPDH was selected for use as a reference gene because it was the most stably expressed in all the experimental conditions investigated compared to ATP synthase 5b and beta actin, the two other candidate reference genes assessed. Expression of IL-1 $\beta$ , IL-6 and the microglial activation marker F4/80 were measured in hippocampus/cortex tissue and compared against cerebellum from young and aged mice 24h after i.p. saline or LPS injection (Figure 4.12). The expression levels of all these genes was not altered by LPS injection 24 hours prior to tissue collection, although there was a nearly significant effect of LPS on F4/80 expression in both cerebellum ( $p = 0.055$ ) and hippocampus/cortex tissue ( $p = 0.053$ ). The data for IL-1 $\beta$  was highly variable and there was no significant effect of age, LPS or age x LPS interaction. IL-6 expression was only assessed in hippocampus/cortex tissue and was not affected by ageing, LPS or age x LPS interaction. F4/80 expression was significantly increased by ageing in the cerebellum but not in hippocampus/cortex tissue. There was no significant age x LPS interaction on F4/80 expression. Table 4.3 contains the statistical analysis of the fold increase from young saline treated tissue.

One experiment was also performed using ELISA to assess IL-6 levels in the serum of young and aged mice 24h after saline or LPS injection ( $n=2-3$  from each condition). IL-6 was not detectable in the serum of any mice tested.

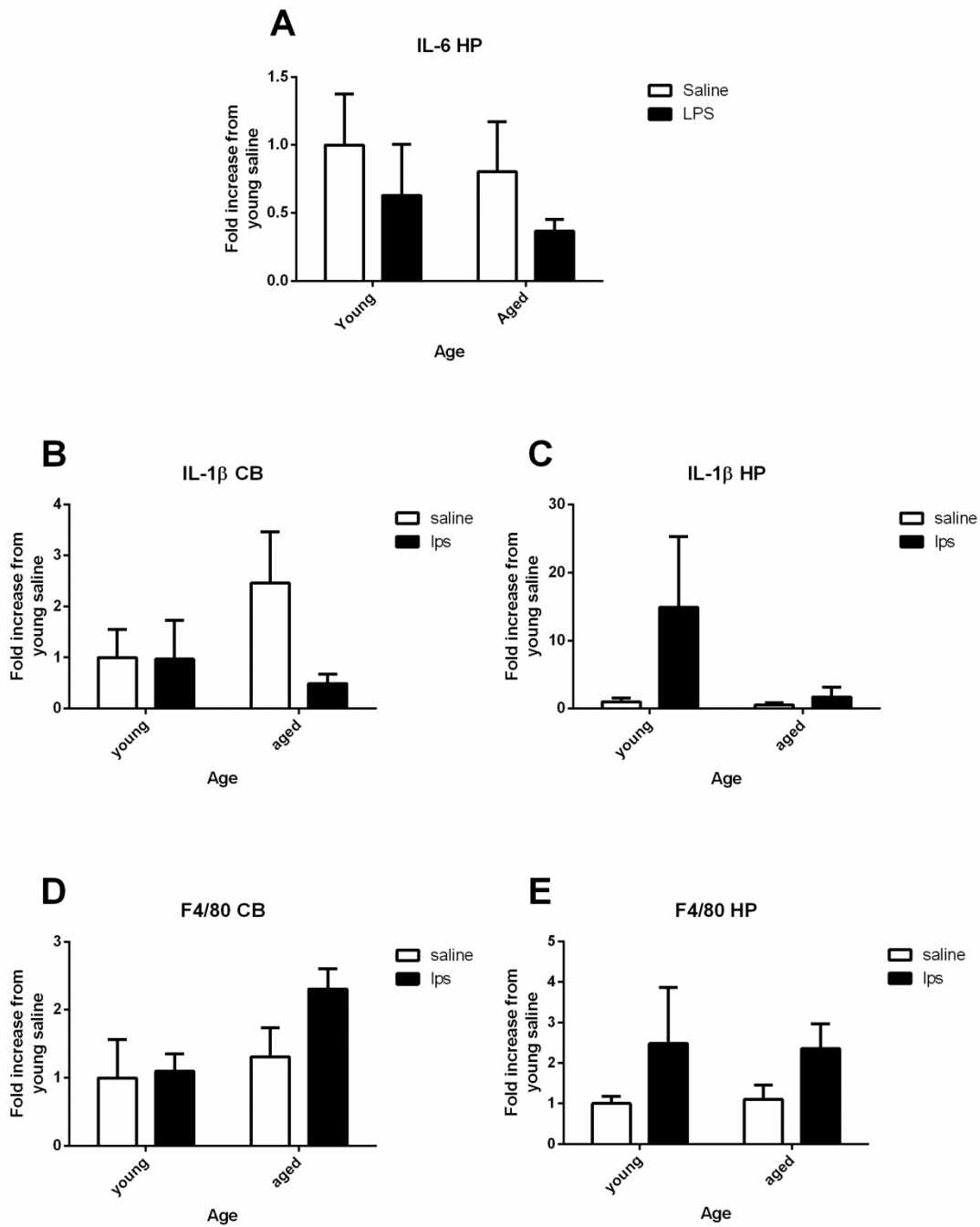


**Figure 4.12. The effect of LPS on expression of IL-1 $\beta$ , IL-6 and F4/80 mRNA levels in young and aged cerebellum and hippocampus/cortex tissue 24h after saline/LPS injection.**

**(A)** IL-6 expression in hippocampus/cortex tissue. **(B)** IL-1 $\beta$  expression in the cerebellum. **(C)** IL-1 $\beta$  expression in hippocampus/cortex tissue. **(D)** F4/80 expression in the cerebellum. **(E)** F4/80 expression in hippocampus/cortex

tissue. There was no significant difference between groups in Holm-Sidak post tests. Data is shown as mean  $\pm$  SEM. N =3-7 per group.

24h LPS	Cerebellum			Hippocampus/ Cortex		
Gene	Age	LPS	Age x LPS	Age	LPS	Age x LPS
IL-6 n = 4- 6/grou p				F (1, 18) = 0.5170	F (1, 18) = 0.001247	F (1, 18) = 0.04122
				P = 0.4814	P = 0.9722	P = 0.8414
IL-1 $\beta$ n = 3- 4/grou p	F (1, 10) = 1.374	F (1, 10) = 1.868	F (1, 10) = 0.8954	F (1, 12) = 4.600	F (1, 12) = 2.597	F (1, 12) = 1.794
	P = 0.2684	P = 0.2017	P = 0.3663	P = 0.0531	P = 0.1330	P = 0.2053
F4/80 n = 5- 7/grou p	F (1, 21) = 4.782	F (1, 21) = 4.133	F (1, 21) = 0.2411	F (1, 23) = 0.07170	F (1, 23) = 4.148	F (1, 23) = 0.4462
	P = 0.0402	P = 0.0549	P = 0.6285	P = 0.7913	P = 0.0533	P = 0.5108

**Table 4.2. Statistical results of analysis of qPCR data from young or aged cerebellum or hippocampus/cortex tissue 24h after saline/LPS injection.**

Data was logarithmic transformed to achieve normality and then analysed using two way ANOVAs.

A second experiment was conducted to investigate the effects of LPS on young or aged mice 3 hours after an intraperitoneal injection of 100 $\mu$ g/kg of LPS. GAPDH was used as a reference gene to quantify expression of IL-1 $\beta$ , COX-2, IL-6 and TNF $\alpha$  in the cerebellum (Figure 4.13) or hippocampus (Figure 4.14). In the cerebellum LPS caused a significant increase in expression of IL-1 $\beta$  and IL-6 and a non-significant increase in expression of COX-2 in aged tissue only. Expression of these molecules was not altered by LPS in young cerebellum tissue. Age had a significant effect on expression of IL-1 $\beta$  and COX-2, but not on IL-6 or TNF $\alpha$ , and there was significant effect of age x LPS interaction on IL-6 expression but not on IL-1 $\beta$ , TNF $\alpha$  or COX-2. In the hippocampus expression

of IL-1 $\beta$ , TNF $\alpha$ , IL-6 and COX-2 was significantly increased by age and LPS. There was no significant effect of age x LPS interaction on expression of any of these molecules in the hippocampus. The changes in expression of these molecules resulting from age or LPS were notably more pronounced in the hippocampus than in the cerebellum. Table 4.4 contains the statistical analysis of the fold increase from young saline treated tissue.

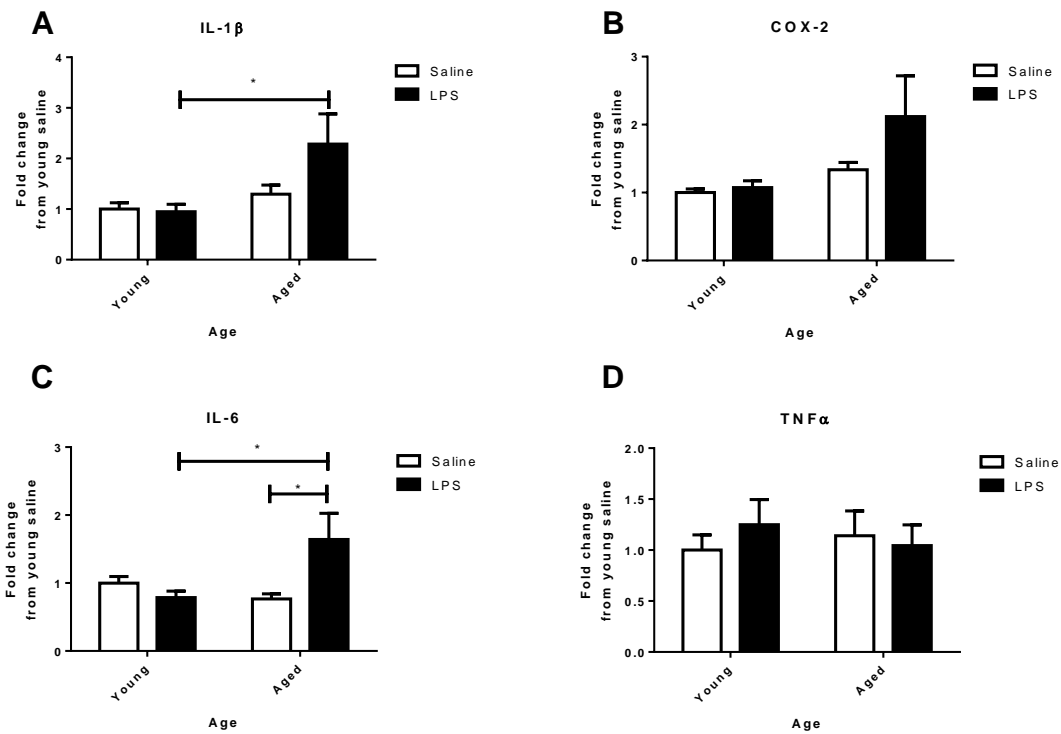


**Figure 4.13. The effect of LPS on expression of expression of inflammatory molecules in young and aged cerebellum 3h after saline/LPS injection.**

Expression of IL-1 $\beta$  (A), COX-2 (B), IL-6 (C), and TNF $\alpha$  (D) were measured by qPCR. Data is shown as mean  $\pm$  SEM. \* denotes p < 0.05 (Holm-Sidak post test). n = 5-6 per group.

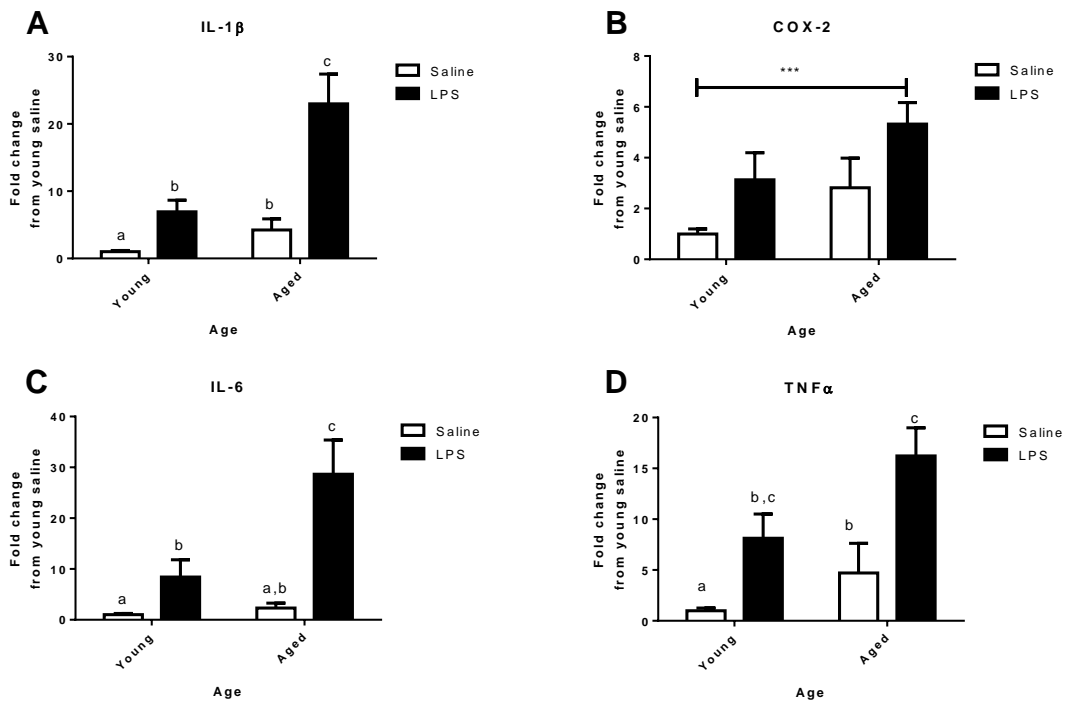


**Figure 4.14. The effect of LPS on expression of IL-1 $\beta$ , IL-6, TNF $\alpha$  and COX-2 mRNA levels in young and aged hippocampus 3h after saline/LPS injection.**

Expression of IL-1 $\beta$  (A), COX-2 (B), IL-6 (C), and TNF $\alpha$  (D) were measured by qPCR. Data is shown as mean  $\pm$  SEM. \*\*\* denotes  $p < 0.001$ . Means with different letters are significantly different to each other ( $p < 0.05$ , Holm-Sidak post tests).  $n = 5-6$  per group.

3h LPS	Cerebellum			Hippocampus		
	Age	LPS	Age x LPS	Age	LPS	Age x LPS
IL-1 $\beta$ n=4- 5/group	F (1, 17) = 8.255	F (1, 17) = 1.158	F (1, 17) = 2.210	F (1, 19) = 23.54	F (1, 19) = 53.48	F (1, 19) = 0.003561
	P = 0.0105	P = 0.2969	P = 0.1554	P = 0.0001	P < 0.0001	P = 0.9530
IL-6 n=4- 5/group	F (1, 17) = 1.676	F (1, 17) = 1.820	F (1, 17) = 9.375	F (1, 19) = 10.78	F (1, 19) = 45.57	F (1, 19) = 1.557
	P = 0.2128	P = 0.1950	P = 0.0071	P = 0.0039	P < 0.0001	P = 0.2272
TNF $\alpha$ n=4- 5/group	F (1, 17) = 0.09111	F (1, 17) = 0.07891	F (1, 17) = 0.5193	F (1, 19) = 10.82	F (1, 19) = 40.01	F (1, 19) = 0.3068
	P = 0.7664	P = 0.7822	P = 0.4809	P = 0.0039	P < 0.0001	P = 0.5861

COX-2 n=4- 5/group	F (1, 17) = 4.537	F (1, 17) = 0.8283	F (1, 17) = 0.3290	F (1, 19) = 8.915	F (1, 19) = 12.80	F (1, 19) = 0.1004
	P = 0.0481	P = 0.3755	P = 0.5738	P = 0.0076	P = 0.0020	P = 0.7549

**Table 4.3. Statistical results of analysis of qPCR data from young or aged cerebellum or hippocampus/cortex tissue 24h after saline/LPS injection.**

Data was analysed by logarithmic transformation to achieve normality and then performing two way ANOVAs.

In summary, these results show that there are significant regional differences in microglial phenotype in the aged brain. This effect of LPS on microglial activation marker expression varied according to age and CNS region. Elevated expression of IL-1 $\beta$  or IL-6 24h after LPS injection was not detectable, but 3h after LPS there was a pronounced increase in expression of IL-1 $\beta$ , TNF $\alpha$ , COX-2 and IL-6 in the hippocampus. This increase was more pronounced in the hippocampus of aged mice. There was a small increase in expression of IL-1 $\beta$ , IL-6 and COX-2 in aged but not young cerebellum tissue 3h after LPS injection.

## 4.4 Discussion

In this study the phenotype and morphological changes of microglia in eight distinct regions of the young and aged mouse brain was investigated. This study shows that age-related phenotype changes of microglial cells are more pronounced in the white matter, with the cerebellum, the most caudal structure studied, showing the greatest differences.

Variations in microglial density have been well described in adult mouse brain with the hippocampus and substantia nigra exhibiting the highest and the cerebellar cortex the lowest density of microglia (Lawson et al., 1990). A number of studies in several areas of the CNS indicate that there is little, if any, change in the distribution or numbers of microglia with age (Deng et al., 2006; Long et al., 1998; Ogura et al., 1994; Peters et al., 2010), but less is known about phenotype changes in different regions of the aged mouse brain. These results are in accord with a recent study describing regional variation in expression levels of immunoregulatory molecules in the healthy adult mouse brain. De Haas et al showed that regional differences between microglial

phenotypes in the adult mouse brain are subtle: expression levels of surface markers such as CD11b, CD40 and the fractalkine receptor CX3CR1 appeared higher in the microglia of the spinal cord and cerebellum than the hippocampus (De Haas et al., 2008). In this study all the functional markers tested displayed the greatest increase in expression with age in white matter regions, particularly in the cerebellum, identifying a clear trend in phenotype changes along the rostro-caudal axis in the aged mouse brain.

The functional markers studied here were selected on a candidate basis, either due to their sensitivity to changes in the activation state of microglia (CD11b, F4/80, CD68, CD11c) or their relevance to microglial function (MHCII, Fc $\gamma$ RI, Fc $\gamma$ RII/III, dectin-1), or both. Table 4.1 describes each one in more depth.

#### **4.4.1 Microglial phenotype changes in response to injury along the rostro-caudal axis**

Phenotype changes in microglia are well described in response to acute and chronic injury or disease, but only a few studies have looked at differential responsiveness of the grey matter versus the white matter along the rostro-caudal axis. Trauma-induced lesions lead to a greater microglial response in the spinal cord than the cortex or corpus callosum and the spinal white matter exhibited a greater microgliosis than spinal grey matter (Batchelor et al., 2008; Schnell et al., 1999a). Regional differences in responsiveness to inflammatory stimuli are partly responsible for these observations, as stereotaxic injections of recombinant cytokines into the striatum fail to evoke a robust response, while similar injections into the spinal cord or brainstem are associated with BBB breakdown, microgliosis and secondary tissue damage (Campbell et al., 2002; Phillips and Lampson, 1999; Phillips et al., 1999; Schnell et al., 1999b). This regional difference in responsiveness to inflammatory stimuli is also evident in EAE, which targets the spinal cord rather than more rostral regions of the brain, such as the forebrain (Sun et al., 2004). Collectively, these studies suggest that the caudal and white matter regions of the CNS are more responsive and therefore more vulnerable to inflammatory stimuli. The experiments described in this chapter suggest that the differential sensitivity of these microglial populations also applies to the ageing process. These data show that in the aged brain there is a greater up-regulation of CD11b, CD11c,

CD68, F4/80 and Fc $\gamma$ RI in white matter than in grey matter and more in caudal areas than rostral areas. These data are in agreement with previous studies in the aged rat brain suggesting a rostral caudal gradient of microglial activation (Kullberg et al., 2001).

#### **4.4.2 Pronounced white matter related changes**

It has been previously reported that the microglia of the white matter express greater levels of microglia associated molecules such as CD68 with age than those of the grey matter (Kullberg et al., 2001), and that the microglia may appear in “clumps” of immunoreactive membranes in white matter (Perry et al., 1993; Stichel and Luebbert, 2007). These aggregates are not directly associated with blood vessels and are not clusters of proliferating cells. Macrophages and microglia are known to form multinucleate giant cells through fusion under a variety of inflammatory conditions (Fendrick et al., 2007; Gasser and Most, 1999; Suzumura et al., 1999). Whether these cells are aggregates of individual microglia or a single syncytium is not clear, but the appearance of multinucleate giant cells during ageing would represent a significant alteration in microglial phenotype.

#### **4.4.3 Pronounced changes in CD11c expression**

A significant increase in CD11c expression levels was observed in aged white matter regions, particularly in the white matter of the cerebellum. Increases in CD11c immunoreactivity in the aged rodent CNS have been reported previously with robust CD11c expression in the aged white matter and occasional CD11c expression throughout the grey matter (Kaunzner et al., 2012; Stichel and Luebbert, 2007). These two studies used immunohistochemistry and FACS to describe CD11c positive cells as dendritic cells, as they co-express DEC-205 and MIDC8 (Stichel and Luebbert, 2007) as well as increased expression of MHCII and the co-stimulatory molecules CD80 and CD86 (Kaunzner et al., 2012). However, only a small portion of CD11c positive cells in the brain were positive for these other molecules, and in this chapter microglial expression of DEC-205 or MHCII was not detectable, despite the presence of positive staining in the spleen, suggesting that the CD11c positive cells observed in this chapter are not dendritic cells. The discrepancy between this study and others with

regard to MHCII expression on aged microglia may be explained by the superior sensitivity of flow cytometry (Henry et al., 2009; Kaunzner et al., 2012).

CD11c is expressed on macrophages, monocytes and dendritic cells and is involved in cell migration and phagocytosis (Cho et al., 2007; Mevorach et al., 1998; Schlesinger and Horwitz, 1991; Wentworth et al., 2010). Various studies also suggest a role for CD11c in the uptake of lipids (Cho et al., 2007; Gower et al., 2011) and show that low density lipoprotein (LDL) exposure can lead to upregulation of CD11c following engagement of low density lipoprotein receptor related protein 1 (LRP-1) (Cho et al., 2007). This may provide an explanation for the robust increase in CD11c expression observed in aged white matter, as myelin is lipid rich and myelin basic protein 1 (MBP-1) has been reported to bind to LRP-1, inducing MBP-1 uptake (Gaultier et al., 2009). We hypothesise that LRP-1 mediated uptake of myelin by microglia leads to a subsequent upregulation of CD11c expression, explaining the localisation of CD11c in the aged white matter. This may have important effects on microglial phenotype and function, as myelin phagocytosis has been shown in vitro to attenuate microglial cytokine responses to IFN $\gamma$ /LPS while simultaneously increasing extracellular ROS levels (Liu et al., 2006). Abnormalities in the myelin sheath, loss of myelinated fibres and decreased stability of myelin have previously been reported in aged rodent and primate brains (Ando et al., 2003; Bowley et al., 2010; Cavallotti et al., 2001; Zhang et al., 2009), supporting the idea of an increased phagocytic load of myelin or myelin breakdown products in the aged brain. This supposition is further supported by the presence of myelin inside the microglia of the optic nerve and fornix of aged rhesus monkeys (Peters et al., 2010; Sandell and Peters, 2002), greater upregulation during ageing of the lysosomal protein CD68 in white than grey matter and the activation of calpain 1, an enzyme involved in the proteolysis of various cytoskeletal proteins and several myelin components, in the microglia in aged white matter (Hinman et al., 2004). Astrocytes and oligodendrocytes on the other hand did not exhibit increases in calpain 1 activity (Hinman et al., 2004).

#### 4.4.4 Neurodegeneration in the ageing brain

It is well recognised that the microglia are exquisitely sensitive to neurodegeneration. However, the extent to which neurodegeneration occurs in the ageing CNS varies considerably from region to region. The substantia nigra (Ma et al., 1999; Mouton et al., 2012) and cerebellum (Sturrock, 1989; Woodruff-Pak et al., 2010) exhibit significantly greater age-related neuronal loss than the hippocampus (Calhoun et al., 1998; Rapp and Gallagher, 1996) or striatum (Pesce and Reale, 1987), and substantial loss of myelinated axons has been reported in white matter regions (Bowley et al., 2010; Cavallotti et al., 2001; Sandell and Peters, 2002, 2003). The areas with greatest neuronal loss are also the regions that exhibit greater changes in microglial phenotype. Whether neuronal loss drives microglial phenotype changes in ageing, or if changes to the microglia precede and contribute towards neuronal loss, is not known. There are however several mechanisms by which neurons keep microglia in a quiescent state, such as via CD200, fractalkine or CD47 and their cognate receptors on microglia (Hoek et al., 2000; Kong et al., 2007; Lyons et al., 2009a). CD200 and CD47 have also been shown to be expressed on oligodendrocytes (Gitik et al., 2011b; Koning et al., 2009). The few studies that have investigated the distribution of these molecules in the healthy adult brain correlate with the changes in microglial phenotype with age observed in this study. Koning et al observed that CD200 is more highly expressed in grey than white matter and that the Purkinje cells of the cerebellum do not express CD200 (Koning et al., 2009). These grey-white matter differences in CD200 expression may contribute to the differences observed in this study between grey and white matter in the phenotype of ageing microglia. Fractalkine transcript expression has been reported to be significantly lower in the cerebellum and other caudal areas such as the brainstem than the hippocampus or striatum, which may help to explain the rostral caudal gradient of microglial changes observed in this study (Tarozzo et al., 2003).

Decreased expression of CD200 in the hippocampus and substantia nigra (Frank et al., 2006; Wang et al., 2011), and of fractalkine in the hippocampus and forebrain have been demonstrated in aged mice (Lyons et al., 2009a; Wynne et al., 2010). Increased numbers of multinuclear giant cells have also been observed in CD200<sup>-/-</sup> mice (Hoek et al., 2000), providing a possible

explanation for their presence in the aged brains of this study. A wider assessment of the expression of these immunoregulatory molecules in different regions of the aged brain and how they may correlate with changes in microglial phenotype would be of interest.

#### **4.4.5 Impact of systemic inflammation on aged-related microglial phenotype**

An increase in expression levels of microglia activation markers after systemic LPS injection was anticipated, which has previously been shown to up-regulate Fc $\gamma$ RI (Lunnon et al., 2011) and CD11b (Buttini et al., 1996). However, the only molecule found to be sensitive to i.p. injection of 100 $\mu$ g/kg of LPS was Fc $\gamma$ RI. CD11b expression was not influenced by systemic LPS. Furthermore, the effect of systemic LPS on Fc $\gamma$ RI expression was subtle, region dependent and primarily observed in the white matter regions and the cerebellum of both young and aged mice. Higher doses of systemic LPS or a later time-point post injection, such as three days, may yield a more robust effect on expression of these molecules (Buttini et al., 1996).

Elevated levels of cytokines within the aged hippocampus have been demonstrated following systemic inflammatory challenge (Barrientos et al., 2009a; Chen et al., 2008; Godbout et al., 2005b), which are likely produced by primed microglia in the ageing brain (Frank et al., 2010b; Wynne et al., 2010). Systemic LPS injection did not lead to elevated levels of IL-1 $\beta$  or IL-6 24 hours after systemic LPS injection in the brain regions studied, in contrast to other studies (Godbout et al., 2005b; Wynne et al., 2010). This discrepancy may be due to the use of a lower dose of LPS (100 $\mu$ g/kg vs 330 $\mu$ g/kg) and a different sex and strain of mouse (male BALB/c vs female C57/BL6) in this study. At a more acute time-point increases in cytokine production were however detectable. An enhanced neuroinflammatory reaction in aged mice was detected at 3 hours after LPS injection, characterised by enhanced induction of IL-1 $\beta$ , IL-6, TNF $\alpha$  and COX-2 mRNA in the hippocampus. LPS only had a measurable effect on cytokine transcript levels in aged cerebellar tissue – cytokine transcription was unaffected in young cerebellar tissue. The enhanced production of cytokines within the aged hippocampus is in line with other studies (Chen et al., 2008), but the relatively small cytokine response in the

cerebellum was unexpected. Previous reports have described a comparable inflammatory reaction in the cerebellum to that seen in the hippocampus 2h after intraperitoneal injection of 100µg/kg LPS in the rat (Hansen et al., 2000b) or i.c.v. injection of 10ng of LPS in mice (Huang et al., 2008). Additional time-points after LPS challenge would have been helpful in this study in determining whether the lack of cytokine induction in the cerebellum is attributable to a difference in the kinetics of inflammatory responses to peripheral inflammation between the hippocampus and cerebellum or to a difference in responsiveness to inflammatory stimuli. Differences in microglial density between the two regions could also contribute to the differences in the inflammatory response, as the hippocampus is more densely populated with microglia than the cerebellum (Lawson et al., 1990) The LPS response only being present in aged, not young cerebellar tissue 3h after injection may be indicative of an exaggerated microglial response to systemic LPS in the aged cerebellum.

#### **4.4.6 Summary**

This study demonstrates that there are significant differences in microglial phenotypes between distinct regions of the aged brain. The microglia of the white matter show more robust changes than those of grey matter and there is evidence of a rostro-caudal gradient in the magnitude of these changes. The age-related changes in microglia phenotype reported here may be of particular interest when comparing studies in rodent and human material. In humans white matter makes up ~40% of the adult human brain (Gur et al., 1999) compared to 10% in the mouse (Zhang and Sejnowski, 2000), and human white matter contains a greater density of microglia than grey matter (Mittelbronn et al., 2001), conversely to the mouse (Lawson et al., 1990). The functional significance of these grey/white matter differences in microglial phenotype during ageing remain to be elucidated. Enhanced cytokine production in response to systemic LPS was detectable in the aged hippocampus and, to a lesser extent, cerebellum, suggesting that microglial priming occurs in both areas of the brain.

## 5. Characterisation of the behavioural response to salmonella typhimurium infection in young and aged mice.

### 5.1 Introduction

There is a growing body of literature suggesting that there is an exaggerated behavioural reaction to systemic inflammation in aged animals. However, the majority of this work has been undertaken using sterile inflammatory stimuli such as LPS or poly I:C, with only a few studies using live infections to investigate differences in the behavioural reaction of young and aged mice to systemic inflammation. The range of non-neurotropic infectious agents used to investigate young/aged differences in sickness behaviour is limited to *Bacillus Calmette-Guérin* (BCG) (Kelley et al., 2013), an intracellular mycobacterium and *E. coli* (Barrientos et al., 2006), a gram negative bacteria that colonises the lower intestine. Studies in rats have shown exaggerated weight loss, fever and an exaggerated deficit in memory performance in *E. coli* infected aged rats compared to infected young rats (Barrientos et al., 2006; Barrientos et al., 2009b), and exaggerated depressive behaviour in BCG infected aged mice compared to infected young mice and delayed recovery of body weight following BCG infection (Kelley et al., 2013).

*Salmonella typhimurium* is an intracellular mycobacterium that causes an infection in mice resembling typhoid fever (Santos et al., 2001). While the immunological reaction to murine *S. typhimurium* infection has been extensively investigated (Mastroeni et al., 2009), the murine behavioural response to *S. typhimurium* infection is not well characterised, as it has not until recently been used as a model of infection in the field of psychoneuroimmunology. The only significant report to date was that of Püntener et al (2012), which described an acute, transient behavioural response to systemic infection with  $1 \times 10^6$  CFU of *S. typhimurium* strain SL3261, including reduced burrowing behaviour (<24h) and an acute weight loss (0-24h) with recovery to 100% of original body weight within 7 days in young mice. The acute effects of *S. typhimurium* infection are likely mediated by circulating LPS, which is present in the serum for the first 24h of *S.*

*typhimurium* infection after i.p. injection (Püntener et al., 2012). Other studies have investigated the metabolic changes associated with *S. typhimurium* infection, demonstrating that a number of metabolic processes are affected during the first few days of *S. typhimurium* infection, including steroid and eicosanoid metabolism (Antunes et al., 2011). This was accompanied by a peripheral cytokine response dominated by IFN $\gamma$  that peaked at 7 days after infection and a central cytokine response that peaked at 3 weeks after infection (Püntener et al., 2012). The cerebral vasculature of these mice was particularly affected by *S. typhimurium* infection, showing a dramatic increase in MHCII reactivity 7 days after infection. The central response to infection in terms of cytokine production was small (~4 fold increase in IL-1 $\beta$  production) but significant at 3 weeks after infection, suggesting a prolonged neuroinflammatory response to peripheral infection.

The study described in this chapter aimed to determine whether there was an exaggerated behavioural and metabolic response to *S. typhimurium* in aged mice compared to young mice, as has been reported using other models of live infection (Barrientos et al., 2009a; Barrientos et al., 2006; Barrientos et al., 2009b; Kelley et al., 2013). This study was also designed to improve the characterisation of the behavioural response to *S. typhimurium* by performing a range of behavioural tests over a more prolonged period of time than previously studied in the literature.

## **5.2 Materials and Methods**

### **5.2.1 Animals**

C57/BL6 female mice aged 3-6 months or 18 months (Harlan, UK, bred in house) were used for pilot experiments to determine an appropriate dose of *S. typhimurium* to use. For the main experiment in this study (experiment 1) and a follow up study (experiment 2) 3 (young) or 18 month old (aged) C57/BL6 female mice were supplied by Charles River, Margate, UK. Mice were housed in groups of 5-6 per cage and housed in the category 2 facilities within the University of Southampton Biomedical Research Facility. All behavioural experiments in this chapter were carried out within these category 2 facilities.

### **5.2.2 Salmonella typhimurium infection**

Mice were injected i.p. with  $1 \times 10^5$ ,  $3 \times 10^5$  or  $1 \times 10^6$  CFU of *S. typhimurium* strain SL3261 (cultured in house by Dr Ursula Püntener, kindly provided by Dr H Atkins, DSTL, Salisbury, UK) or saline. Body weights were taken daily for 4 weeks after infection and every other day after 4 weeks, or until the mouse was culled. If a mouse's body weight dropped to below 85% of their original body weight then they were culled as specified in the Home Office Licence used in this experiment. Assistance was received from Ursula Püntener (University of Southampton) in collecting some body weight measurements and during injection of mice with *S. typhimurium*.

### **5.2.3 Food intake measurement**

Food intake was measured in experiment 2 by weighing the remaining amount of food pellets in the hopper of each cage between 9.00-10.00AM daily.

### **5.2.4 Behavioural testing regime**

Behavioural testing was performed between the hours of 08:00-18:00. Behavioural tests were performed as described in chapter 2. The habituation and testing regime used in experiment 1 are described in figures 5.1 and 5.2. D represents days post injection. At each behavioural time-point two separate groups for tissue collection were pooled to give behavioural data from naïve mice (saline injected (D0) and *S. typhimurium* injected D1), 7 days post injection (D8 and D15) and 21 days after injection (D22 and 2 months).

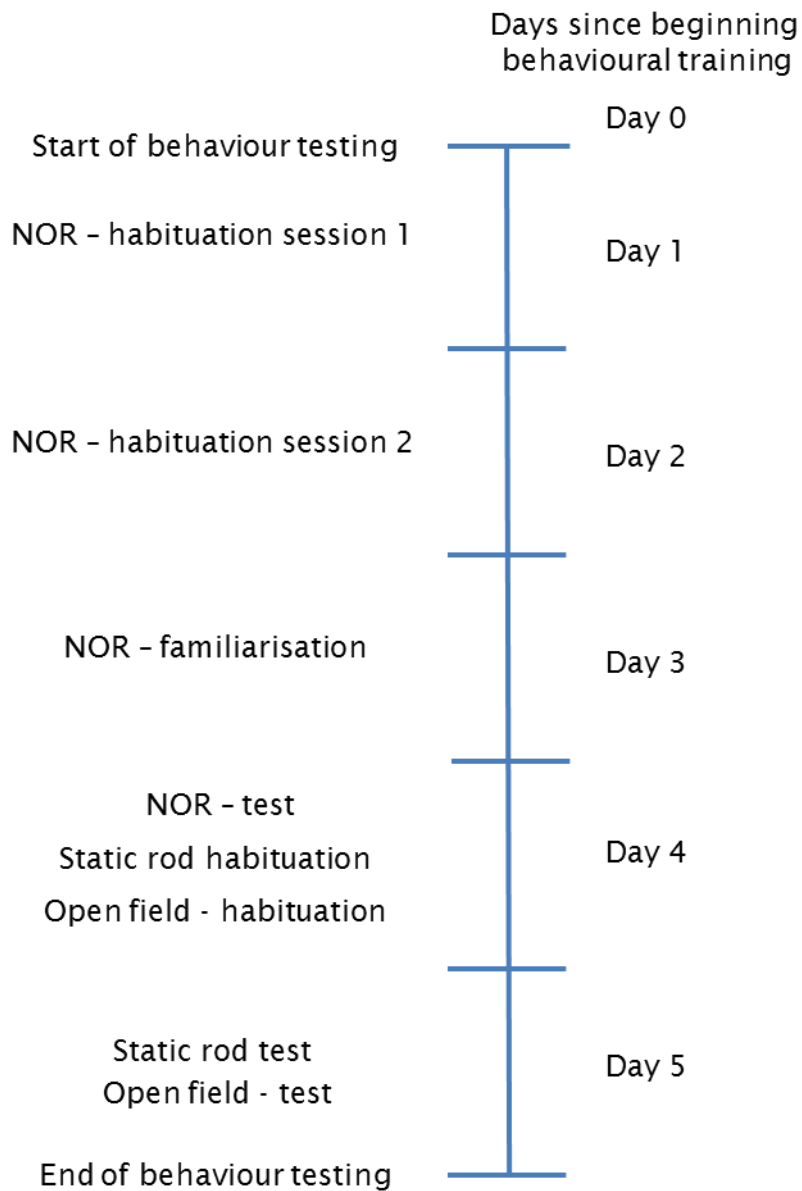


**Figure 5.1. Experimental design for behavioural testing in experiment 1.**

The training and testing regime for each time point (naïve (D0), 7 days after infection or 21 days after infection) used in experiment 1. NOR stands for the novel object recognition test.

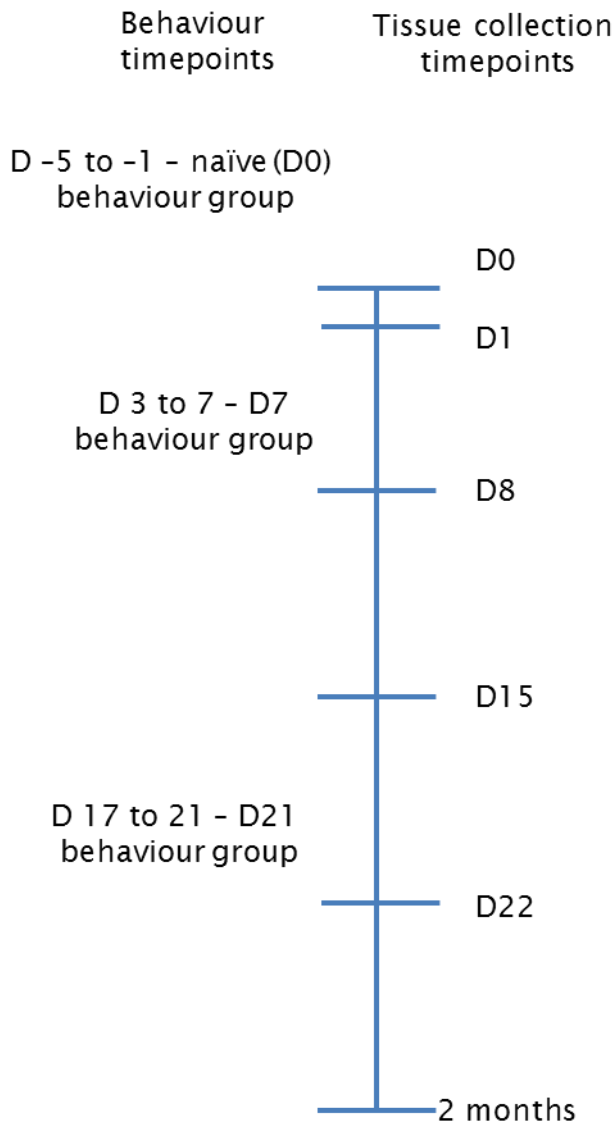


**Figure 5.2 The overall experimental design for experiment 1.**

Behavioural groups were made of pooled D0 (saline injected) & D1, D8 & D15 and D22 & 2 month groups to give n = 11-12 per group. D represents days post injection. D0 is the day of injection.

### 5.2.5 Novel Object Recognition Test

The object pairings for the novel object recognition test (NOR) were chosen by recording the time mice spent attending a variety of different objects within a box that they had been habituated to for 5 minutes at a time in 2 sessions spaced 24h apart. Objects which were attended for a similar amount of time and for at least 5s on average during a 5 minute testing session were paired with each other. Two pairs of objects were deemed suitable pairs – a glass

beaker and an inverted glass funnel (pair 1), and an inverted coverslip box and a metal bottle lid (pair 2).

Initial experiments during validation of the novel object recognition test had a 5 minute familiarisation session and a 10 minute test session. The protocol was adapted from that used in Mazarati et al, 2011. This was further adapted for experiment 1 to allowing the mouse to investigate the two “familiar” objects for exactly 30s, then removing the mouse and placing it back in its home cage, using a similar protocol to that of Orr et al. (2012).

The kappa opiate agonist U50,488 (Sigma, Poole, UK) was injected at 0.3mg/kg i.p. 15 minutes before the test phase of novel object recognition during assay validation to disrupt novel object recognition (Carey et al., 2009; Schindler et al., 2010) and provide a positive control to validate the protocol used in this assay.

#### **5.2.6 Static rod test**

The static rod test was carried out as described in chapter 2 for experiments using *S. typhimurium*. Briefly, 9, 12 and 15mm rods were clamped directly to the bench and mice were trained on one occasion on all three rods 24h before testing began. Any occasion where the mouse slipped and turned upside down or fell was marked as a fail. If this occurred during recording of transit time the stopwatch was paused, the mouse was replaced on the rod in the same location as the slip and the stopwatch started again.

#### **5.2.7 Manual Open field test**

The manual open field test was conducted as described in chapter 2. Mice were habituated to the open field box 24h before testing, immediately after being tested in the novel object recognition test.

A control experiment was performed to validate the results from experiment 1 to control for the effects of daily handling of the mice. The mice were weighed daily, and the mice were tested after 1, 8 or 22 days of daily weight taking.

## 5.3 Results

### 5.3.1 Pilot experiments

To establish what dose of *S. typhimurium* was suitable for use in young and aged mice pilot experiments were conducted using different doses of *S. typhimurium*. The aim was to find a dose sufficient to cause sickness behaviour without causing weight loss exceeding 15% of original body weight, which is the maximum amount of weight loss permitted in the Home Office licence used. A dose of  $1 \times 10^6$  CFU was tested first, consistent with doses used in previous experiments (Püntener et al., 2012). This dose elicited a 5.5% loss of body weight in the first 24h after infection in young mice and recovery to close to 100% of original body weight within the next 7 days. In aged mice this dose elicited a progressive decline in body weight over the next 7 days, with a mean reduction in body weight of 15% by 7 days after infection (Figure 5.3 A). A smaller dose of  $1 \times 10^5$  CFU only elicited a 1-2% decline in body weight 24h after infection in both young and aged mice (Figure 5.3 B). Therefore an intermediate dose of  $3 \times 10^5$  CFU was deemed suitable for aged mice.

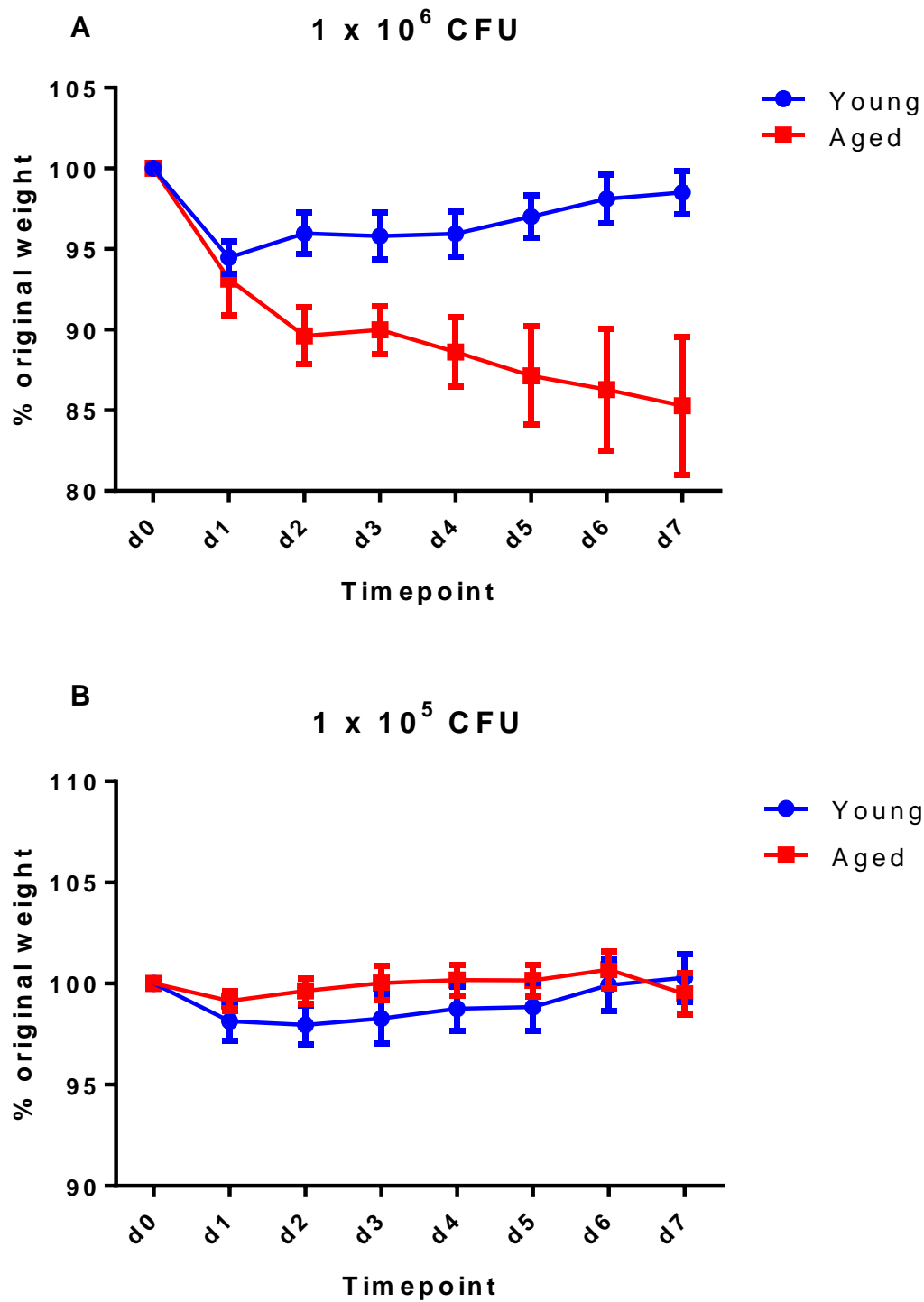


**Figure 5.3. Optimisation of *S. typhimurium* doses for aged mice.**

Mice were given a dose of either  $1 \times 10^6$  CFU (A) or  $1 \times 10^5$  (B) CFU *S. typhimurium* strain SL3261 and body weights were recorded every 24h. Error bars represent standard error. n = 5-6 per group.

Before beginning experiment 1 several pilot experiments were carried out to establish and validate a protocol for the novel object recognition test. Pilot experiments were initially carried out with a variety of different objects to find object pairs that mice had approximately equal preference for and were sufficiently engaging to induce at least 5s of attendance from mice during a 5 minute testing period. 2 suitable pairs of objects were identified during this optimisation. Pair 1 was a glass beaker and an inverted glass funnel. Pair 2 was an inverted plastic coverslip box and a metal bottle lid. Mice exposed to both objects from either pair 1 or pair 2 showed equal preference for the two objects (Figure 5.4 A), demonstrating the suitability of both object pairs for novel object recognition testing.

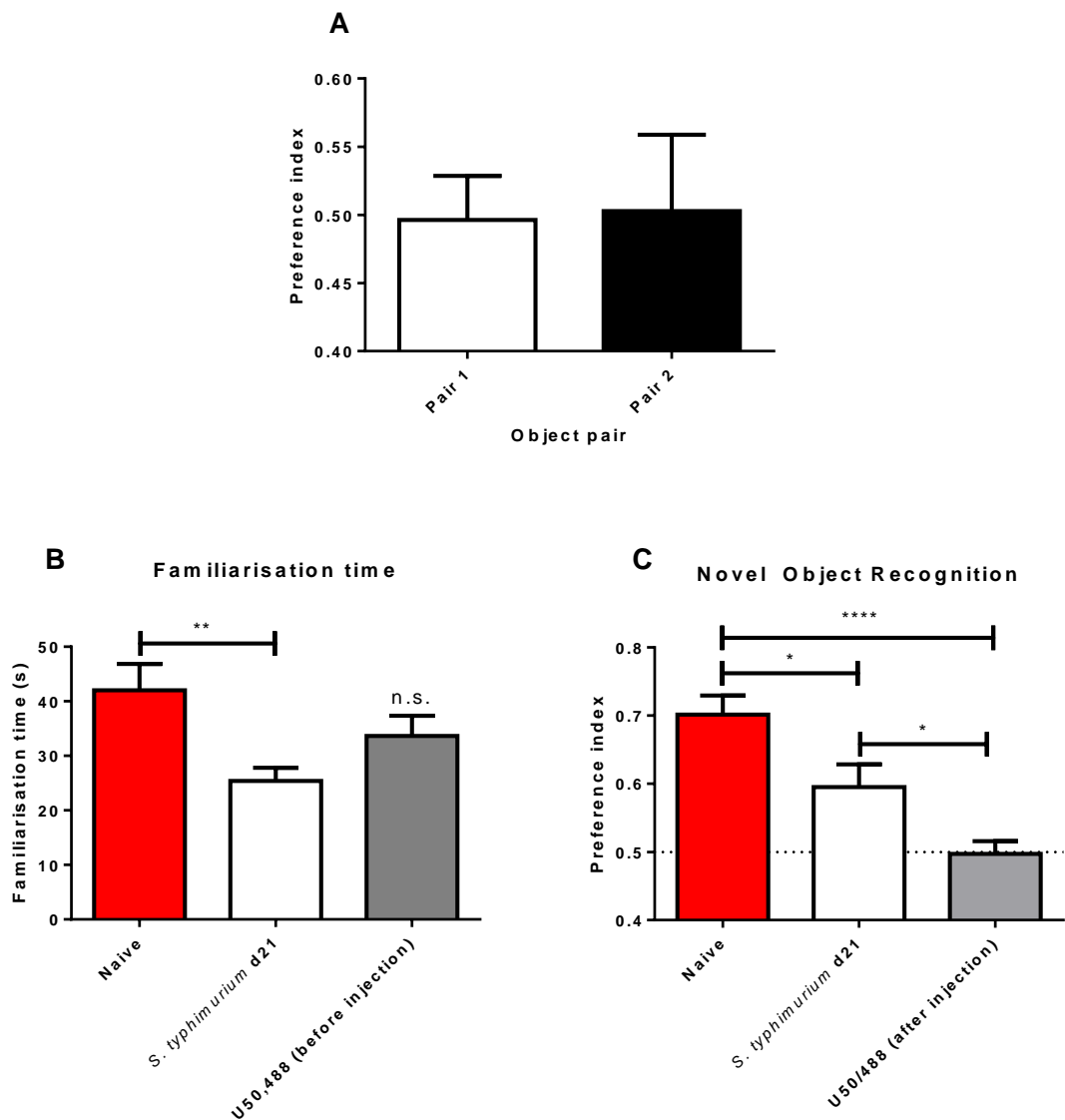


Figure 5.4. Optimisation of the novel object recognition test.

Naive mice exposed to pair 1 or pair 2 for the first time did not show any innate bias for either object (A). n=5-8 per group. Mice were either naïve, three weeks post *S. typhimurium* infection ( $1 \times 10^6$  CFU) or injected 15 minutes before the test phase with U50,488. The amount of time spent attending objects during the familiarisation phase was similar in naïve and U50,488/ injected mice, but reduced in *S. typhimurium* infected mice (B). n = 8 per group, except for *S. typhimurium* infected mice familiarisation times (B) which had n = 19. Errors bars represent standard error of the mean. Preference for the novel over the familiar object was strongest in naïve mice, reduced in *S. typhimurium* infected mice and abolished in U50,488 injected mice (B). \*= $p < 0.05$ , \*\*= $p < 0.01$ , \*\*\*= $p < 0.001$ , \*\*\*\*= $p < 0.0001$  in Holm-Sidak post-test.

To validate the NOR protocol a pilot experiment was performed using naïve mice, *S. typhimurium* infected mice (3 weeks of infection) or mice injected with U50,488, a kappa opiate agonist (Vonvoigtlander et al., 1983). Mice were first familiarised with 2 glass beakers for 10 minutes. 24h later one beaker was replaced with an inverted glass funnel and the time spent attending each object measured. The preference index for the novel object (glass funnel) was 0.71 in the naïve mice (Figure 5.4 C), showing that naïve mice preferred the novel object over the familiar object. A separate group of mice infected with  $1 \times 10^6$  *S. typhimurium* for 3 weeks were tested with pair 1, scoring a preference index of 0.595, indicating a reduced preference for the novel object. Finally the original naïve group of mice were familiarised to two coverslip boxes and 15 minutes before the 24h time-point injected with 0.3mg/kg U50,488, a kappa opiate agonist shown to disrupt memory (Carey et al., 2009; Schindler et al., 2010). 15 minutes after injection mice were tested with the novel object and they showed no preference for the novel object. These data show that naïve mice tested using this protocol had a substantial preference for novel objects compared to familiar objects that could be removed through application of a drug with known disruptive effects on memory recall.

The time spent attending the two identical objects during the familiarisation phase was also recorded. Naïve mice spent a mean time of 42.0s attending the identical objects, whereas the *S. typhimurium* infected mice spent only 25.4s attending the objects during familiarisation (Figure 5.4 B). This difference was statistically significant (t test:  $t_{(25)} = 3.43$ ,  $p = 0.0021$ ). The mice used for U50,488 injections were the same as those used as the naïve group and they

spent a mean of 33.7s attending the 2 familiar objects. In light of the reduction in familiarisation time following *S. typhimurium* infection, the protocol was adjusted to control for reduced drive to investigate novel objects during familiarisation. Instead of the familiarisation time being limited to 5 minutes per mouse, the mouse was allowed as much time as necessary to spend a total of 30s attending the two identical objects during familiarisation, thus ensuring that all mice spent the same time attending the objects.

### 5.3.2 Experiment 1 (main experiment)

After establishing a suitable dose and protocol for the novel object recognition test the main experiment was initiated (experiment 1). Young and aged mice were housed in groups of 5-6 mice per cage and injected with saline or  $3 \times 10^5$  CFU *S. typhimurium*. Each group/cage was culled at a separate time-point in the experiment, as described in figure 5.2. Body weights were taken daily for all mice, and the weights from the young and aged 21 day and 2 month post infection groups ( $n = 12$ ) were pooled together for analysis. Young and aged mice both lost a significant amount of body weight within the first 24h of infection (d0 vs d1 Holm-Sidak post test -  $p < 0.05$ ), although weight loss appeared slightly attenuated in aged mice (mean = 4%) compared to young mice (mean = 6.5%) (Figure 5.5). Young mice recovered their body weight over the course of the next 9 days, reaching 100% of their original body weight by day 10 after infection. In contrast, aged mice did not recover any significant amount of body weight between day 1 to day 8 after infection and began to progressively lose weight from day 8 onwards, with their weight differing significantly from that of young mice at the same time-point from day 11 onwards ( $p < 0.05$ , Holm-Sidak post test). There was a significant effect of days post infection (two way repeated measures ANOVA:  $F_{22,484} = 13.89$ ,  $p < 0.0001$ ), age ( $F_{1,22} = 7.221$ ,  $p < 0.0135$ ), subject matching ( $F_{22,484} = 55.33$ ,  $p < 0.0001$ ) and interaction between age and days post infection ( $F_{22,484} = 13.89$ ,  $p < 0.0001$ ). Body weights in this cohort were measured until day 22 when some of the mice were culled for tissue collection.

A smaller group of mice were followed until 2 months after infection ( $n=4$  aged, 6 young) (Figure 5.6). Aged mice continued to lose weight until 26 days after infection, when their mean weight stabilised at approximately 93% of their original body weight. The aged mice then began to recover their body

weight from day 30 until day 53 after infection, when their mean body weight reached 100% of their original body weight. The mean body weight of young mice varied between 98-102% of their original body weight between day 10-43, after which the mice began to increase their mean body weight, reaching 110.8% of their original body weight by day 55 after infection. The changes in weight were found to be significant in young mice between day 0 and days 1-3 and 48-55, and in aged mice between day 0 and days 22-29 ( $p < 0.05$ , Holm-Sidak post tests). There was a significant effect of days post infection (two way repeated measures ANOVA:  $F_{44,352} = 6.925$ ,  $p < 0.0001$ ), subject matching ( $F_{8,352} = 81.76$ ,  $p < 0.0001$ ), and interaction between age and days post infection ( $F_{44,352} = 4.217$ ,  $p < 0.0001$ ), but not age ( $F_{1,8} = 2.705$ ,  $p = 0.1386$ ).

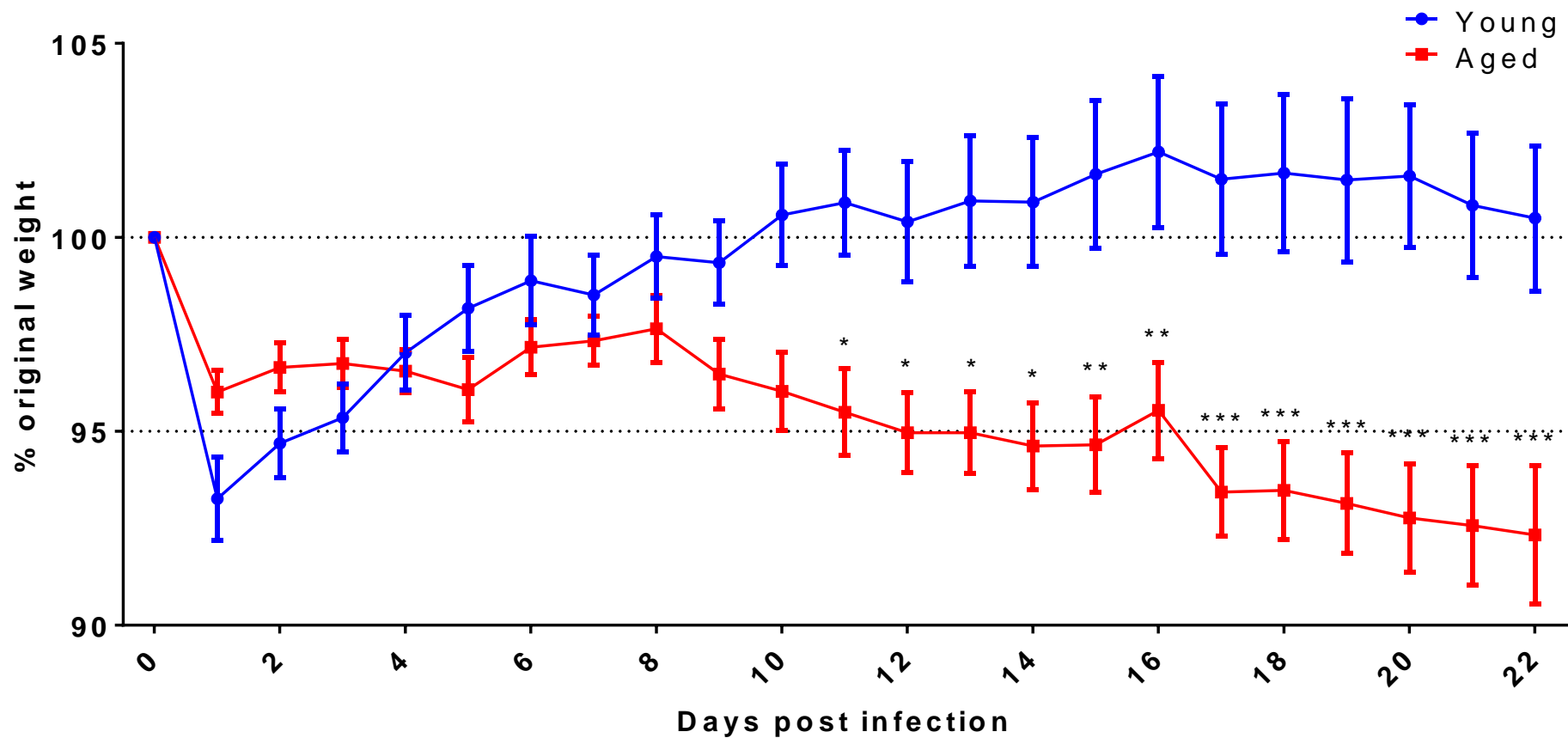


Figure 5.5. Changes in body weight of young or aged mice followed infection with  $3 \times 10^5$  CFU *S. typhimurium*.

Body weights were recorded daily for 22 days. n = 12 per group. All data is expressed as percentage of the mouse's starting body weight on the day of injection. Error bars represent standard error of the mean. \* represent significant difference from age matched time-point with Holm-Sidak post test. \*=p<0.05, \*\*=p<0.01, \*\*\*=p<0.001, \*\*\*\*=p<0.0001 in Holm-Sidak post-test.

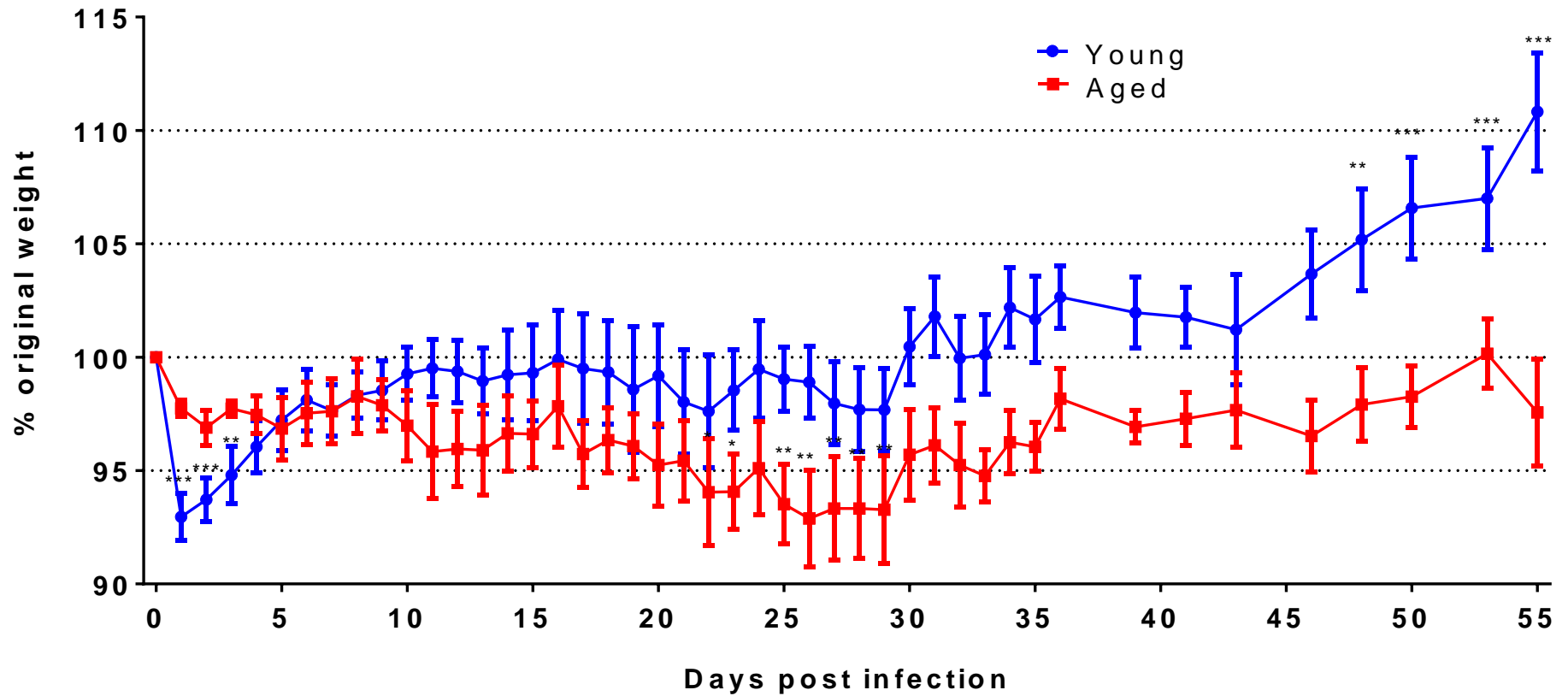
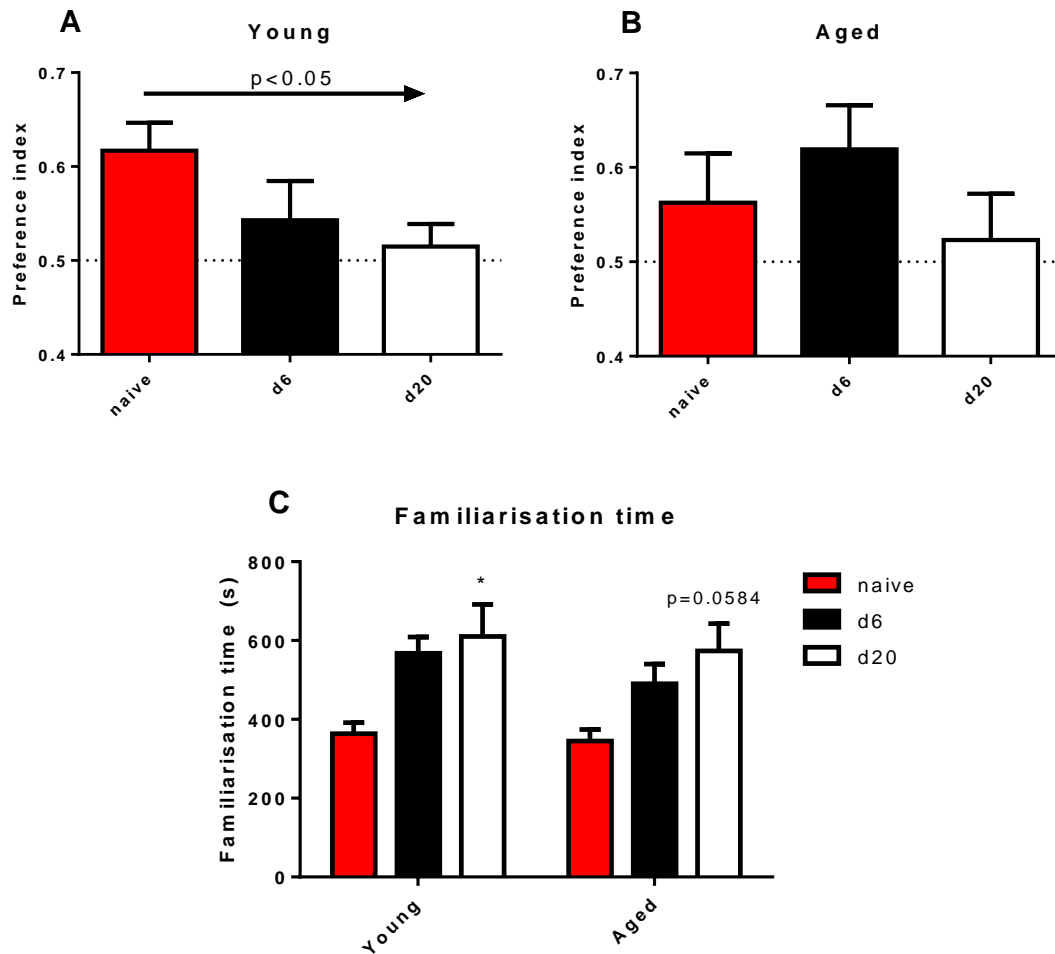


Figure 5.6 Changes in body weight of young or aged mice followed infection with  $3 \times 10^5$  CFU *S. typhimurium* over a prolonged period of time (55 days).

Body weights were recorded daily for 36 days and then every 2-3 days until day 55.  $n = 6$  for 3 month old mice,  $n = 4$  for 18 month old mice. All data is expressed as percentage of the mouse's starting body weight on the day of injection. Error bars represent standard error of the mean. \* represent significant difference from weight at day 0 with Holm-Sidak post test.  $*=p<0.05$ ,  $**=p<0.01$ ,  $***=p<0.001$ ,  $****=p<0.0001$  in Holm-Sidak post-test.

Various behavioural assays were performed on the mice over the course of the experiment, beginning with the novel object recognition test. Young naïve mice had a mean preference index of 0.62, while aged naïve mice had a mean preference index of 0.56, which made it difficult to observe changes in novel object recognition test performance as the aged mice were already impaired in their performance. For this reason novel object recognition performance was analysed in 2 separate one way ANOVAs rather than a single 2 way ANOVA. Young mice demonstrated a progressive reduction in novel object recognition test performance over the course of *S. typhimurium* infection (Figure 5.7 A) with their mean novel object preference index dropping to 0.54 7 days after infection and 0.51 21 days after infection. This trend was not significant when tested by one way ANOVA ( $F_{2,31} = 2.663$ ,  $p = 0.0857$ ), but post testing for a linear trend with time showed a significant effect of infection ( $R^2 = 0.139$ ,  $p = 0.0319$ ). Aged mice already showed reduced novel object preference before infection and there was no significant effect of days post infection ( $F_{2,30} = 0.946$ ,  $p = 0.400$ ) (Figure 5.7 B). The time taken for the mice to attend the objects for 30s during the familiarisation phase was also recorded (Figure 5.7 C). Infection caused a significant increase in time taken to spend 30s attending objects during familiarisation ( $F_{2,63} = 9.885$ ,  $p = 0.0002$ ), although age ( $F_{1,63} = 0.968$ ,  $p = 0.329$ ) and age x days post infection ( $F_{2,63} = 0.148$ ,  $p = 0.862$ ) had no impact.



**Figure 5.7. The effect of *S. typhimurium* infection on novel object recognition test performance in young or aged mice.**

Young mice showed a progressive decline in novel object preference over the course of *S. typhimurium* infection (A). Aged mice showed no clear pattern of changes in novel object preference (B) and showed less novel object preference before infection compared to young mice. The time required to spend a total of 30s attending the identical objects in the familiarisation phase increased significantly in both young and aged mice during infection (C). Error bars represent standard error of the mean. \*= $p < 0.05$ , \*\*= $p < 0.01$ , \*\*\*= $p < 0.001$ , \*\*\*\*= $p < 0.0001$  in Holm-Sidak post-test.

Co-ordination and balance was assessed using the static rod test. 3 rods of different diameters (9, 12 and 15mm) were used to test mice, with one training session 24h prior to testing. The effects of ageing and *S. typhimurium* infection were most pronounced using the 9mm rod (Figure 5.8 A), with a significant effect of both age, infection and an interaction between age and

infection on static rod transit time (two way ANOVA: age:  $F_{1,63} = 79.71$ ,  $p < 0.0001$ , days post infection:  $F_{2,63} = 3.193$ ,  $p = 0.0478$ , age x days post infection:  $F_{2,63} = 3.355$ ,  $p = 0.0413$ ). The failure rate of mice on the 9mm rod was also significantly increased in naïve aged mice compared to young mice (Figure 5.8 B) ( $\chi^2$  test:  $\chi^2 = 27.99$ , d.f. = 5,  $p < 0.0001$ ; aged d0 vs aged d7:  $p < 0.05$ ) and in aged mice at 1 week of infection compared to naïve aged mice ( $p < 0.05$ ) or 3 weeks ( $p < 0.01$ ) after infection. The failure rate on the 9mm rod did not change in young mice following infection.

There was a significant effect of ageing alone and an interaction between ageing and infection on transit times on the 12mm rod (Figure 5.8 C) (age:  $F_{1,63} = 77.21$ ,  $p < 0.0001$ , days post infection:  $F_{2,63} = 1.478$ ,  $p = 0.236$ , age x days post infection:  $F_{2,63} = 3.989$ ,  $p = 0.0234$ ), although post testing did not show any significant difference between aged naïve mice and aged mice 7 days after infection. The failure rate on this rod was not significantly different between any of the groups tested (Figure 5.8 D) (partitioned  $\chi^2$  test:  $\chi^2 = 7.065$ , d.f. = 5,  $p = 0.216$ ).

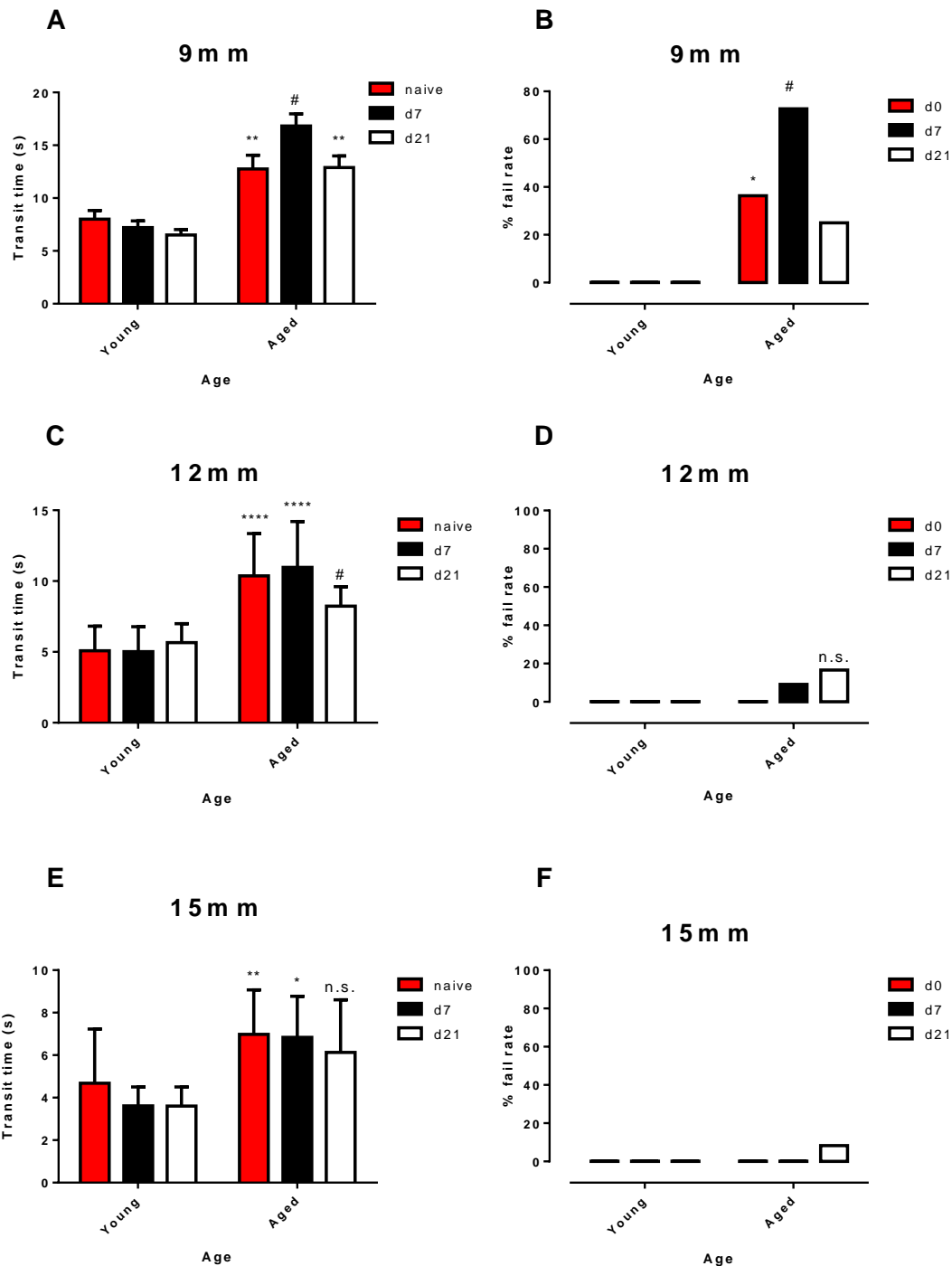


**Figure 5.8. The effects of *S. typhimurium* infection on static rod test performance in young and aged mice.**

Mice were tested on 9mm (A, B), 12mm (C, D) or 15mm (E, F) diameter rods. Aged mice performed worse than young mice on all three diameter rods, and a further impairment in static rod performance was detectable 7 days after infection in aged but not young mice on 9mm (A, B) and 12mm rods (C, D). Error bars represent standard error of the mean. \*=p<0.05, \*\*=p<0.01,

\*\*\*= $p < 0.001$ , \*\*\*\*= $p < 0.0001$  in Holm-Sidak post-test or partitioned Chi squared test. # represents significant difference from unmarked and \* marked columns in the Holm-Sidak post-test or partitioned chi squared test.

The effects of ageing on static rod transit time were less pronounced using the 15mm rod than the 9 or 12mm rod (Figure 5.8 E) but still significant, and there was no significant interaction between age and infection or effect of infection alone (age:  $F_{1,62} = 49.41$ ,  $p < 0.0001$ , days post infection:  $F_{2,62} = 1.535$ ,  $p = 0.224$ , age x days post infection:  $F_{2,62} = 0.408$ ,  $p = 0.667$ ). The failure rate on this rod was not significantly different between any of the groups tested (Figure 5.8 F) (partitioned  $\chi^2$  test:  $\chi^2 = 4.82$ , d.f. = 5,  $p = 0.438$ ).

To assess locomotor and exploratory activity the open field test was performed on mice. Young and aged mice both exhibited a decline in locomotor behaviour of a similar magnitude due to infection (Figure 5.9 B) (young d21 – 51.2% of baseline, aged d21 – 63.8% of baseline). To ensure that this decline in locomotor activity was a genuine effect of *S. typhimurium* infection and not an artefact of reduced anxiety from daily handling, a control experiment was carried out with naïve mice which were handled and weighed daily, similarly to the mice in experiment 1. Locomotor activity also progressively reduced in mice that were handled daily for 3 weeks (naïve d21 – mean = 69.7% of baseline), but the declines in percentage of baseline locomotor activity were significantly greater in 21 days post infection young mice (Figure 5.9 B) (naïve d21 vs young infected d21 –  $p < 0.05$ , Holm-Sidak post test). There was no statistically significant effect of group (young infected, aged infected or naïve control) (two way ANOVA:  $F_{2,90} = 0.717$ ,  $p = 0.491$ ) or of group x days post infection ( $F_{4,90} = 0.472$ ,  $p = 0.756$ ), but there was a significant effect of days post infection ( $F_{2,90} = 20.71$ ,  $p < 0.0001$ ). The post test results show that at 21 days after infection *S. typhimurium* infected mice did have a greater decline in locomotor activity than naïve mice.

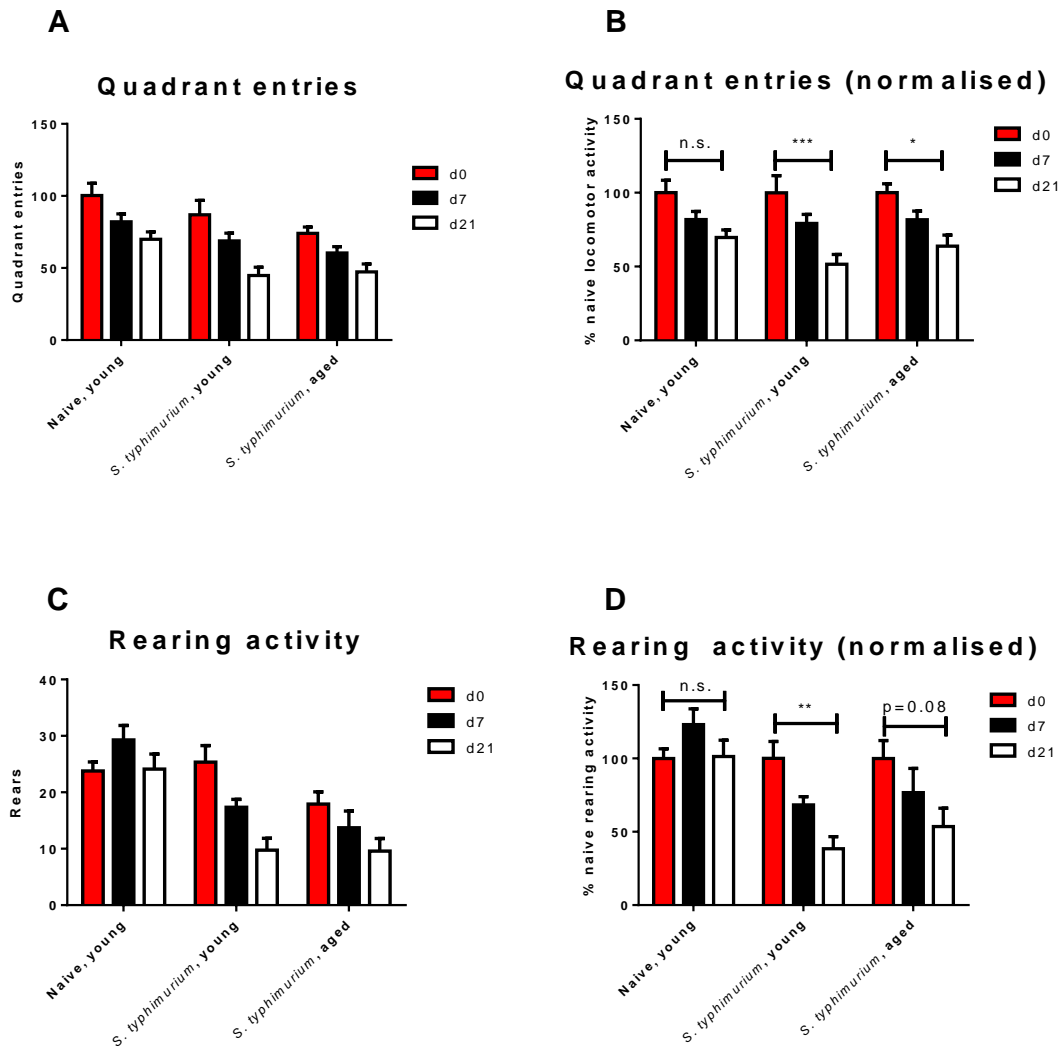


**Figure 5.9. The effect of *S. typhimurium* infection on open field test performance in young and aged mice.**

The number of quadrant entries and rears made at D0 varied between groups (A, C), so data was normalised to activity at D0 within groups (B, D). The level of locomotor activity (quadrant entries) changed over time in naïve and infected mice, but the change was more pronounced in young infected mice (B). Rearing activity was unaffected by daily handling of naïve mice, but was significantly reduced by *S. typhimurium* infection in young and aged mice (D). Error bars represent standard error of the mean. \*= $p < 0.05$ , \*\*= $p < 0.01$ , \*\*\*= $p < 0.001$ , \*\*\*\*= $p < 0.0001$  in Holm-Sidak post-test.

Rearing activity was unaltered by daily handling in the control experiment, but progressively declined during *S. typhimurium* infection (Figure 5.9 D). There was a significant effect of group (two way ANOVA:  $F_{2,90} = 10.14$ ,  $p = 0.0001$ ),

days post infection ( $F_{2,90} = 8.24$ ,  $p = 0.0005$ ) and group x days post infection in percentage of baseline rearing activity (Figure 5.9 D) ( $F_{4,90} = 2.55$ ,  $p = 0.0445$ ). 21 days after infection young mice rearing activity was significantly reduced compared to D0 ( $p < 0.01$ , Holm-Sidak post-test), whereas rearing activity was unaffected by time-point in naïve mice after 21 days of handling and weighing. The rearing activity of aged mice 21 days after infection was not quite significantly different from D0 ( $p = 0.0845$ , Holm-Sidak post-test). There was no significant difference in percentage of baseline rearing activity between young and aged mice at D7 or D21 after infection (Holm-Sidak post-test).

### 5.3.3 Experiment 2

A follow up experiment was conducted following the completion of these behavioural tests, referred to here as experiment 2. The primary purpose of this experiment was to provide tissue for use in chapter 6, but food intake and body weight were also recorded to provide additional data regarding weight loss in young and aged mice during *S. typhimurium* infection. Young and aged mice of 3 or 18 months of age were given  $3 \times 10^5$  CFU of *S. typhimurium* or saline. Daily body weights and food intake were recorded in this experiment for 21 days. *S. typhimurium* infection caused similar patterns of weight loss to those previously observed in figure 5.5 – young mice had an acute (24h) mean weight loss of approximately 5.3% of their original body weight, which they recovered rapidly over the next few days (Figure 5.10). Aged mice lost a slightly smaller amount of weight initially (4.3%) in the first 24h after infection, but failed to recover to their initial weight and started to gradually lose weight again from day 8 onwards, with weight loss accelerating from day 10 onwards and slowing at approximately day 16. Young and aged mice injected with saline did not lose any significant amount of weight throughout the experiment (Holm-Sidak post test). There was a significant effect of group ID ( $F_{3,19} = 8.733$ ,  $p = 0.0008$ ), days post infection ( $F_{21,399} = 2.424$ ,  $p = 0.0005$ ) and an interaction between the two ( $F_{63,399} = 5.600$ ,  $p < 0.0001$ ) in a 2 way repeated measures ANOVA. The difference in weight loss between aged *S. typhimurium* infected mice and aged saline mice became significant from day 12 onwards (Holm-Sidak post test:  $p < 0.05$ ).

Daily food consumption per cage was also measured. There was an acute reduction in food intake following *S. typhimurium* injection in both young and

aged mice which appeared more pronounced in aged mice (Figure 5.11). There was a significant effect of group (two way ANOVA without replication: group -  $F_{3,57} = 30.20$ ,  $p < 0.0001$ ) and days post infection ( $F_{19,57} = 1.874$ ,  $p = 0.0354$ ). Food intake of *S. typhimurium* infected young mice recovered to levels similar to saline injected young or aged mice and remained similar until between day 11-15, when young saline treated mice increased their food intake by approximately 2-3g per cage per day while young *S. typhimurium* infected mice maintained a steady food intake of approximately 16g per cage per day. Aged infected mice ate less than any other group tested in the study (Holm-Sidak post test:  $p < 0.0001$ ), particularly between days 10-16 when the mice were losing 0.5-1.0% of body weight per day. Young *S. typhimurium* infected mice also ate less than young saline mice across the study (Holm-Sidak post test:  $p < 0.01$ ), but this reduction in food intake was more pronounced in aged mice.

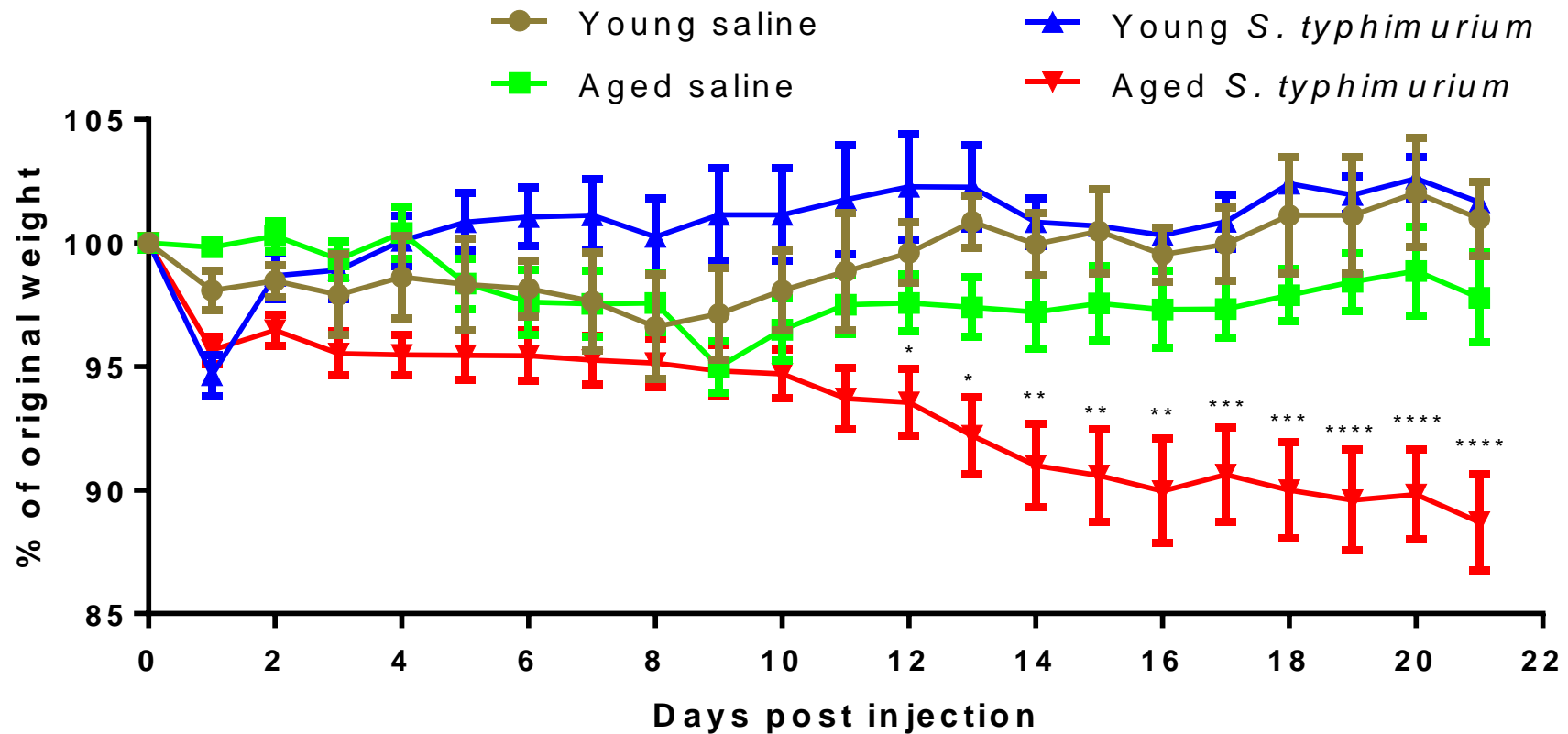


Figure 5.10. Changes in body weight of young or aged mice followed infection with  $3 \times 10^5$  CFU *S. typhimurium* – experiment 2.

Body weights were recorded daily for 21 days. n = 5-6 per group. All data is expressed as percentage of the mouse's starting body weight on the day of injection. Error bars represent standard error of the mean. \* represent significant difference between aged *S.*

*typhimurium* treated and from age matched time-point with Holm-Sidak post test. \*=p<0.05, \*\*=p<0.01, \*\*\*=p<0.001, \*\*\*\*=p<0.0001 in Holm-Sidak post-test.

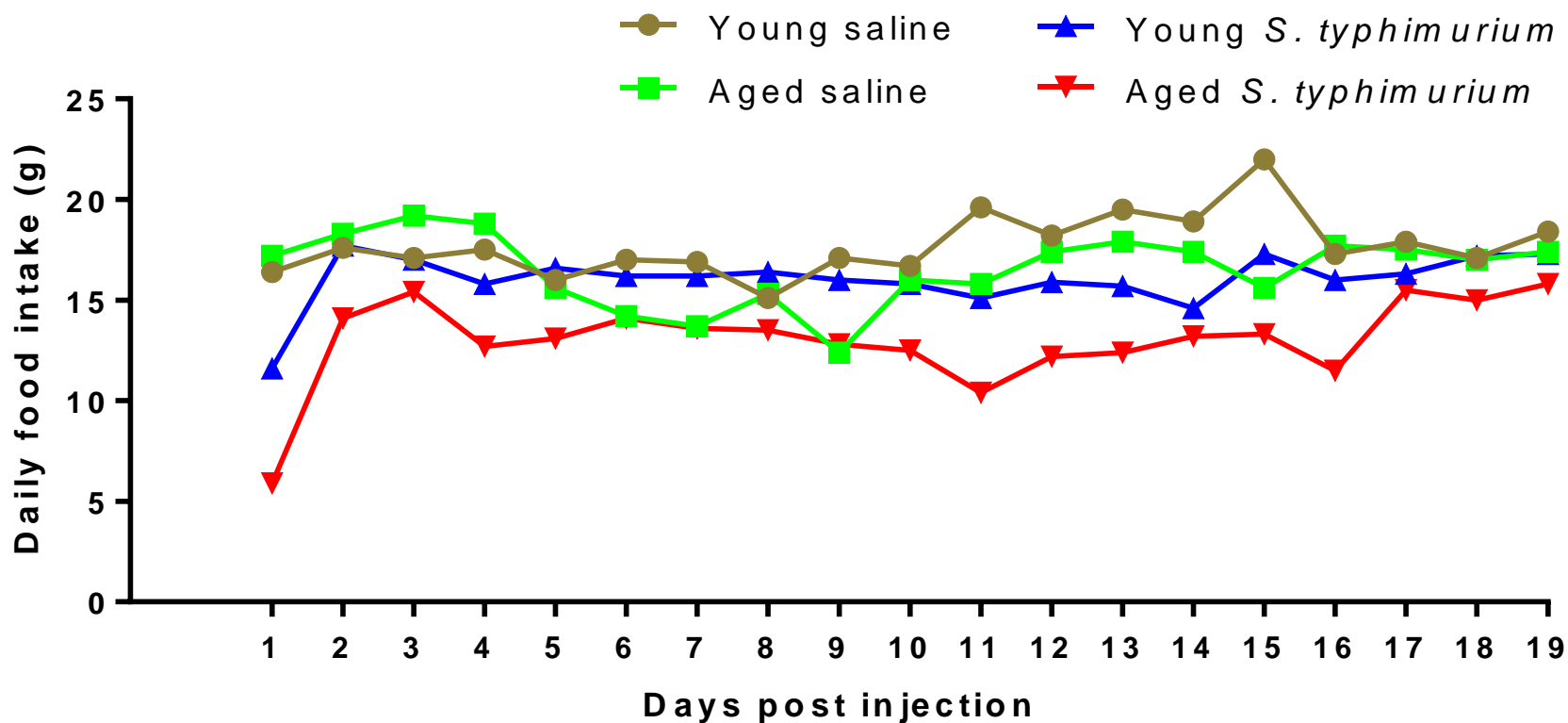


Figure 5.11 Changes in daily food intake of young or aged mice followed infection with  $3 \times 10^5$  CFU *S. typhimurium* – experiment 2.

Food consumption was recorded daily for 20 days. n = 1 cage per group, each cage housing 5-6 mice.

## 5.4 Discussion

*S. typhimurium* infection caused a sustained behavioural response in both young and aged mice, lasting for at least three weeks after infection. Open field rearing and locomotor activity was reduced to a similar extent in both young and aged mice. Static rod performance was only impaired in aged mice 7 days post *S. typhimurium* infection, and by 21 days after infection static rod performance returned to baseline levels. Body weight was reduced in the first 24h after infection in both young and aged mice, but whereas young mice recovered their body weight, aged mice did not and a second phase of chronic weight loss began at approximately 8-10 days after infection in aged mice. This weight loss coincided with decreased food intake. Young mice also demonstrated a progressive reduction in novel object preference during infection. Aged mice were already impaired in novel object recognition test performance at baseline, preventing the accurate assessment of the effects of *S. typhimurium* infection on novel object preference in aged mice.

### 5.4.1 Preliminary experiments

Preliminary experiments were designed with two goals in mind – to determine what dose of *S. typhimurium* was most suitable for an experiment using both young and aged mice, and to establish and validate a protocol for the novel object recognition test. When  $1 \times 10^6$  CFU *S. typhimurium* was administered to aged mice weight loss was no longer transient, but instead continued progressively over the next 7 days until several mice reached the 15% weight loss limit set by the Home Office licence used and therefore were culled. 6 month old mice responded to an injection of  $1 \times 10^6$  CFU by losing approximately 5% of their original body weight in the first 24h following infection and then gradually recovering weight over the next 7 days, in agreement with the kinetics of weight loss described by Püntener et al 2012 following *S. typhimurium* infection. The more severe weight loss experienced by aged mice in response to *S. typhimurium* infection suggests that aged mice fail to control *S. typhimurium* infection at this dose. A dose of  $1 \times 10^5$  CFU did not cause significant weight loss in either young or aged mice. Therefore an intermediate dose of  $3 \times 10^5$  CFU was deemed suitable for young and aged mice.

The novel object recognition test is principally a test of memory encoding and recall. The test depends on two main assumptions – that the two objects tested are of equal initial preference to a mouse and that the mouse will prefer to spend time investigating a novel object rather than a familiar object. Two pairs of objects were identified, first through identification of objects that were sufficiently salient to mice to attract their attention and then by presenting these object pairs to naive mice to ensure that both objects in a pair were equally attractive to a mouse that had seen neither object before. These object pairs, identified in the methods section of this chapter as pair 1 and pair 2, were used to validate the assay protocol that was designed based on that used by Materazi et al. (2011). Naive mice exhibited a strong preference for the novel object over a familiar object (mean preference index of 69.5%), demonstrating that mice recalled having encountered the familiar object previously and therefore preferred to investigate the novel object. This preference was impaired in young mice that had been infected with *S. typhimurium* for 3 weeks (mean preference index of 60%) and abolished in mice treated with U50,488, a kappa opiate agonist (mean preference index of 51%). U50,488 has been shown in multiple studies to abolish novel object preference (Carey et al., 2009; Schindler et al., 2010), possibly by acting on kappa opiate receptors expressed in the temporal lobe and hippocampus (Carey et al., 2009; Mansour et al., 1996). The endogenous kappa opiate agonist dynorphin is thought to mediate some of the disruptive effects of chronic stress on memory recall (Carey et al., 2009), and it is likely U50,488 acts in the same way.

The reduction in novel object preference 20 days post infection in young mice suggested that *S. typhimurium* infection may have an effect on memory function, but it was accompanied by a reduction in the amount of time spent attending to the two identical objects during the familiarisation phase of the protocol. This introduces a confounding factor when interpreting this data, as the decreased time spent attending the objects could lead to decreased encoding of the familiar objects and therefore poorer recall of the familiar objects, leading to reduced preference for the novel object during the testing phase. To address this possibility the protocol was adapted to ensure that all mice spent the same amount of time (30 seconds) attending the identical objects during the familiarisation phase.

#### 5.4.2 Anorexic weight loss

$3 \times 10^5$  CFU of *S. typhimurium* induced an acute monophasic loss of body weight in young mice and a prolonged biphasic loss of weight in aged mice. The second phase of weight loss was prolonged in aged mice, beginning at day 8-10 and continuing until day 26. A second experiment showed that these results were reproducible and that young infected mice recovered their body weight to a level very similar to that of young saline injected mice, whereas aged mice lost more weight than aged saline injected mice over the course of the 21 days of the experiment.

The close coincidence of decreased food intake with peak periods of weight loss suggests an anorexic rather than a cachexic cause of weight loss due to *S. typhimurium* infection. The initial phase of weight loss (day 0-1) is most likely mediated by activation of immune to brain communication pathways by PRR ligands derived from *S. typhimurium*, such as LPS, which is detectable in serum in the first few days of infection (Püntener et al., 2012). These ligands may activate TLRs on vagal afferents or brain endothelium directly or mediate their actions through induction of cytokine production in the periphery. By 24h after infection serum LPS and cytokine levels are much lower than in the first few hours of infection and cytokines are not robustly expressed in the brain or serum (Püntener et al., 2012), which would explain why the first phase of weight loss only lasts 24h. LPS is undetectable in the serum of young mice by 7 days after injection (Püntener et al., 2012), suggesting that the second phase of weight loss is not LPS mediated. Increased sensitivity to peripheral cytokine levels, an enhanced central inflammatory reaction to peripheral inflammation or enhanced sensitivity of specific neuronal circuits in aged mice could all potentially contribute to the induction of this second phase of weight loss.

Control of food intake is complex and mediated by several different nuclei of the brain, including several areas of the hypothalamus, NTS, ventral tegmental area, lateral parabrachial nucleus nucleus accumbens and the amygdala (Gautron and Laye, 2009). An exaggerated production of central inflammatory mediators in response to peripheral cytokines in any of these areas could contribute to the induction of a second phase of weight loss. Increased BBB permeability, which has been reported in ageing (Farrall and Wardlaw, 2009), in particular areas could also underlie some of these changes, leading to

increased exposure of neurons to blood components or inflammatory mediators. These areas have not been systematically studied in the ageing brain for their responsiveness to peripheral inflammation, and barely studied at all in the context of the brain's response to live infection. Neurons and microglia in the aged mouse hypothalamus have an increased neuroinflammatory status, expressing higher levels of TNF $\alpha$  and NF $\kappa$ B signalling, leading to a subsequent decrease in gonadotrophin releasing hormone (Zhang G. et al., 2013). An enhanced basal inflammatory state in the aged hypothalamus could potentially render this particular brain area more likely to exert anorexic behavioural effects in response to peripheral inflammation, either through neuroendocrine changes or neuronal modification of behaviours e.g. food seeking behaviours. Enhanced c-fos activity in several brain nuclei associated with enhanced anorexic behaviour has been reported in response to an i.p. injection of 10 $\mu$ g of LPS per mouse in young and aged mice (Gaykema et al., 2007a), including the NTS, PVN of the hypothalamus, area postrema, amygdala and parabrachial nucleus. Whether this enhanced neuronal activity is caused by enhanced local cytokine production, enhanced neuronal activation due to signalling from the CVOs or vagal afferents or a mixture of the two is not addressed by Gaykema et al. (2007a). During *S. typhimurium* infection in the aged brain a similar enhanced neuronal response to systemic inflammation could occur in specific brain regions e.g. the hypothalamus.

#### **5.4.3 Static rod test performance**

The static rod test is a well characterised assay of co-ordination and balance (Contet et al., 2001). Deficits in co-ordination and balance have not been widely reported as a consequence of systemic inflammation. *S. typhimurium* infection caused a significant increase in transit time and the failure rate on the 9mm diameter rod at 7 days after infection in aged mice. Static rod performance returned to baseline levels 21 days after infection in aged mice, indicating that this impairment in co-ordination and balance was transient. In contrast young mice did not perform any worse in the static rod test when infected with *S. typhimurium*. Aged mice also performed worse than young mice at baseline, in agreement with data from chapter 3. Age and infection induced deficits in static rod performance were less pronounced when using

the 12 or 15mm diameter rod, as the larger diameter rods are easier for the mice to traverse and are therefore less discriminatory than the 9mm diameter rod. The increases in transit time were caused by an increased number of foot faults by the mice, where their foot slipped from the rod and the mouse gripped the rod using its legs rather than its feet, rather than any change in normal walking speed.

One study that has previously reported acute motor deficits following systemic inflammation is that of Cunningham et al 2009, which found an acute effect (6h) of a 500µg/kg LPS injection on inverted screen performance and horizontal bar performance, but only in mice that had existing prion pathology (14 weeks post inoculation). Mice injected with normal brain homogenate did not show any change in performance in these tests following LPS injection, suggesting the necessity of either pre-existing neuronal pathology or an exaggerated neuroinflammatory response for motor deficits to appear. There was no effect of 100µg/kg LPS on static rod test performance in aged mice as described in chapter 3. This may be due to the lower dose of LPS used in this study compared to that of Cunningham et al and a possible ceiling effect on co-ordination and balance due to ageing in this experiment. Ageing is known to induce deficits in cerebellum dependent behaviour in the absence of systemic inflammation, possibly due to loss of Purkinje neurons during ageing (Woodruff-Pak et al., 2010), and in the case of *S. typhimurium* infection it may be that pre-existing age-related pathology in the cerebellum renders this brain area particularly susceptible to systemic inflammation (Woodruff-Pak et al., 2010). Purkinje neurons express IL-1 receptors and EP1, 2 and 4 receptors (Candelario-Jalil et al., 2005; Cunningham et al., 1992; Zhang and Rivest, 1999), so it is possible that the effects of peripheral infection on co-ordination and balance may be mediated by inflammatory signalling to Purkinje neurons.

#### **5.4.4 Open field and novel object recognition test**

The data from the open field test showed a progressive decrease in locomotor and rearing activity following *S. typhimurium* infection, with changes most pronounced 21 days after infection. However, as these mice were being handled daily and the open field test is sensitive to changes in anxiety (Carola et al., 2002), a control experiment was designed to assess the effects of daily handling on open field test performance in naïve mice. Daily handling did

reduce locomotor activity, but not to the same degree observed in *S. typhimurium* infected mice at the same time-points. Rearing activity was also assessed and was not altered by daily handling, whereas the reduction in rearing activity following *S. typhimurium* infection was clear (~40-50%). This experiment indicated that the open field deficits observed during *S. typhimurium* infection were truly a result of *S. typhimurium* infection and not an artefact resulting from daily handling.

There was no difference between young and aged mice in how *S. typhimurium* affected their open field performance. This lack of age related differences in the rearing activity and locomotor activity changes does not fit with the general pattern of an exaggerated behavioural response to systemic inflammation in aged animals described by multiple authors (Barrientos et al., 2006; Godbout et al., 2005b). One explanation may be that the behavioural changes observed in the experiments described in this chapter are initiated via different immune to brain communication routes than studies using systemic LPS injections, in which the direct actions of LPS on endothelial cells at the BBB and subsequent central production of inflammatory mediators are likely to contribute significantly to changes in open field behaviour (Godbout et al., 2005b). The open field deficits induced by BCG infection were not more pronounced in aged mice than in young mice, although recovery of open field activity was delayed (Kelley et al., 2013). It would be interesting to see whether recovery of open field activity is also delayed in aged mice infected with *S. typhimurium*.

These changes in open field activity could reflect reduced anxiety in *S. typhimurium* infected mice (Carola et al., 2002), but most reports of the effects of peripheral infection on anxiety behaviour have described an anxiogenic rather than an anxiolytic effect of infection on behaviour (Goehler et al., 2008; Lyte et al., 2006). An alternative explanation would be a state of decreased motivation to engage in exploratory behaviour, indicating a state of apathy or fatigue. It has been proposed previously that catecholaminergic pathways between the NTS and forebrain regions such as the hypothalamus, hippocampus, dorsal striatum and ventral tegmental area may be a neural correlate for aspects of behaviour involved in behavioural arousal and fatigue (Gaykema and Goehler, 2011). The NTS acts as a relay station for vagus afferent fibres (Berthoud and Neuhuber, 2000) and it may be that vagal input or input from the CVOs mediates the changes in open field activity observed

here. Decreased behavioural arousal would lead to a decreased desire to explore novel environments such as the open field arena and a decreased desire to escape from the arena, and therefore offers a plausible explanation for the decreased open field activity of *S. typhimurium* infected mice. Another explanation would be decreased motivation resulting from depressive behaviour, but work from Ursula Püntener and Steven Booth has shown a peak of immobility in the forced swim test in young mice 7 days after infection, not 21 days after infection (Ursula Püntener and Steven Booth, personal communication), coinciding with the peak of peripheral cytokine levels. If these changes in open field activity were representative of depressive behaviour then one would expect the largest reduction in open field activity to occur 1 week after infection, when depressive behaviour is most pronounced, not 3 weeks after infection, as was observed in this study.

The changes in novel object recognition behaviour observed in young mice can be interpreted in one of two ways – either a deficiency in memory formation/recall during infection, and therefore loss of memory of the familiar object, or an apathetic attitude towards novel stimuli and therefore a lack of impetus to preferentially investigate the novel object. Impaired memory consolidation has been described following infection previously in *E. coli* infected rats using fear conditioning (Barrientos et al., 2006). Decreased interest in novel objects in general would be supported by the decreased time spent attending the two identical objects during the familiarisation session in both the pilot study and in experiment 1, as well as a decreased preference for the novel object over the familiar object during the testing phase. The time taken to reach 30s of time spent with the identical objects during familiarisation increased by ~40% in experiment 1 and the mean time spent investigating the identical objects during the familiarisation phase in the pilot study was ~40% lower than that of naïve mice. Decreased interest in novel objects could be interpreted as indicative of an apathetic state, resulting from increased fatigue and decreased arousal. Distinguishing which of these interpretations is correct is not possible without further experiments to investigate the extent of decreased memory or arousal using different behavioural assays, such as the alternating Y maze or fear conditioning test to assess memory and the social interaction test to test arousal or the quinine avoidance test to test apathy (Martinowich et al., 2012). It is also possible that

decreased memory consolidation and arousal interact to produce a decreased novel object preference in this test.

Aged mice performed poorly in the novel object recognition test at baseline, only scoring a preference index of ~56%. This is in line with the previous observations of other authors that novel object recognition test performance is impaired in aged rodents (de Lima et al., 2005). This poor baseline performance meant that it was not possible to meaningfully assess further changes in novel object recognition resulting from *S. typhimurium* infection.

The variability in novel object recognition performance between the preliminary experiments and experiment 1 is not easily explained. The mice used in pilot experiments were from a different breeding colony, having been bred in house from Harlan stocks, whereas the mice used for experiment 1 were ordered directly from Charles River. Whether these differences in origin may impact on baseline novel object recognition performance is not known. However, there is a clear reduction in novel object preference following *S. typhimurium* infection in mice used from both sources of approximately 9%, showing the reproducibility of decreased novel object preference following *S. typhimurium* infection despite the variability in baseline performance.

#### 5.4.5 Summary

*S. typhimurium* infection causes a range of prolonged metabolic and behavioural alterations in both young and aged mice. Data from the open field test may be indicative of a state of increased apathy or fatigue or reduced anxiety three weeks after infection in both young and aged mice. The novel object recognition test data may also indicate a state of apathy, or may be indicative of memory deficits during *S. typhimurium* infection. The response to *S. typhimurium* infection differed between young and aged mice in the static rod test, which is a measure of co-ordination and balance, where aged mice performed significantly worse 1 week after infection while young mice were unaffected by infection. Aged mice experienced a second, chronic phase of weight loss that began at day 8-10 after infection, probably due to decreased food intake over this time period. In summary, aged mice showed a selective vulnerability to weight loss and co-ordination/balance deficits which young mice did not and both young and aged mice showed reduced open field

activity and in the case of young mice novel object preference that may be indicative of a decreased state of motivation.



## 6. A longitudinal study of the effects of *Salmonella* infection and ageing on microglial phenotype and function.

### 6.1 Introduction

Systemic administration of TLR ligands such as LPS can activate microglia within the CNS to produce inflammatory cytokines and to modulate their expression of functionally relevant molecules such as MHCII (Corona et al., 2010; Henry et al., 2009; Laflamme et al., 2001). The effects of LPS-induced systemic inflammation on microglia are enhanced in the aged brain (Henry et al., 2009). However, the effects of live systemic infections on microglia are not as well characterised. The systemic and central immune response to bacterial infections can be considerably more prolonged than to sterile mimetics of infection such as LPS (Godbout et al., 2005b; O'Connor et al., 2009b; Püntener et al., 2012) and central inflammatory responses may be induced via different immune-to-brain communication pathways to those induced by systemic administration of TLR agonists such as LPS.

Intraperitoneal inoculation of the attenuated *S. typhimurium* strain SL3261 results in a prolonged systemic inflammatory response characterised by increased levels of cytokines such as IFN $\gamma$  peaking at 7 days after infection (Mittrucker and Kaufmann, 2000; Püntener et al., 2012). The CNS response to *S. typhimurium* infection is characterised by increased levels of IL-1 $\beta$  and IL-12 in the CNS 3 weeks after infection, increased expression of MHCII, ICAM and VCAM on endothelial cells and CD11b on microglial cells and exaggerated inflammatory responses to a secondary central LPS challenge 4 weeks after infection (Püntener et al., 2012). BCG infections in aged mice cause exaggerated sickness behaviour and prolonged depressive behaviour (Kelley et al., 2013) and *E. coli* infection in aged rats causes memory deficits accompanied by increased production of IL-1 $\beta$  and decreased BDNF expression in the hippocampus (Barrientos et al., 2009a).

The effects of infections on aged microglia outside the hippocampus have not been thoroughly investigated. A rostral caudal gradient of microglial sensitivity

to inflammation and ageing has been suggested (Kullberg et al., 2001; Schnell et al., 1999b) and Chapter 4 of this thesis describes grey-white matter differences in age-related changes in microglia. Therefore rostral-caudal and grey-white matter differences may exist in the responsiveness of the CNS to systemic infections such as *S. typhimurium*. This study investigates the effects of *S. typhimurium* infection on microglial phenotypes in different areas of the young and aged CNS and the effect of ageing on the central inflammatory response to *S. typhimurium*.

## **6.2 Methods**

### **6.2.1 Animals**

Female, C57/Bl6J mice aged either 3 (young) or 18 (aged) months old were obtained from Charles River, Margate, UK. Mice were injected with  $3 \times 10^5$  CFU of *S. typhimurium* strain SL3261. These mice were the same as those used for behavioural experiments in Chapter 5. The data presented in this chapter is derived from two independent experiments, experiment 1 and experiment 2. Both experiments were designed to study the effect of systemic *S. typhimurium* infection on the CNS over time. Experiment 1 had six different groups – saline treated mice culled 1 day after injection and mice infected with *S. typhimurium* for 1, 8, 15, 22 or 57 days. The 57 day time-point is referred to as 2 months throughout this chapter. Experiment 2 had three different groups – saline treated mice culled 21 days after injection and mice infected with *S. typhimurium* for 7 or 21 days. Within each group were 5-6 young and 5-6 aged mice, with the exception of the aged 57 day group of experiment 1 which only contained 3 mice due to some mice losing excessive amounts of weight and therefore being culled early under the terms of the home office licence used.

### **6.2.2 Tissue collection**

After perfusion with heparinised saline the brain was rapidly dissected and tissue was either embedded directly in OCT for immunohistochemistry or flash frozen in liquid nitrogen for qPCR. In experiment 1 the cerebellum was removed and embedded in OCT and the rest of the brain was cut sagittally. One half of the brain was embedded in OCT for fresh frozen

immunohistochemistry. A hippocampal punch was obtained from the other half of the brain using a sterile RNase free pipette tip to capture hippocampus enriched tissue. Serum was collected as described in chapter 2. In experiment 2 a hippocampal punch and cerebellar tissue were snap frozen for qPCR to allow comparison of the two regions. Assistance was received from Ursula Püntener and Steven Booth (University of Southampton) in collecting tissue from these experiments.

### **6.2.3 Cytokine measurements**

Serum cytokine measurements were obtained using a MSD multiplex kit ((K15012B) MesoScale Discovery, Gaithersburg, MD, USA) as described in chapter 2. Ursula Püntener (University of Southampton) assisted in performing the assay and data interpretation.

### **6.2.4 Immunohistochemistry**

Fresh frozen immunohistochemistry was performed as described in chapter 2. To maximise consistency within experiments, sections from several different mice were mounted on the same slide, allowing the simultaneous staining of all sections for one marker within one experiment. Sections were taken from within 0.3mm of bregma -2.2mm (hippocampus, corpus callosum, alveus) or -6.0mm (cerebellar white matter of the inferior cerebellar peduncle, cerebellar nuclei, molecular layer). Sections from spinal cord were collected from ventral lumbar spinal cord at all time-points except for 2 months after infection.

### **6.2.5 Quantification of immunohistochemistry**

Images were analysed and quantified using ImageJ. The DAB and haematoxylin channels were isolated using a plugin and a threshold was determined for quantification. Thresholds were determined for each experiment to control for variation in DAB staining intensity between experiments. Background or excessively dark haematoxylin staining was removed using the “despeckle” setting and, when required, by superimposing a mask of the haematoxylin channel onto the image. The region of interest was traced “freehand” from the image and the average pixel density within the selected area was calculated. For each animal two images per region of interest were captured at x20

magnification for quantification, using a brain atlas to identify matching regions of interest in each hemisphere. The average of the two images was calculated and data expressed as either fold increase over saline treated expression levels in the same region from age matched saline injected mice (Cd11b or CD68 and F4/80) or percentage of image above threshold (CD11c and Fc $\gamma$ RI). Fc $\gamma$ RI expression in the spinal cord grey matter was excluded from analysis due to non-specific nuclear binding in this particular region. The identity of sections was blinded during image capture and quantification.

### 6.2.6 qPCR

All data was quantified using the delta delta Ct method described in chapter 2. PGK1 was used as the housekeeping gene in all experiments. Assistance was received from Steven Booth and Ursula Püntener (University of Southampton) in performing some of the RNA extractions and reverse transcription reactions.

## 6.3 Results

### 6.3.1 The effect of *S. typhimurium* infection on circulating cytokine levels in young and aged mice

In experiment 1 young (3 months old) and aged mice (18 months old) were infected with  $3 \times 10^5$  CFU of *S. typhimurium* and culled 1, 8, 15, 22 or 57 days (2 months) later or injected with saline and culled 1 day later. Serum samples were collected at these time-points and the serum levels of the cytokines IL-1 $\beta$ , TNF $\alpha$ , IL-6, IL-12, IFN $\gamma$  and IL-10 determined using a multiplex immunoassay (Figure 6.1). Circulating cytokine levels peaked at 8 days after infection and the biggest increase in cytokine levels were in IFN $\gamma$  (Figure 6.1 A). IFN $\gamma$  concentrations were elevated in serum up to 22 days after infection, but progressively declined between day 8 and day 22. The peak concentration of TNF $\alpha$ , IL-1 $\beta$ , IL-6 and IL-10 was also 8 days after infection, although the increase from saline injected levels was smaller than that of IFN $\gamma$ . Infection had a significant effect on the concentrations of all cytokines measured ( $p < 0.01$ ) except for IL-12. Age did not affect the expression of any of the cytokines measured at baseline or after *S. typhimurium* infection apart from IL-10. Age had a significant effect on IL-10 expression ( $p < 0.001$ ) and IL-10 was generally

more elevated between days 1-22 after infection in aged than in young mice. There was no significant effect of age x infection on circulating cytokine levels. The results of the statistical analysis of these data are compiled in table 6.1.

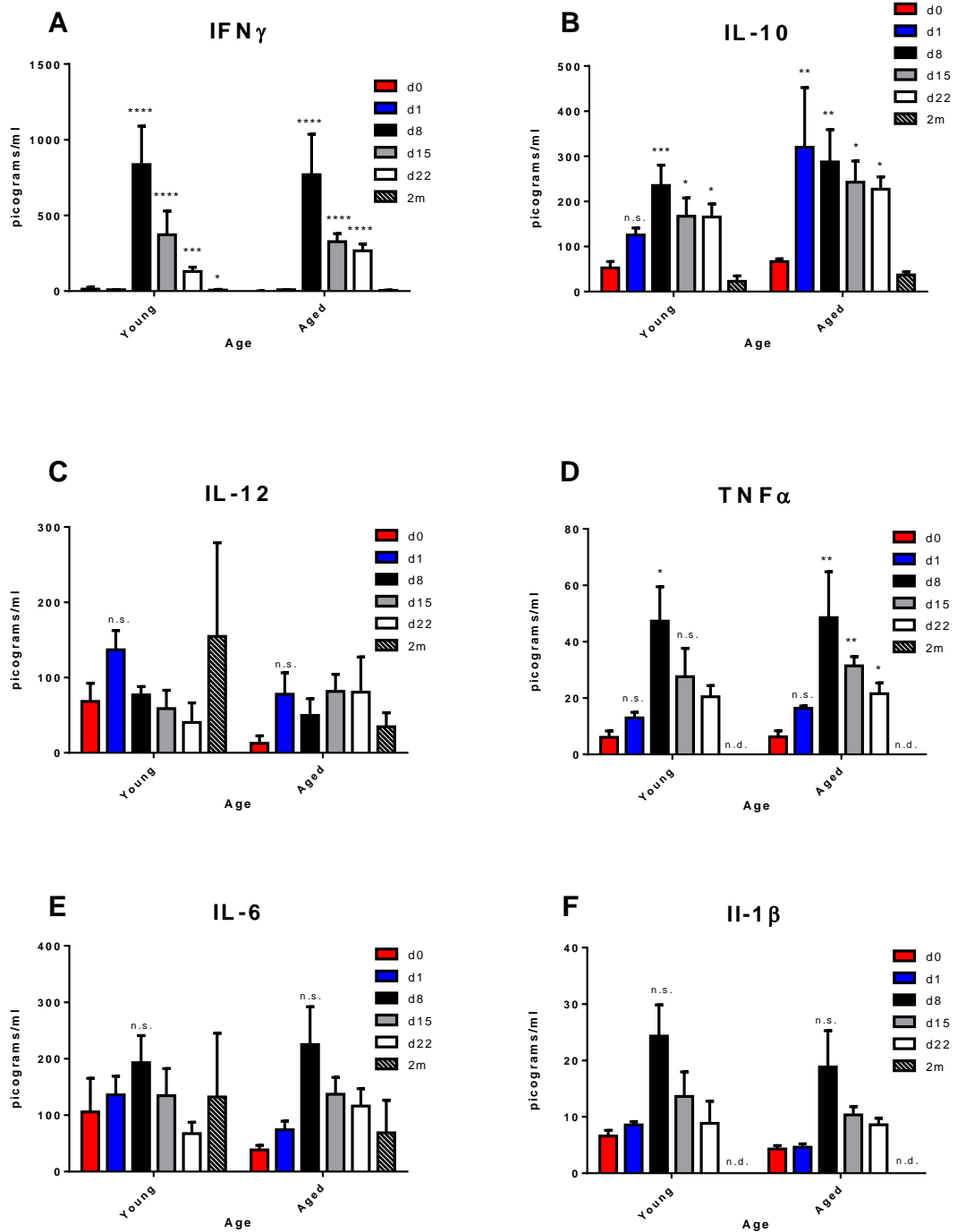


**Figure 6.1.** The effect of *S. typhimurium* infection on serum cytokine levels in young and aged mice. Levels of IFN $\gamma$  (A), IL-10 (B), IL-12 (C), TNF $\alpha$  (D), IL-6 (E), IL-1 $\beta$  (F) were measured using a multiplex immunoassay. Data is shown as

mean  $\pm$  SEM. Stars denote a significant difference compared to age matched D0 expression. \* denotes  $p < 0.05$ ; \*\* denotes  $p < 0.01$ ; \*\*\* denotes  $p < 0.001$ ; \*\*\*\* denotes  $p < 0.0001$ .

Cytokine	Serum		
	Age	Infection	Age x Infection
IL-1 $\beta$ n = 5-6	F (1, 45) = 2.126	F (4, 45) = 5.019	F (4, 45) = 0.9125
	P = 0.1517	P = 0.0020	P = 0.4649
IL-6 n = 5-6	F (1, 52) = 0.1357	F (5, 52) = 3.837	F (5, 52) = 0.7325
	P = 0.7141	P = 0.0049	P = 0.6024
TNF $\alpha$ n = 5-6	F (1, 45) = 0.04506	F (4, 45) = 7.920	F (4, 45) = 0.3999
	P = 0.8328	P < 0.0001	P = 0.8076
IFN $\gamma$ n = 5-6	F (1, 52) = 0.008024	F (5, 52) = 32.38	F (5, 52) = 1.058
	P = 0.9290	P < 0.0001	P = 0.3941
IL-12 n = 5-6	F (1, 50) = 0.7085	F (5, 50) = 2.258	F (5, 50) = 2.507
	P = 0.4040	P = 0.0628	P = 0.0421
IL-10 n = 5-6	F (1, 52) = 13.31	F (5, 52) = 26.85	F (5, 52) = 0.5661
	P = 0.0006	P < 0.0001	P = 0.7255

**Table 6.1. Statistical analysis of the effects of *S. typhimurium* infection and ageing on circulating levels of IL-1 $\beta$ , IL-6, TNF $\alpha$ , IFN $\gamma$ , IL-12 and IL-10.**

Data was logarithmically transformed to obtain a normal distribution and then analysed using two way ANOVAs.

### 6.3.2 An immunohistological assessment of microglial phenotype in different regions of the young and aged CNS after *S. typhimurium* infection

Fresh frozen sections were stained for the same molecules selected for investigation in chapter 4, namely CD11b, CD68, F4/80, Fc $\gamma$ RI and CD11c. The regions investigated were cerebellar white matter, the cerebellar nuclei (mixed grey/white matter), the molecular layer of the cerebellum (grey matter), the dentate gyrus and CA1 regions of the hippocampus (grey matter), the alveus of the hippocampus (white matter), the corpus callosum (white matter), and the lateral white matter tracts and grey matter of the ventral lumbar spinal cord. Expression levels of these molecules was quantified for each region (Figure 6.2) and expressed as fold increase from young saline treated mice for CD11b, CD68 and F4/80 and as percentage of image above threshold for Fc $\gamma$ RI and CD11c due to the negligible expression of these proteins in some regions.

The increase in expression of CD11b in aged mice was most pronounced in the cerebellum and in the corpus callosum and alveus (Figure 6.2 A), although the effect of region was not significant (Kruskal-Wallis test: d.f. = 7,  $\chi^2 = 10.90$ ,  $p = 0.143$ ). Increases in CD68 expression during ageing were most pronounced in the cerebellum and region had a significant effect on CD68 expression (Kruskal-Wallis test: d.f. = 7,  $\chi^2 = 16.07$ ,  $p = 0.0245$ ) (Figure 6.2 B). F4/80 expression was only increased during ageing in white matter or mixed grey/white matter areas, although the effect of region was not quite statistically significant (Kruskal-Wallis test: d.f. = 7,  $\chi^2 = 13.64$ ,  $p = 0.0580$ ) (Figure 6.2 C). Fc $\gamma$ RI expression was also only increased during ageing in white matter or mixed grey/white matter areas and region and age had a significant effect (2 way ANOVA: age:  $F_{1,68} = 42.14$ ,  $p < 0.0001$ , region:  $F_{6,68} = 8.54$ ,  $p < 0.0001$ , age x region:  $F_{6,68} = 0.932$ ,  $p = 0.478$ ) (Figure 6.2 D). CD11c expression was only increased during ageing in white matter areas and age, region and age x region had a statistically significant effect on CD11c expression (2 way ANOVA: age:  $F_{1,68} = 17.30$ ,  $p < 0.0001$ , region:  $F_{7,68} = 3.16$ ,  $p = 0.0054$ , age x region:  $F_{7,68} = 2.57$ ,  $p = 0.0193$ ) (Figure 6.2 E).

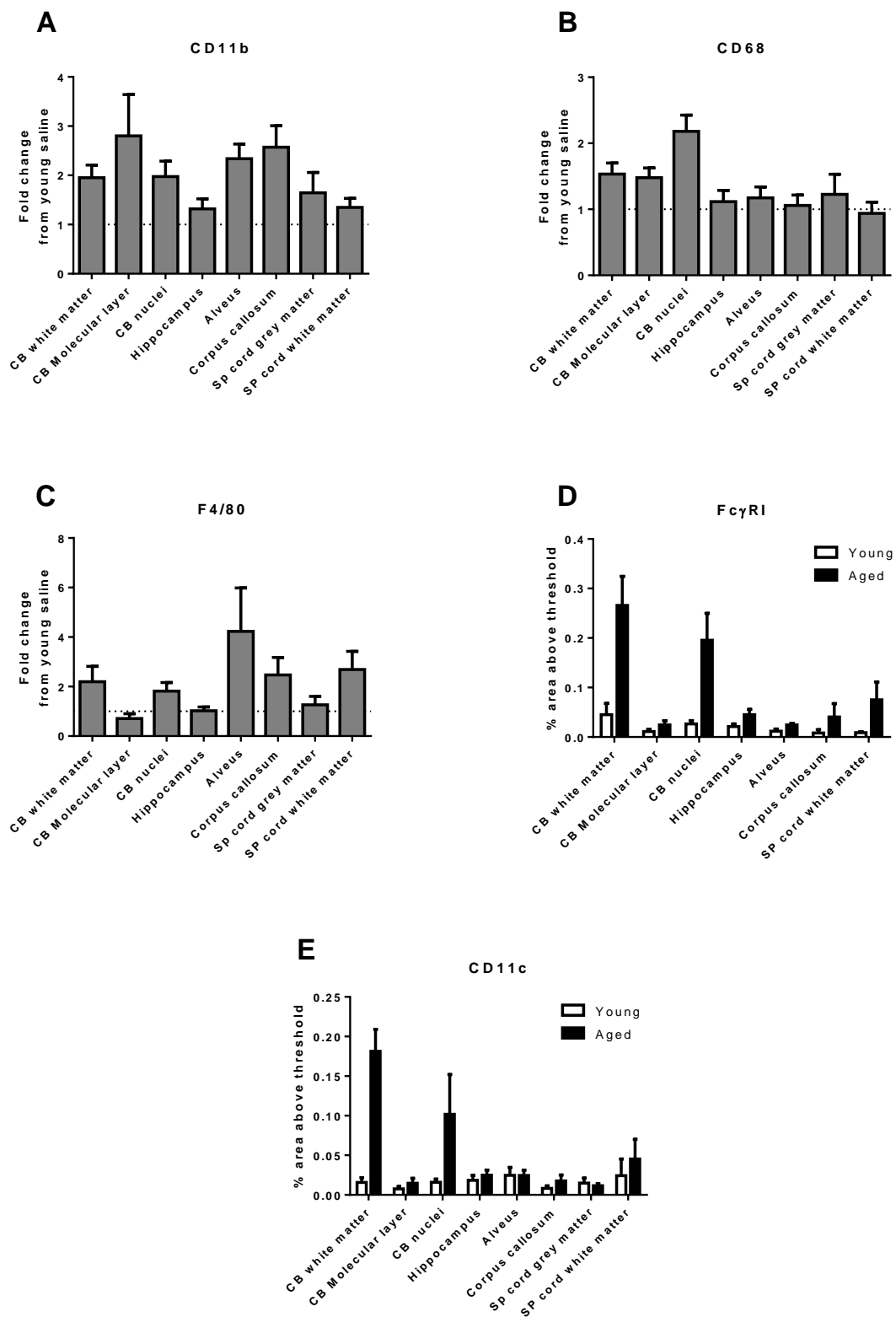


**Figure 6.2.** The effect of ageing on expression of microglia markers in various regions of the aged CNS.

Expression of CD11b (A), CD68 (B), F4/80 (C), Fc $\gamma$ RI (D) and CD11c (E) increases with ageing. Data is shown as mean  $\pm$  SEM.

The effect of *S. typhimurium* infection on expression of the selected microglial activation markers was also quantified in each of the regions tested. CD11b expression was increased by *S. typhimurium* infection in all CNS regions examined (Figure 6.3), with no detectable regional differences in sensitivity of microglial CD11b expression to *S. typhimurium* infection. The variability of these data meant that infection or age x infection did not have a statistically significant effect in any region examined (table 6.2). Increases in CD11b expression were slightly more pronounced in young than in aged cerebellum and hippocampus regions, although the molecular layer of the cerebellum was the only region where the effect of age was significant. In the spinal cord increases in CD11b expression were comparable between ages. Representative images from hippocampus (Figure 6.4), spinal cord (Figure 6.5) and cerebellar white matter (Figure 6.6) illustrate the general increase in CD11b expression observed in these brain areas.

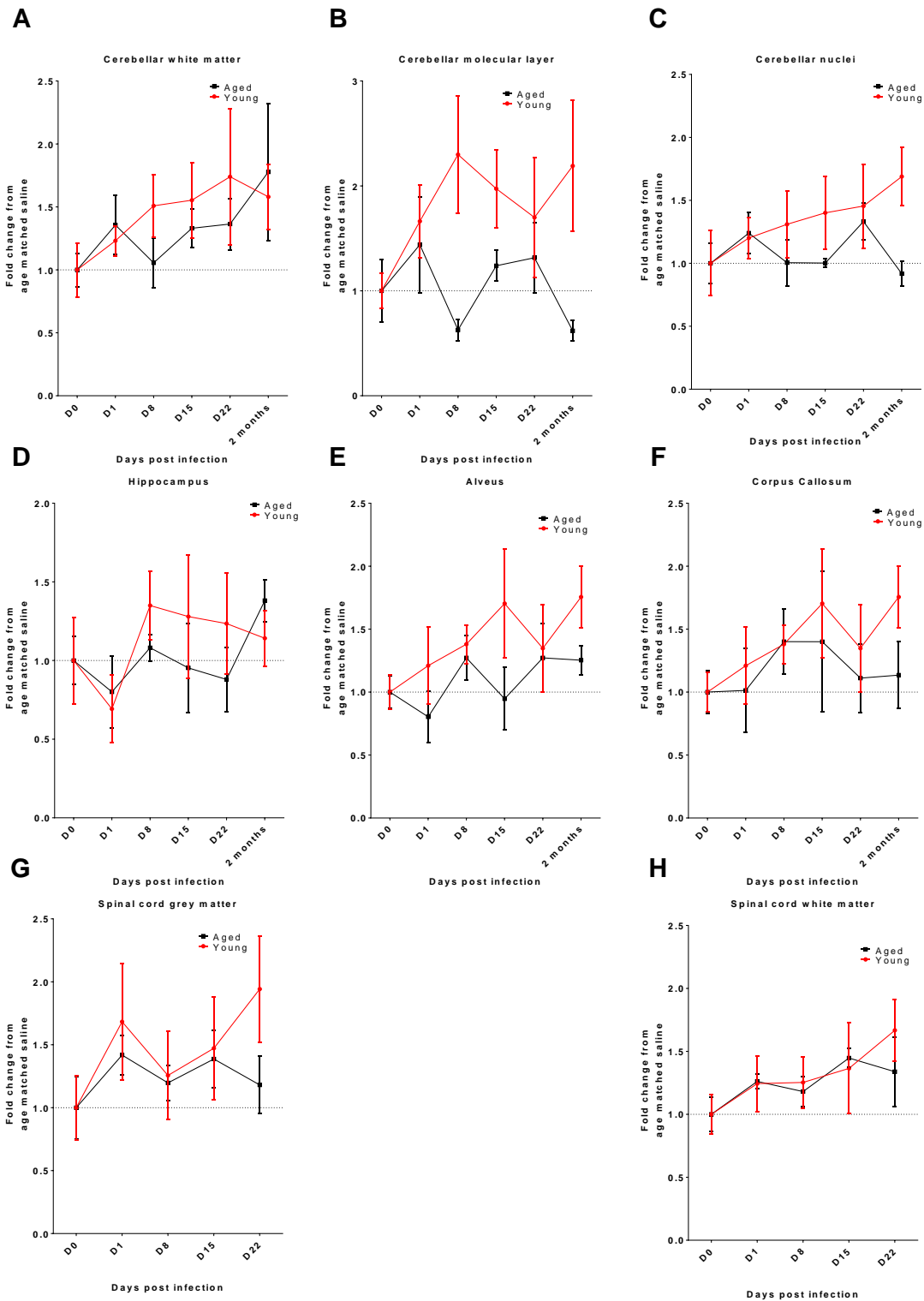


**Figure 6.3. The effect of *S. typhimurium* infection on CD11b expression in various regions of the young and aged CNS.**

CD11b expression was quantified in cerebellar white matter (A), the molecular layer of the cerebellum (B), the cerebellar nuclei (C), the dentate gyrus and CA1

region of the hippocampus (D), the alveus of the hippocampus (E), the corpus callosum (F), the grey matter of the ventral spinal cord (G) and the white matter of the ventral spinal cord (H). Stars denote a significant increase in expression of CD11b compared to age matched saline injected mice in that region. Stars denote a significant difference compared to age matched D0 expression. \* denotes  $p < 0.05$ ; \*\* denotes  $p < 0.01$ ; \*\*\* denotes  $p < 0.001$ .

Region	Age	Time-point	Age x Time-point
Cerebellar white matter	F (1, 54) = 0.04735	F (5, 54) = 1.367	F (5, 54) = 0.1973
	P = 0.8286	P = 0.2511	P = 0.9622
Cerebellar molecular layer	F (1, 53) = 7.916	F (5, 53) = 1.026	F (5, 53) = 0.9346
	P = 0.0069	P = 0.4116	P = 0.4662
Cerebellar nuclei	F (1, 51) = 0.3880	F (5, 51) = 0.7826	F (5, 51) = 0.4505
	P = 0.5361	P = 0.5670	P = 0.8110
Hippocampus	F (1, 54) = 0.01353	F (5, 54) = 1.352	F (5, 54) = 0.3431
	P = 0.9078	P = 0.2568	P = 0.8844
Alveus	F (1, 54) = 3.118	F (5, 54) = 1.323	F (5, 54) = 0.4789
	P = 0.0831	P = 0.2682	P = 0.7904
Corpus callosum	F (1, 49) = 1.891	F (5, 49) = 0.5460	F (5, 49) = 0.2379
	P = 0.1753	P = 0.7405	P = 0.9438
Spinal cord grey matter	F (1, 46) = 0.1323	F (4, 46) = 1.288	F (4, 46) = 0.4567
	P = 0.7178	P = 0.2886	P = 0.7670
Spinal cord white matter	F (1, 46) = 0.1086	F (4, 46) = 0.8060	F (4, 46) = 0.5988
	P = 0.7433	P = 0.5277	P = 0.6653

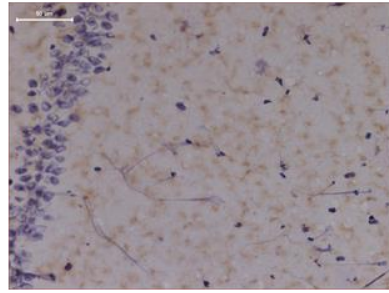
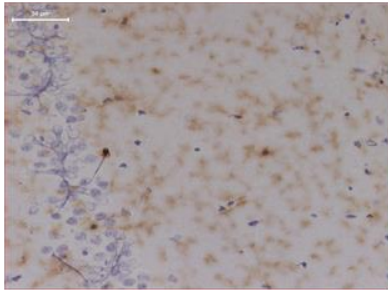
**Table 6.2. Statistical analysis of the effects of *S. typhimurium* infection and ageing on expression of CD11b.**

Data was logarithmically transformed to obtain a normal distribution and then analysed by two way ANOVA.

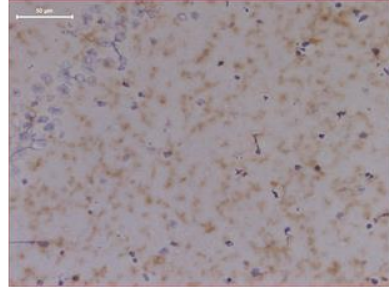
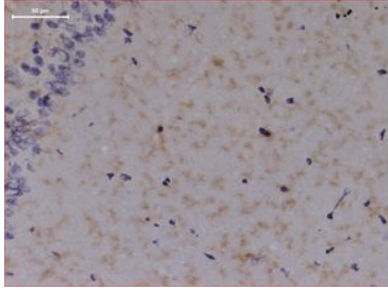
**Young**

**Aged**

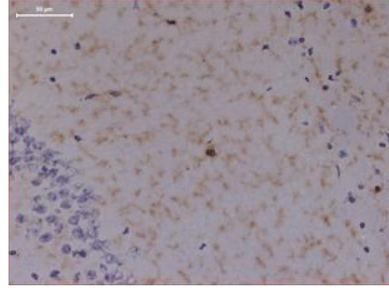
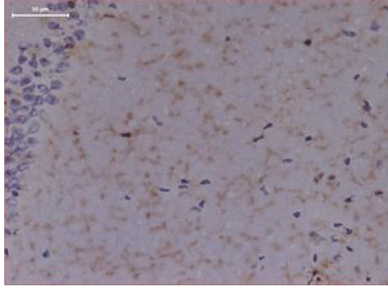
**D0**



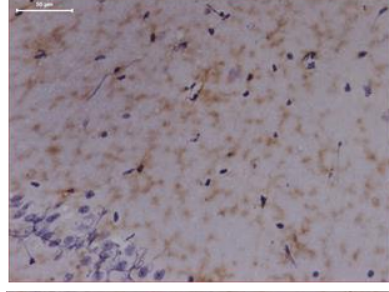
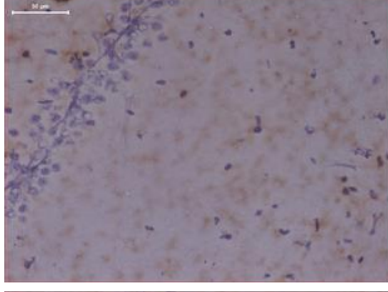
**D1**



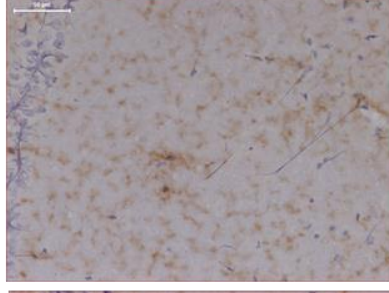
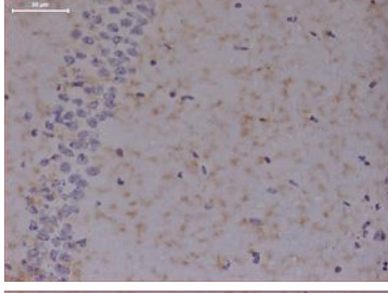
**D8**



**D15**



**D22**



**2 mo**

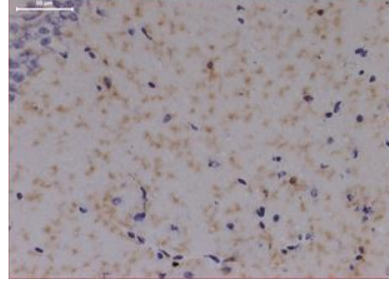
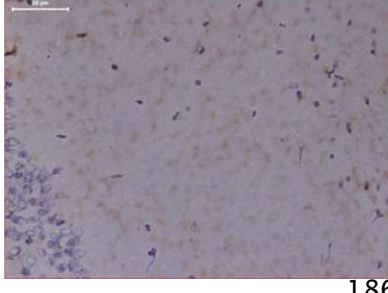


**Figure 6.4. Representative images of CD11b expression in the hippocampus of young or aged mice following *S. typhimurium* infection.**

Images were captured at x40 magnification. The blue staining is a haematoxylin nuclear counterstain, brown staining is for CD11b. The scale bar represents 50µm.

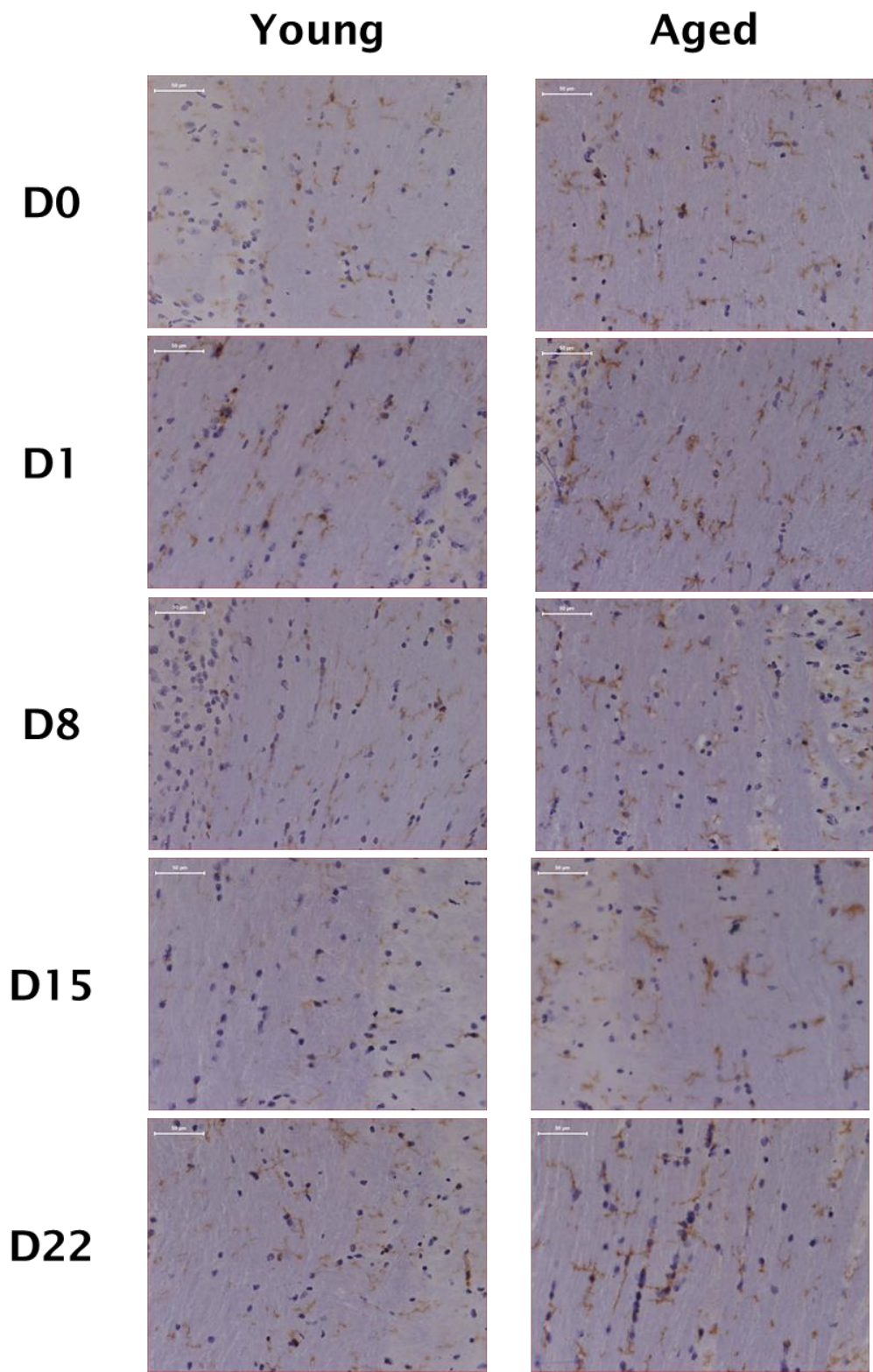


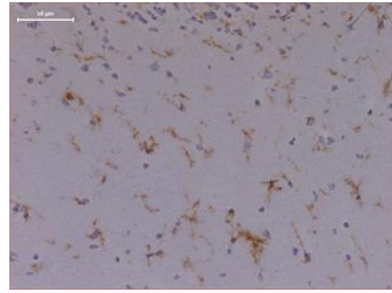
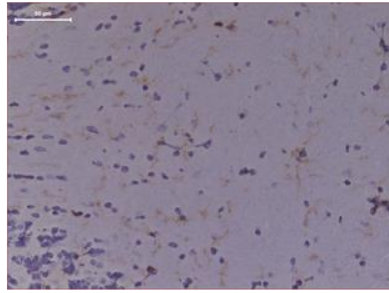
**Figure 6.5. Representative images of CD11b expression in spinal cord white matter tracts of young or aged mice following *S. typhimurium* infection.**

Images were captured at x40 magnification. Blue staining is a haematoxylin nuclear counterstain, brown staining is for CD11b. Scale bar represents 50µm.

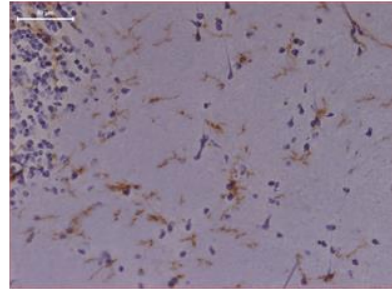
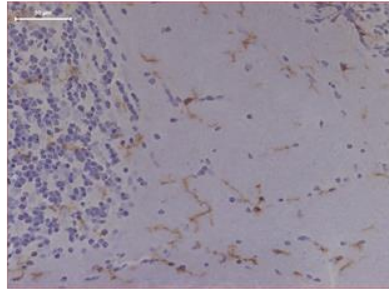
**Young**

**Aged**

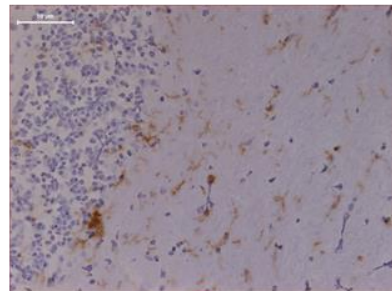
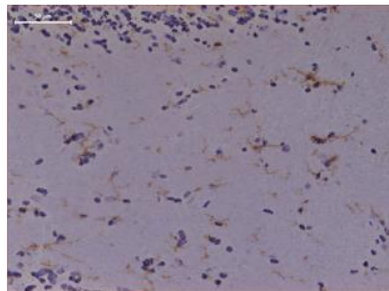
**D0**



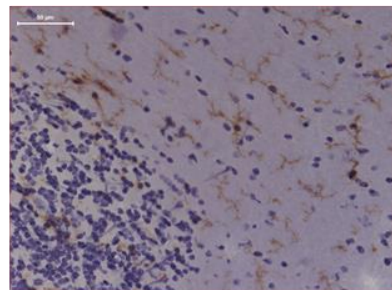
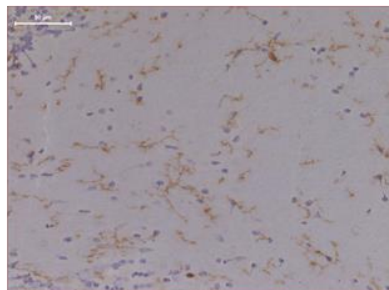
**D1**



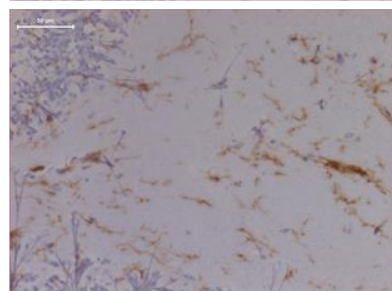
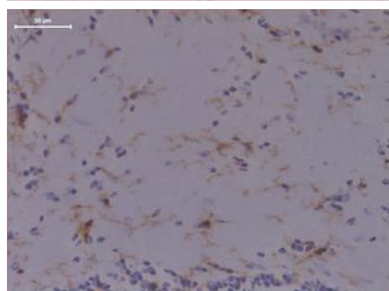
**D8**



**D15**



**D22**



**2 mo**

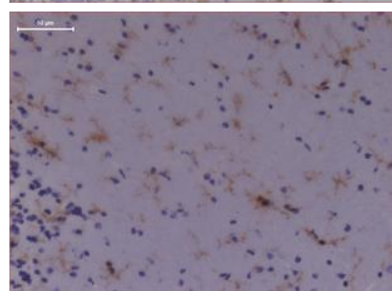
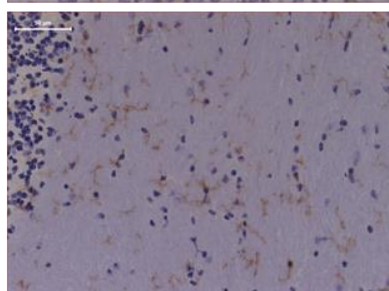


**Figure 6.6. Representative images of CD11b expression in the cerebellar white matter tracts of young or aged mice following *S. typhimurium* infection.**

Images were captured at x40 magnification. The blue staining is a haematoxylin nuclear counterstain, brown staining is for CD11b. The scale bar represents 50µm.

Changes in CD68 expression during infection were most pronounced in the grey and white matter of the aged spinal cord, where a progressive increase in CD68 expression was observed peaking at 22 days after infection (Figure 6.7). A weaker increase in CD68 expression during *S. typhimurium* infection occurs in the young spinal cord. There was no discernible increase in CD68 expression during infection in any regions of the young cerebellum, hippocampus, alveus or corpus callosum, whereas CD68 expression did slightly increase in the aged cerebellum, hippocampus, alveus and corpus callosum. The statistical analysis of these data is presented in table 6.3. Representative images illustrating the changes in CD68 expression that occur during infection in hippocampus (Figure 6.8), spinal cord (Figure 6.9) and cerebellar white matter (Figure 6.10) illustrate the changes in CD68 expression that occur during *S. typhimurium* infection and show increases in CD68 expression in both parenchymal microglial cells and cells associated with blood vessels.

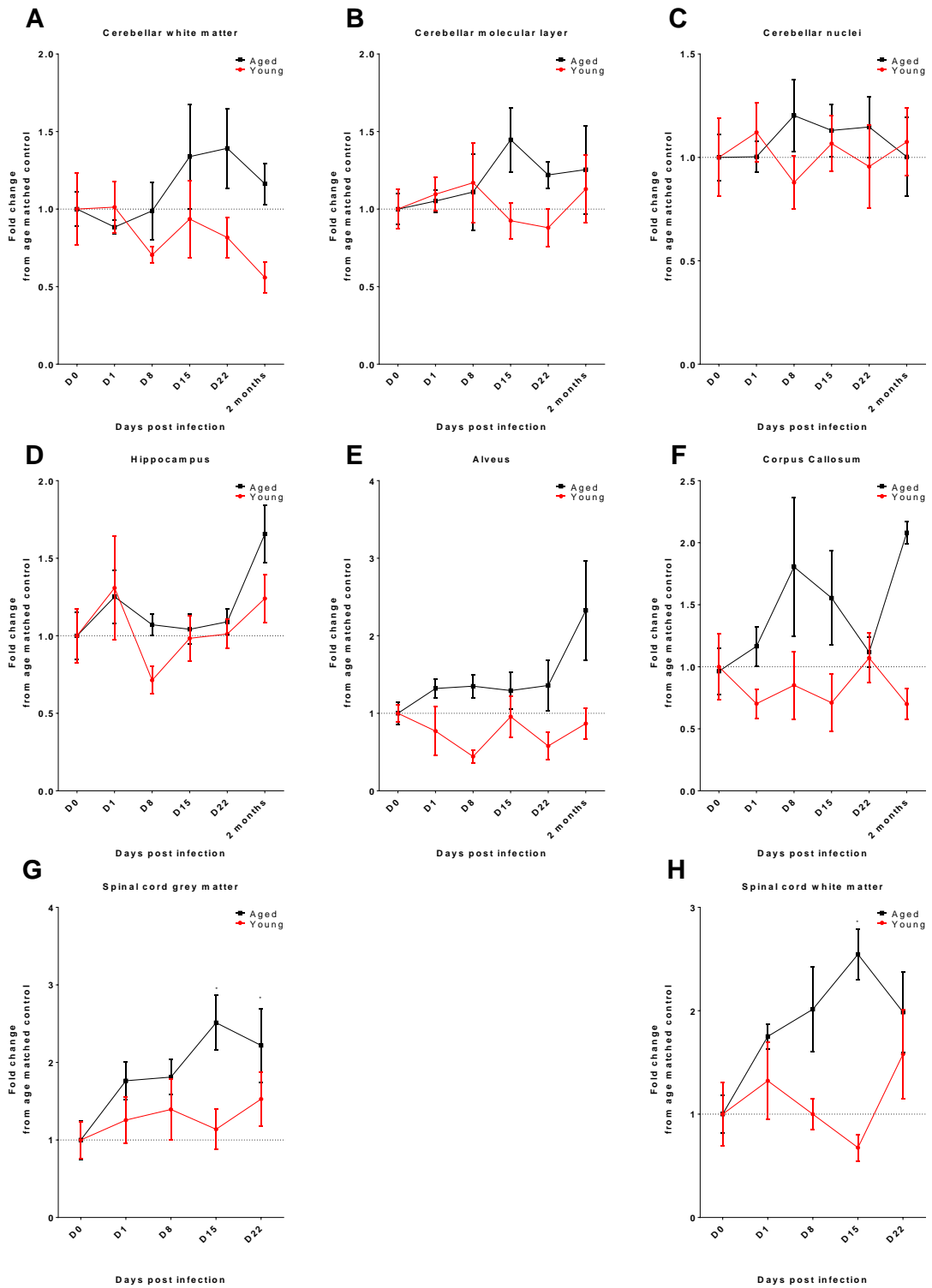


**Figure 6.7. The effect of *S. typhimurium* infection on CD68 expression in various regions of the young and aged CNS.**

CD68 expression was quantified in cerebellar white matter (A), the molecular layer of the cerebellum (B), the cerebellar nuclei (C), the dentate gyrus and CA1

region of the hippocampus (D), the alveus of the hippocampus (E), the corpus callosum (F), the grey matter of the ventral spinal cord (G) and the white matter of the ventral spinal cord (H). Stars denote a significant increase in expression of CD68 compared to age matched saline injected mice in that region. Stars denote a significant difference compared to age matched D0 expression. \* denotes  $p < 0.05$ ; \*\* denotes  $p < 0.01$ ; \*\*\* denotes  $p < 0.001$ .

Region	Age	Time-point	Age x Time-point
Cerebellar white matter	F (1, 53) = 8.910	F (5, 53) = 0.4362	F (5, 53) = 1.089
	P = 0.0043	P = 0.8213	P = 0.3775
Cerebellar molecular layer	F (1, 53) = 2.696	F (5, 53) = 0.2319	F (5, 53) = 0.9762
	P = 0.1065	P = 0.9469	P = 0.4409
Cerebellar nuclei	F (1, 53) = 0.9755	F (5, 53) = 0.1701	F (5, 53) = 0.4730
	P = 0.3278	P = 0.9726	P = 0.7947
Hippocampus	F (1, 53) = 3.737	F (5, 53) = 2.678	F (5, 53) = 0.6688
	P = 0.0586	P = 0.0313	P = 0.6488
Alveus	F (1, 53) = 21.28	F (5, 53) = 1.026	F (5, 53) = 1.190
	P < 0.0001	P = 0.4120	P = 0.3267
Corpus callosum	F (1, 45) = 14.59	F (5, 45) = 0.3687	F (5, 45) = 1.634
	P = 0.0004	P = 0.8674	P = 0.1706
Spinal cord grey matter	F (1, 46) = 2.686	F (4, 46) = 2.561	F (4, 46) = 1.108
	P = 0.1081	P = 0.0509	P = 0.3642
Spinal cord white matter	F (1, 46) = 17.64	F (4, 46) = 2.529	F (4, 46) = 2.020
	P = 0.0001	P = 0.0532	P = 0.1073

**Table 6.3. Statistical analysis of the effects of *S. typhimurium* infection and ageing on expression of CD68.**

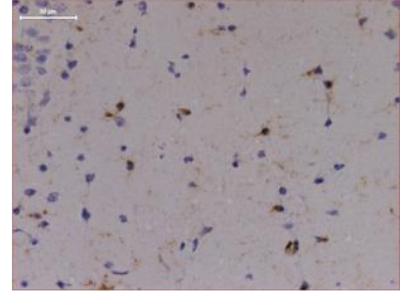
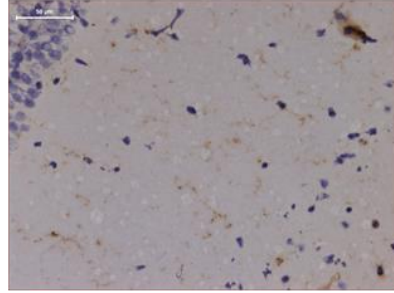
Data was logarithmically transformed to obtain a normal distribution and then analysed by two way ANOVA.

**Figure 6.8. Representative images of CD68 expression in the hippocampus of young or aged mice following *S. typhimurium* infection.** Images were captured at x40 magnification. The blue staining is a haematoxylin nuclear counterstain, brown staining is for CD68. The scale bar represents 50 $\mu$ m.

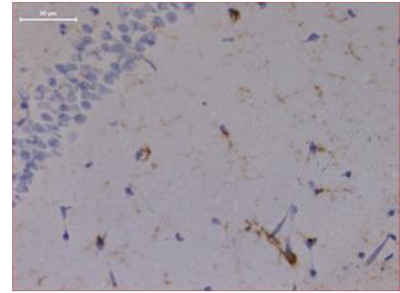
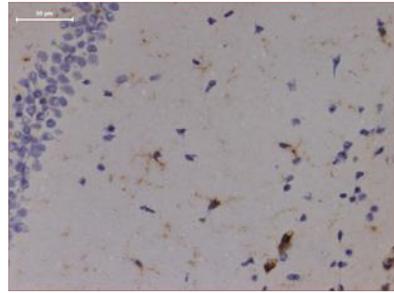
**Young**

**Aged**

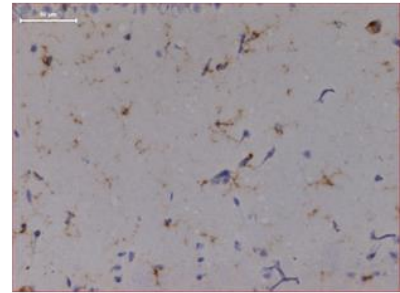
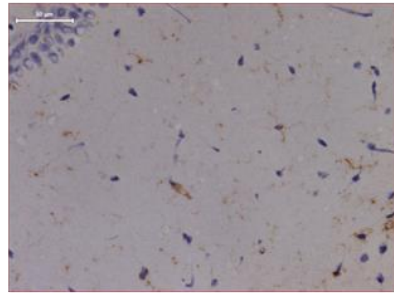
**D0**



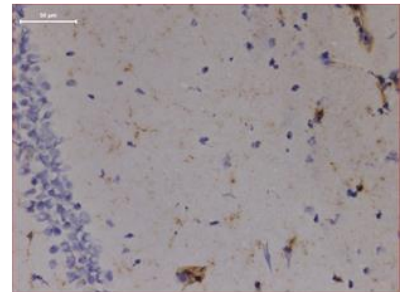
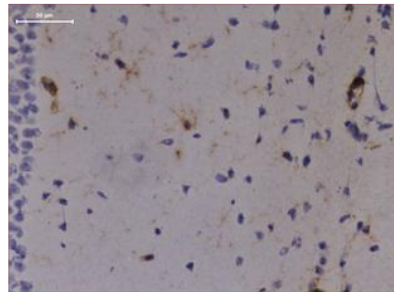
**D1**



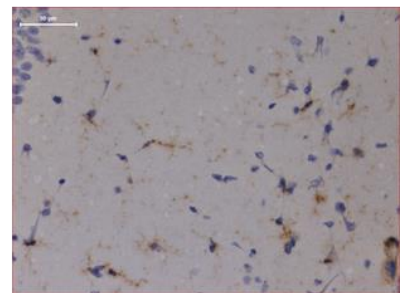
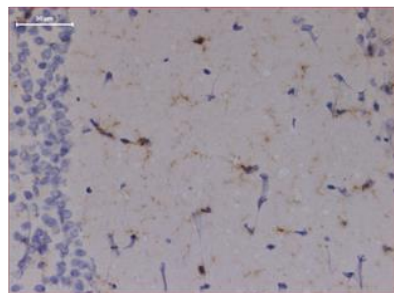
**D8**



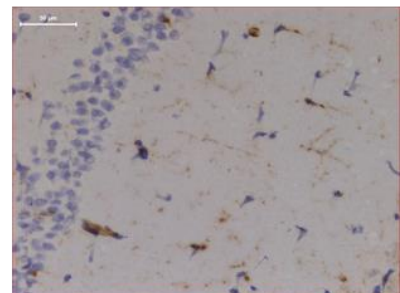
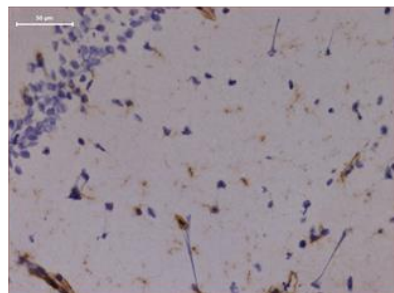
**D15**



**D22**



**2 mo**



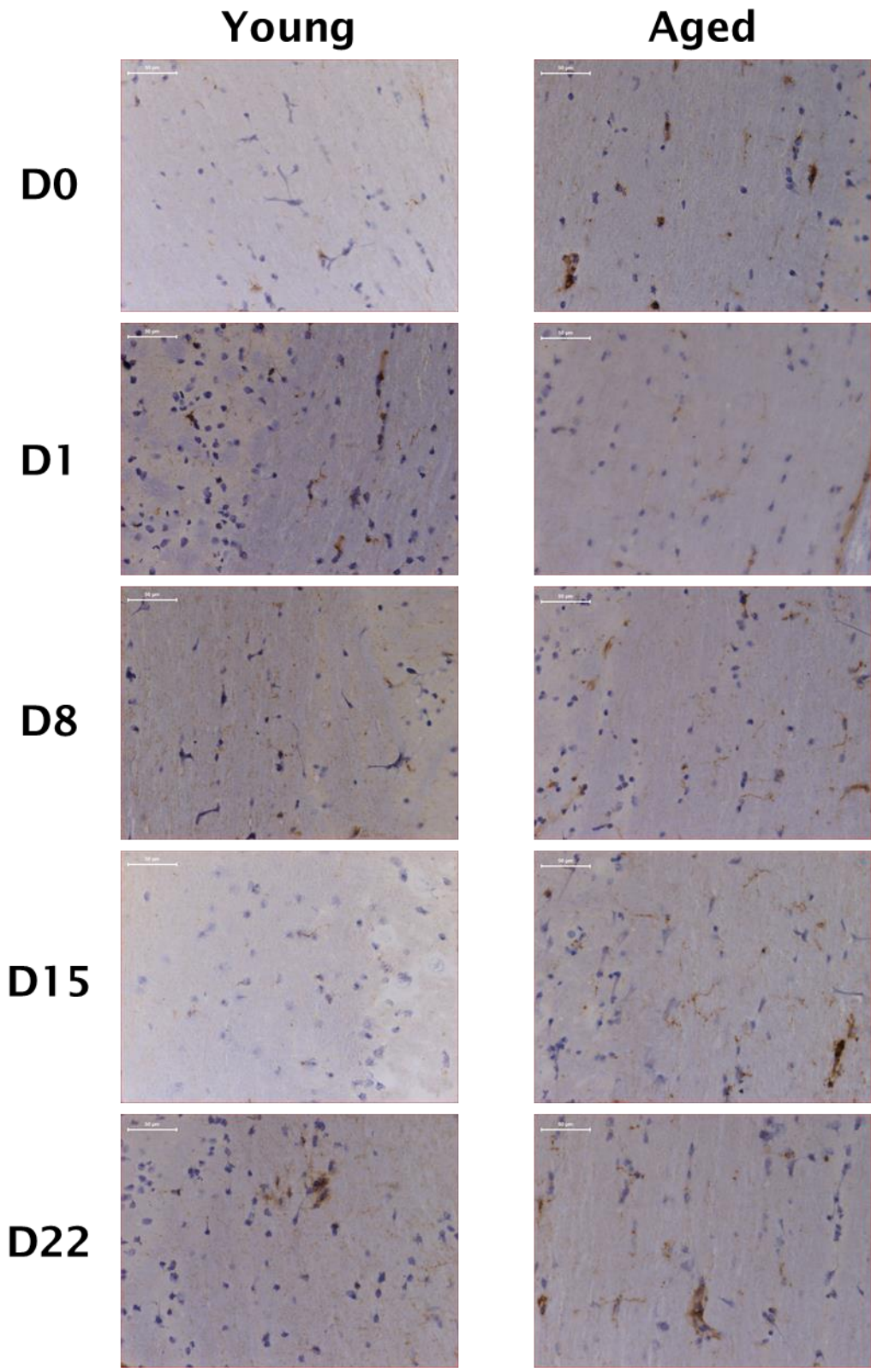


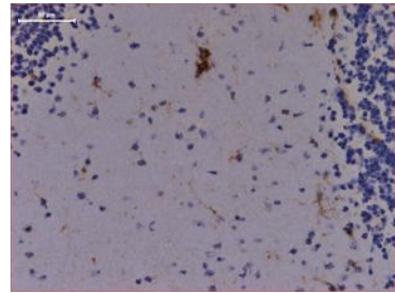
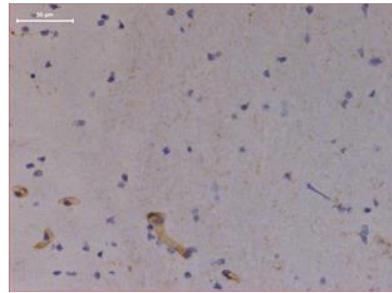
Figure 6.9. Representative images of CD68 expression in spinal cord white matter tracts of young or aged mice following *S. typhimurium* infection.

Images were captured at x40 magnification. Blue staining is a haematoxylin nuclear counterstain, brown staining is for CD68. Scale bar represents 50µm.

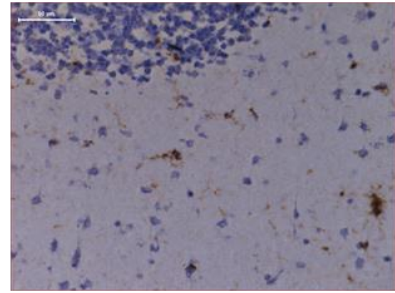
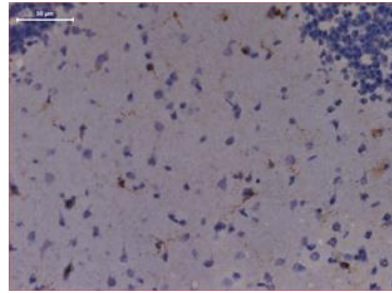
**Young**

**Aged**

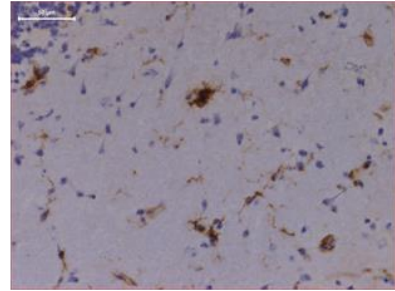
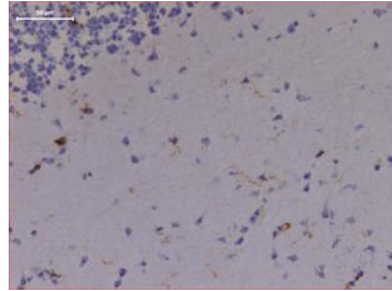
**D0**



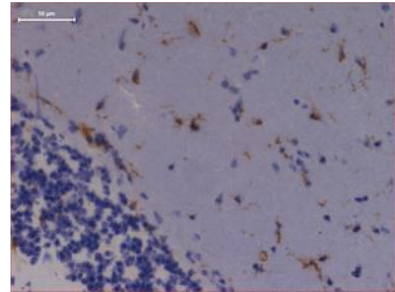
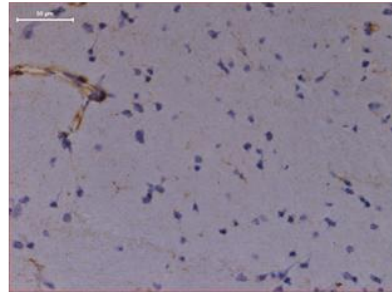
**D1**



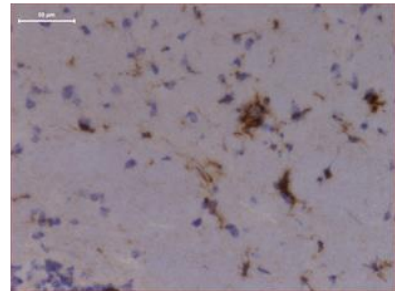
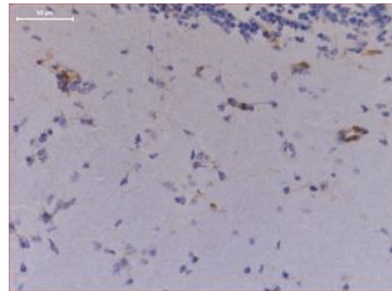
**D8**



**D15**



**D22**



**2 mo**

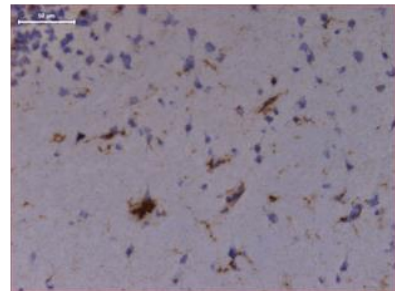
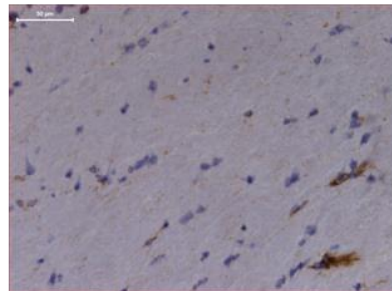


**Figure 6.10. Representative images of CD68 expression in the cerebellar white matter tracts of young or aged mice following *S. typhimurium* infection.**

Images were captured at x40 magnification. The blue staining is a haematoxylin nuclear counterstain, brown staining is for CD68. The scale bar represents 50µm.

F4/80 expression was increased by *S. typhimurium* infection (Figure 6.11). This increase in expression was most pronounced in the spinal cord. Young and aged mice show a progressive increase in F4/80 expression of similar magnitude in spinal cord grey matter, whereas in white matter the fold increase in F4/80 expression is larger in young mice. There was a statistically significant effect of infection on F4/80 expression in the white matter and molecular layer of the cerebellum as well as the spinal cord grey and white matter. In the cerebellum, hippocampus, alveus and corpus callosum the kinetics and the extent of change in F4/80 expression varied greatly, making it difficult to identify specific trends in expression of F4/80. There was however an overall trend towards increased F4/80 expression during infection in these regions, particularly at later time-points such as 15 or 22 days after infection. Most cells that were F4/80 positive were associated with blood vessels, but in the white matter of *S. typhimurium* infected mice F4/80 positive cells with a microglial morphology were more prevalent (Figure 6.12).

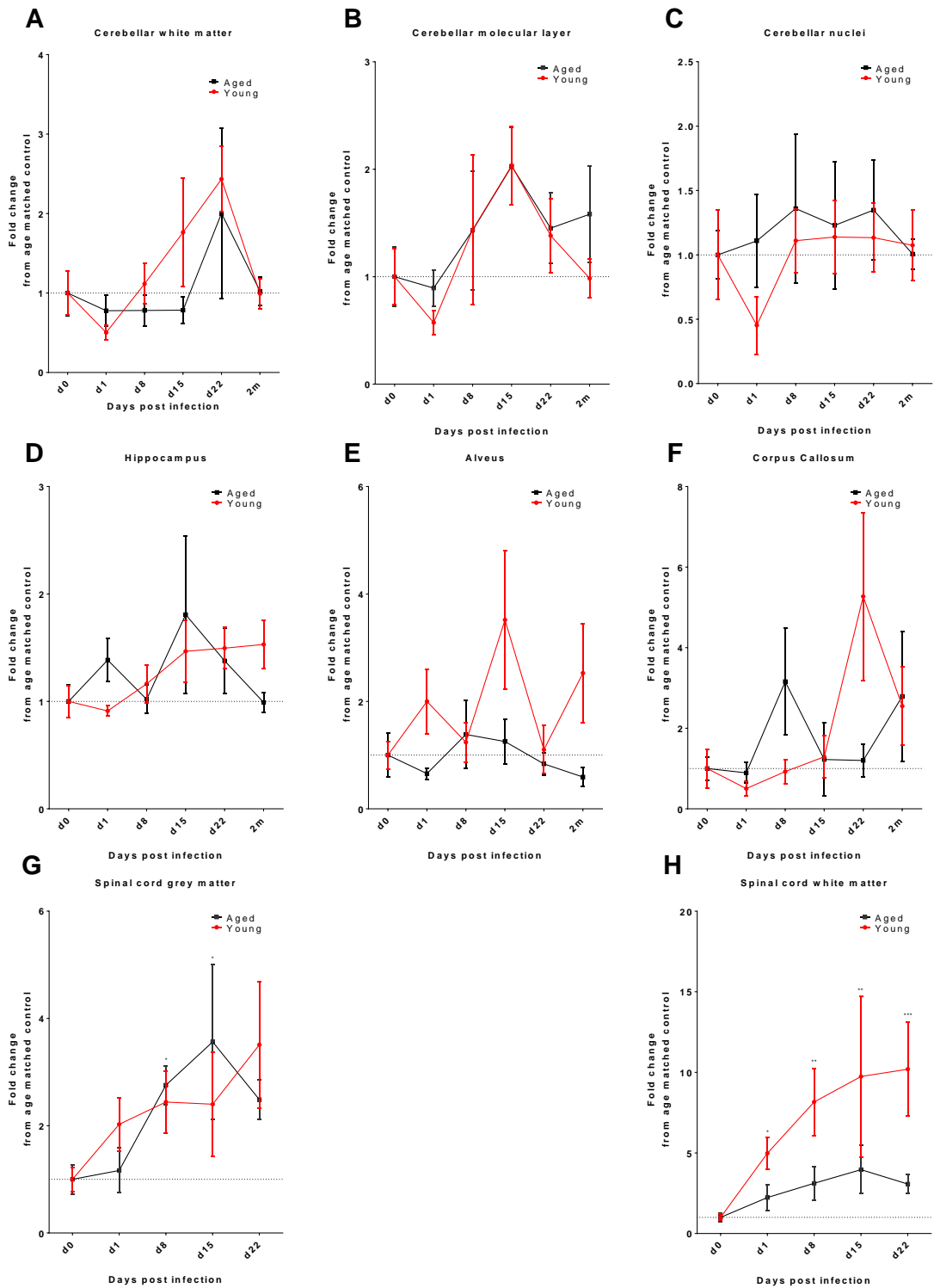


**Figure 6.11. The effect of *S. typhimurium* infection on F4/80 expression in various regions of the young and aged CNS.**

F4/80 expression was quantified in cerebellar white matter (A), the molecular layer of the cerebellum (B), the cerebellar nuclei (C), the dentate gyrus and CA1

region of the hippocampus (D), the alveus of the hippocampus (E), the corpus callosum (F), the grey matter of the ventral spinal cord (G) and the white matter of the ventral spinal cord (H). Stars denote a significant increase in expression of F4/80 compared to age matched saline injected mice in that region. Stars denote a significant difference compared to age matched D0 expression. \* denotes  $p < 0.05$ ; \*\* denotes  $p < 0.01$ ; \*\*\* denotes  $p < 0.001$ .

Region	Age	Time-point	Age x Time-point
Cerebellar white matter	F (1, 53) = 1.037	F (5, 53) = 3.274	F (5, 53) = 0.8678
	P = 0.3131	P = 0.0119	P = 0.5090
Cerebellar molecular layer	F (1, 53) = 1.281	F (5, 53) = 3.270	F (5, 53) = 0.2426
	P = 0.2628	P = 0.0120	P = 0.9417
Cerebellar nuclei	F (1, 51) = 0.9036	F (5, 51) = 1.183	F (5, 51) = 0.7201
	P = 0.3463	P = 0.3305	P = 0.6114
Hippocampus	F (1, 54) = 0.1044	F (5, 54) = 1.347	F (5, 54) = 0.8791
	P = 0.7479	P = 0.2588	P = 0.5014
Alveus	F (1, 52) = 4.249	F (5, 52) = 0.6458	F (5, 52) = 0.2904
	P = 0.0443	P = 0.6659	P = 0.9162
Corpus callosum	F (1, 50) = 0.2410	F (5, 50) = 1.379	F (5, 50) = 1.303
	P = 0.6256	P = 0.2479	P = 0.2777
Spinal cord grey matter	F (1, 45) = 0.06802	F (4, 45) = 5.478	F (4, 45) = 0.9044
	P = 0.7954	P = 0.0011	P = 0.4695
Spinal cord white matter	F (1, 45) = 12.06	F (4, 45) = 8.037	F (4, 45) = 0.7079
	P = 0.0011	P < 0.0001	P = 0.5908

**Table 6.4. Statistical analysis of the effects of *S. typhimurium* infection time-point and ageing on expression of F4/80.**

Data was logarithmically transformed to obtain a normal distribution and then analysed by two way ANOVA.

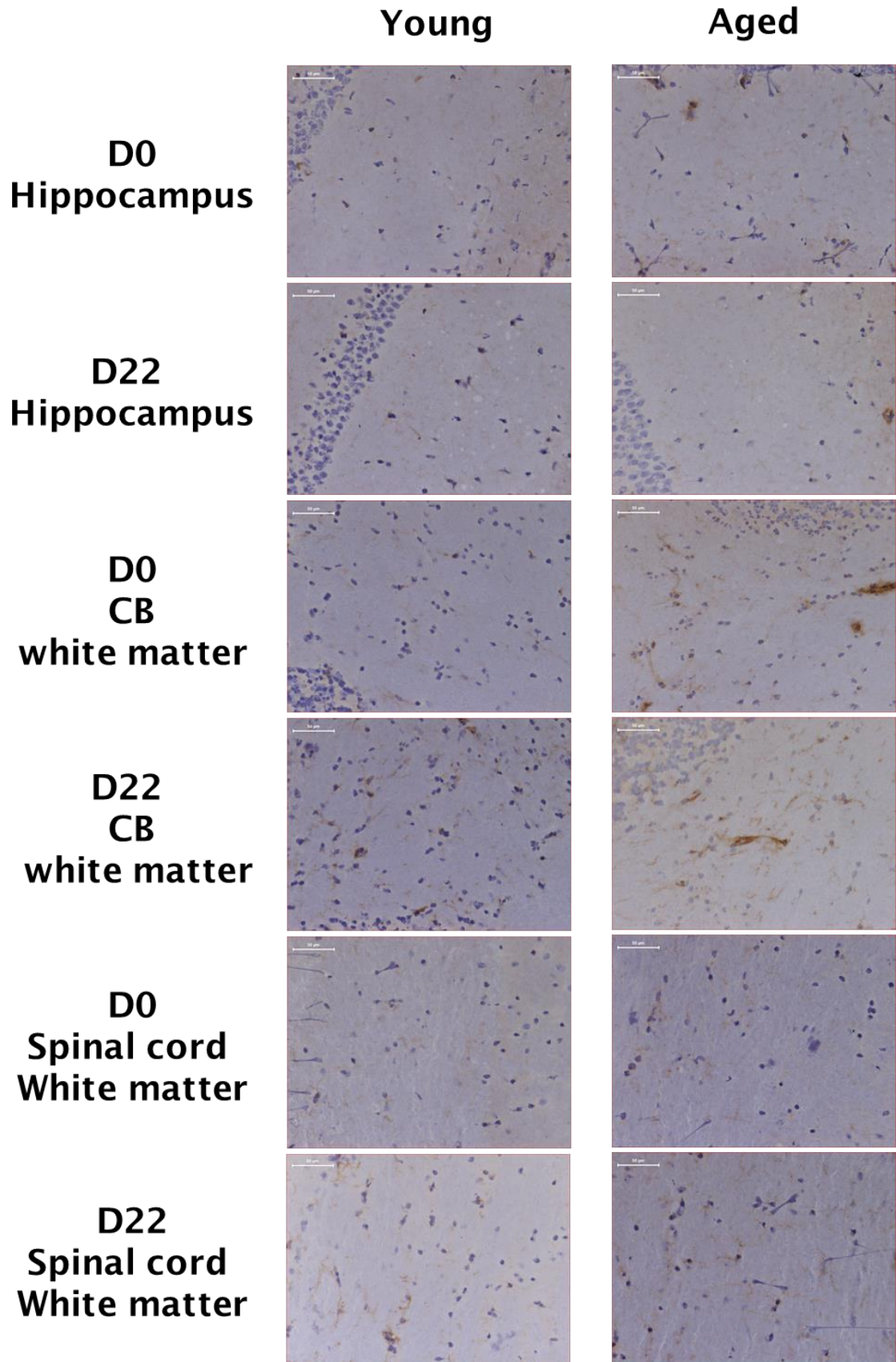
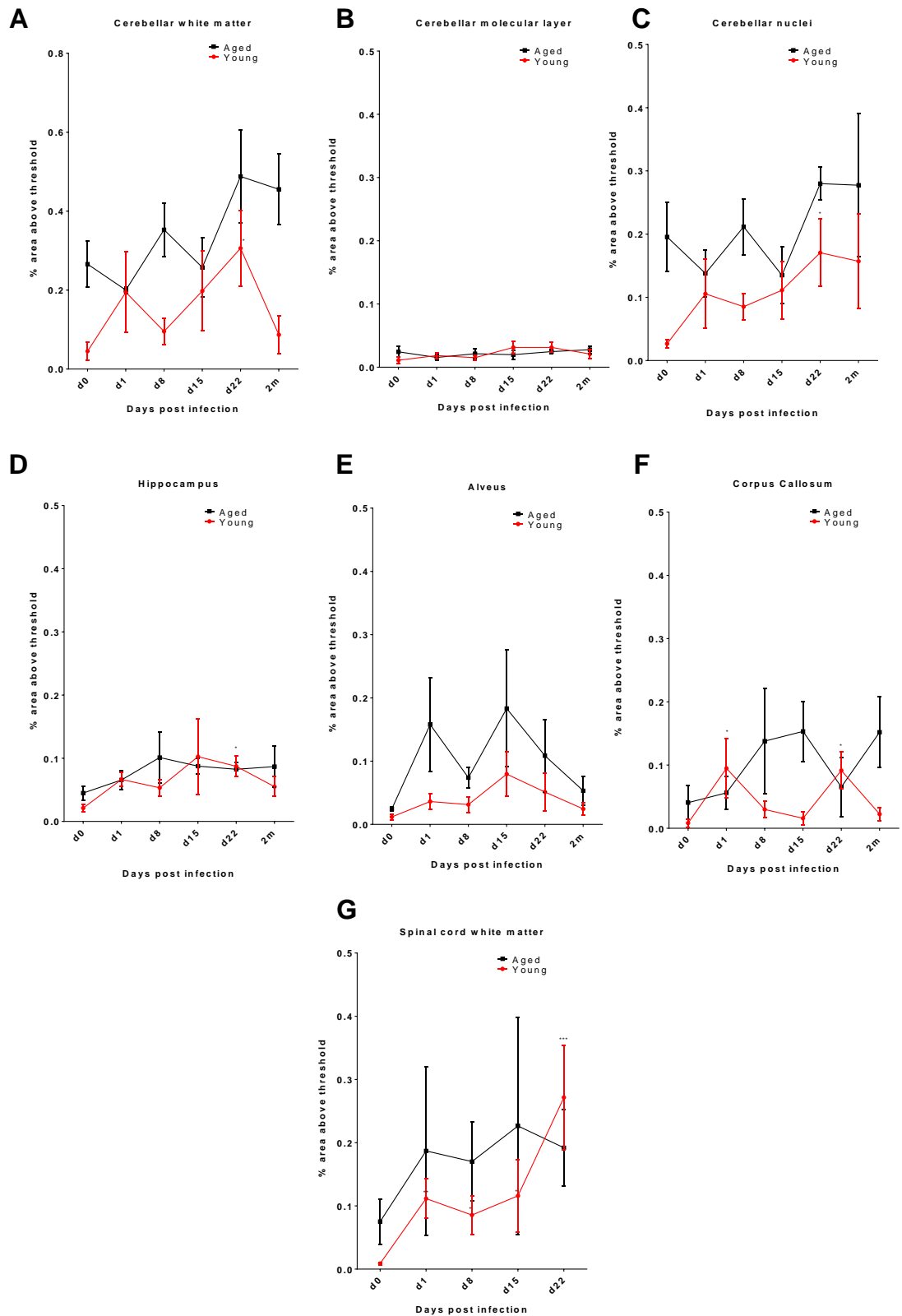


Figure 6.12. Representative images of F4/80 expression in the CNS of young or aged mice following *S. typhimurium* infection.

Images were captured at x40 magnification. The blue staining is a haematoxylin nuclear counterstain, brown staining is for F4/80. The scale bar represents 50µm.

FcγRI expression was negligible after saline injection in young mice, so data is represented as percentage area covered instead of fold increase from age matched saline injected mice. Increases in FcγRI expression were detectable following infection throughout the CNS, including areas such as the hippocampus where there was no detectable expression prior to infection – although the amount of detectable of FcγRI expression was still very limited in such areas (Figure 6.14). Increases in expression were most pronounced in young and aged spinal cord white matter (Figure 6.13 G) and young cerebellar nuclei and white matter. There was a significant effect of infection on expression of FcγRI in the cerebellar nuclei, hippocampus, corpus callosum and spinal cord white matter and a nearly significant effect in cerebellar white matter. Most cells that were positive for FcγRI had a microglial morphology (Figure 6.14).



**Figure 6.13.** The effect of *S. typhimurium* infection on Fc $\gamma$ RI expression in various regions of the young and aged CNS.

Fc $\gamma$ RI expression was quantified in cerebellar white matter (A), the molecular layer of the cerebellum (B), the cerebellar nuclei (C), the dentate gyrus and CA1 region of the hippocampus (D), the alveus of the hippocampus (E), the corpus callosum (F), the grey matter of the ventral spinal cord (G) and the white matter of the ventral spinal cord (H). Stars denote a significant increase in expression of Fc $\gamma$ RI compared to age matched saline injected mice in that region. \* denotes p<0.05; \*\* denotes p< 0.01; \*\*\* denotes p< 0.001.

Region	Age	Time-point	Age x Time-point
Cerebellar white matter	F (1, 53) = 28.47	F (5, 53) = 2.048	F (5, 53) = 1.099
	P < 0.0001	P = 0.0867	P = 0.3721
Cerebellar molecular layer	F (1, 53) = 0.4759	F (5, 53) = 1.689	F (5, 53) = 0.8125
	P = 0.4933	P = 0.1534	P = 0.5461
Cerebellar nuclei	F (1, 49) = 13.65	F (5, 49) = 3.101	F (5, 49) = 0.8884
	P = 0.0006	P = 0.0165	P = 0.4961
Hippocampus	F (1, 54) = 4.139	F (5, 54) = 3.281	F (5, 54) = 0.5663
	P = 0.0468	P = 0.0117	P = 0.7253
Alveus	F (1, 54) = 9.104	F (5, 54) = 1.843	F (5, 54) = 0.1290
	P = 0.0039	P = 0.1199	P = 0.9852
Corpus callosum	F (1, 51) = 11.14	F (5, 51) = 2.359	F (5, 51) = 2.809
	P = 0.0016	P = 0.0531	P = 0.0257
Spinal cord white matter	F (1, 46) = 4.074	F (4, 46) = 6.185	F (4, 46) = 1.314
	P = 0.0494	P = 0.0005	P = 0.2788

**Table 6.5. Statistical analysis of the effects of *S. typhimurium* infection and ageing on expression of Fc $\gamma$ RI.**

Data was logarithmically transformed to obtain a normal distribution and then analysed by two way ANOVA.

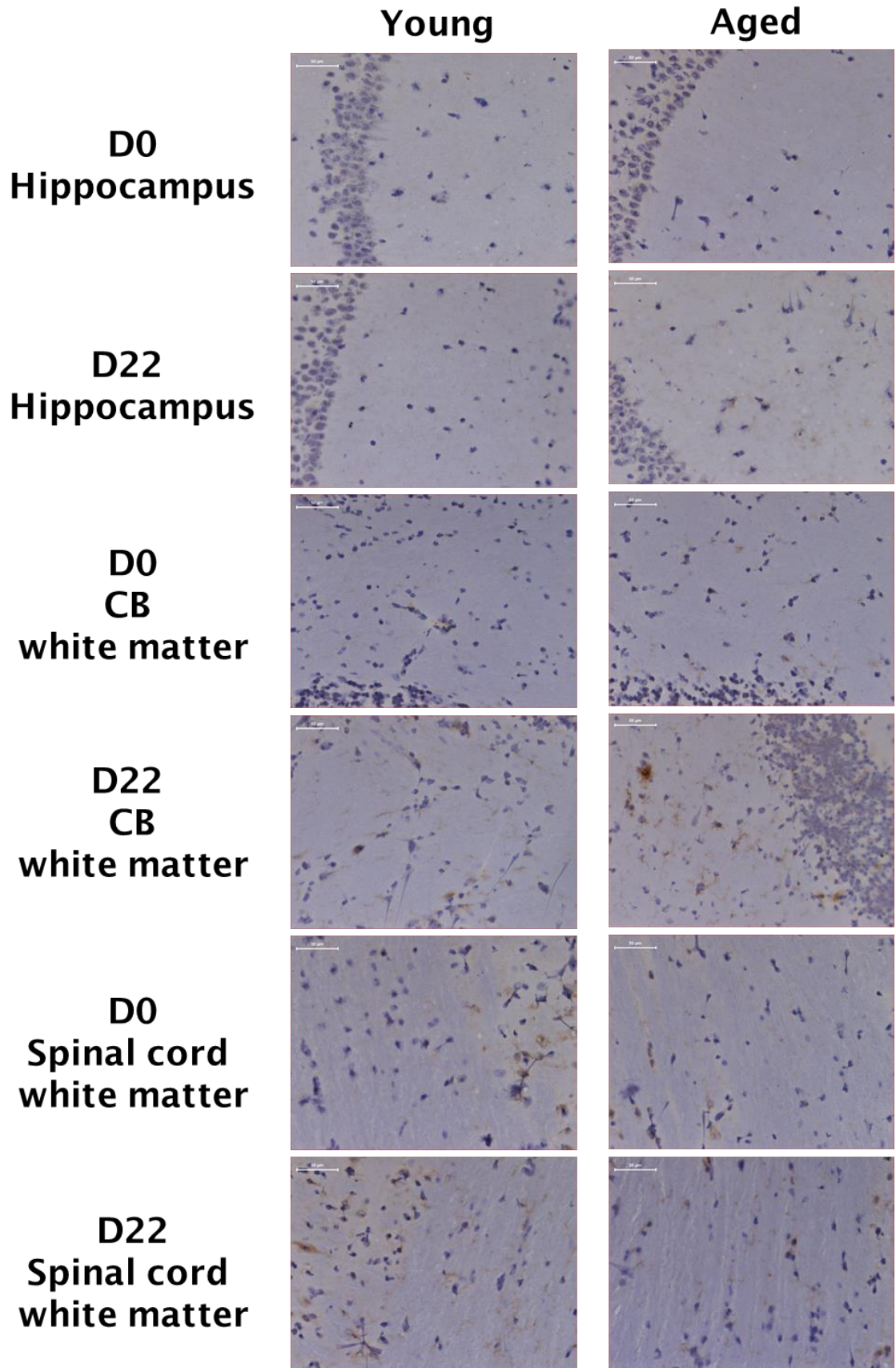
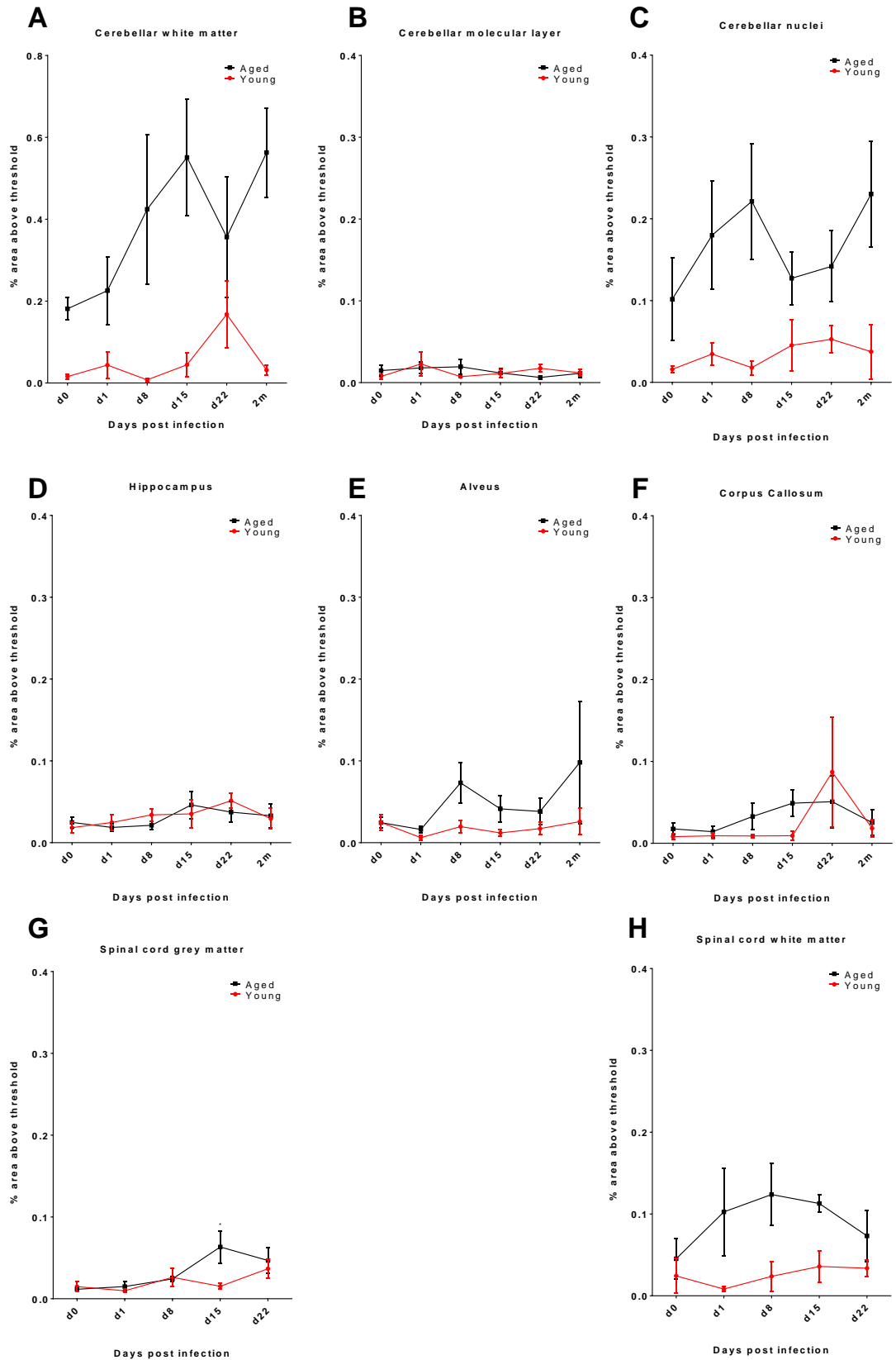


Figure 6.14. Representative images of Fc $\gamma$ RI expression in the CNS of young or aged mice following *S. typhimurium* infection.

Images were captured at x40 magnification. The blue staining is a haematoxylin nuclear counterstain, brown staining is for Fc $\gamma$ RI. The scale bar represents 50 $\mu$ m.

CD11c expression was not detectable except in aged white matter/ mixed grey and white matter regions, so data was represented as percentage of area covered instead of fold increase from age matched saline controls. A trend towards increased CD11c expression during infection was present in all aged white matter tracts, but were most pronounced in cerebellar white matter and spinal cord white matter (Figure 6.15 A & H). Increased CD11c expression was typically associated with cells of a microglial morphology (Figure 6.16). There was also an increase in expression of CD11c in aged spinal cord grey matter and young cerebellar white matter 22 days after infection, but not at other time-points. The increases in CD11c expression caused by infection were only significant in spinal cord grey matter, although there was a nearly significant effect of infection on CD11c expression in cerebellar white matter.



**Figure 6.15.** The effect of *S. typhimurium* infection on CD11c expression in various regions of the young and aged CNS.

CD11c expression was quantified in cerebellar white matter (A), the molecular layer of the cerebellum (B), the cerebellar nuclei (C), the dentate gyrus and CA1 region of the hippocampus (D), the alveus of the hippocampus (E), the corpus callosum (F), the grey matter of the ventral spinal cord (G) and the white matter of the ventral spinal cord (H). Stars denote a significant increase in expression of CD11c compared to age matched saline injected mice in that region. \* denotes  $p < 0.05$ ; \*\* denotes  $p < 0.01$ ; \*\*\* denotes  $p < 0.001$ .

Region	Age	Time-point	Age x Time-point
Cerebellar white matter	F (1, 53) = 84.79	F (5, 53) = 2.204	F (5, 53) = 2.010
	P < 0.0001	P = 0.0675	P = 0.0922
Cerebellar molecular layer	F (1, 52) = 0.009767	F (5, 52) = 0.1966	F (5, 52) = 1.040
	P = 0.9217	P = 0.9624	P = 0.4042
Cerebellar nuclei	F (1, 51) = 53.88	F (5, 51) = 0.7180	F (5, 51) = 1.290
	P < 0.0001	P = 0.6129	P = 0.2827
Hippocampus	F (1, 54) = 0.01865	F (5, 54) = 1.130	F (5, 54) = 0.9735
	P = 0.8919	P = 0.3558	P = 0.4424
Alveus	F (1, 52) = 9.821	F (5, 52) = 0.7771	F (5, 52) = 0.6077
	P = 0.0028	P = 0.5707	P = 0.6943
Corpus callosum	F (1, 50) = 4.867	F (5, 50) = 0.6841	F (5, 50) = 0.7716
	P = 0.0320	P = 0.6377	P = 0.5747
Spinal cord grey matter	F (1, 45) = 5.063	F (4, 45) = 5.278	F (4, 45) = 1.195
	P = 0.0294	P = 0.0014	P = 0.3260
Spinal cord white matter	F (1, 45) = 26.04	F (4, 45) = 1.410	F (4, 45) = 1.059
	P < 0.0001	P = 0.2461	P = 0.3879

**Table 6.6. Statistical analysis of the effects of *S. typhimurium* infection and ageing on expression of CD11c.**

Data was logarithmically transformed to obtain a normal distribution and then analysed by two way ANOVA.

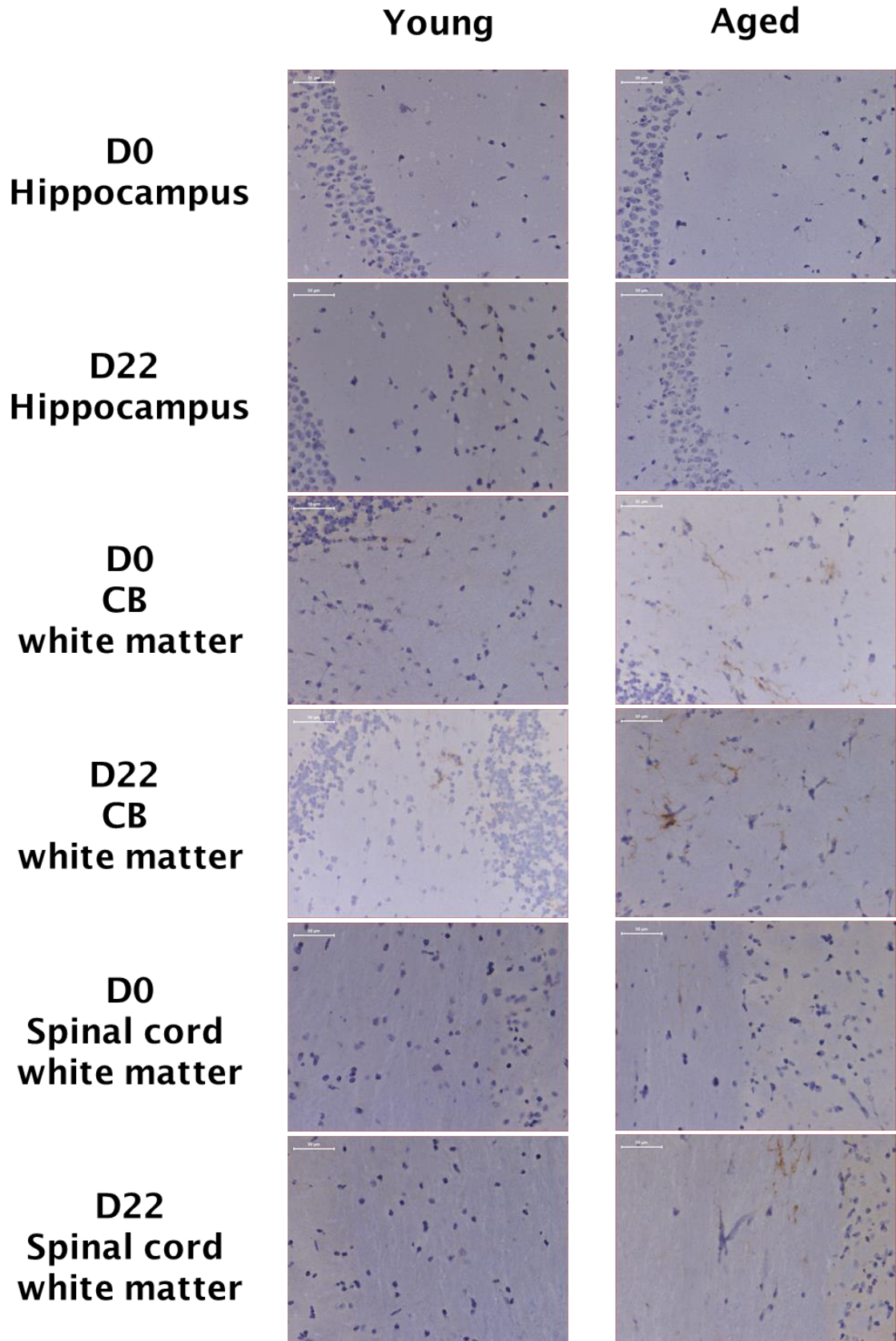
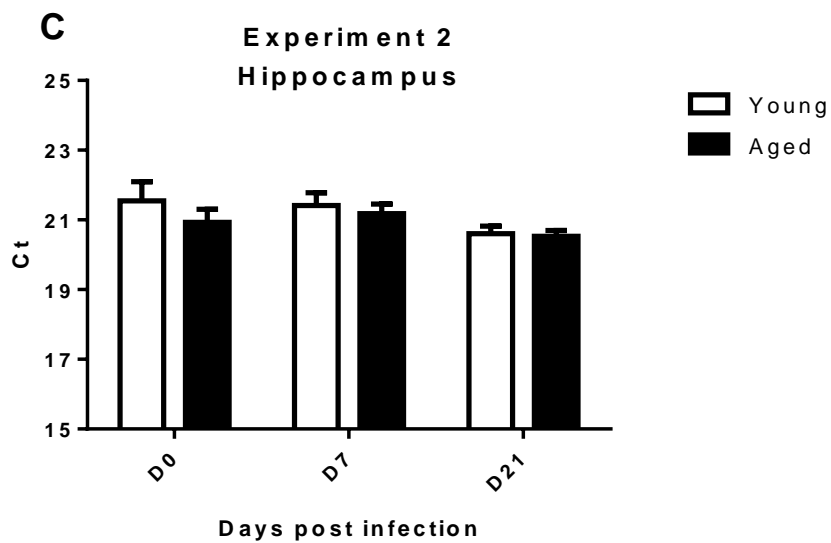
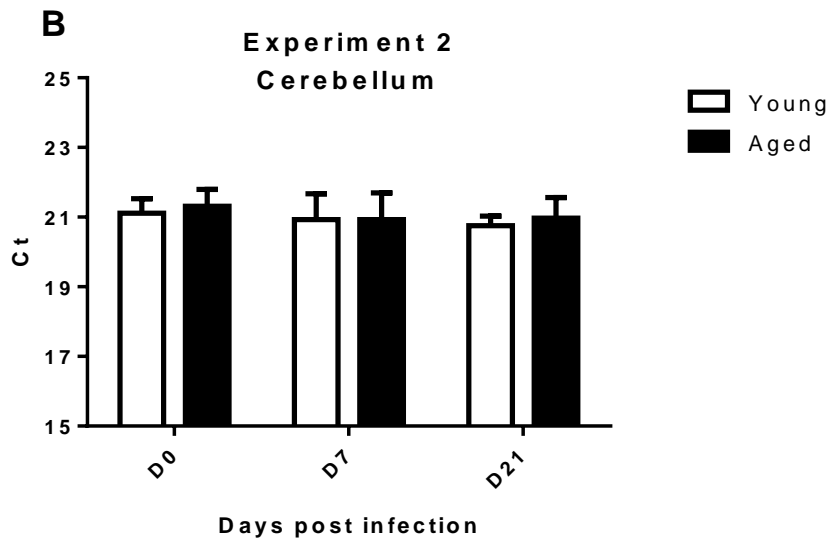
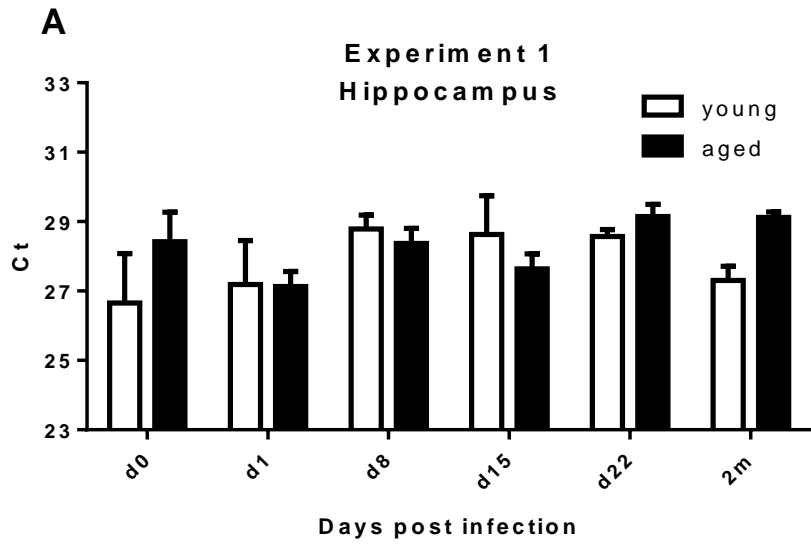


Figure 6.16. Representative images of CD11c expression in the CNS of young or aged mice following *S. typhimurium* infection. Images were

captured at x40 magnification. The blue staining is a haematoxylin nuclear counterstain, brown staining is for CD11c. The scale bar represents 50µm.

### **6.3.3 The effect of *S. typhimurium* infection on production of pro-inflammatory molecules in the young and aged CNS**

Hippocampal punches collected from experiment 1 were used to measure expression of several cytokines by qPCR. The reference gene used in Chapter 4, GAPDH, produced melting curves with multiple peaks instead of one single peak when tested using samples collected from mice in experiment 1, indicating the potential presence of multiple amplicons. Therefore a new reference gene was identified and characterised. PGK1 has been suggested to be a more stable reference gene for ageing studies compared to several other genes such as GAPDH and beta actin (Boda et al., 2009) and was therefore selected for use in this chapter as a reference gene. PGK1 expression was not altered by ageing or *S. typhimurium* infection in either experiment 1 or experiment 2 (Figure 6.17).



### Figure 6.17. Characterisation of PGK1 as a reference gene for qPCR.

There was no significant difference between groups in Holm-Sidak post tests. Data is shown as mean  $\pm$  SEM.

Expression of transcripts for several inflammatory molecules was determined in hippocampal punches from experiment 1 using qPCR (Figure 6.18). *S. typhimurium* infection had an overall statistically significant effect on IL-1 $\beta$  expression, although there was no effect of age or age x infection interaction. In young mice, an approximately 2 fold increase in IL-1 $\beta$  transcript was observed from day 1, and remained elevated up to 22 days after infection. In aged mice IL-1 $\beta$  was increased at day 22 after infection only. IFN $\beta$  also showed a trend towards increased expression during infection, although this was not significant, but a significant effect of age on IFN $\beta$  expression was observed. Brain derived neurotrophic factor (BDNF) expression was significantly decreased by ageing and infection and there was a significant interaction between age and infection. Aged mice expressed significantly less BDNF transcript before infection and during infection showed a much greater reduction in BDNF expression than young mice, with the exception of the 22 day time-point where expression was similar to that of saline treated mice. *S. typhimurium* infection and ageing did not significantly alter expression of COX-1, COX-2 or TNF $\alpha$ . TNF $\alpha$  measurements were also confounded by the lack of detectable transcript in some samples. The statistical analysis of these genes are summarised in table 6.7.

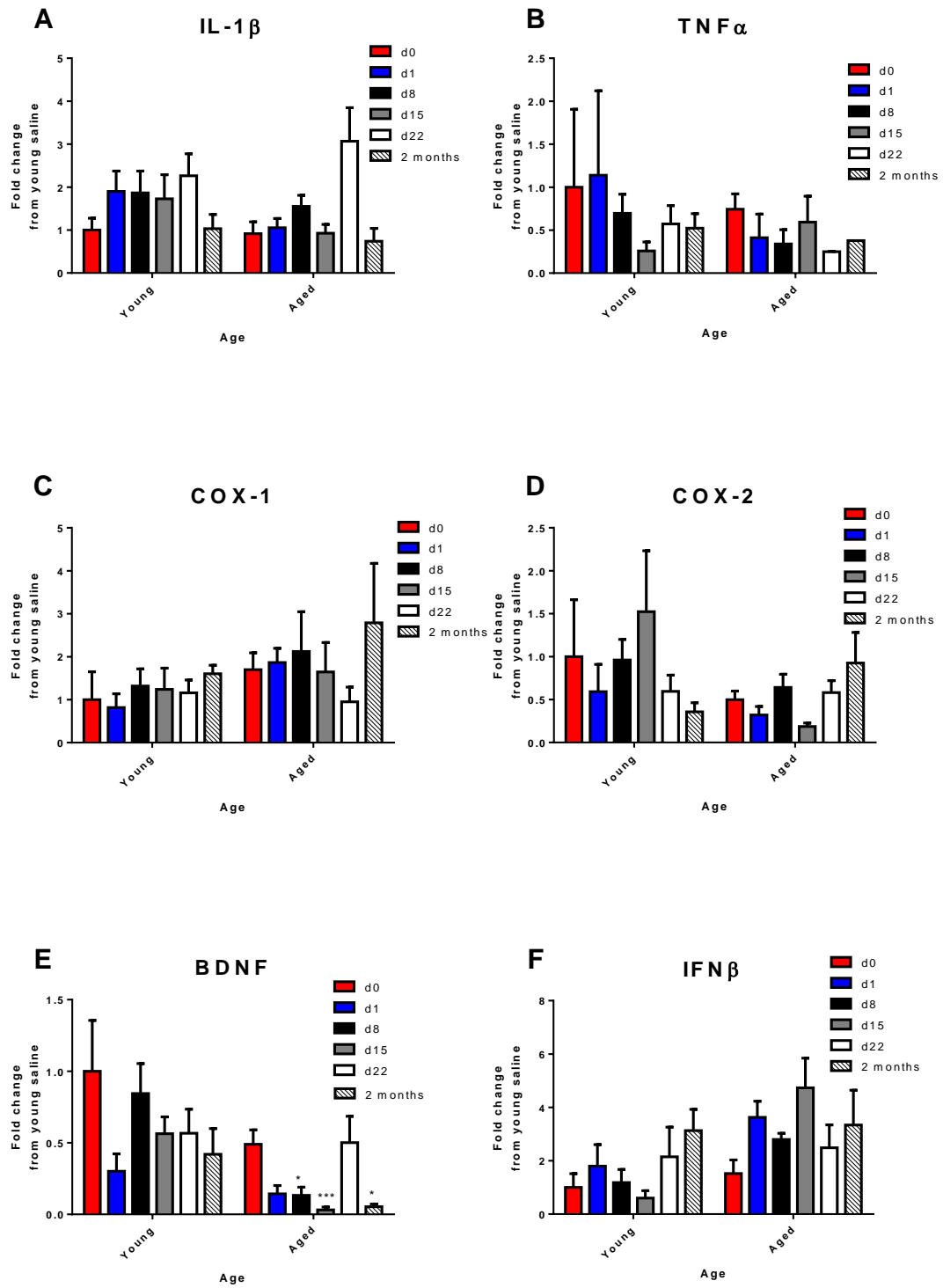


**Figure 6.18.** The effect of *S. typhimurium* infection on expression of pro-inflammatory molecules in the young and aged hippocampus.

Expression of IL-1 $\beta$  (A), TNF $\alpha$  (B), COX-1 (C), COX-2 (D), BDNF (E) and IFN $\beta$  (F) was determined by qPCR. Data is shown as mean  $\pm$  SEM. \* denotes  $p < 0.05$ , \*\*  $p < 0.01$ , \*\*\*  $p < 0.001$  (Holm-Sidak post test).

Gene	Age	Infection	Age x Infection
IL-1 $\beta$	F (1, 54) = 1.083	F (5, 54) = 4.226	F (5, 54) = 0.3446
	P = 0.3027	P = 0.0026	P = 0.8835
TNF $\alpha$	F (1, 37) = 0.3568	F (5, 37) = 0.1539	F (5, 37) = 1.139
	P = 0.5539	P = 0.9775	P = 0.3572
COX-1	F (1, 53) = 2.428	F (5, 53) = 0.7715	F (5, 53) = 1.704
	P = 0.1251	P = 0.5745	P = 0.1498
COX-2	F (1, 53) = 0.05589	F (5, 53) = 1.116	F (5, 53) = 1.488
	P = 0.8140	P = 0.3630	P = 0.2095
BDNF	F (1, 53) = 34.14	F (5, 53) = 5.492	F (5, 53) = 3.530
	P < 0.0001	P = 0.0004	P = 0.0079
IFN $\beta$	F (1, 54) = 17.13	F (5, 54) = 1.523	F (5, 54) = 1.669
	P = 0.0001	P = 0.1982	P = 0.1579

**Table 6.7. Statistical results of analysis of qPCR data from young or aged cerebellum or hippocampus after *S. typhimurium* infection (experiment 1).**

Data was logarithmic transformed to achieve normality and then analysed using two way ANOVAs.

A second experiment (experiment 2) was conducted to investigate potential regional differences in the CNS inflammatory response to *S. typhimurium* infection by comparing cytokine responses in the hippocampus to those in the cerebellum. The inflammatory response in the hippocampus was marked by an increase in IL-1 $\beta$ , IL-6 and TNF $\alpha$  expression 7 days after infection, but not 21 days after infection (Figure 6.19). The overall effect of *S. typhimurium* infection was significant for these three cytokines. There was also a significant effect of age on expression of these cytokines, although there was no age x infection interaction. COX-2 expression was increased in young but not aged infected mice, although there was only a non-significant trend towards an interaction between infection and age. The effect of *S. typhimurium* infection on inflammatory mediator expression was also investigated in the cerebellum (Figure 6.20). *S. typhimurium* infection did not significantly increase expression of IL-1 $\beta$ , IL-6, TNF $\alpha$  or COX-2 in the cerebellum. There was also no significant effect of age or age x infection interaction on expression of any of these transcripts. Table 6.8 contains the statistical analysis of the fold increase from young saline treated tissue.

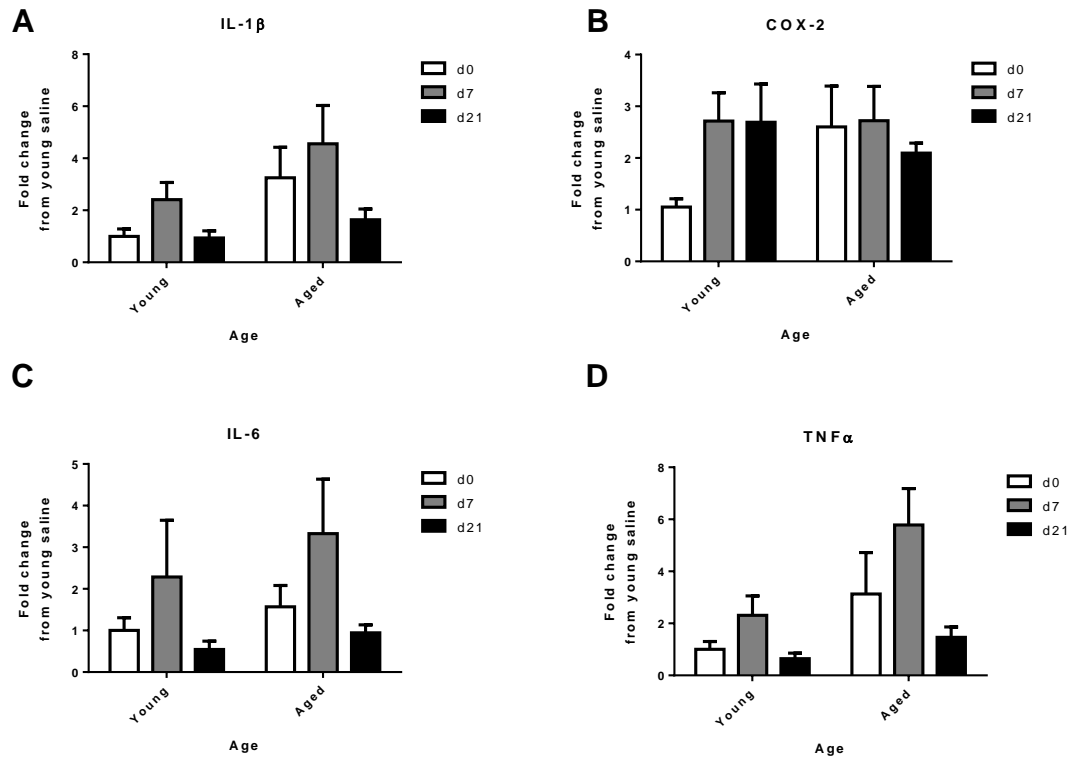


**Figure 6.19. The effect of *S. typhimurium* infection on expression of pro-inflammatory molecules in the young and aged hippocampus.**

Expression of IL-1 $\beta$  (A), COX-2 (B), IL-6 (C) and TNF $\alpha$  (D) was determined by qPCR. There was no significant difference between groups in Holm-Sidak post tests. Data is shown as mean  $\pm$  SEM.

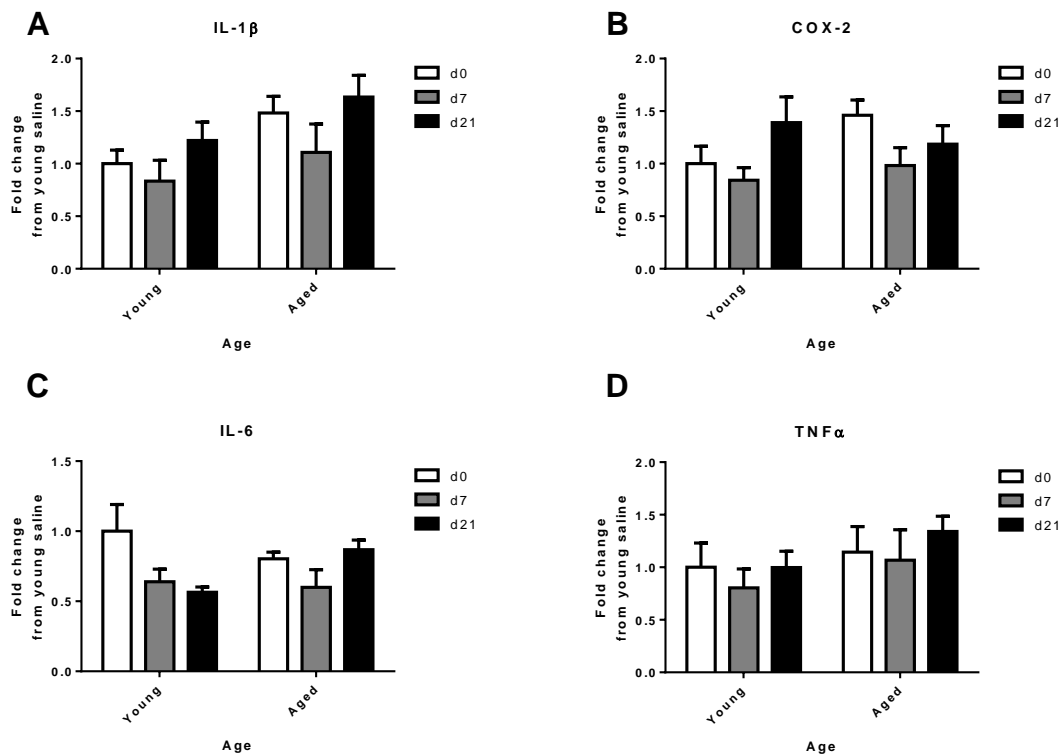


**Figure 6.20.** The effect of *S. typhimurium* infection on expression of pro-inflammatory molecules in the young and aged cerebellum.

Expression of IL-1 $\beta$  (A), COX-2 (B), IL-6 (C) and TNF $\alpha$  (D) was determined by qPCR. There was no significant difference between groups in Holm-Sidak post tests. Data is shown as mean  $\pm$  SEM.

Region	Cerebellum			Hippocampus		
	Age	Infection	Age x Infection	Age	Infection	Age x Infection
IL-1 $\beta$ n = 5-6	F (1, 27) = 3.943	F (2, 27) = 3.182	F (2, 27) = 0.1198	F (1, 28) = 9.687	F (2, 28) = 4.573	F (2, 28) = 0.3716
	P = 0.0573	P = 0.0589	P = 0.8875	P = 0.0042	P = 0.0191	P = 0.6930
IL-6 n = 5-6	F (1, 28) = 0.02315	F (2, 28) = 2.321	F (2, 28) = 1.451	F (1, 28) = 5.927	F (2, 28) = 4.230	F (2, 28) = 0.08335
	P = 0.8802	P = 0.1168	P = 0.2513	P = 0.0215	P = 0.0248	P = 0.9203
TNF $\alpha$ n = 5-6	F (1, 28) = 0.7241	F (2, 28) = 1.229	F (2, 28) = 0.1429	F (1, 28) = 11.80	F (2, 28) = 6.799	F (2, 28) = 0.05623
	P = 0.4020	P = 0.3078	P = 0.8675	P = 0.0019	P = 0.0039	P = 0.9454
COX-2 n = 5-6	F (1, 28) = 0.8678	F (2, 28) = 2.084	F (2, 28) = 0.9978	F (1, 28) = 1.558	F (2, 28) = 3.079	F (2, 28) = 2.826

	P = 0.3595	P = 0.1434	P = 0.3814	P = 0.2223	P = 0.0618	P = 0.0762
--	------------	------------	------------	------------	------------	------------

**Table 6.8. Statistical results of analysis of qPCR data from young or aged cerebellum or hippocampus after *S. typhimurium* infection (experiment 2).**

Data was logarithmic transformed to achieve normality and then analysed using two way ANOVAs.

## 6.4 Discussion

### 6.4.1 The peripheral cytokine response to *S. typhimurium*

The systemic cytokine response to *S. typhimurium* infection was similar between young and aged mice, peaking at day 8 after infection. Previous studies have shown similar kinetics of the circulating cytokine response to that reported here, with a cytokine response peaking at 1 week after infection in which IFN $\gamma$  is the most responsive cytokine measured (Püntener et al., 2012), despite the use of a lower dose of *S. typhimurium* in the experiments described in this chapter. Cytokines which play an important role in immune to brain communication such as IL-1 $\beta$ , IL-6 or TNF $\alpha$  were also upregulated at 8 days after infection, but this elevation was much less pronounced by 15 days after infection. The lack of difference between the peripheral cytokine responses of young and aged mice suggest that any differences observed between microglia or the central cytokine responses infection of young or aged mice is due to differences in the responsiveness of the CNS compartment rather than age related changes in the peripheral immune response.

### 6.4.2 Regional differences in the effects of ageing on microglial phenotype.

Ageing caused an increase in expression of the five microglial activation markers investigated, CD11b, CD68, F4/80, Fc $\gamma$ RI and CD11c. These changes tended to be more pronounced in white matter areas and more caudal areas of the CNS, which is in agreement with data from chapter 4. One difference between the data in this chapter compared to that in chapter 4 is the use of spinal cord instead of striatum. The spinal cord was selected because few age related changes in microglia in the striatum were detected in chapter 4 and the

spinal cord is more caudal to the cerebellum, providing an opportunity to investigate further the evidence of a rostral to caudal gradient. Age related changes in CD11b, CD68, CD11c and FcγRI expression were less pronounced in spinal cord areas than in the cerebellum - only changes in F4/80 expression were similar in magnitude between the two regions. This suggests that there is not a straight forward, linear rostral to caudal gradient in microglial reactivity to ageing. The white matter and nuclei of the cerebellum were generally the areas with the greatest increase in expression of microglial activation markers, while the microglia of the dentate gyrus and CA1 of the hippocampus showed the smallest changes. The reason why the white matter and mixed grey/white matter areas of the cerebellum are more susceptible to age related changes in microglial phenotype is not immediately clear, but could relate to the loss of Purkinje neurons (Woodruff-Pak et al., 2010), their axonal projections through cerebellar white matter and the concomitant demyelination that would accompany neuronal and axonal loss.

#### **6.4.3 The effects of *S. typhimurium* infection on microglial phenotype in the young and aged CNS.**

When *S. typhimurium* had an effect on expression of CD11b, CD68, F4/80, FcγRI and CD11c it was generally to cause a progressive and sustained increase in expression of these markers. The effects of *S. typhimurium* on microglial phenotype were highly variable within groups, possibly reflecting the success of different mice within groups in resisting *S. typhimurium* infection and the strength of their immune response.

Increases in expression of CD11b were detectable in all the CNS regions studied, with a greater fold increase observed in young mice than aged mice, contrary to expectations. This may be due to the increased basal expression of CD11b in the aged CNS and an inherent limitation of quantification by percentage above threshold, where if there is a very strong signal one will observe a “ceiling effect” where the stained epitope is maximally detected using that threshold setting. CD11b is constitutively expressed in resting microglia at levels high enough to detect by immunohistochemistry, so fold increases in CD11b expression detected by threshold analysis are usually indicative of increases in intensity of staining of microglia rather than detection of previously unstained microglial cells. CD11b expression has been shown

previously to be sensitive to peripheral LPS challenge (Buttini et al., 1996) and whatever causes this increase in CD11b expression appears to do so universally.

CD68 expression was more increased in aged than in young mice following *S. typhimurium* infection, with the most pronounced changes detected in the spinal cord grey and white matter. CD68 expression in the spinal cord of aged saline injected mice was typically localised around blood vessels, whereas following *S. typhimurium* infection CD68 was clearly also detectable in parenchymal microglia. Increases in expression were also present during infection in more rostral areas of the aged CNS such as the hippocampus, but they were smaller and highly variable, making it difficult to state conclusively whether *S. typhimurium* infection increases CD68 expression in these brain areas. Increases in F4/80 and Fc $\gamma$ RI expression induced by *S. typhimurium* infection were also more pronounced in the young and aged spinal cord than other CNS areas. Fc $\gamma$ RI expression was also increased following infection in cerebellar white matter and nuclei and to a lesser degree in the hippocampus, while F4/80 expression was increased in other brain areas but not as clearly or consistently as in the grey and white matter of the spinal cord. CD11c expression was also increased in the aged spinal cord and in aged cerebellar white matter or nuclei, but less so in more rostral regions such as the alveus or corpus callosum where there was little expression of CD11c initially.

These data provide evidence for a rostral to caudal gradient of microglial reactivity to *S. typhimurium* infection in which the spinal cord is the region which demonstrates the most pronounced changes in microglial phenotype, particularly regarding CD68 expression. Other studies have shown that the spinal cord is more responsive to mechanical or inflammatory insult than forebrain regions such as the striatum, particularly the spinal white matter (Batchelor et al., 2008; Raghavendra et al., 2004; Schnell et al., 1999a; Schnell et al., 1999b). Blood brain barrier breakdown was also reportedly more pronounced in the spinal cord or brain stem following stereotaxic injection of IL-1 $\beta$  or TNF $\alpha$  (Schnell et al., 1999b).

It is not clear from these data whether the integrity of the BBB is compromised during *S. typhimurium* infection, but there is a substantial increase in expression of molecules such as ICAM, VCAM and MHCII on endothelial cells in

the hippocampus of *S. typhimurium* infected mice (Püntener et al., 2012). Increased BBB permeability has also been reported following systemic inflammation induced by an i.p. injection of 100µg/kg LPS. This increase in BBB permeability was more pronounced in the spinal cord than in the brain (Lu et al., 2009). Increased BBB permeability could lead to infiltration of blood components such as fibrinogen, which can induce stress or damage in neurons and glia and directly induce inflammatory responses in microglia by binding to CD11b, leading to increases in expression of iNOS and the activation marker Iba-1 (Davalos et al., 2012). Other blood components that could contribute to microglial activation and increase expression of microglial activation markers include IgG acting at Fc receptors (He et al., 2002; Lunnion et al., 2011; Teeling et al., 2012) or thrombin (Fujimoto et al., 2007; Weinstein et al., 2005). Fibrinogen can also contribute to demyelination and axonal loss (Davalos et al., 2012), which may explain the increase in CD11c expression observed during *S. typhimurium* infection. CD11c expression in macrophages is linked to lipid processing and microglial CD11c expression by the microglia of aged white matter tracts may be a result of increased myelin phagocytosis and breakdown, as discussed in chapter 4 (Cho et al., 2007; Gaultier et al., 2009).

Alternatively differential sensitivity to peripheral cytokines in different brain areas could underlie regional differences in changes in activation marker expression levels. One potential cause of such rostral caudal differences in sensitivity to systemic inflammation could be differences in expression of immunoregulatory molecules such as fractalkine, which is more highly expressed in rostral regions such as the hippocampus than caudal regions such as the cerebellum (Tarozzo et al., 2003), or CD200, which is more highly expressed in grey than white matter (Koning et al., 2009). Decreased expression of immunoregulatory molecules in specific regions could cause microglia in those regions to be more reactive to inflammatory stimuli.

#### **6.4.4 The CNS inflammatory response to *S. typhimurium* infection.**

The only previous report on the effect of *S. typhimurium* infection on production of inflammatory mediators in the CNS showed an increase in hippocampal IL-1β and IL-12 levels 21 days after infection (Püntener et al., 2012). In experiment 1 COX-1, COX-2 and TNFα levels were not altered by *S. typhimurium* infection, whereas IL-1β expression was slightly increased in

young mice and at day 22 in aged mice. IFN $\beta$  expression was also slightly elevated by infection, although this increase was not significant. In experiment 2 a different inflammatory response in the hippocampus was detected, with IL-1 $\beta$ , TNF $\alpha$  and IL-6 expression peaking at 1 week after infection and then returning to baseline. The increase in expression of IL-1 $\beta$ , TNF $\alpha$  and IL-6 was still only approximately two fold over hippocampus from age matched saline treated mice, and therefore comparable in size to the increase in IL-1 $\beta$  expression observed in experiment 1. Together these data show a mild inflammatory response in the hippocampus that peaks between 1-3 weeks after initial infection. This study used a low dose of *S. typhimurium* ( $3 \times 10^5$  CFU compared to  $1 \times 10^6$  CFU) due to excessive weight loss in aged mice caused by the use of the higher dose, and this may explain the small changes in cytokines observed in this study.

BDNF expression was decreased during *S. typhimurium* infection in experiment 1, and this decrease in BDNF expression was especially pronounced in aged mice. BDNF is a neurotrophic factor with roles in neuroplasticity, LTP and memory (Bramham and Messaoudi, 2005; Lu et al., 2005; Tyler et al., 2002). Decreases in BDNF expression in response to increased hippocampal IL-1 $\beta$  levels has been suggested to underlie memory deficits observed during *E. coli* infection in aged rats (Cortese et al., 2011) and a similar mechanism may occur during *S. typhimurium* infection. BDNF expression is increased by tasks that involve memory and learning such as the novel object recognition test (Goulart et al., 2010) and the mice used in this study were exposed to extensive behavioural testing as detailed in chapter 5 which could have affected BDNF expression. Ageing and infection have been shown to attenuate increases in BDNF expression caused by fear conditioning (a test of memory) in rats (Chapman et al., 2012). Whether the decreased expression of BDNF observed in these data reflects impaired induction of BDNF expression during learning or reduced basal expression of BDNF is not clear and requires further study.

In experiment 2 expression of IL-1 $\beta$ , TNF $\alpha$ , IL-6 and COX-2 was also measured in the cerebellum. However, no change in expression of these genes was detected in the young or aged cerebellum during *S. typhimurium* infection, in contrast to the hippocampus. This suggests that the regional differences observed in age related changes to microglial expression of proteins such as CD68 do not necessarily reflect enhanced cytokine production in response to

infection. It should be noted that the homogenised cerebellum sample will also contain a large amount of cerebellar cortex and therefore molecular layer, which was not as susceptible to age related changes in microglial phenotype as the cerebellar white matter tracts or cerebellar nuclei. In chapter 4 a smaller inflammatory response to LPS was present in the cerebellum than in the hippocampus, suggesting that it is not just *S. typhimurium* infection which elicits a smaller inflammatory response in the cerebellum than in the hippocampus. In contrast several studies have reported similar responsiveness of the cerebellum to i.p. or i.c.v. LPS challenge (Hansen et al., 2000b; Huang et al., 2008), although the mechanisms underlying the central inflammatory response elicited by *S. typhimurium* may differ from those elicited by systemic LPS injection.

#### **6.4.5 Summary**

These data show that young and aged mice have a similar systemic cytokine response to *S. typhimurium* infection and that there is a rostral caudal gradient of responsiveness of microglial expression of F4/80 and Fc $\gamma$ RI in the young and aged CNS and CD68 and CD11c in aged white matter. This rostral to caudal gradient in activation marker expression during *S. typhimurium* infection contrasts with analysis of pro-inflammatory mediator expression, where the hippocampus is more responsive to *S. typhimurium* infection than the cerebellum. The effect on hippocampal cytokine production was small but statistically significant, peaking at 1 week after infection. This cytokine response was not enhanced in aged mice, suggesting that the concept of age associated microglial priming might not be applicable to the inflammatory response generated by low grade systemic *S. typhimurium* infection.

## **7. The effect of systemic inflammation on the organisation of the paranodal junction in the spinal cord.**

### **7.1 Introduction**

Systemic infections exert a diverse range of effects on an organism's behaviour and ability to function. This can include effects on co-ordination and balance as shown in chapter 5, and comparatively mild infections such as upper respiratory tract infections can affect reaction time in both simple and more complex reaction time tasks (Bucks et al., 2008; Smith, 2013). The molecular basis underlying the broad range of effects exerted by infections on the CNS are not yet fully elucidated.

Evidence has emerged in the last decade of the vulnerability of paranodal junctions, the junction between the oligodendrocyte and the axon, to inflammatory conditions – particularly EAE and MS. In these diseases paranodal junctions elongate and the paranodal/juxtaparanodal compartmentalisation is compromised (Howell et al., 2006; Howell et al., 2010). It has been proposed that these changes in the paranodal junctions may be an early sign of demyelination and could disrupt or slow axonal conduction (Howell et al., 2006; Sherman et al., 2005). More recent work has demonstrated that systemic inflammation induced by subcutaneous injection of complete Freund's adjuvant (an emulsion of mycobacterium and mineral oil) and pertussis toxin is sufficient to cause a transient elongation of paranodal junctions and increased overlapping of paranodal/juxtaparanodal domains (Howell et al., 2010). Ageing has also been associated with changes in paranodal organisation, leading to elongated paranodal regions and overlap between paranodal and juxtaparanodal compartments (Hinman et al., 2006; Shepherd et al., 2010). The physiological relevance of dysfunction at the paranodal junction is clearly demonstrated by the effects of genetic deletion of any of the paranodal junction components – knocking out neurofascin 155, caspr or contactin leads to reduced conduction velocity, ataxia, axonal transport deficits, tremor and in the case of neurofascin 155 (Nfasc155) early death (Bhat et al., 2001; Boyle et al., 2001; Sherman et al., 2005).

There is no published data on the effect of systemic non-neurotropic infections on paranodal integrity. *S. typhimurium* infection evokes a prolonged systemic inflammatory response and a low grade but chronic central inflammatory response (chapter 6). The experiments in this chapter aimed to investigate whether *S. typhimurium* infection induces changes in paranodal morphology, particularly in aged mice, in which exaggerated central inflammatory reactions to systemic inflammatory challenges have previously been described (Godbout et al., 2005b). Disruption to paranodal junction integrity and subsequent changes in the efficiency of axonal conduction could contribute to some of the behavioural changes observed during *S. typhimurium* infection, particularly those that rely on reaction speed such as co-ordination and balance.

## 7.2 Materials and Methods

### 7.2.1 Complete Freund's adjuvant (CFA) experiment

4 month old female C57/BL6J mice were used in the CFA experiment. Mice from the CFA group (n = 4) were injected intraperitoneally with 200ng of pertussis toxin (PTX) in a volume of 200µL sterile saline on day 0, 1, 7 and 8 of the experiment. On day 0 of the experiment mice were injected with a 1:1 emulsion of complete Freund's adjuvant (BD Biosciences, Oxford, UK, catalogue number: 263810) and sterile saline. 200µL of this emulsion was subcutaneously injected into each flank of the mouse. On day 7 of the experiment mice were injected with a 1:1 emulsion of incomplete Freund's adjuvant (IFA) (BD Biosciences, Oxford, UK) and sterile saline. 200µL of this emulsion was subcutaneously injected into each flank of the mouse. Mice were culled 10 days after the first pertussis toxin injection. Saline injected mice (n = 5) were injected intraperitoneally with 200µL of saline on day 0, 1, 7 and 8. An additional control group of 3 mice were injected with pertussis toxin on day 0, 1, 7 and 8, but were not injected with CFA. This protocol was derived from Howell et al's protocol for CFA challenge (Howell et al., 2010), with the principle difference between the protocols being the use of incomplete instead of complete Freund's adjuvant on day 7 due to the terms of the Home Office licence used in this study. Figure 7.1 provides a schematic showing the schedule for the experiment. Body weights were recorded on a daily basis between 12.30-14.30.

Mice were deeply anaesthetised, perfused with heparinised saline and perfusion fixed with ice cold 4% PFA. The lumbar spinal cord was dissected out, post fixed in ice cold 4% PFA for 4-6 hours and left in 30% sucrose overnight. The tissue was then embedded in OCT and stored at -20°C.

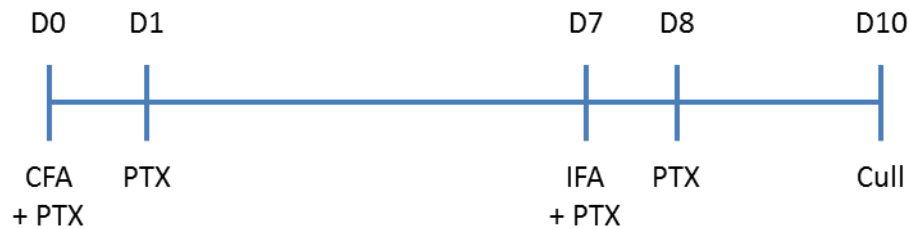


**Figure 7.1. A schematic showing the schedule for the CFA experiment.**

### 7.2.2 EAE experiment

EAE was induced in DBA mice using recombinant MOG, complete Freund's adjuvant and pertussis toxin. Tissue was kindly provided by Dr Karl Goodyear (University of Glasgow). Tissue was harvested at the peak of clinical symptoms, perfused with heparinised saline and embedded in OCT (i.e. tissue was fresh frozen). Tissue was screened for lesions by F4/80 staining, and two spinal cords were found to have prevalent F4/80 positive lesions and good enough quality tissue to use for immunohistochemical analysis.

### 7.2.3 *S. typhimurium* experiment

Tissue from mice infected with *S. typhimurium* for 8 or 22 days or injected with saline was collected from the mice described in experiment 1 of chapter 5. After perfusion with heparinised saline a portion of lumbar spinal cord was dissected out and post fixed in ice cold 4% PFA overnight (~16 hours). After fixation spinal cords were transferred to 30% sucrose for 24 hours and embedded in OCT. Perfusion fixation with 4% PFA was not carried out because of the use of other tissue from this experiment for analysis by qPCR or fresh frozen immunohistochemistry.

### 7.2.4 Immunofluorescence

Fresh frozen slides were dried and then immersed in ice cold 4% PFA for 20 minutes. Once tissue had been fixed in 4% PFA sections were post fixed in

Bouin's fixative (Appendix 1) for 30 seconds (if embedded fresh frozen) or 60 seconds (if embedded PFA fixed). The sections were then washed 3 x 1 minutes in PBS and enclosed using a wax pen.

Initial experiments using Nfasc155 antibodies in PFA fixed or fresh frozen tissue resulted in staining with very high background levels, so after advice from Dr Barbara Zonta (University of Edinburgh) a specific blocking protocol was adopted for stains using Nfasc155 antibodies. The blocking medium consisted of 5% gelatin, 0.2% triton, 1% BSA and 1% normal animal serum. All reagents were diluted in this block up until the counterstaining step of the protocol and all incubations were performed at approximately 30°C to prevent the gelatin in the blocking diluent from solidifying on the section, which occurs at temperatures under approximately 25°C.

The antibodies used in this chapter are listed in table 7.1. Primary antibodies were incubated overnight at 30°C in a tightly sealed humidified chamber. Secondary antibodies were incubated for 40 minutes, streptavidin (when used) for 30 minutes and DAPI/Hoeschst for 10 minutes. All washes were performed using 0.1% PBS-triton. Immunofluorescence was otherwise carried out as described in chapter 2.

Sections from EAE mice were stained using a mouse-on-mouse (M.O.M.) kit (Vector Laboratories, Peterborough, UK) to reduce background staining from endogenous mouse IgG. All steps were carried out as described above, with the addition of M.O.M. kit protein concentrate (1:13) to the blocking medium used throughout the experiment, M.O.M. Ig Blocking Reagent (1:28) to the blocking medium used during the blocking step and the secondary antibody used was the M.O.M. biotinylated anti-mouse IgG reagent (1:250).

The single SMI-32 stain used for quantification was performed using the M.O.M. kit without gelatin or triton as described above to obtain maximum staining intensity with minimal background or IgG staining.

### **7.2.5 Microscopy**

Epifluorescence images were captured using a Leica DM5000B microscope. Confocal stacks were captured using a Leica SP5 confocal microscope. Some of the representative images from confocal microscope images are maximal

projections – they are a 2D representation of the points of maximum intensity within that pixel's Z plane. The individual figure legends indicate how each image was captured. All pictures taken were of the lateral white matter tracts of the ventral spinal cord.

### 7.2.6 Quantitative analysis

All analysis was carried out using Volocity software (version 6.1.1 - PerkinElmer, Waltham, USA). Automated protocols were used to identify individual paranodes based on staining intensity for Nfasc155 and morphological characteristics. The skeletal length of each paranode was estimated using the same automated protocols. The skeletal length value provides a measurement of paranodal length in three dimensions (X, Y and Z) and is capable of accounting for shape differences between different paranodes. The accuracy of each skeletal length measurement was confirmed by visually inspecting each individual paranodal skeleton and comparing it to the morphology of the paranode. An example is provided in figure 7.2. The skeletal lengths of the first 20 clearly identifiable paranodes per confocal stack were recorded for three confocal stacks per section. All quantifications of material from *S. typhimurium* or CFA experiments were performed blinded to sample identity.

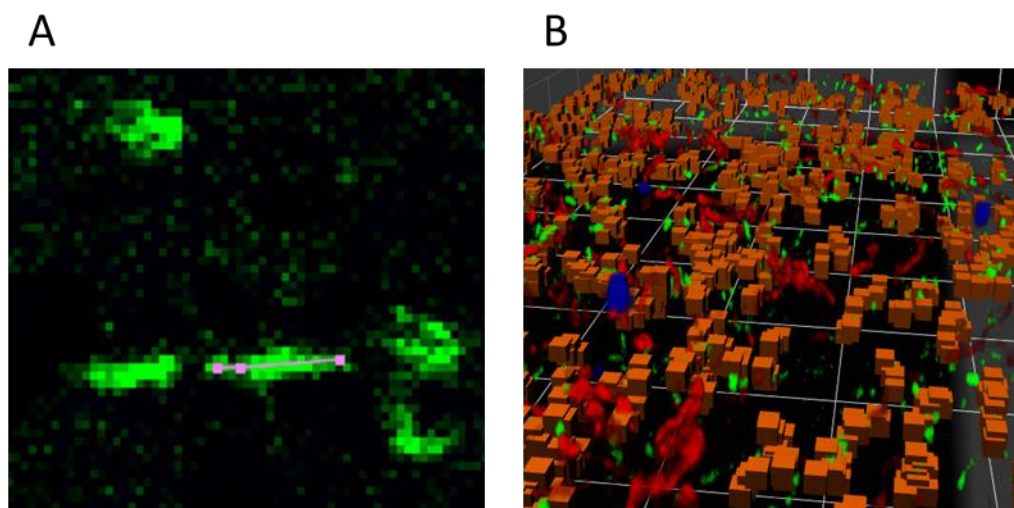


**Figure 7.2. An example demonstrating how skeletal lengths are obtained using Volocity software.**

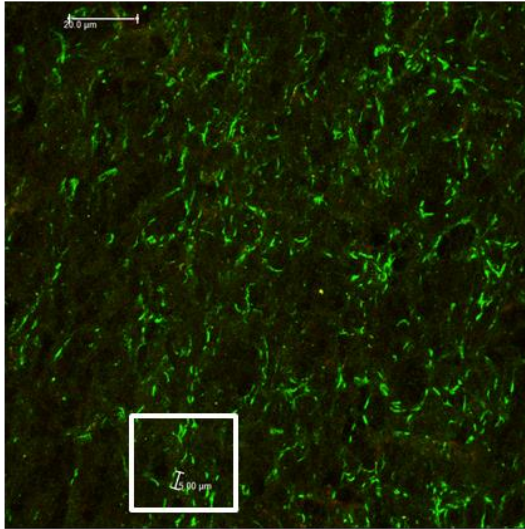
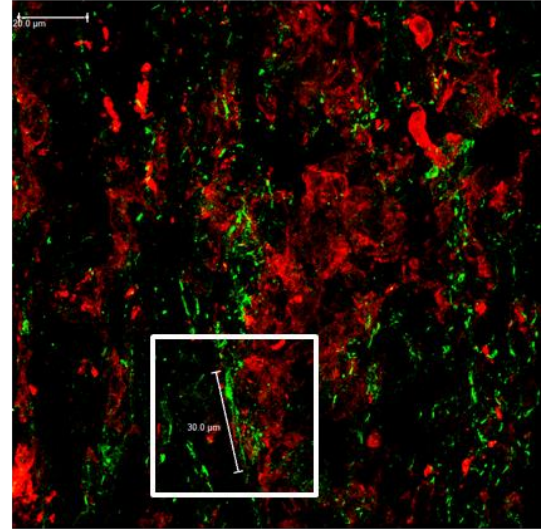
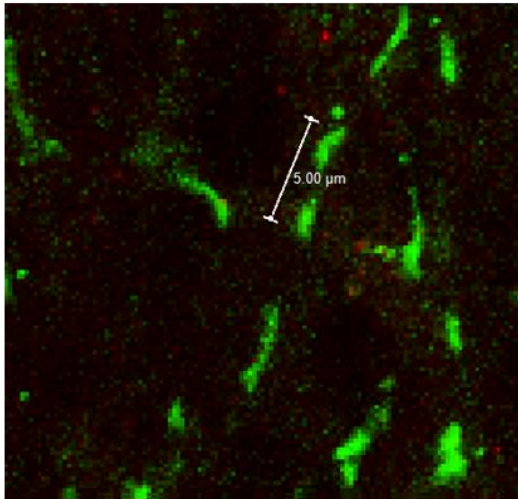
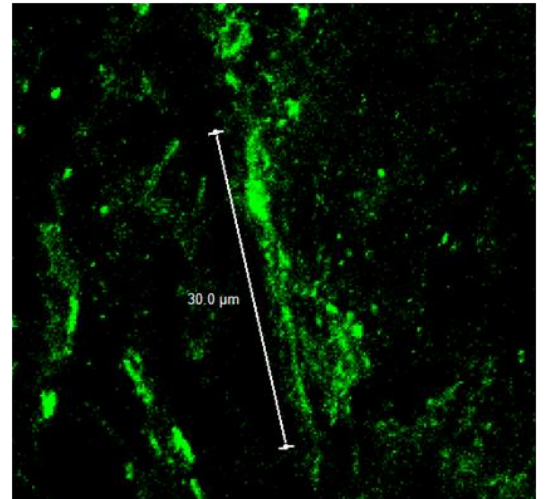
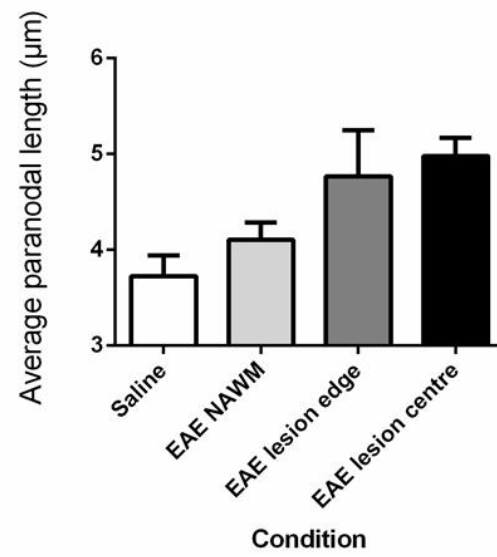
(A) A skeletal length drawn through X, Y and Z planes to map the longest length through the Nfasc155 (green) positive paranode. The purple line represents the skeletal length and the boxes mark changes in the direction of the line. (B) A 3D representation of a confocal stack after identification of Nfasc155 (green) positive paranodes and estimation of their skeletal length. The red staining is for SMI-32 reactive axons and the blue staining is for DAPI stained nuclei.

For EAE sections the 3 categories of normal appearing white matter (NAWM), lesion edge and lesion centre were determined by the extent of F4/80 staining. Intense F4/80 staining of many closely associated cells was taken to indicate the presence of a lesion. In such areas of intense F4/80 staining there was dramatically reduced Nfasc155 staining, indicating the occurrence of demyelination (Howell et al., 2006). NAWM areas were defined as white matter tracts which did not contain a lesion edge or centre within the captured field.

## 7.3 Results

### 7.3.1 EAE experiment

To establish the effects of CNS inflammation on paranodal integrity and to validate the quantification protocols developed in Volocity software, fresh frozen spinal cords from saline treated mice ( $n = 3$ ) or mice that had developed clinical symptoms of EAE following MOG immunisation ( $n = 2$ ) were stained for F4/80, Nfasc155, Kv1.2 or SMI-32. In EAE spinal cords F4/80 reactivity was significantly increased (Figure 7.3 B) compared to saline treated mice (Figure 7.3 A). Paranodal staining was reduced in the vicinity of EAE lesions compared to saline treated mice (Figure 7.3 A & B). Individual paranodes were longer in length and staining was less evenly distributed throughout paranodes (Figure 7.3 D) compared to paranodes from saline treated mice (Figure 7.3 C). Quantification of paranodal length in EAE tissue showed a trend towards increasing paranodal length in EAE NAWM (mean length:  $4.11\mu\text{m}$ ) compared to saline injected mice ( $3.72\mu\text{m}$ ), and further increases in paranodal length at the edge ( $4.77\mu\text{m}$ ) or centre ( $4.98\mu\text{m}$ ) of lesions (Figure 7.3 E).

**A****B****C****D****E**

### **Figure 7.3. The effect of EAE on paranodal integrity.**

Images A and C show tissue from a young saline treated mouse spinal cord stained for F4/80 (red) and Nfasc155 (green). The lack of F4/80 staining is evidence of a resting microglial phenotype without substantial infiltration of cells. Images B and D show tissue from a mouse with EAE. There is widespread F4/80 staining on individual microglia/macrophages and in focal areas of the spinal cord. Paranodes stained with Nfasc155 near areas of intense F4/80 staining are longer in length and are not as evenly stained (**D**) as paranodes from saline treated mice (**C**). Images A and B are maximum projections from confocal stacks captured at x100 magnification on a Leica SP5 microscope. C and D are magnifications of the parts of A & B respectively marked by white boxes and only show Nfasc155 staining. Scale bars are 20 $\mu$ m in length. Paranodal (Nfasc155+) length was quantified from confocal images of mice with EAE or mice injected with saline (**E**) (n = 2-3 per group). Columns represent mean  $\pm$ SEM.

Antibodies against SMI-32 label non-phosphorylated neurofilaments in axons, which have previously been described as a marker of damaged or stressed axons in EAE (Trapp et al., 1998). In the vicinity of presumed lesions (determined by the high density of DAPI stained nuclei and absence of Nfasc155 staining) (Figure 7.4 A) SMI-32 reactivity was increased compared to normal appearing white matter (Figure 7.4 B). Antibodies against Kv1.2 clearly stained juxtaparanodal regions in saline treated mice (Figure 7.4 D), but attempts to stain for Kv1.2 in EAE spinal cord were unsuccessful due to high background, probably caused by the presence of endogenous IgG (Figure 7.4 C).

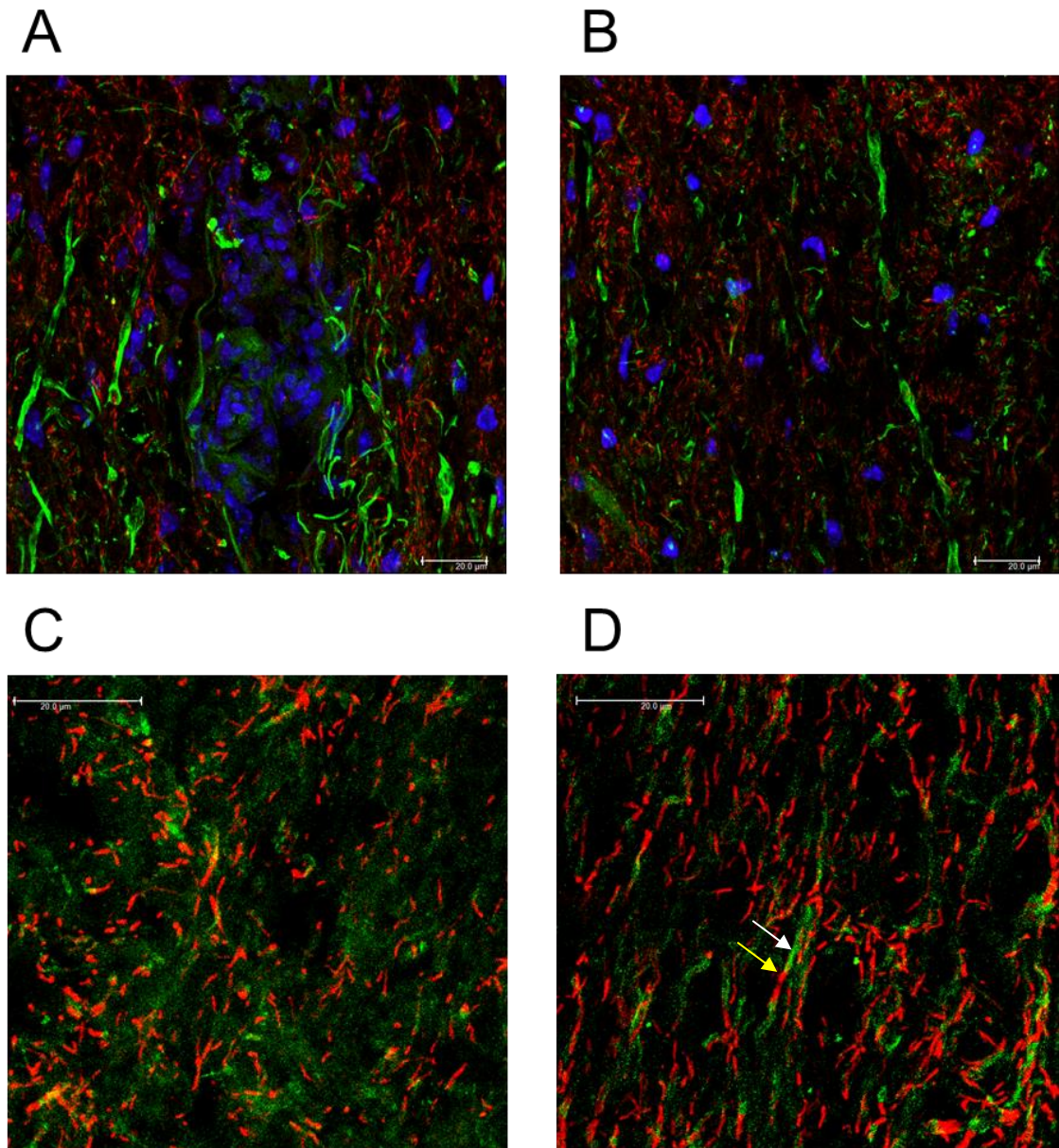


**Figure 7.4. The effect of EAE on paranodal length and SMI-32 reactivity.**

**A-B** Paranodes are stained for Nfasc155 in red, damaged axons are stained for SMI-32 in green, nuclei are stained blue with DAPI. **(A)** Axons in the vicinity of a presumed lesion (identified by the increased density of nuclei and absence of Nfasc155 staining) stain positively for SMI-32 more frequently than in normal appearing white matter **(B)**, where most paranodes are not associated with SMI-32 positive axons. Images are maximum projections from confocal stacks captured at x100 magnification on a Leica SP5 microscope. **C-D** Paranodes are stained for Nfasc155 in red, juxtaparanodal regions are stained for Kv1.2 in green. Kv1.2 staining was not discernible from background staining in tissue

from EAE treated mice (C), whereas in tissue from saline treated mice Kv1.2 staining localises to the juxtapanode (white arrow) flanking paranodal regions (yellow arrow) (D). Images are maximum projections from confocal stacks captured at x100 magnification on a Leica SP5 microscope and magnified x2. Scale bars are 20µm in length. n = 2-3 per group.

### 7.3.2 CFA experiment

The next experiment undertaken investigated the effect of a subcutaneous CFA challenge accompanied by pertussis toxin injections on paranodal integrity. This protocol was designed to be as similar as possible to the protocol used by Howell et al's 2010 study (Howell et al., 2010) in which they showed significant lengthening of paranodes 10 days after CFA injection. Mice were either given subcutaneous injections of CFA followed by IFA accompanied by pertussis toxin injections, pertussis toxin alone or saline alone. Pertussis toxin injection alone and pertussis toxin with CFA/IFA caused an increase in weight across the course of the experiment (two way repeated measures ANOVA: time x treatment:  $F_{18,90} = 8.778$ ,  $p = 0.001$ ) (Figure 7.5 E). Mice of the same age injected with saline did not change in weight over the same time period.

Mice were perfusion fixed 10 days after the initial CFA injection with 4% PFA and spinal cords were stained for Kv1.2 (green) and Nfasc155 (red). Paranodal (Nfasc155 positive) and juxtapanodal (Kv1.2 positive) domains of the axon did not appear to be significantly altered by CFA injection compared to saline injected animals and co-localisation did not increase following CFA injection (Figure 7.5 A-D). Quantification of paranodal length showed that there was no significant increase in paranodal length 10 days after the CFA injection (mean length: 4.42µm) compared to saline injected mice (mean length: 4.36µm) (student's t test:  $t_{(6)} = 0.379$ ,  $p = 0.717$ ) (Figure 7.5 F).

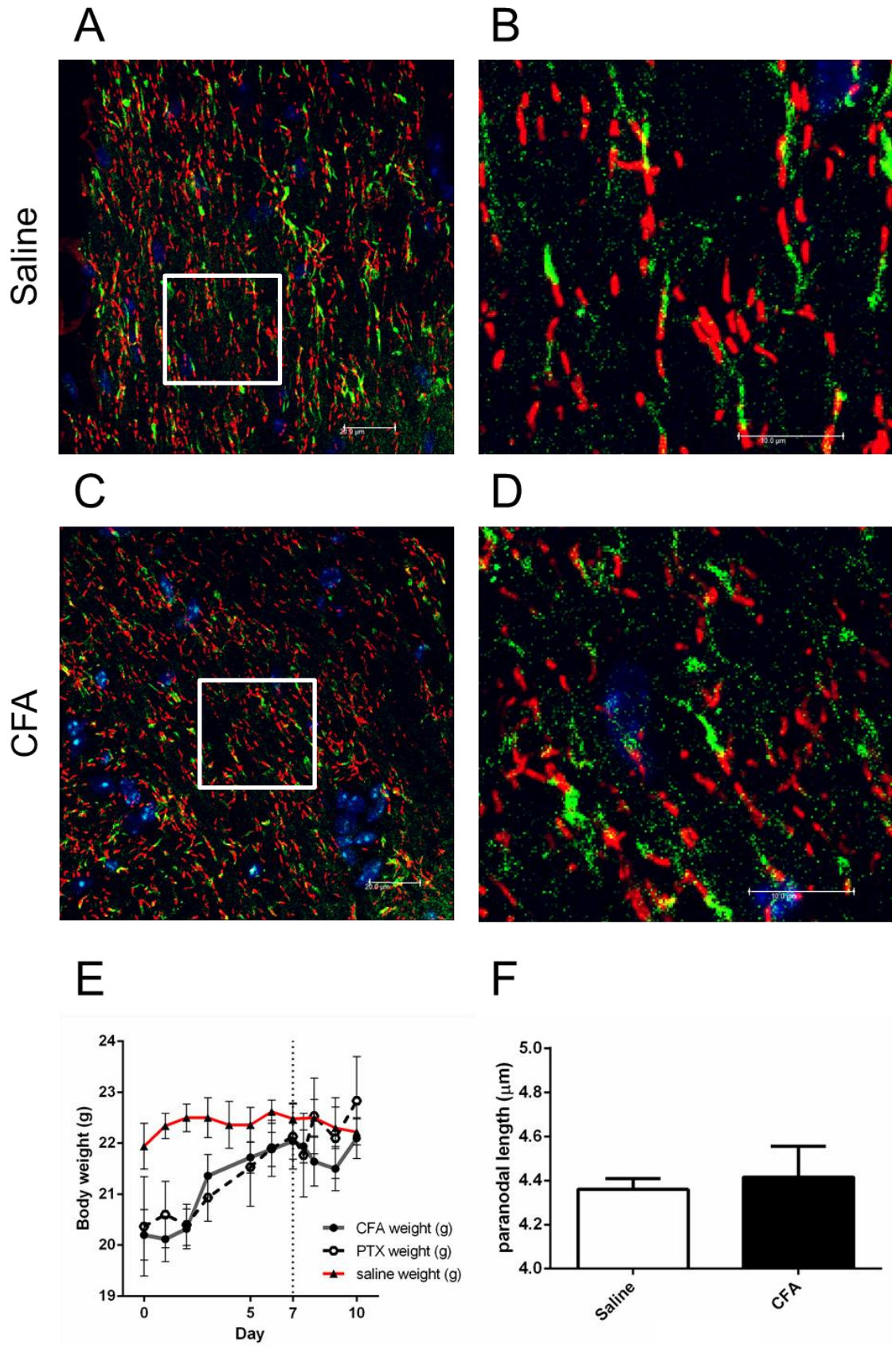


Figure 7.5. The effects of CFA and PTX injection on paranodal length and paranodal/juxtaparanodal compartmentalisation.

Paranodes are stained for Nfasc155 in red, juxtaparanodes are stained for Kv1.2 in green and nuclei are stained blue with DAPI. Both saline treated (A, B) and CFA treated (C, D) mice had strongly stained neurofascin 155 positive paranodes (red) of approximately 4-5µm size. Some of these paranodes were flanked by Kv1.2 (green) positive juxtaparanodes. There was no co-localisation of Kv1.2 and Nfasc155, indicating that there is efficient compartmentalisation of the paranodal and juxtaparanodal compartments. Injection of PTX alone or PTX + CFA induced weight gain in the days following injection, whereas saline did not (E). CFA challenge did not cause any significant increase in mean paranodal length compared to saline challenge (n = 4-5 per group) (F). B & D are x2 magnifications of the parts of A & C respectively indicated by white boxes. Paranodal length was analysed by two tailed student's t test. Images are maximum projections from confocal stacks captured at x100 magnification on a Leica SP5 microscope. Scale bars are 20µm in length in A and C and 10µm in length in B and D.

### 7.3.3 *S. typhimurium* experiment

To examine whether *S. typhimurium* infection had any effect on the paranodal junctions of young or aged mice, spinal cords from mice injected with saline or infected with *S. typhimurium* for 8 or 22 days were post fixed in 4% PFA and stained for SMI-32 and Nfasc155. Initial examination of confocal images did not reveal pronounced differences in paranodal morphology as a result of ageing or *S. typhimurium* infection (Figure 7.6 A-F). Quantification of paranodal length showed that in SMI-32 negative axons (Figure 7.7 A) there was not a significant effect of *S. typhimurium* on paranodal length (two way ANOVA:  $F_{2,27} = 3.313$ ,  $p = 0.0517$ ), but that ageing did have a small effect on paranodal length ( $F_{1,27} = 9.448$ ,  $p = 0.0048$ ). There was no interaction between ageing and *S. typhimurium* infection ( $F_{2,27} = 0.561$ ,  $p = 0.5772$ ).

Quantification of paranodal length in SMI-32 positive axons (Figure 7.7 B) revealed a significant effect of *S. typhimurium* infection which, contrary to expectation, decreased the mean length of paranodes (two way ANOVA:  $F_{2,24} = 7.875$ ,  $p = 0.0023$ ). Age had no effect on paranodal length in SMI-32 positive axons ( $F_{1,24} = 0.00032$ ,  $p = 0.9859$ ) and there was no interaction between age and infection ( $F_{2,24} = 0.03434$ ,  $p = 0.9663$ ).

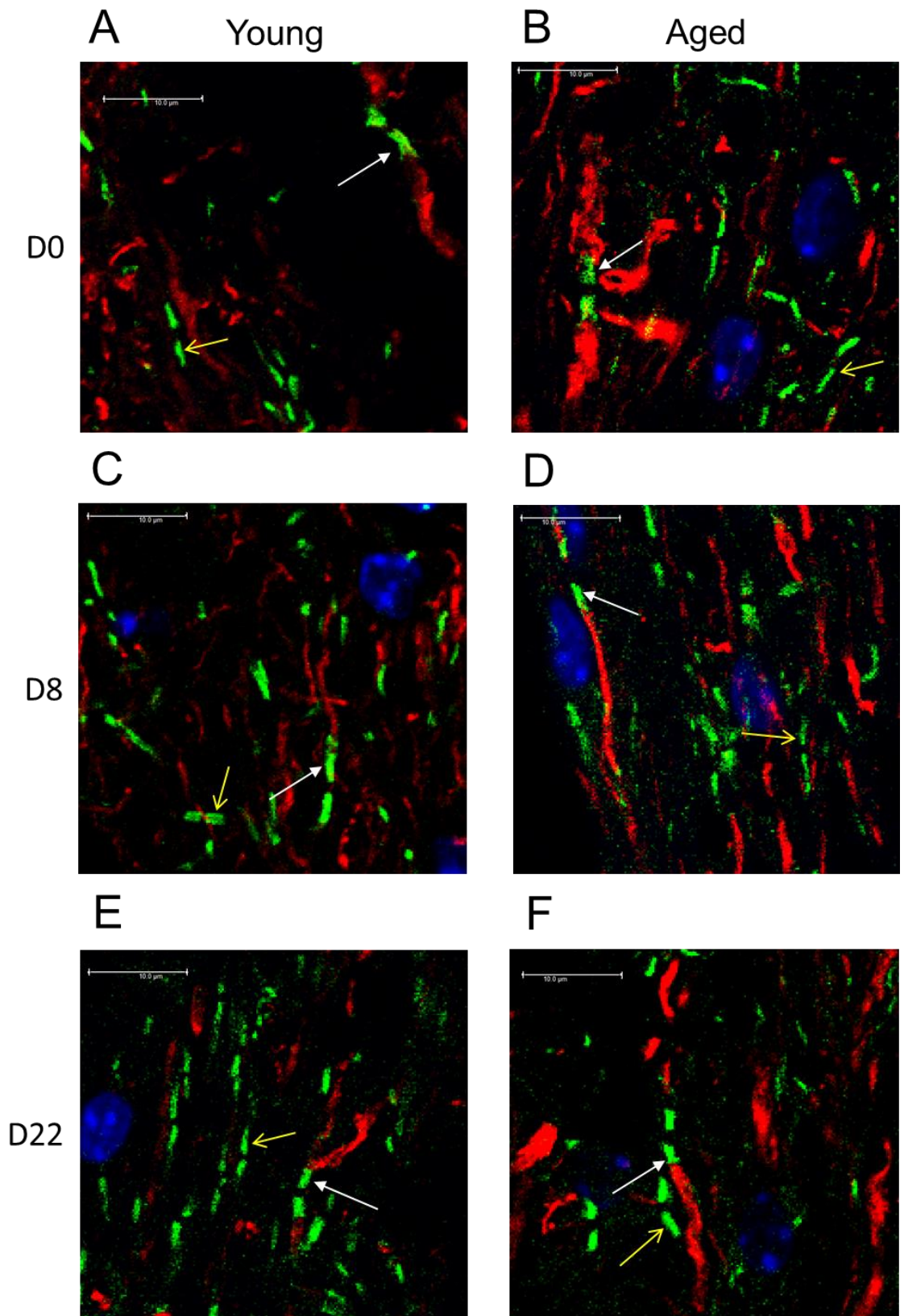
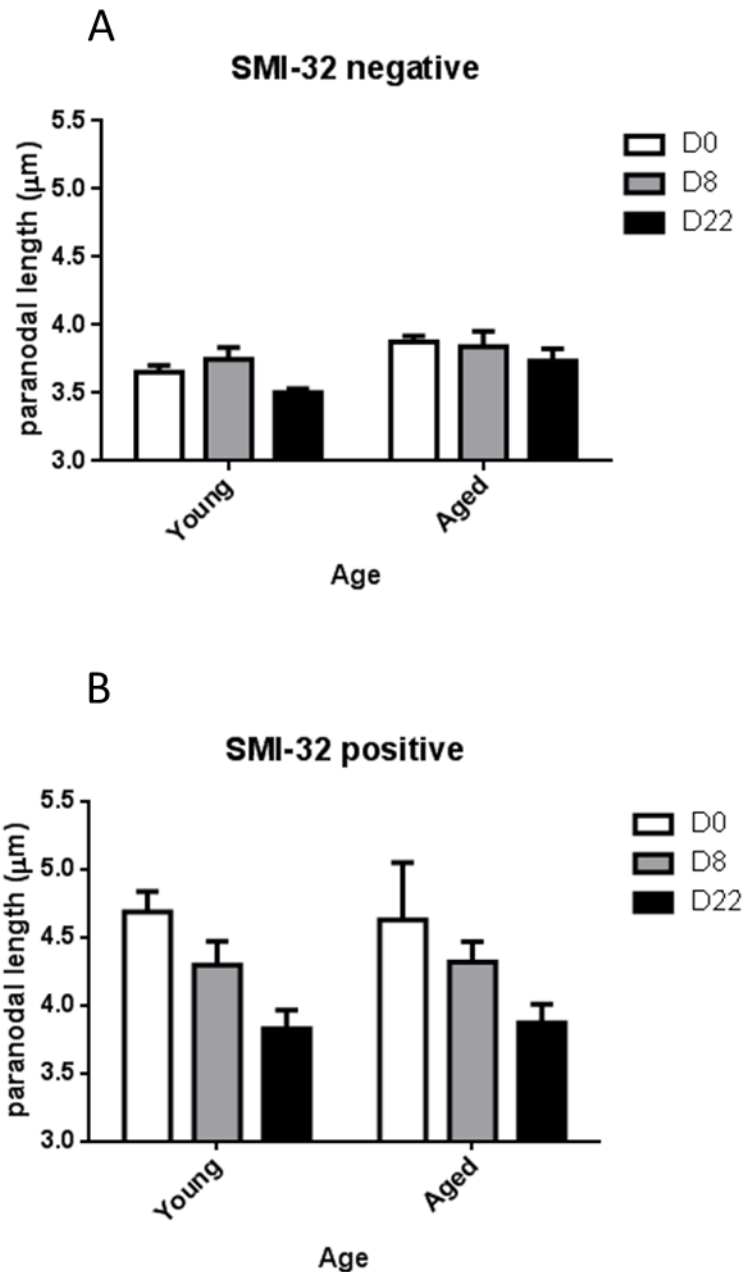


Figure 7.6. The effect of *S. typhimurium* infection on paranodal integrity in SMI-32 negative and positive axons of young and aged mice.

Paranodes are stained for Nfasc155 in green, damaged axons are stained for SMI-32 in red, nuclei are stained blue with DAPI. Examples of SMI-32 positive paranodes are indicated by white arrows with closed heads and SMI-32 negative paranodes are indicated by yellow arrows with open heads. Images are taken from spinal cord of young (**A, C, E**) or aged (**B, D, F**) mice injected with saline (**A,B**) or infected with *S. typhimurium* for 8 (**C, D**) or 22 days (**E, F**). Scale bar represents 10µm. Images are taken from a single Z plane of confocal stacks captured at x100 magnification on a Leica SP5 microscope. n = 4-5 per group.

Total SMI-32 immunoreactivity was assessed by measuring average pixel intensity in a single SMI-32 stain from 3 x40 magnification images from an epifluorescence microscope per subject (n = 4-5 per group). There was a significant effect of time-point on SMI-32 immunoreactivity (2 way ANOVA:  $F_{2,22} = 8.541$ ,  $p = 0.0018$ ), but not of age ( $F_{1,22} = 0.156$ ,  $p = 0.697$ ) or any interaction between age and time-point ( $F_{2,22} = 2.641$ ,  $p = 0.0937$ ). SMI-32 staining intensity was increased at 1 week after infection in both young and aged mice, although this change appeared more pronounced and prolonged in aged mice. Spinal cord from saline injected aged mice had slightly less SMI-32 reactivity compared to spinal cord from saline injected young mice, although this difference was not significant.



**Figure 7.7. Quantification of paranodal (Nfasc155) length on SMI-32 negative or positive axons.**

Paranodes on SMI-32 negative axons did not change in length during *S. typhimurium* infection (A), although paranodes from aged mice were slightly elongated compared to paranodes from young mice ( $p < 0.05$ ). Paranodal length in SMI-32 positive axons decreased during *S. typhimurium* infection to an equal degree in both young and aged mice (B) ( $p < 0.01$ ), reaching a similar mean length to SMI-32 negative paranodes ( $< 4 \mu\text{m}$ ). Columns represent means  $\pm$  SEM.  $n = 4-5$  per group.

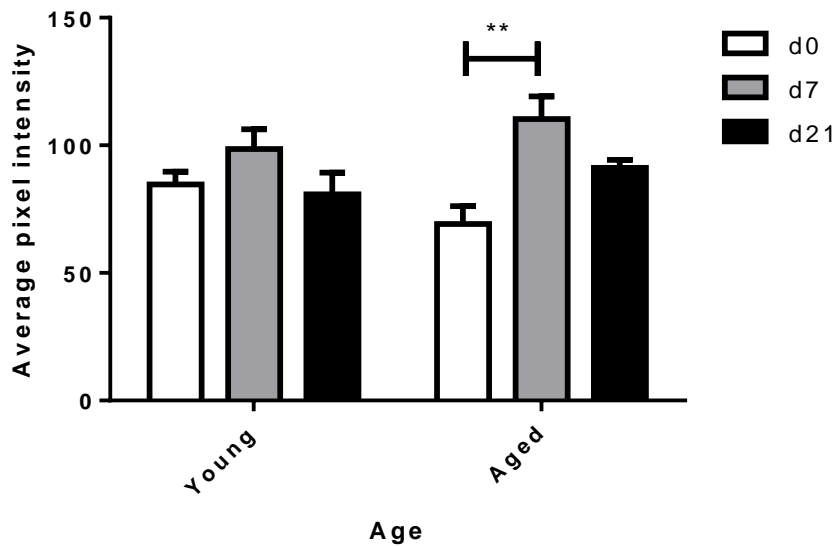


**Figure 7.8. Quantification of SMI-32 immunoreactivity in *S. typhimurium* infected young and aged mice.**

SMI-32 immunoreactivity was increased one week after infection. This increase was more pronounced in aged mice. Columns represent means  $\pm$ SEM. \*\* denotes  $p < 0.01$  in Holm-Sidak post test.  $n = 4-5$  per group.

Spinal cords from young and aged mice infected with *S. typhimurium* were stained for juxtaparanodal Kv1.2 and paranodal Nfasc155 ( $n = 4-5$  per group). After qualitative assessment of staining in these sections it was concluded that there was no noticeable increase in Kv1.2/Nfasc155 co-localisation associated with ageing or *S. typhimurium* infection (Figure 7.9). A qualitative assessment of staining for Nfasc155 and caspr, the cognate partner of Nfasc155 in the paranodal junction (Salzer, 2003), also showed no effect of age or *S. typhimurium* infection on the degree of co-localisation between these two proteins, as the majority of paranodes clearly stained for both proteins (Figure 7.10) ( $n = 4-5$  per group).

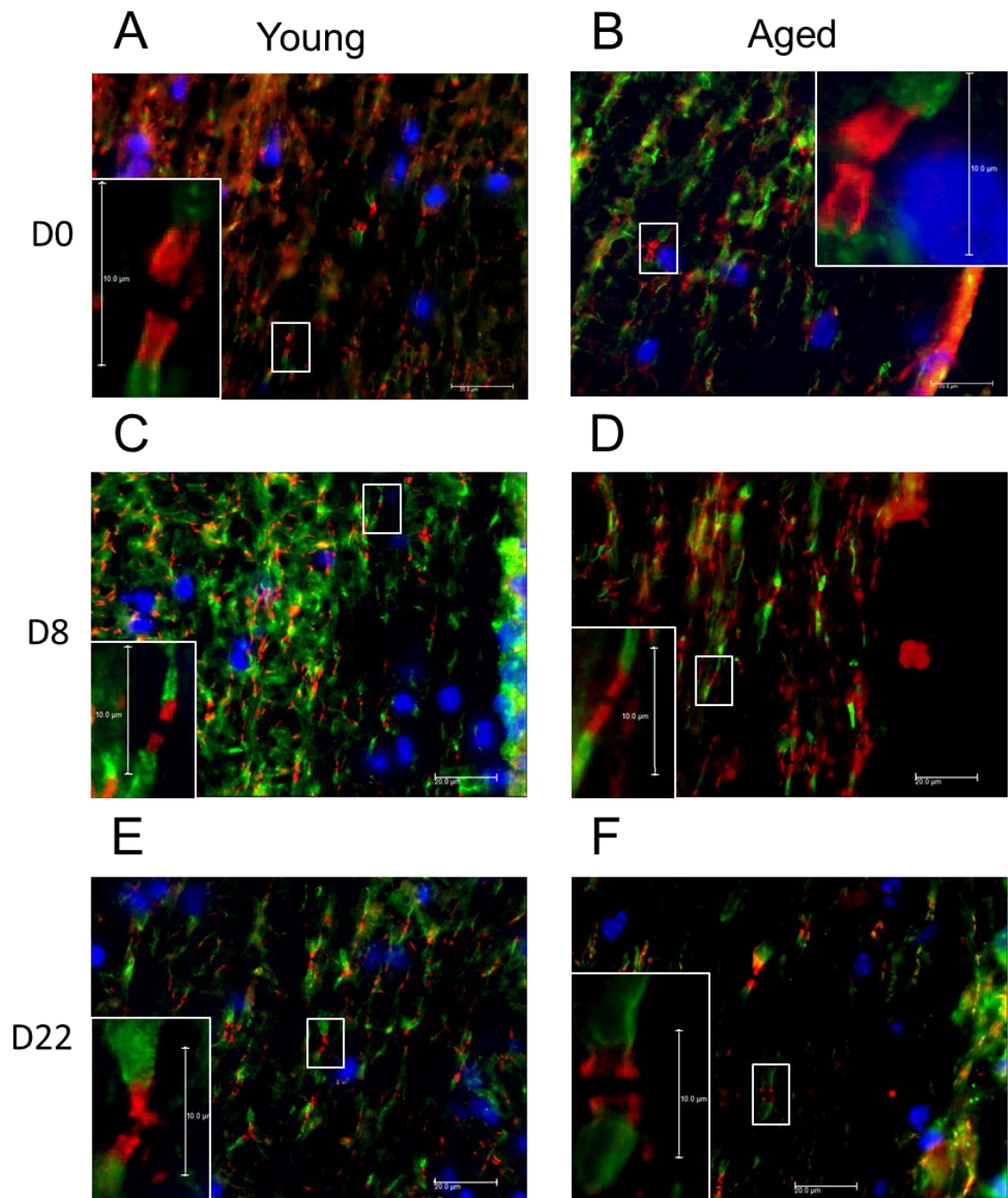


**Figure 7.9. The effect of *S. typhimurium* infection on paranodal/juxtaparanodal compartmentalisation in young and aged mice.**

Paranodes are stained for Nfasc155 in red, Kv1.2 for juxtaparanodes in green, nuclei are stained blue with DAPI. The Nfasc155 positive (red) paranodes did not usually co-localise with Kv1.2 (green) during *S. typhimurium* infection in young or aged mice, indicating maintenance of paranodal/juxtaparanodal compartmentalisation. Young and aged mice were either injected with saline (A, B) or infected with *S. typhimurium* for 8 days (C, D) or 22 days (E, F).

Images were captured using at x100 magnification using an epifluorescence microscope. Insets are x4 magnifications the area indicated by the white box in each image. n = 4-5 per group.

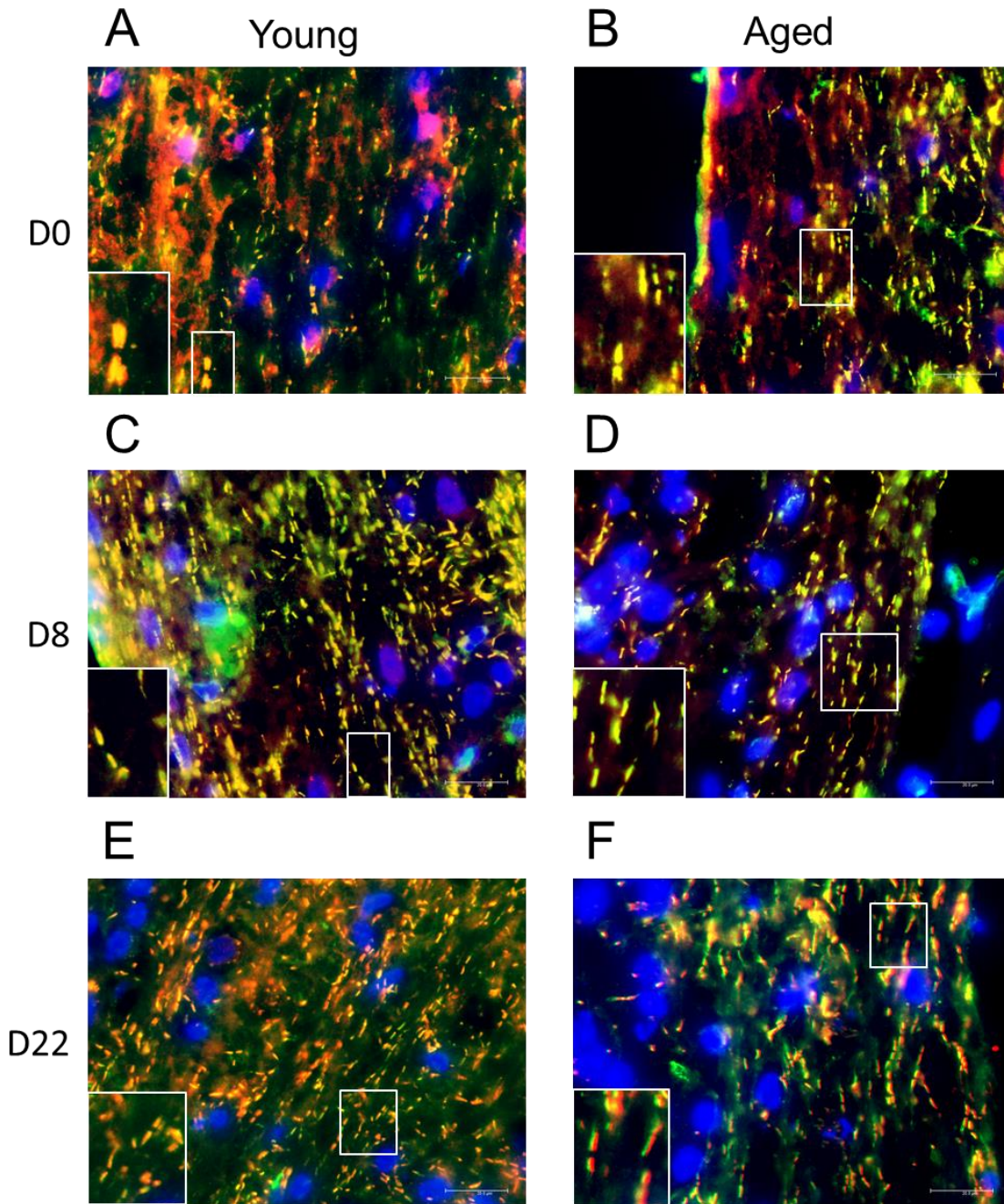


**Figure 7.10.** The effect of *S. typhimurium* infection on caspr and Nfasc155 co-localisation in young and aged mice.

Paranodes are stained for Nfasc155 in red and CASPR in green, nuclei are stained blue with DAPI. Young and aged mice were either injected with saline (A, B) or infected with *S. typhimurium* for 8 days (C, D) or 22 days (E, F). There

was no difference in the degree of caspr/nfasc155 co-localisation following infection in young or aged mice. Images were captured using at x100 magnification using an epifluorescence microscope. Insets are x2 magnifications of the areas indicated by the white box in each image. n =4-5 per group.

## **7.4 Discussion**

### **7.4.1 The effects of EAE on paranodal organisation**

As anticipated, EAE caused disruption of paranodal junctions. Nfasc155 positive paranodes were longer in length in EAE spinal cord than spinal cord from saline treated mice and tended to have less evenly distributed staining along the length of a paranode. These effects on paranodal integrity were more pronounced with increasing proximity to EAE lesions, in agreement with the findings of other authors (Howell et al., 2006). The increase of SMI-32 staining around lesion sites shown here validates the use of this epitope as a marker for “stressed” or “damaged” axons in these experiments. These data demonstrated that the quantification techniques devised for measuring Nfasc155 length were valid and suitable in the lateral white matter tracts of the spinal cord. Double staining for Kv1.2 and Nfasc155 was attempted, but proved technically challenging due to the Kv1.2 antibody used being of mouse origin and EAE tissue having a very high endogenous IgG content. This problem proved surmountable for SMI-32 through the use of a mouse on mouse kit (Vector Laboratories, Peterborough, UK), but background levels were too high when staining for Kv1.2.

### **7.4.2 Selection of spinal cord as site of study**

All the experiments conducted in this chapter were carried out using the lateral white matter tracts of the spinal cord. Data from Howell et al 2010 demonstrated an effect of CFA and EAE on paranodal length in these tracts of the spinal cord, but these authors did not investigate the effects of CFA on paranodal integrity on other areas of the CNS. Therefore the lateral white matter tracts of the spinal cord were deemed a suitable location to look for systemic inflammation induced paranodal disruption. From a technical perspective the spinal cord is also well suited for studying paranodal integrity,

with large well defined white matter tracts and most fibres orientated in a similar plane, as opposed to the cerebellar peduncles for example, where there are bundles of axons orientated in many different planes. Studies from other authors have also suggested a rostral-caudal gradient in the CNS in the scale of immune responses to local inflammatory stimuli, with more caudal areas such as the spinal cord exhibiting greater BBB breakdown and microglial responses to mechanical injury or stereotaxic injection of cytokines (Phillips et al., 1999; Schnell et al., 1999a; Schnell et al., 1999b) and greater increases in BBB leakiness in response to an i.p. injection of 100µg/kg of LPS (Lu et al., 2009). Microglia in the spinal cord also generally exhibited greater changes in phenotype during *S. typhimurium* infection than other areas of the CNS (Chapter 6). This increased reactivity of the spinal cord to inflammatory stimuli and the previous demonstration of paranodal changes in the spinal cord following CFA injection led to the decision to select the spinal cord for use in the experiments described in this chapter.

### **7.4.3 The effect of CFA on paranodal organisation**

CFA is an emulsion of mineral oil and heat-killed mycobacterium that provokes a long lasting immune response in the CNS, including increased expression of markers of microglial and astrocyte activation and of the cytokines IL-1 $\beta$ , TNF $\alpha$  and IL-6 up to 14 days after injection (Raghavendra et al., 2004). It is often used as an adjuvant for the induction of EAE (Howell et al., 2010), as is pertussis toxin, which is believed to facilitate EAE induction by increasing BBB permeability (Kugler et al., 2007; Yong et al., 1993) and through its actions promoting T cell responses to CNS antigens (Hofstetter et al., 2002). Injections of CFA and PTX has previously been reported to cause increases in paranodal length and increased incidence of Nfasc155/Kv1.2 co-localisation (Howell et al., 2010), but in the experiments described in this chapter no such changes were observed. This lack of an effect may be explained by differences in the protocol used for CFA challenge between this study and Howell et al's. Howell et al's study challenged the mice with CFA on day 7 as well as day 0 of the experiment, whereas in this study CFA was only administered on day 0 and incomplete Freund's adjuvant was administered on day 7, due to restrictions in the Home Office licence used regarding multiple challenges with complete Freund's adjuvant. The CFA used in the experiments described in this chapter

had a slightly different composition, containing 200µg of *Mycobacterium butyricum*, whereas the CFA used in Howell et al's study contained 320µg of *Mycobacterium tuberculosis* and 80µg of *Mycobacterium butyricum*. These differences in the protocol and reagents used may have contributed to the lack of any effect of CFA seen in this experiment.

#### **7.4.4 The effect of *S. typhimurium* and ageing on paranodal organisation**

The most striking result of the *S. typhimurium* study was that mean paranodal length progressively decreased in SMI-32 positive axons during infection, whereas mean paranodal length in SMI-32 negative axons was unaffected by infection. The intensity of Nfasc155 staining on SMI-32 positive axons was not noticeably affected by infection – only the average length seemed to decrease. The paranodes of SMI-32 positive axons of young saline treated mice (4.68µm) were significantly longer than those of SMI-32 negative axons from young saline treated mice (3.65µm). However, after 3 weeks of infection paranodal length was nearly equal between SMI-32 negative and positive axons (SMI-32 negative d22 young – 3.5µm, SMI-32 positive d22 young – 3.8 µm). This progressive reduction in paranodal length is difficult to explain, particularly as paranodal elongation rather than contraction has been reported in SMI-32 positive axons in EAE and following CFA administration (Howell et al., 2010).

Shortening of paranodal domains has not been widely reported in the literature previously. One study that reported shortening paranodes used a model of mild cerebral hypoperfusion (Reimer et al., 2011) and observed progressively decreasing intensity of Nfasc155 staining and paranodal length. Staining for caspr, which is localised to the axon and not the myelin loop as Nfasc155 is, was not altered by hypoperfusion and was still organised into paranodal domains despite the absence of Nfasc155. To investigate whether there were differences in Nfasc155 and caspr localisation in the spinal cords of *S. typhimurium* infected mice, double staining for caspr and Nfasc155 staining was performed (Figure 7.8). Caspr/ Nfasc155 co-localisation was visible in almost all paranodes under all conditions and did not appear to be altered by *S. typhimurium* infection or ageing. This finding suggests that local hypoperfusion is not responsible for the changes in paranodal length observed in SMI-32 positive axons. Kv1.2/ Nfasc155 compartmentalisation also did not

appear to change due to *S. typhimurium* infection (Figure 7.6), suggesting that this shortening of paranodes in SMI-32 positive axons does not compromise paranodal/juxtaparanodal compartmentalisation.

One potential cause of decreased paranodal length in SMI-32 positive axons may be that the paranodes are actually unchanged, but previously SMI-32 negative axons become SMI-32 positive following systemic *S. typhimurium* infection. SMI-32 immunoreactivity increases 1 week after infection, correlating with the peak of peripheral cytokine levels (chapter 6), but SMI-32 immunoreactivity decreases again 3 weeks after infection towards control levels. There also appears to be a difference between young and aged mice in *S. typhimurium* induced changes in SMI-32 reactivity, with aged mice exhibiting a greater increase in SMI-32 reactivity. This is not reflected in the progressive decreases in paranodal length observed in SMI-32 positive axons during infection, which are similar between young and aged mice. These data suggest that these changes in paranodal length cannot be explained by increased numbers of SMI-32 positive axons during *S. typhimurium* infection.

The peak of increased SMI-32 immunoreactivity occurred 1 week after infection, co-inciding with the peak of peripheral cytokines and hippocampal cytokine expression (chapter 6). The cause of increased SMI-32 reactivity was not directly investigated in this thesis, but could include increased infiltration of blood components such as fibrinogen or thrombin caused by elevated circulating cytokines (Huynh and Dorovinizis, 1993; Mayhan, 2002) and their subsequent effects acting either directly on axons (Donovan et al., 1997; Shavit et al., 2008) or on local microglial cells (Davalos et al., 2012; Fujimoto et al., 2007; Lunnon et al., 2011). Alternatively production of cytokine and reactive oxygen/nitrogen species by microglia or BBB associated cells could be induced by circulating cytokines (Skelly et al., 2013; Teeling et al., 2010) and these inflammatory molecules could cause axonal stress/damage and cause increased SMI-32 immunoreactivity (di Penta et al., 2013; Nikic et al., 2011; Redford et al., 1997). Changes in SMI-32 reactivity in the spinal of cord EAE mice has been associated with mitochondrial dysfunction (Mahad et al., 2009), which has been linked to decreased conduction of axons (Redford et al., 1997). Therefore the increased SMI-32 immunoreactivity of axons 8 days after infection may reflect changes in axonal conduction or mitochondrial function.

Paranodal length was slightly longer in the paranodes of aged mice compared to those of young mice. Morphologically there was little difference between paranodes from young or aged mice, and a slight change to paranodes with ageing is consistent with previous studies (Shepherd et al., 2010). However there was no noticeable increase in Kv1.2/Nfasc155 co-localisation, which has previously been reported in aged monkeys and rats (Hinman et al., 2006).

*S. typhimurium* infection clearly has an effect on mean paranodal length in SMI-32 positive axons, but not on SMI-32 negative axons. These data are difficult to explain without further experiments. Performing electron microscopy to examine transverse band organisation in SMI-32 positive axons following *S. typhimurium* infection would provide some perspective into the nature of the changes occurring at the paranodal junction, for example whether the number or density of transverse bands was altered during infection or whether shortening of paranodes is associated with withdrawal of paranodal loops. The functional relevance of changes in paranodal length and SMI-32 reactivity could be investigated by measuring conduction velocity in spinal cord white matter tracts, either in spinal cord explants or using in vivo recordings.

#### **7.4.5 Summary**

In agreement with previous studies these data showed that EAE leads to paranodal disorganisation in lateral spinal cord white matter tracts. However, CFA administration had no effect on paranodal organisation. Contrary to expectations, *S. typhimurium* infection caused a reduction in paranodal length in SMI-32 positive axons, although paranodal/juxtaparanodal compartmentalisation was preserved and caspr/Nfasc155 co-localisation was unaffected by infection. SMI-32 reactivity increased during *S. typhimurium* infection, peaking at 1 week after infection, and this increase was more pronounced in aged mice. Paranodal length in SMI-32 negative axons was unaffected by *S. typhimurium* infection, but ageing caused a slight increase in paranodal length in these axons. The reason for the decrease in paranodal length in SMI-32 positive axons is not clear and requires further investigation to establish the functional relevance of these changes.

## 8. General discussion

Microglia have been shown to alter their phenotype during ageing, adopting a primed response to pro-inflammatory stimuli and increasing their expression of activation markers such as CD68 and CD11b (Deng et al., 2006; Godbout et al., 2005b; Henry et al., 2009). However, most literature investigating age-related changes to microglia, including microglial priming, has focused on the microglia of the hippocampus. Furthermore there are very few studies investigating the effects of live, non-neurotropic infections instead of sterile mimetics of infection on the aged CNS, despite substantial differences in the kinetics and the mediators of inflammatory responses to LPS compared to many live infections. This thesis aimed to provide insight into regional differences in phenotype between microglia in the aged CNS, how their responses to systemic inflammation induced by live infection or LPS differed and to characterise the behavioural response of young and aged mice to LPS or live infection. The model of live infection used in this thesis, an attenuated strain of *S. typhimurium*, was selected for its prolonged systemic and CNS inflammatory response and the systemic, non-neurotropic infection *S. typhimurium* inoculation produces (Püntener et al., 2012). LPS was used to assess the inflammatory response of microglia in different areas of the CNS to a well characterised inflammatory stimulus.

### 8.1 Changes in microglia

Studies undertaken in this thesis demonstrate that regional differences in microglial phenotypes are exacerbated by the ageing process. Regional differences in microglia were especially pronounced between grey and white matter in the ageing brain, most strikingly in expression of CD11c but also in expression of other molecules such as CD68 and Fc $\gamma$ RI. Microglia in the grey or white matter of different areas of the brain also responded differently to ageing, with the most striking increases in expression of several markers occurring in the cerebellar white matter or nuclei. This does not necessarily reflect a straightforward rostral to caudal gradient, as changes in microglial phenotypes in the spinal cord were not as pronounced as in the cerebellum. These data contrast the findings of Kullberg et al, 2001, who reported greater changes in microglial phenotype in the spinal cord of the aged rat than in the

inferior cerebellar peduncle. The reason for greater changes in microglia in the cerebellum is not known but could be due to the high levels of neuronal loss reported in the cerebellum compared to other brain areas during ageing (Woodruff-Pak et al., 2010).

The studies using LPS in this thesis support the concept of microglial priming in the ageing brain, with an exaggerated inflammatory response detected in both the hippocampus and the cerebellum three hours after a systemic LPS challenge. This is in agreement with several previous studies showing exaggerated microglial responses to systemic LPS challenge in the ageing brain (Godbout et al., 2005b; Henry et al., 2009; Wynne et al., 2010). The cerebellar response to LPS in the young and aged brain was however considerably smaller than that of the hippocampus. Other authors have reported a similar increase in cytokine transcription between the cerebellum and hippocampus in response to systemic LPS injection (Hansen et al., 2000b) or an i.c.v. LPS injection (Huang et al., 2008), in contrast to the data reported in this thesis. Differences in microglial density between the two regions could contribute to the differences in the inflammatory response, as the hippocampus is more densely populated with microglia than the cerebellum (Lawson et al., 1990). Data from different time-points after LPS injection would help to establish whether these differences are a result of differences in the kinetics of cytokine responses between the two regions. This inflammatory reaction was not accompanied by a detectable increase in expression of the microglial activation markers investigated using immunohistochemistry (CD11b, CD68, F4/80, CD11c), with the exception of Fc $\gamma$ RI in the cerebellum.

These data contrast with the effects of *S. typhimurium* infection on microglia in several aspects. There was a general increase in expression of microglial activation markers such as CD11b and F4/80 during *S. typhimurium* infection. The inflammatory reaction measured in the hippocampus was much smaller than the acute response to LPS, inducing a maximum two fold increase in IL-1 $\beta$ , TNF $\alpha$  and IL-6 expression compared to a 7-8 fold increase after LPS injection in young mice, and in the cerebellum no increase in cytokine expression was detected during *S. typhimurium* infection. There were no differences in the central cytokine response to *S. typhimurium* infection between young and aged mice, and expression of CD11b, Fc $\gamma$ RI and F4/80 were increased to a similar degree in most regions or to a greater extent in

young than in aged mice. Overall these data do not support the idea that aged microglia have an enhanced inflammatory response to *S. typhimurium* infection. Increases in CD68 and CD11c expression were observed in aged white matter tracts and in particular the aged spinal cord, which may indicate increased phagocytic activity of cells in these regions (Kettenmann et al., 2011). The cause of any such increased phagocytic activity is open to speculation.

A possible explanation of the lack of differences between the young and aged cytokine response to *S. typhimurium* infection compared to systemic LPS injection is differences in the stimuli activating microglia. Systemic LPS injection is believed to primarily activate microglia through production of inflammatory mediators such as IL-1 $\beta$  and PGE<sub>2</sub> by endothelial cells and perivascular macrophages which then act on microglia (Laflamme and Rivest, 1999, 2001). The inflammatory reaction produced by *S. typhimurium* infection differs from that produced by systemic LPS injection. The kinetics of the circulating cytokine response differ substantially, with *S. typhimurium* infection causing a prolonged cytokine response that lasts for several weeks (Chapter 6), whereas the cytokine response induced by i.p. injection of 1-100 $\mu$ g/kg LPS lasts approximately 6 hours (Teeling et al., 2010; Teeling et al., 2007). The effects of prolonged cytokine elevation on cytokine production in cerebral endothelial cells have not been investigated in vivo, but the data in this thesis suggest that chronically elevated cytokine expression results in at most a small (two fold) increase in cytokine expression in the brain. In contrast i.p. injection of 100 $\mu$ g/kg of LPS produces an acute elevation of central cytokine transcription that resolves within 24 hours (Chapter 4). The composition of the circulating inflammatory response differs between *S. typhimurium* infection and LPS injection as well, with *S. typhimurium* infection leading to greater increases in circulating IFN $\gamma$  and smaller increases in IL-1 $\beta$  than LPS injection (Püntener et al., 2012). IL-6 and TNF $\alpha$  are also robustly increased by systemic LPS challenge (Skelly et al., 2013), whereas the data presented in this thesis showed only a small elevation of IL-6, while TNF $\alpha$  was more robustly elevated during *S. typhimurium* infection.

Elevated levels of peripheral cytokines such as IFN $\gamma$  or TNF $\alpha$  can lead to disruption of the BBB and increased extrusion of blood components (Huynh and Dorovinizis, 1993; Mayhan, 2002). Extruding blood components such as

IgG, fibrinogen or thrombin could produce a low grade inflammatory response in microglia and could contribute to the general microglial activation observed in the CNS during *S. typhimurium* infection and the low grade inflammatory response observed during infection (Davalos et al., 2012; Fujimoto et al., 2007; He et al., 2002; Lunnon et al., 2011). A rostral caudal gradient in the sensitivity of the BBB to inflammation induced disruption have been reported previously (Lu et al., 2009) and that could explain the rostral to caudal gradient of microglial marker expression observed in response to *S. typhimurium* infection. Extruding blood components could also contribute to axonal stress either directly or through their effects on microglia (Davalos et al., 2012; Fujimoto et al., 2007; Shavit et al., 2008), potentially explaining the elevated SMI-32 reactivity observed in white matter tracts of the CNS during *S. typhimurium* infection. Despite the increased SMI-32 immunoreactivity observed in the spinal cord during *S. typhimurium* infection no increase in paranodal length was detected. Increased paranodal length and juxtaparanodal/paranodal overlap has been suggested to precede demyelination (Howell et al., 2006), and the absence of paranodal lengthening observed in this thesis indicates that demyelination is not induced in the spinal cord of *S. typhimurium* infected mice. This thesis did not investigate whether microglial proliferation increased or monocyte infiltration occurred during *S. typhimurium* infection, but these could both also make a contribution to the changes in microglial expression of surface markers observed in the CNS.

## **8.2 Sickness behaviour after LPS injection or *S. typhimurium* infection**

An important aspect of this thesis was to define the differences between the behavioural changes induced in young and aged mice by LPS injection or *S. typhimurium* infection. Following LPS injection there was an exaggerated and prolonged reduction in burrowing activity in aged mice and a greater loss of body weight, whereas open field activity, rotarod performance and glucose water consumption was reduced to a similar extent in both young and aged mice. No change in static rod test performance was detected in mice of either age following LPS injection. Recovery of open field and burrowing activity was ongoing at the 24 hour time-point when mice were sacrificed.

The behavioural reaction to *S. typhimurium* infection differed markedly. The principle difference was the longevity of the behavioural changes observed in *S. typhimurium* infected mice – behavioural differences were apparent at one and three weeks after infection. This correlates with the prolonged cytokine reaction to infection in the circulation and to a lesser extent within the CNS. Open field activity was reduced to a similar extent in young and aged mice, and this reduction in activity was most pronounced three weeks after infection. Novel object recognition test performance was also reduced in young mice at three weeks after infection and the second phase of weight loss observed in aged mice lasted between 1-4 weeks after infection. In contrast, static rod performance was only affected one week after infection in aged mice and was completely unaffected by infection in young mice. Previous studies in young mice using a higher dose of *S. typhimurium* ( $1 \times 10^6$  compared  $3 \times 10^5$  CFU) showed no effect of *S. typhimurium* infection on burrowing between 2-21 days after infection (Püntener et al., 2012). Together these data form a diverse collection of behavioural changes that occur during *S. typhimurium* infection, and differences in their kinetics and their age dependent sensitivity to infection illustrates the complexity of sickness behaviour in response to a live infectious agent.

Increased central production of inflammatory mediators such as IL-1 $\beta$  and PGE<sub>2</sub> plays a key role in mediating sickness behaviour induced by systemic LPS challenge (Bluthe et al., 2000a; Kent et al., 1992; Pecchi et al., 2006; Teeling et al., 2007). The exaggerated deficits observed in burrowing activity, a hippocampus dependent behaviour (Deacon et al., 2002), fits with the exaggerated hippocampal cytokine induction observed 3 hours after LPS injection. However, the data in this thesis do not support such an important role for the central inflammatory response in *S. typhimurium* infection. The increase in expression of cytokines was small in the hippocampus (maximum of a two fold increase from saline) or non-existent in the cerebellum and the peak of hippocampal cytokine expression appeared to be at one week rather than three weeks after infection, contrasting to data published using a higher dose of *S. typhimurium* strain SL3261 (Püntener et al., 2012). It is feasible that the second phase of weight loss observed in aged mice is attributable to increased hypothalamic expression of inflammatory mediators, but this was not measured in this thesis.

There are several alternative explanations for the sickness behaviours observed during *S. typhimurium* infection that do not depend on elevated central cytokine or prostaglandin expression. Sickness behaviour-like symptoms have been reported during chronic liver disease, especially fatigue (D'Mello and Swain, 2011). The liver is one of the organs colonised by *S. typhimurium* during systemic infection and a site of localised inflammation (Simon et al., 2007). A study using another *Salmonella enterica* serovar, *Salmonella Dublin*, showed that the cytokine response to salmonella infection in the liver is prolonged, lasting at least 30 days and consisting of the same cytokines induced in circulation, including IFN $\gamma$  and TNF $\alpha$  (Eckmann et al., 1996). One aspect of an apathetic or fatigued state in a mouse would be a decreased desire to initiate exploratory behaviour (Chaudhuri and Behan, 2000; Gaykema and Goehler, 2011; Stone et al., 2006), which is reflected in the decreased rearing and locomotor activity observed in the open field test, the decreased preference for the novel object in the NOR test and the reduced interest in investigating objects during the familiarisation phase of the NOR test. The precise causes of fatigue during liver disease are not completely understood, but are believed to be caused by changes in neurotransmission within the CNS involving serotonergic and noradrenergic circuits (Swain, 2006). The liver inflammation that occurs during *Salmonella* infections could potentially cause similar effects on fatigue. Several recent publications have suggested that liver disease causes increased fatigue through endothelial adhesion and infiltration of inflammatory monocytes into discrete brain areas involved with initiating and executing motor behaviour including the hippocampus, basal ganglia and motor cortex and that blocking infiltration into the CNS with anti-P-selectin antibodies can attenuate reductions in social interaction and locomotor activity (D' Mello et al., 2013; D'Mello et al., 2009).

An alternative mechanism that may transduce liver inflammation induced behavioural changes is vagal afferent signalling, which has been suggested to contribute to several aspects of sickness behaviour, including anorexia (Bret Dibat et al., 1995), reduced locomotor activity and fatigue (Gaykema and Goehler, 2011). Vagal afferent projections extensively innervate the liver and other visceral organs and can sense inflammatory molecules such as prostaglandins, TNF $\alpha$  and IL-1 $\beta$  (Ek et al., 1998; Goehler et al., 1997; Rogers and Hermann, 2012), so they may also play a role in *S. typhimurium* induced

sickness behaviour. This idea is supported by the acute activation of c-fos in vagal afferents and the network of brain areas they project to within the CNS following *S. typhimurium* infection in the gut (Riley et al., 2013; Wang et al., 2002). Longer term studies into vagal activation by *S. typhimurium* infection have not been carried out, possibly due to the difficulty in using c-fos, an immediate early response protein, to examine chronic changes in neuronal activity (Chaudhuri, 1997). Persistent vagal signalling could also induce plastic changes in neurotransmission in the NTS or other CNS areas, as has been reported for other chronic inflammatory stimuli of vagal afferents such as tobacco smoke or house dust mite in the lung (Chen et al., 2001; Sekizawa et al., 2008; Sekizawa et al., 2010). Such plastic changes could contribute to the chronic behavioural changes that occur during *S. typhimurium* infection and which persist beyond the peak of circulating cytokine levels.

Neuronal control of appetite is complex and involves multiple brain areas, but the hypothalamus plays a central role in controlling food intake (Gautron and Laye, 2009). Gastrointestinal *S. typhimurium* infection has previously been shown by c-fos to acutely activate vagal afferents and neurons in the paraventricular nucleus of the hypothalamus (Riley et al., 2013; Wang et al., 2002), an area which vagal afferent fibres project to via the NTS (Gaykema et al., 2007b). Increases in c-fos staining were more pronounced in several areas associated with vagal afferent signalling, including the PVN of the hypothalamus, in aged mice compared to young mice following systemic LPS injection (Gaykema et al., 2007a), suggesting that enhanced vagus nerve mediated signalling could contribute to the increased anorexic response to systemic inflammation observed in aged mice. Neurons and microglia in the mediobasal hypothalamus (MBH), an area of the hypothalamus with roles in nutrient sensing (Blouet et al., 2013), adopt a more pro-inflammatory phenotype in ageing characterised by increased NF $\kappa$ B signalling and microglial production of TNF $\alpha$  (Zhang G. et al., 2013), and this could also indicate increased sensitivity to inflammation of hypothalamic nuclei in ageing. The MBH also has a leakier BBB than neighbouring areas of the hypothalamus and CNS in general, as demonstrated using several different size tracers (Morita and Miyata, 2012), which may render it more susceptible to systemic inflammation than other areas of the CNS. The hypothalamus also plays important roles in regulating behaviour, include motivation for exploratory

activity (Gaykema and Goehler, 2009; Grossberg et al., 2011), and in modulating immune responses, for example through induction of cortisol release via the HPA axis (Engelmann et al., 2004), making it a structure of particular interest for investigations into the effects of *S. typhimurium* infection on sickness behaviour.

The co-ordination and balance deficits observed following *S. typhimurium* infection of aged mice are particularly interesting as they do not fit within the usual constellation of sickness behaviours described in the literature in response to systemic LPS (Dantzer, 2004). The deficits in static rod test performance observed in aged mice were only observed 7 days after infection, which differed from the progressive decrease in open field activity, body weight of aged mice and novel object preference from 7 days to 21 days after infection. This co-ordination and balance deficit co-occurred with the increased SMI-32 reactivity observed in the spinal cord of mice which indicates increased axonal stress in the white matter tracts of both young and aged mice. Whether this axonal stress could affect axonal conduction in these fibres is not clear, but impaired axonal conduction of action potentials in the spinal cord could contribute to co-ordination and balance deficits. A potential source of such axonal stress could be extravasation of blood components such as fibrinogen (Davalos et al., 2012), IgG (Lunnon et al., 2011; Teeling et al., 2012) or thrombin (Donovan et al., 1997; Shavit et al., 2008) and their effects on axons, either directly or via activation of microglial cells.

The susceptibility of aged but not young mice to infection induced co-ordination and balance deficits may be caused by the pre-existing deficits in co-ordination and balance present in aged mice, as demonstrated by impaired static rod test performance. Loss of neurons in the cerebellum (Woodruff-Pak et al., 2010) and hair cells in the vestibular system (Rauch et al., 2001) both contribute to decreased co-ordination and balance during ageing and a pre-existing loss of function in these circuits may pre-dispose them to further dysfunction during *S. typhimurium* infection. Alternatively the inflammatory response to *S. typhimurium* infection in the aged spinal cord could be more pronounced than in the cerebellum or hippocampus and therefore underlie these inflammatory changes, in concurrence with the rostral caudal gradient of *S. typhimurium* infection induced changes in microglial expression in response of various surface molecules such as F4/80.

The changes in novel object recognition test performance could be caused either by reduced motivation caused by a state of fatigue or apathy in *S. typhimurium* infected mice or impaired memory function, or an interaction of apathy/fatigue and impaired memory. Impaired memory during *S. typhimurium* infection could be explained by the reduced BDNF expression observed in the hippocampus. Reduced hippocampal BDNF expression resulting from elevated IL-1 $\beta$  levels has been suggested to underlie the impairments in fear conditioning behaviour observed in *E. Coli* infected rats (Barrientos et al., 2009a; Cortese et al., 2011; Frank et al., 2010a). The increase in hippocampal IL-1 $\beta$  observed following *S. typhimurium* infection is similar in size to that observed in the aged rat hippocampus (approximately 2-3 fold from saline treated mice) (Barrientos et al., 2009a), suggesting that in the case of memory related tasks the increases in hippocampal IL-1 $\beta$  may be sufficient to negatively impact performance. Fatigue and apathy could reduce the motivation drive of an animal to engage in exploratory activity, as discussed earlier.

The spectrum of changes induced by systemic LPS injection and *S. typhimurium* infection are summarised below in Figure 6.1 and 6.2.

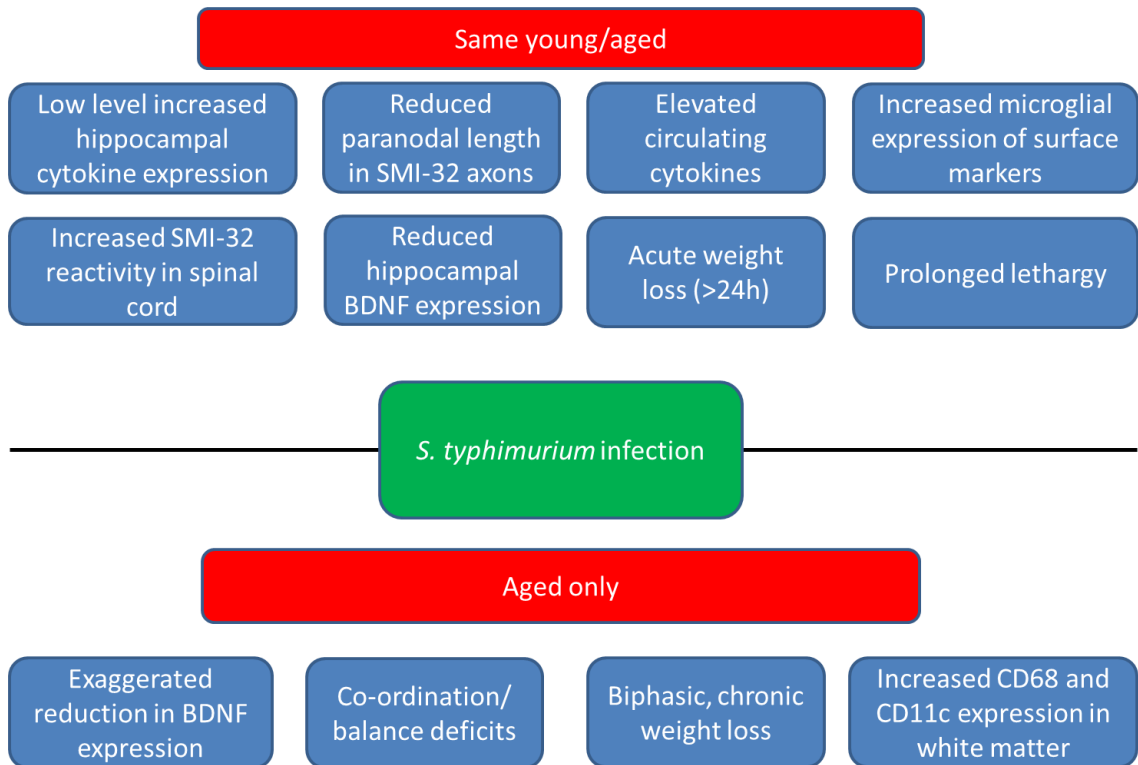


**Figure 8.1.** A summary figure showing the changes induced by *S. typhimurium* infection in the young and aged CNS.

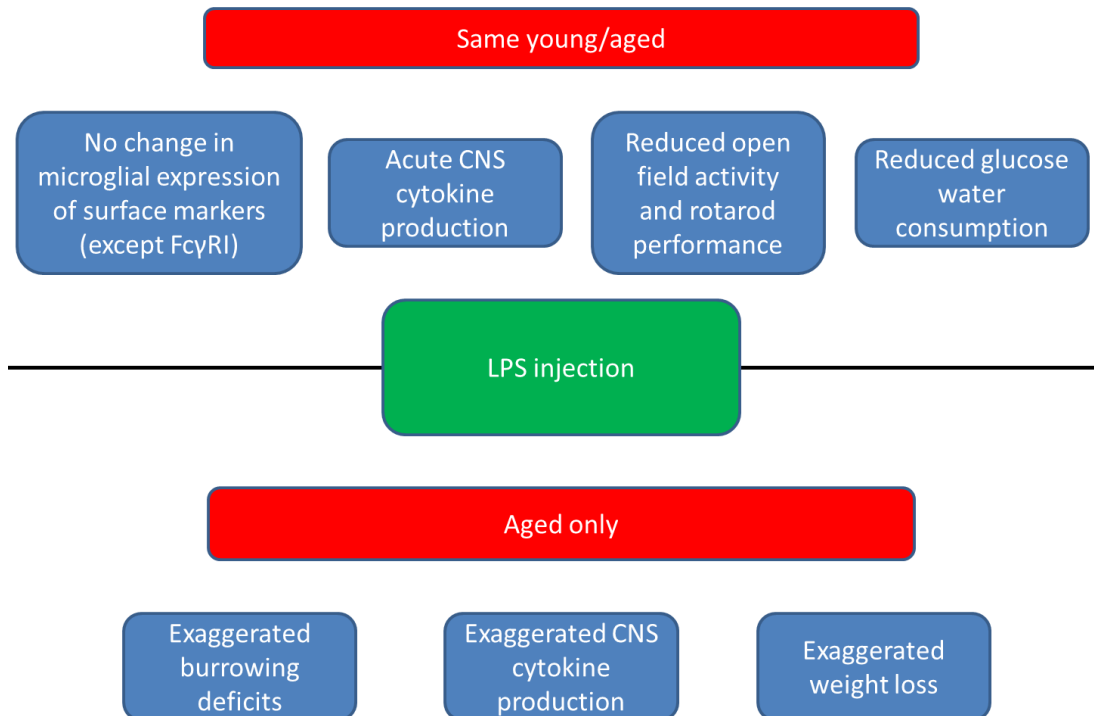


**Figure 8.2.** A summary figure showing the changes induced by systemic LPS injection in young and aged mice.

### 8.3 Implications

These data challenge the assumption that ageing enhances the CNS inflammatory response to live infections. The induction of inflammatory mediators was comparable between young and aged mice, and these data suggest that behavioural changes and changes in microglial phenotype during *S. typhimurium* infection may be driven by other means than de novo production of the cytokines IL-1 $\beta$ , TNF $\alpha$ , IL-6 or IFN $\beta$  or PGE<sub>2</sub> within the CNS. These differences might not be reflected in all other models of bacterial or viral infection – for example the hippocampal IL-1 $\beta$  response is more pronounced in aged than young *E. Coli* infected rats (Barrientos et al., 2009a), but these data demonstrate the importance of using live infections to verify how applicable the biological phenomena observed using mimetics of infection are to real infections. The changes in microglial phenotype observed during infection may also contribute to the activation of microglia during normal human ageing (Cribbs et al., 2012), which differs from ageing in mice as we are constantly exposed to pathogenic stimuli which require immune responses. Identifying the precise mechanisms underlying changes to microglia induced by live systemic infections may present new therapeutic avenues to reduce age related microglial dysfunction.

The regional differences in microglial phenotypes induced by ageing and infection highlights an important question – how universal are the changes termed microglial priming within the ageing brain? The differences observed between aged microglia in white compared to grey matter in this thesis have particular relevance for the study of the ageing human CNS, which consists of approximately 40% white matter (Gur et al., 1999) in contrast to the 10% white matter in the rodent brain (Zhang and Sejnowski, 2000). Human white matter also contains higher concentrations of microglia than grey matter (Mittelbronn et al., 2001), conversely to the mouse (Lawson et al., 1990). These data also raise the question of whether microglia actively contribute to age related white matter changes or the white matter specific changes in microglial phenotype are a bystander effect.

Finally the data in this thesis contribute significantly to the characterisation of the attenuated *S. typhimurium* strain SL3261 as a model of systemic bacterial infection and resulting immune to brain communication. These data showed

that exploratory activity was equally impaired in young and aged mice whereas aged mice experienced co-ordination and balance impairments and a second phase of weight loss which was not present in young mice. These observations open up new lines of inquiry for researchers to follow regarding the impact of systemic infections on the elderly and how seemingly subclinical infection might impact on function in previously unnoticed ways, for example impaired co-ordination and balance. The data in this thesis also shows that concepts about immune to brain communication developed using mimetics of infection may not be applicable to all infections, especially those of a chronic nature.

## **8.4 Future experiments**

Several unanswered questions that arise from this thesis could be addressed with further experiments. This thesis has described regional differences in microglial expression of various markers, particularly between grey and white matter, but it only addresses whether microglia in different regions of the aged CNS have different cytokine responses to systemic inflammation in a limited fashion, by comparing whole cerebellum and hippocampus. Regional differences between microglia could be investigated in much greater depth by injecting young and aged mice intraperitoneally with LPS and assessing the inflammatory response of microglia at an acute time-point when microglia are at their peak cytokine production e.g. 4-6 hours after injection. Microglial production of inflammatory mediators could then be assessed in situ by laser capture microdissection to isolate specific regions. Techniques have been described to capture individual immunohistochemically stained cells for laser capture from histological sections (Waller et al., 2012), raising the prospect of measuring microglia specific transcripts and comparing the influence of microenvironment on microglial phenotype within the young and aged brain. Using this approach one could also assess the contribution of endothelial cells and perivascular macrophages compared to parenchymal microglial cells to the exaggerated cytokine response to systemic inflammation.

To investigate what role myelin phagocytosis plays in the induction of CD11c expression an in vitro approach could be used. Myelin isolated from young or aged brains could be incubated with primary adult microglia and the subsequent changes in surface markers such as CD11c measured by fluorescence activated cell sorting (FACS). The surface molecule expression of

these cells could then be compared to microglia isolated from aged cerebellum and FACS sorted for CD11c expression. This would allow one to determine to what extent the phenotype of microglia in aged white matter tracts is driven directly by uptake of myelin by phagocytosis.

Further behavioural experiments would be useful to expand our understanding of different aspects of the behavioural response to *S. typhimurium*, such as establishing whether deficits in novel object recognition test performance are due to decreased memory or a lack of motivation to explore novel objects. This could be achieved through use of memory tasks that do not rely on novelty seeking behaviour, such as the alternating Y maze test or fear conditioning. Further characterisation of the seemingly apathetic or fatigued state of *S. typhimurium* infected mice could be established through use of a quinine avoidance test. Quinine is a bitter tasting compound that naïve mice preferentially avoid, but mice in a non-depressed apathetic state induced by chronic restraint stress show no preference for water over quinine (Martinowich et al., 2012). If using males the female estrous urine sniffing test could also provide a measure of decreased exploratory driven behaviour (Martinowich et al., 2012). The social interaction test would also be a suitable test of exploratory activity, but there are practical difficulties in using a healthy conspecific juvenile for social interaction when the mouse it is interacting with has a live infection. A variety of other behavioural assays could also be used to assess anxiety related behaviour such as the elevated plus maze or holeboard assay which would help to differentiate whether the deficits in exploratory behaviour seen following *S. typhimurium* infection are caused by heightened anxiety or a lethargic/apathetic state. Additional experiments with longer time-points, for example 8 weeks after infection, would provide interesting information regarding whether open field activity and novel object preference eventually recovers following *S. typhimurium* infection.

Experiments to establish what mechanisms underlie behavioural and microglial changes during *S. typhimurium* infection could provide interesting insights with applications for preventing maladaptive responses to infection in humans. The role of hippocampal inflammatory mediator production in *S. typhimurium* sickness behaviours could be clarified by using an osmotic pump to deliver an anti-inflammatory drug such as minocycline into the hippocampus of infected mice. Minocycline have been shown to attenuate microglial inflammatory

responses (Henry et al., 2008). To assess whether there is increased permeability of the BBB during *S. typhimurium* infection, tracer studies could be undertaken by injecting fluorescently labelled dextran beads of different molecular weights or Evans blue intravenously shortly before perfusing a mouse at various time-points during the infection and determining the extent of extravasation of the tracer by immunohistochemistry in different regions of the CNS. Similar studies have been performed following systemic inflammation induced by LPS and shown increased extravasation of Evans blue (Lu et al., 2009). These data could then be compared with the prevalence of blood components in the parenchyma which may affect microglial function such as fibrinogen and IgG.

The role the vagus nerve in *S. typhimurium* induced sickness behaviour could be determined by performing a subdiaphragmatic vagotomy on mice several weeks before infection and then performing a range of behavioural assays, including those performed in this thesis and those already mentioned designed to further investigate lethargic/apathetic behaviour, anxiety and memory, and comparing the behavioural response to sham operated mice. Experiments to determine the contribution of infiltrating cells such as monocytes to the CNS response to *S. typhimurium* infection could be undertaken through adoptive transfer of fluorescently labelled monocytes to establish whether any successfully infiltrate the CNS during *S. typhimurium* infection and by using anti-P-selectin antibodies to prevent infiltration if any were detected (D'Mello et al., 2009). Confirming the presence of a robust inflammatory response in the liver and defining the kinetics of cytokine production using this particular strain of *S. typhimurium* could provide useful information about how well liver inflammation correlates with behavioural changes in the brain.

Characterisation of the hypothalamic response to *S. typhimurium* infection, including release of hormones such as corticotrophin releasing hormone, would also add important information regarding the mechanisms underlying *S. typhimurium* sickness behaviour. Experiments to confirm the absence of *S. typhimurium* from the CNS parenchyma would also help to further characterise this model of infection.

To establish the basis of the increased susceptibility of aged mice to coordination and balance deficits one could model the loss of Purkinje neurons that occurs during ageing using diphtheria toxin (Riedel et al., 1990). The

specific depletion of Purkinje neurons would compromise cerebellar circuitry involved with co-ordination and balance, but the mouse would in all other aspects be a young healthy mouse. This would allow one to establish whether the increased susceptibility to co-ordination and balance deficits during infection is due to pre-existing cerebellar pathology in aged mice. A similar toxin based approach could be used to model the effects of vestibular hair cell loss in the cochlea, for example by using an existing genetic model in which mice recombinantly express the gene for diphtheria toxin receptor in the vestibular hair cell specific gene *pou4f3* (Golub et al., 2012). Measurements of conduction velocity in spinal cord white matter tracts would also help to determine the cause of impaired static rod performance during *S. typhimurium* infection. Subjecting mice to the eye blink conditioning test would establish whether there are deficits in the function of cerebellar circuitry following *S. typhimurium* infection (Woodruff-Pak et al., 2010).

## 8.5 Summary

In summary, this thesis has highlighted regional differences in microglial phenotypes in the ageing brain and how they respond to a live systemic bacterial infection or LPS injection. It has also contributed significantly to the characterisation of *S. typhimurium* infection as a model for immune to brain communication and shown that there are significant differences in the behavioural responses to LPS compared to a live bacterial infection. The behavioural effects of *S. typhimurium* infection are prolonged and differentially affect young and aged mice. This work will hopefully provide a platform for further investigations into how immune to brain communication affects the elderly and the heterogeneity of microglia within the young and aged CNS. The most important observations made in this thesis are summarised below in table 8.1.

Chapter(s)	Key point
3	Some aspects of sickness behaviour, e.g. burrowing, are exaggerated in aged mice injected i.p. with 100µg/kg LPS, whereas other aspects e.g. changes in open field activity were comparable between young and aged mice.

3	Aged mice exhibit deficits in co-ordination and balance compared to young mice, but these deficits were not enhanced by LPS injection in these experiments.
4 & 6	Microglial expression of activation markers exhibits differential sensitivity to ageing depending on CNS region. The microglia of the white matter and the cerebellum in particular are more susceptible to age related changes in expression of the markers investigated.
4	Aged mice have a greater acute central cytokine response than young mice to i.p. LPS injection.
5	<i>S. typhimurium</i> causes prolonged changes in behaviour in both young and aged mice, including reduced exploratory activity and possible deficits in memory.
5	Aged mice infected with <i>S. typhimurium</i> exhibited a second phase of weight loss that younger mice did not experience and deficits in their co-ordination and balance, which was unaffected in young mice. The second phase of weight loss in aged mice was associated with decreased food intake.
6	Microglial expression of activation markers increased during <i>S. typhimurium</i> infection, with the microglia of the spinal cord exhibiting the greatest changes in expression.
6	<i>S. typhimurium</i> infection produces a peripheral and central inflammatory response of similar magnitude in the hippocampus of young and aged mice and no measurable response at all in the cerebellum, contrasting to the effects of LPS.
6	BDNF expression was reduced in <i>S. typhimurium</i> infected mice. This reduction in BDNF expression was enhanced in aged mice.
7	Mean paranodal length progressively decreased in SMI-32 positive axons over the course of <i>S. typhimurium</i> infection.
7	<i>S. typhimurium</i> infection caused an increase in the number of SMI-32 positive axons 1 week after infection.

**Table 8.1. A summary table listing the key observations made during this thesis.**



# Appendices

## Appendix 1: Preparation of buffers and solutions.

### A1.1 Fixatives

4% Paraformaldehyde (PFA): Prepared by adding 40g of Paraformaldehyde (Fisher, Loughborough, UK) to 400ml of distilled water heated to 60°C and stirring gently for 3 hours. Once the powder had dissolved and the solution had taken on a milky appearance the solution was cleared by adding 25% NaOH drop by drop. When the solution became clear the volume was topped up to 500ml with distilled water and 500ml of 0.2M phosphate buffer was added to the solution. After stirring the 4% PFA was cooled to 4°C for immediate use or frozen for use at a later date.

Bouin's fixative: 7.5ml of saturated picric acid, 2.5ml of 40% formaldehyde and 0.5ml of glacial acetic acid were mixed and stored at room temperature out of direct light.

### A1.2 Mouse food pellets composition

Standard chow: 5.3% fat (corn oil), 21.2% protein, 49.2% carbohydrate; Special Diet Services, Witham, Essex, UK

High fat: Standard chow diet supplemented 18% (w/w) with animal lard with additional vitamins and minerals, protein and choline [final composition in percentage of grams (w/w): lard 17.8; casein 26.5; choline chloride 0.3; L-cystine 0.4; rice starch 28.3; cellulose 6.1; soya oil 4.3; sucrose 10.4; minerals 4.3; vitamins 1.2; Special Diet Services) (Lanham S.A. et al., 2010)

### A1.3 Immunohistochemistry reagents

DAB Solution: 5ml DAB (Sigma, Poole, UK), 125µl H<sub>2</sub>O<sub>2</sub>, 250ml 0.1M phosphate buffer.

Acid Alcohol: 70% absolute ethanol with 1% conc. HCl

Scott's Tap Water: 0.2% (w/v) potassium bicarbonate, 2% MgSO<sub>4</sub>, in distilled water.

Mowiol mounting medium: 2.4 g of mowiol, 6 g of glycerol, and 6 mL of distilled water were mixed together for 3 h. 12 mL of 0.2 M Tris-Cl (pH 8.5) was then added and the solution incubated with mixing at 50°C for 10 min. The solution was then centrifuged at 5000RCF for 15 min to pellet insoluble material and DABCO added at a final concentration of 2.5% to the solution as an antibleaching agent. The mounting medium was then stored in 500µL aliquots at -20°C.

Gelatinised slides: Slides were washed in 10% Decon in tap water for 15-20 minutes, rinsed in distilled water and dried overnight at 37°C. Slides were then dipped in gelatin solution (500ml distilled water, 2.5g of gelatin and 0.25g chromium potassium sulphate, heated to 40°C) for 30-60s and dried overnight at 37°C.

## A1.4 Buffers

50 x TAE buffer: 242g of tris base was dissolved in 600ml of distilled water. Once the tris had dissolved, 57.1 ml of glacial acetic acid and 100ml of 0.5M EDTA were added to the water and the volume adjusted to 1L with distilled water.

0.2M phosphate buffer: 15.6g sodium dihydrogen orthophosphate in 500ml distilled water made and dissolved separately to 68g Sorenson's Salt (disodium hydrogen orthophosphate dihydrate) in 2L distilled water. Then the two solutions were mixed and brought to pH 7.4 using either 1M NaOH or HCl.

Citrate Buffer: 2.1g citric acid powder in 1L distilled water, brought to pH 6 using NaOH or HCl. The final solution was stored at 4°C.

10x PBS (phosphate buffered saline): 80g NaCl, 2g KCl, 26.8g Na<sub>2</sub>HPO<sub>4</sub>·7H<sub>2</sub>O and 2.4g KH<sub>2</sub>PO<sub>4</sub> were dissolved in 800 ml of distilled water. The volume was then adjusted to 1L with distilled water and the pH of the solution adjusted to 7.4 with HCl or NaOH.

Loading buffer: 47.5ml formamide (95%), 250µL Tris 2M, 100µL of EDTA (0.5M), 1.5ml bromophenol blue (1%) and 1.5ml xylene cyanol were well mixed and stored at +4°C.

## List of References

- Abbas, A.K., Murphy, K.M., Sher, A., 1996. Functional diversity of helper T lymphocytes. *Nature* 383, 787-793.
- Abraham, J., Jang, S., Godbout, J.P., Chen, J., Kelley, K.W., Dantzer, R., Johnson, R.W., 2008. Aging sensitizes mice to behavioral deficits induced by central HIV-1 gp120. *Neurobiology of Aging* 29, 614-621.
- Abraham, J., Johnson, R.W., 2009a. Central inhibition of interleukin-1 beta ameliorates sickness behavior in aged mice. *Brain Behavior and Immunity* 23, 396-401.
- Abraham, J., Johnson, R.W., 2009b. Consuming a Diet Supplemented with Resveratrol Reduced Infection-Related Neuroinflammation and Deficits in Working Memory in Aged Mice. *Rejuvenation Research* 12, 445-453.
- Adamson, J., Lawlor, D.A., Ebrahim, S., 2004. Chronic diseases, locomotor activity limitation and social participation in older women: cross sectional survey of British Women's Heart and Health Study. *Age and Ageing* 33, 293-298.
- Aderem, A., Underhill, D.M., 1999. Mechanisms of phagocytosis in macrophages. *Annual Review of Immunology* 17, 593-623.
- Ajami, B., Bennett, J.L., Krieger, C., Tetzlaff, W., Rossi, F.M.V., 2007. Local self-renewal can sustain CNS microglia maintenance and function throughout adult life. *Nature Neuroscience* 10, 1538-1543.
- Alblas, J., Honing, H., de Lavalette, C.R., Brown, M.H., Dijkstra, C.D., van den Berg, T.K., 2005. Signal regulatory protein alpha ligation induces macrophage nitric oxide production through JAK/STAT- and phosphatidylinositol 3-kinase/Rac1/NAPDH oxidase/H<sub>2</sub>O<sub>2</sub>-dependent pathway. *Molecular and Cellular Biology* 25, 7181-7192.
- Aloisi, F., 2001. Immune function of microglia. *Glia* 36, 165-179.
- Ambrosini, E., Aloisi, F., 2004. Chemokines and glial cells: A complex network in the central nervous system. *Neurochemical Research* 29, 1017-1038.
- Ando, S., Tanaka, Y., Toyoda, Y., Kon, K., 2003. Turnover of myelin lipids in aging brain. *Neurochemical Research* 28, 5-13.
- Aneja, R.K., Tsung, A., Sjodin, H., Geffer, J.V., Delude, R.L., Billiar, T.R., Fink, M.P., 2008. Preconditioning with high mobility group box 1 (HMGB1) induces lipopolysaccharide (LPS) tolerance. *Journal of Leukocyte Biology* 84, 1326-1334.
- Antunes, L.C.M., Arena, E.T., Menendez, A., Han, J., Ferreira, R.B.R., Buckner, M.M.C., Lolic, P., Madilao, L.L., Bohlmann, J., Borchers, C.H., Finlay, B.B., 2011. Impact of Salmonella Infection on Host Hormone Metabolism Revealed by Metabolomics. *Infection and Immunity* 79, 1759-1769.
- Arimoto, T., Bing, G.Y., 2003. Up-regulation of inducible nitric oxide synthase in the substantia nigra by lipopolysaccharide causes microglial activation and neurodegeneration. *Neurobiology of Disease* 12, 35-45.
- Aston-Jones, G., Rogers, J., Shaver, R.D., Dinan, T.G., Moss, D.E., 1985. Age-impaired impulse flow from nucleus basalis to cortex. *Nature* 318, 462-464.
- Austyn, J.M., Gordon, S., 1981. F4-80, a monoclonal-antibody directed specifically against the mouse macrophage. *European Journal of Immunology* 11, 805-815.
- Bachstetter, A.D., Morganti, J.M., Jernberg, J., Schlunk, A., Mitchell, S.H., Brewster, K.W., Hudson, C.E., Cole, M.J., Harrison, J.K., Bickford, P.C., Gemma, C., 2011. Fractalkine and CX(3)CR1 regulate hippocampal neurogenesis in adult and aged rats. *Neurobiology of Aging* 32, 2030-2044.

Bake, S., Friedman, J.A., Sohrabji, F., 2009. Reproductive age-related changes in the blood brain barrier: Expression of IgG and tight junction proteins. *Microvascular Research* 78, 413-424.

Banks, W.A., 2009. Characteristics of compounds that cross the blood-brain barrier. *Bmc Neurology* 9.

Barreto, G., Huang, T.-T., Giffard, R.G., 2010. Age-related Defects in Sensorimotor Activity, Spatial Learning, and Memory in C57BL/6 Mice. *Journal of Neurosurgical Anesthesiology* 22, 214-219.

Barrientos, R.M., Frank, M.G., Hein, A.M., Higgins, E.A., Watkins, L.R., Rudy, J.W., Maier, S.F., 2009a. Time course of hippocampal IL-1 beta and memory consolidation impairments in aging rats following peripheral infection. *Brain Behavior and Immunity* 23, 46-54.

Barrientos, R.M., Higgins, E.A., Biedenkapp, J.C., Sprunger, D.B., Wright-Hardesty, K.J., Watkins, L.R., Rudy, J.W., Maier, S.F., 2006. Peripheral infection and aging interact to impair hippocampal memory consolidation. *Neurobiology of Aging* 27, 723-732.

Barrientos, R.M., Watkins, L.R., Rudy, J.W., Maier, S.F., 2009b. Characterization of the sickness response in young and aging rats following *E. coli* infection. *Brain Behavior and Immunity* 23, 450-454.

Batchelor, P.E., Tan, S., Wills, T.E., Porritt, M.J., Howells, D.W., 2008. Comparison of Inflammation in the Brain and Spinal Cord following Mechanical Injury. *Journal of Neurotrauma* 25, 1217-1225.

Baurle, J., Grussercornehl, U., 1994. Axonal torpedoes in cerebellar purkinje-cells of 2 normal mouse strains during aging. *Acta Neuropathologica* 88, 237-245.

Beal, M.F., Lang, A.E., Ludolph, A., 2005. *Neurodegenerative Diseases*. Cambridge University Press.

Benjamin, W.H., Hall, P., Roberts, S.J., Briles, D.E., 1990. The primary effect of the *ity* locus is on the rate of growth of *Salmonella-typhimurium* that are relatively protected from killing. *Journal of Immunology* 144, 3143-3151.

Berthoud, H.R., Neuhuber, W.L., 2000. Functional and chemical anatomy of the afferent vagal system. *Autonomic Neuroscience-Basic & Clinical* 85, 1-17.

Bette, M., Kaut, O., Schafer, M.K.H., Weihe, E., 2003. Constitutive expression of p55TNFR mRNA and mitogen-specific up-regulation of TNF alpha and p75TNFR mRNA in mouse brain. *Journal of Comparative Neurology* 465, 417-430.

Bhat, M.A., Rios, J.C., Lu, Y., Garcia-Fresco, G.P., Ching, W., St Martin, M., Li, J.J., Einheber, S., Chesler, M., Rosenbluth, J., Salzer, J.L., Bellen, H.J., 2001. Axon-glia interactions and the domain organization of myelinated axons requires Neurexin IV/Caspr/Paranodin. *Neuron* 30, 369-383.

Bhutta, Z.A., 2006. Current concepts in the diagnosis and treatment of typhoid fever. *British Medical Journal* 333, 78-82B.

Bianchi, R., Adami, C., Giambanco, I., Donato, R., 2007. S100B binding to RAGE in microglia stimulates COX-2 expression. *Journal of Leukocyte Biology* 81, 108-118.

Bilbo, S., 2010. Early-life infection is a vulnerability factor for aging-related glial alterations and cognitive decline *Neurobiology of Learning and Memory*.

Bilbo, S.D., Tsang, V., 2010. Enduring consequences of maternal obesity for brain inflammation and behavior of offspring. *Faseb Journal* 24, 2104-2115.

Biswas, S.K., Lopez-Collazo, E., 2009. Endotoxin tolerance: new mechanisms, molecules and clinical significance. *Trends in Immunology* 30, 475-487.

Blank, U., Launay, P., Benhamou, M., Monteiro, R.C., 2009. Inhibitory ITAMs as novel regulators of immunity. *Immunological Reviews* 232, 59-71.

Blouet, C., Jo, Y.H., Li, X., Schwartz, G.J., 2013. Rapid glutamate release in the mediobasal hypothalamus accompanies feeding and is exaggerated by an obesogenic food. *Journal of Neuroscience* 29, 8302-8311.

BlumDegen, D., Muller, T., Kuhn, W., Gerlach, M., Przuntek, H., Riederer, P., 1995. Interleukin-1 beta and interleukin-6 are elevated in the cerebrospinal fluid of Alzheimer's and de novo Parkinson's disease patients. *Neuroscience Letters* 202, 17-20.

Bluthe, R.M., Crestani, F., Kelley, K.W., Dantzer, R., 1992. Mechanisms of the behavioral-effects of interleukin-1 - role of prostaglandins and CRF.

Bluthe, R.M., Laye, S., Michaud, B., Combe, C., Dantzer, R., Parnet, P., 2000a. Role of interleukin-1 beta and tumour necrosis factor-alpha in lipopolysaccharide-induced sickness behaviour: a study with interleukin-1 type I receptor-deficient mice. *European Journal of Neuroscience* 12, 4447-4456.

Bluthe, R.M., Michaud, B., Poli, V., Dantzer, R., 2000b. Role of IL-6 in cytokine-induced sickness behavior: a study with IL-6 deficient mice. *Physiology & behavior* 70, 367-373.

Boche, D., Cunningham, C., Docagne, F., Scotta, H., Perry, V.H., 2006. TGF beta 1 regulates the inflammatory response during chronic neurodegeneration. *Neurobiology of Disease* 22, 638-650.

Boda, E., Pini, A., Hoxha, E., Parolisi, R., Tempia, F., 2009. Selection of Reference Genes for Quantitative Real-time RT-PCR Studies in Mouse Brain. *Journal of Molecular Neuroscience* 37, 238-253.

Borovikova, L.V., Ivanova, S., Zhang, M.H., Yang, H., Botchkina, G.I., Watkins, L.R., Wang, H.C., Abumrad, N., Eaton, J.W., Tracey, K.J., 2000. Vagus nerve stimulation attenuates the systemic inflammatory response to endotoxin. *Nature* 405, 458-462.

Bowley, M.P., Cabral, H., Rosene, D.L., Peters, A., 2010. Age Changes in Myelinated Nerve Fibers of the Cingulate Bundle and Corpus Callosum in the Rhesus Monkey. *Journal of Comparative Neurology* 518, 3046-3064.

Boyle, M.E.T., Berglund, E.O., Murai, K.K., Weber, L., Peles, E., Ranscht, B., 2001. Contactin orchestrates assembly of the septate-like junctions at the paranode in myelinated peripheral nerve. *Neuron* 30, 385-397.

Bramham, C.R., Messaoudi, E., 2005. BDNF function in adult synaptic plasticity: The synaptic consolidation hypothesis. *Progress in Neurobiology* 76, 99-125.

Bretdibat, J.L., Bluthe, R.M., Kent, S., Kelley, K.W., Dantzer, R., 1995. Lipopolysaccharide and interleukin-1 depress food-motivated behavior in mice by a vagal-mediated mechanism. *Brain Behavior and Immunity* 9, 242-246.

Bruunsgaard, H., Pedersen, A.N., Schroll, M., Skinhoj, P., Pedersen, B.K., 1999. Impaired production of proinflammatory cytokines in response to lipopolysaccharide (LPS) stimulation in elderly humans. *Clinical and Experimental Immunology* 118, 235-241.

Bucks, R.S., Gidron, Y., Harris, P., Teeling, J., Wesnes, K.A., Perry, V.H., 2008. Selective effects of upper respiratory tract infection on cognition, mood and emotion processing: A prospective study. *Brain Behavior and Immunity* 22, 399-407.

Buttini, M., Limonta, S., Boddeke, H., 1996. Peripheral administration of lipopolysaccharide induces activation of microglial cells in rat brain. *Neurochemistry International* 29, 25-35.

Buxbaum, J.D., Oishi, M., Chen, H.I., Pinkaskramarski, R., Jaffe, E.A., Gandy, S.E., Greengard, P., 1992. Cholinergic agonists and interleukin-1 regulate processing and secretion of the Alzheimer beta/a4 amyloid protein-precursor. *Proceedings of the National Academy of Sciences of the United States of America* 89, 10075-10078.

Calhoun, M.E., Kurth, D., Phinney, A.L., Long, J.M., Hengemihle, J., Mouton, P.R., Ingram, D.K., Jucker, M., 1998. Hippocampal neuron and synaptophysin-positive bouton number in aging C57BL/6 mice. *Neurobiology of Aging* 19, 599-606.

Campbell, S.J., Wilcockson, D.C., Butchart, A.G., Perry, V.H., Anthony, D.C., 2002. Altered chemokine expression in the spinal cord and brain contributes to differential interleukin-1 beta-induced neutrophil recruitment. *Journal of Neurochemistry* 83, 432-441.

Campisi, J., Hansen, M.K., O'Connor, K.A., Biedenkapp, J.C., Watkins, L.R., Maier, S.F., Fleshner, M., 2003. Circulating cytokines and endotoxin are not necessary for the activation of the sickness or corticosterone response produced by peripheral E-coli challenge. *Journal of Applied Physiology* 95, 1873-1882.

Candelario-Jalil, E., Slawik, H., Ridelis, I., Waschbisch, A., Akundi, R.S., Hull, M., Fiebich, B.L., 2005. Regional distribution of the prostaglandin E-2 receptor EP1 in the rat brain - Accumulation in Purkinje cells of the cerebellum. *Journal of Molecular Neuroscience* 27, 303-310.

Capuron, L., Neuraeter, G., Musselman, D.L., Lawson, D.H., Nemeroff, C.B., Fuchs, D., Miller, A.H., 2003. Interferon-alpha-induced changes in tryptophan metabolism: Relationship to depression and paroxetine treatment. *Biological Psychiatry* 54, 906-914.

Cardona, A.E., Pioro, E.P., Sasse, M.E., Kostenko, V., Cardona, S.M., Dijkstra, I.M., Huang, D.R., Kidd, G., Dombrowski, S., Dutta, R., Lee, J.C., Cook, D.N., Jung, S., Lira, S.A., Littman, D.R., Ransohoff, R.M., 2006. Control of microglial neurotoxicity by the fractalkine receptor. *Nature Neuroscience* 9, 917-924.

Carey, A.N., Lyons, A.M., Shay, C.F., Dunton, O., McLaughlin, J.P., 2009. Endogenous kappa Opioid Activation Mediates Stress-Induced Deficits in Learning and Memory. *Journal of Neuroscience* 29, 4293-4300.

Carola, V., D'Olimpio, F., Brunamonti, E., Mangia, F., Renzi, P., 2002. Evaluation of the elevated plus-maze and open-field tests for the assessment of anxiety-related behaviour in inbred mice. *Behavioural Brain Research* 134, 49-57.

Cavallotti, D., Cavallotti, C., Pescosolido, N., Iannetti, G.D., Pacella, E., 2001. A morphometric study of age changes in the rat optic nerve. *Ophthalmologica* 215, 366-371.

Cerejeira, J., Firmino, H., Vaz-Serra, A., Mukaetova-Ladinska, 2010. The neuroinflammatory hypothesis of delirium. *Acta Neuropathologica*.

Chakravarty, S., Herkenham, M., 2005. Toll-like receptor 4 on nonhematopoietic cells sustains CNS inflammation during endotoxemia, independent of systemic cytokines. *Journal of Neuroscience* 25, 1788-1796.

Chan, D.C., 2006. Mitochondria: Dynamic organelles in disease, aging, and development. *Cell* 125, 1241-1252.

Chang, H.Y., Mashimo, H., Goyal, R.K., 2003. Musings on the wanderer: What's new in our understanding of vago-vagal reflex? IV. Current concepts of vagal efferent projections to the gut. *American Journal of Physiology-Gastrointestinal and Liver Physiology* 284, G357-G366.

Chapman, T.R., Barrientos, R.M., Ahrendsen, J.T., Hoover, J.M., Maier, S.F., Patterson, S.L., 2012. Aging and infection reduce expression of specific brain-derived neurotrophic factor mRNAs in hippocampus. *Neurobiology of Aging* 33.

Chaudhuri, A., 1997. Neural activity mapping with inducible transcription factors. *Neuroreport* 8, R3-R7.

Chaudhuri, A., Behan, P.O., 2000. Fatigue and basal ganglia. *Journal of the Neurological Sciences* 179, 34-42.

Chelvarajan, R.L., Collins, S.M., Van Willigen, J.M., Bondada, S., 2005. The unresponsiveness of aged mice to polysaccharide antigens is a result of a defect in macrophage function. *Journal of Leukocyte Biology* 77, 503-512.

Chen, C., Liu, Y., Liu, Y., Zheng, P., 2009. mTOR Regulation and Therapeutic Rejuvenation of Aging Hematopoietic Stem Cells. *Science Signaling* 2.

Chen, C.Y., Bonham, A.C., Schelegle, E.S., Gershwin, L.J., Plopper, C.G., Joad, J.P., 2001. Extended allergen exposure in asthmatic monkeys induces neuroplasticity in nucleus tractus solitarius. *Journal of Allergy and Clinical Immunology* 108, 557-562.

Chen, J., Buchanan, J.B., Sparkman, N.L., Godbout, J.P., Freund, G.G., Johnson, R.W., 2008. Neuroinflammation and disruption in working memory in aged mice after acute stimulation of the peripheral innate immune system. *Brain Behavior and Immunity* 22, 301-311.

Chen, L., Bao, S.W., Lockard, J.M., Kim, J.J., Thompson, R.F., 1996. Impaired classical eyeblink conditioning in cerebellar-lesioned and Purkinje cell degeneration (pcd) mutant mice. *Journal of Neuroscience* 16, 2829-2838.

Chen, Y., Liu, L., 2012. Modern methods for delivery of drugs across the blood-brain barrier. *Advanced Drug Delivery Reviews* 64, 640-665.

Cho, H.J., Shashkin, P., Gleissner, C.A., Dunson, D., Jain, N., Lee, J.K., Miller, Y., Ley, K., 2007. Induction of dendritic cell-like phenotype in macrophages during foam cell formation. *Physiological Genomics* 29, 149-160.

Choi, D., Zhang, J., Bing, G., 2008. Aging enhances the neuroinflammatory response and  $\alpha$ -synuclein nitration in rats *Neurobiology of Aging*.

Chorinchath, B.B., Kong, L.Y., Mao, L., McCallum, R.E., 1996. Age-associated differences in TNF-alpha and nitric oxide production in endotoxic mice. *Journal of Immunology* 156, 1525-1530.

Clarke, R.M., Lyons, A., O'Connell, F., Deighan, B.F., Barry, C.E., Anyakoha, N.G., Nicolaou, A., Lynch, M.A., 2008. A pivotal role for interleukin-4 in atorvastatin-associated neuroprotection in rat brain. *Journal of Biological Chemistry* 283, 1808-1817.

Colton, C.A., 2009. Heterogeneity of Microglial Activation in the Innate Immune Response in the Brain. *Journal of Neuroimmune Pharmacology* 4.

Colton, C.A., Mott, R.T., Sharpe, H., Xu, Q., Van Nostrand, W.E., Vitek, M.P., 2006. Expression profiles for macrophage alternative activation genes in AD and in mouse models of AD. *Journal of Neuroinflammation* 3.

Conde, J.R., Streit, W.J., 2006. Microglia in the aging brain. *Journal of Neuropathology and Experimental Neurology* 65, 199-203.

Connor, T.J., Song, C., Leonard, B.E., Merali, Z., Anisman, H., 1998. An assessment of the effects of central interleukin-1 beta, -2, -6, and tumor necrosis factor-alpha administration on some behavioural, neurochemical, endocrine and immune parameters in the rat. *Neuroscience* 84, 923-933.

Contet, C., Rawlins, J.N.P., Deacon, R.M.J., 2001. A comparison of 129S2/SvHsd and C57BL/6JO1aHsd mice on a test battery assessing sensorimotor, affective and cognitive behaviours: implications for the study of genetically modified mice. *Behavioural Brain Research* 124, 33-46.

Corona, A.W., Huang, Y., O'Connor, J.C., Dantzer, R., Kelley, K.W., Popovich, P.G., Godbout, J.P., 2010. Fractalkine receptor (CX(3)CR1) deficiency sensitizes mice to the behavioral changes induced by lipopolysaccharide. *Journal of Neuroinflammation* 7.

Cortese, G.P., Barrientos, R.M., Maier, S.F., Patterson, S.L., 2011. Aging and a Peripheral Immune Challenge Interact to Reduce Mature Brain-Derived Neurotrophic Factor and Activation of TrkB, PLC gamma 1, and ERK in Hippocampal Synaptoneurosomes. *Journal of Neuroscience* 31, 4274-4279.

Cribbs, D.H., Berchtold, N.C., Perreau, V., Coleman, P.D., Rogers, J., Tenner, A.J., Cotman, C.W., 2012. Extensive innate immune gene activation accompanies brain aging, increasing vulnerability to cognitive decline and neurodegeneration: a microarray study. *Journal of Neuroinflammation* 9.

Crump, J.A., Luby, S.P., Mintz, E.D., 2004. The global burden of typhoid fever. *Bulletin of the World Health Organization* 82, 346-353.

Cunningham, A.F., Gaspal, F., Serre, K., Mohr, E., Henderson, I.R., Scott-Tucker, A., Kenny, S.M., Khan, M., Toellner, K.-M., Lane, P.J.L., MacLennan, I.C.M., 2007a. Salmonella induces a switched antibody response without germinal centers that impedes the extracellular spread of infection. *Journal of Immunology* 178, 6200-6207.

Cunningham, C., Champion, S., Lunnon, K., Murray, C.L., Woods, J.F.C., Deacon, R.M.J., Rawlins, J.N.P., Perry, V.H., 2009. Systemic Inflammation Induces Acute Behavioral and Cognitive Changes and Accelerates Neurodegenerative Disease. *Biological Psychiatry* 65, 304-312.

Cunningham, C., Champion, S., Teeling, J., Felton, L., Perry, V.H., 2007b. The sickness behaviour and CNS inflammatory mediator profile induced by systemic challenge of mice with synthetic double-stranded RNA (poly I : C). *Brain Behavior and Immunity* 21, 490-502.

Cunningham, C., Wilcockson, D.C., Champion, S., Lunnon, K., Perry, V.H., 2005. Central and systemic endotoxin challenges exacerbate the local inflammatory response and increase neuronal death during chronic neurodegeneration. *Journal of Neuroscience* 25, 9275-9284.

Cunningham, E.T., Wada, E., Carter, D.B., Tracey, D.E., Battey, J.F., Desouza, E.B., 1992. In situ histochemical-localization of type-i interleukin-1 receptor messenger-RNA in the central-nervous-system, pituitary, and adrenal-gland of the mouse. *Journal of Neuroscience* 12, 1101-1114.

D' Mello, C., Riazi, K., Le, T., Stevens, K.M., Wang, A., McKay, D.M., Pittman, Q.J., Swain, M.G., 2013. P-selectin-mediated monocyte-cerebral endothelium adhesive interactions link peripheral organ inflammation to sickness behaviors. *Journal of Neuroscience* 33, 25989-14888.

D'Andrea, M.R., 2003. Evidence linking neuronal cell death to autoimmunity in Alzheimer's disease. *Brain Research* 982, 19-30.

D'Autreaux, B., Toledano, M.B., 2007. ROS as signalling molecules: mechanisms that generate specificity in ROS homeostasis. *Nature Reviews Molecular Cell Biology* 8, 813-824.

D'Mello, C., Le, T., Swain, M.G., 2009. Cerebral Microglia Recruit Monocytes into the Brain in Response to Tumor Necrosis Factor alpha Signaling during Peripheral Organ Inflammation. *Journal of Neuroscience* 29, 2089-2102.

D'Mello, C., Swain, M.G., 2011. Liver-brain inflammation axis. *American Journal of Physiology-Gastrointestinal and Liver Physiology* 301, G749-G761.

Dantzer, R., 2004. Cytokine-induced sickness behaviour: a neuroimmune response to activation of innate immunity. *European Journal of Pharmacology* 500, 399-411.

Dasaraju, P.V., Liu, C., 1996. Infections of the Respiratory System. In: Baron, S. (Ed.), *Medical Microbiology*, 4th edition.

Davalos, D., Grutzendler, J., Yang, G., Kim, J.V., Zuo, Y., Jung, S., Littman, D.R., Dustin, M.L., Gan, W.B., 2005. ATP mediates rapid microglial response to local brain injury in vivo. *Nature Neuroscience* 8, 752-758.

Davalos, D., Ryu, J.K., Merlini, M., Baeten, K.M., Le Moan, N., Petersen, M.A., Deerinck, T.J., Smirnoff, D.S., Bedard, C., Hakozaki, H., Murray, S.G., Ling, J.B., Lassmann, H., Degen, J.L., Ellisman, M.H., Akassoglou, K., 2012. Fibrinogen-

induced perivascular microglial clustering is required for the development of axonal damage in neuroinflammation. *Nature Communications* 3.

Daws, M.R., Sullam, P.M., Niemi, E.C., Chen, T.T., Tchao, N.K., Seaman, W.E., 2003. Pattern recognition by TREM-2: Binding of anionic ligands. *Journal of Immunology* 171, 594-599.

De Haas, A.H., Boddeke, H., Biber, K., 2008. Region-specific expression of immunoregulatory proteins on microglia in the healthy CNS. *Glia* 56, 888-894.

de Lima, M.N., Laranja, D.C., Caldana, F., Bromberg, E., Roesler, R., Schroder, N., 2005. Reversal of age-related deficits in object recognition memory in rats with L-deprenyl. *Experimental Gerontology* 40, 506-511.

de Rooij, S.E., van Munster, B.C., Korevaar, J.C., Levi, M., 2007. Cytokines and acute phase response in delirium. *Journal of Psychosomatic Research* 62, 521-525.

Deacon, R.M.J., 2009. Burrowing: A sensitive behavioural assay, tested in five species of laboratory rodents. *Behavioural Brain Research* 200, 128-133.

Deacon, R.M.J., Croucher, A., Rawlins, J.N.P., 2002. Hippocampal cytotoxic lesion effects on species-typical behaviours in mice. *Behavioural Brain Research* 132, 203-213.

Dei, R., Takeda, A., Niwa, H., Li, M., Nakagomi, Y., Watanabe, M., Inagaki, T., Washimi, Y., Yasuda, Y., Horie, K., Miyata, T., Sobue, G., 2002. Lipid peroxidation and advanced glycation end products in the brain in normal aging and in Alzheimer's disease. *Acta Neuropathologica* 104, 113-122.

del Rey, A., Balschun, D., Wetzel, W., Randolph, A., Besedovsky, H.O., 2013. A cytokine network involving brain-borne IL-1 $\beta$ , IL-1ra, IL-18, IL-6, and TNF $\alpha$  operates during long-term potentiation and learning. *Brain, Behavior, and Immunity*.

Dello Russo, C., Lisi, L., Tringali, G., Navarra, P., 2009. Involvement of mTOR kinase in cytokine-dependent microglial activation and cell proliferation. *Biochemical Pharmacology* 78, 1242-1251.

Denes, A., Ferenczi, S., Halasz, J., Kornyei, Z., Kovacs, K.J., 2008. Role of CX3CR1 (fractalkine receptor) in brain damage and inflammation induced by focal cerebral ischemia in mouse. *Journal of Cerebral Blood Flow and Metabolism* 28, 1707-1721.

Deng, X.H., Bertini, G., Xu, Y.Z., Yan, Z., Bentivoglio, M., 2006. Cytokine-induced activation of glial cells in the mouse brain is enhanced at an advanced age. *Neuroscience* 141, 645-661.

Denieffe, S., Kelly, R.J., McDonald, C., Lyons, A., Lynch, M.A., 2013. Classical activation of microglia in CD200-deficient mice is a consequence of blood brain barrier permeability and infiltration of peripheral cells. *Brain, Behavior, and Immunity* Epub.

di Penta, A., Moreno, B., Reix, S., Fernandez-Diez, B., Villanueva, M., Errea, O., Escala, N., Vandenbroeck, K., Comella, J.X., Villoslada, P., 2013. Oxidative Stress and Proinflammatory Cytokines Contribute to Demyelination and Axonal Damage in a Cerebellar Culture Model of Neuroinflammation. *Plos One* 8.

Dickstein, D.L., Kabaso, D., Rocher, A.B., Luebke, J.I., Wearne, S.L., Hof, P.R., 2007. Changes in the structural complexity of the aged brain. *Aging Cell* 6, 275-284.

DiPatre, P.L., Gelman, B.B., 1997. Microglial cell activation in aging and Alzheimer disease: Partial linkage with neurofibrillary tangle burden in the hippocampus. *Journal of Neuropathology and Experimental Neurology* 56, 143-149.

Diz-Chaves, Y., Pernia, O., Carrero, P., Garcia-Segura, L.M., 2012. Prenatal stress causes alterations in the morphology of microglia and the inflammatory

response of the hippocampus of adult female mice. *Journal of Neuroinflammation* 9.

Dong, L.W., Kong, X.N., Yan, H.X., Yu, L.X., Chen, L., Yang, W., Liu, Q., Huang, D.D., Wu, M.C., Wang, H.Y., 2008. Signal regulatory protein alpha negatively regulates both TLR3 and cytoplasmic pathways in type I interferon induction. *Molecular Immunology* 45, 3025-3035.

Donnini, A., Argentati, K., Mancini, R., Smorlesi, A., Bartozzi, B., Bernardini, G., Provinciali, M., 2002. Phenotype, antigen-presenting capacity, and migration of antigen-presenting cells in young and old age. *Experimental Gerontology* 37, 1097-1112.

Donovan, F.M., Pike, C.J., Cotman, C.W., Cunningham, D.D., 1997. Thrombin induces apoptosis in cultured neurons and astrocytes via a pathway requiring tyrosine kinase and RhoA activities. *Journal of Neuroscience* 17, 5316-5326.

Dougan, G., John, V., Palmer, S., Mastroeni, P., 2011. Immunity to salmonellosis. *Immunological Reviews* 240, 196-210.

Droge, W., Schipper, H.M., 2007. Oxidative stress and aberrant signaling in aging and cognitive decline. *Aging Cell* 6, 361-370.

Eckmann, L., Fierer, J., Kagnoff, M.F., 1996. Genetically resistant (Ity(r)) and susceptible (Ity(s)) congenic mouse strains show similar cytokine responses following infection with *Salmonella dublin*. *Journal of Immunology* 156, 2894-2900.

Edwards, J.P., Zhang, X., Frauwirth, K.A., Mosser, D.M., 2006. Biochemical and functional characterization of three activated macrophage populations. *Journal of Leukocyte Biology* 80, 1298-1307.

Ek, M., Arias, C., Sawchenko, P., Ericsson-Dahlstrand, A., 2000. Distribution of the EP3 prostaglandin E-2 receptor subtype in the rat brain: Relationship to sites of interleukin-1-induced cellular responsiveness. *Journal of Comparative Neurology* 428, 5-19.

Ek, M., Kurosawa, M., Lundberg, T., Ericsson, A., 1998. Activation of vagal afferents after intravenous injection of interleukin-1 beta: Role of endogenous prostaglandins. *Journal of Neuroscience* 18, 9471-9479.

Emborg, M.E., Ma, S.Y., Mufson, E.J., Levey, A.I., Taylor, M.D., Brown, W.D., Holden, J.E., Kordower, J.H., 1998. Age-related declines in nigral neuronal function correlate with motor impairments in rhesus monkeys. *Journal of Comparative Neurology* 401, 253-265.

Engblom, D., Saha, S., Engstrom, L., Westman, M., Audoly, L.P., Jakobsson, P.J., Blomqvist, A., 2003. Microsomal prostaglandin E synthase-1 is the central switch during immune-induced pyresis. *Nature Neuroscience* 6, 1137-1138.

Engelmann, M., Landgraf, R., Wotjak, C.T., 2004. The hypothalamic-neurohypophysial system regulates the hypothalamic-pituitary-adrenal axis under stress: An old concept revisited. *Frontiers in Neuroendocrinology* 25, 132-149.

Erickson, C.A., Barnes, C.A., 2003. The neurobiology of memory changes in normal aging. *Experimental Gerontology* 38, 61-69.

Ericsson, A., Liu, C., Hart, R.P., Sawchenko, P.E., 1995. Type-1 interleukin-1 receptor in the rat-brain - distribution, regulation, and relationship to sites of IL-1-induced cellular activation. *Journal of Comparative Neurology* 361, 681-698.

Evans, D.J., Evans, D.G., 1996. *Escherichia Coli* in Diarrheal Disease. In: Baron, S. (Ed.), *Medical Microbiology*, 4th edition.

Fadok, V.A., Bratton, D.L., Konowal, A., Freed, P.W., Westcott, J.Y., Henson, P.M., 1998. Macrophages that have ingested apoptotic cells in vitro inhibit proinflammatory cytokine production through autocrine/paracrine mechanisms

involving TGF-beta, PGE2, and PAF. *Journal of Clinical Investigation* 101, 890-898.

Faggioni, R., Fantuzzi, G., Villa, P., Buurman, W., Vantits, L.J.H., Ghezzi, P., 1995. Independent down-regulation of central and peripheral tumor-necrosis-factor production as a result of lipopolysaccharide tolerance in mice. *Infection and Immunity* 63, 1473-1477.

Fang, F., Lue, L.F., Yan, S.Q., Xu, H.W., Luddy, J.S., Chen, D., Walker, D.G., Stern, D.M., Yan, S.F., Schmidt, A.M., Chen, J.X., Yan, S.S., 2010. RAGE-dependent signaling in microglia contributes to neuroinflammation, A beta accumulation, and impaired learning/memory in a mouse model of Alzheimer's disease. *Faseb Journal* 24, 1043-1055.

Faraco, G., Pittelli, M., Cavone, L., Fossati, S., Porcu, M., Mascagni, P., Fossati, G., Moroni, F., Chiarugi, A., 2009. Histone deacetylase (HDAC) inhibitors reduce the glial inflammatory response in vitro and in vivo. *Neurobiology of Disease* 36, 269-279.

Farrall, A.J., Wardlaw, J.M., 2009. Blood-brain barrier: Ageing and microvascular disease-systematic review and meta-analysis. *Neurobiology of Aging* 30, 337-352.

Fendrick, S.E., Xue, Q.S., Streit, W.J., 2007. Formation of multinucleated giant cells and microglial degeneration in rats expressing a mutant Cu/Zn superoxide dismutase gene. *Journal of Neuroinflammation* 4.

Fernando, M.S., Simpson, J.E., Matthews, F., Brayne, C., Lewis, C.E., Barber, R., Kalaria, R.N., Forster, G., Esteves, F., Wharton, S.B., Shaw, P.J., O'Brien, J.T., Ince, P.G., Function, M.R.C.C., Ageing Neuropathology Study, G., 2006. White matter lesions in an unselected cohort of the elderly - Molecular pathology suggests origin from chronic hypoperfusion injury. *Stroke* 37, 1391-1398.

Field, R., Champion, S., Warren, C., Murray, C., Cunningham, C., 2010. Systemic challenge with the TLR3 agonist poly I:C induces amplified IFNalpha/beta and IL-1beta responses in the diseased brain and exacerbates chronic neurodegeneration. *Brain Behavior and Immunity*.

Franceschi, C., Capri, M., Monti, D., Giunta, S., Olivieri, F., Sevini, F., Panourai, M.P., Invidia, L., Celani, L., Scurti, M., Cevenini, E., Castellani, G.C., Salvioli, S., 2007. Inflammaging and anti-inflammaging: A systemic perspective on aging and longevity emerged from studies in humans. *Mechanisms of Ageing and Development* 128, 92-105.

Frank, M.G., Barrientos, R.A., Biedenkapp, J.C., Rudy, J.W., Watkins, L.R., Maier, S.F., 2006. mRNA up-regulation of MHC II and pivotal pro-inflammatory genes in normal brain aging. *Neurobiology of Aging* 27, 717-722.

Frank, M.G., Barrientos, R.M., Hein, A.M., Biedenkapp, J.C., Watkins, L.R., Maier, S.F., 2010a. IL-1RA blocks E. coli-induced suppression of Arc and long-term memory in aged F344 x BN F1 rats. *Brain Behavior and Immunity* 24, 254-262.

Frank, M.G., Barrientos, R.M., Watkins, L.R., Maier, S.F., 2010b. Aging sensitizes rapidly isolated hippocampal microglia to LPS ex vivo. *Journal of Neuroimmunology* 226, 181-184.

Frank, M.G., Thompson, B.M., Watkins, L.R., Maier, S.F., 2012. Glucocorticoids mediate stress-induced priming of microglial pro-inflammatory responses. *Brain Behavior and Immunity* 26, 337-345.

Franklin, K.B.J., Paxinos, G., 2008. The mouse brain in stereotaxic coordinates.

Frost, P., Barrientos, R.M., Makino, S., Wong, M.L., Sternberg, E.M., 2001. IL-1 receptor type I gene expression in the amygdala of inflammatory susceptible Lewis and inflammatory resistant Fischer rats. *Journal of Neuroimmunology* 121, 32-39.

Fry, M., Ferguson, A.V., 2007. The sensory circumventricular organs: Brain targets for circulating signals controlling ingestive behavior. *Physiology & behavior* 91, 413-423.

Fujimoto, S., Katsuki, H., Ohnishi, M., Takagi, M., Kume, T., Akaike, A., 2007. Thrombin induces striatal neurotoxicity depending on mitogen-activated protein kinase pathways in vivo. *Neuroscience* 144, 694-701.

Garcia-Fresco, G.P., Sousa, A.D., Pillai, A.M., Moy, S.S., Crawley, J.N., Tessarollo, L., Dupree, J.L., Bhat, M.A., 2006. Disruption of axo-glial junctions causes cytoskeletal disorganization and degeneration of Purkinje neuron axons. *Proceedings of the National Academy of Sciences of the United States of America* 103, 5137-5142.

Gardner, I.D., 1980. The Effect of Aging on Susceptibility to Infection. *Reviews of Infectious Diseases* 2, 801-810.

Gasic-Milenkovic, J., Dukic-Stefanovic, S., Deuther-Conrad, W., Gartner, U., Munch, G., 2003. beta-amyloid peptide potentiates inflammatory responses induced by lipopolysaccharide, interferon-gamma and 'advanced glycation endproducts' in a murine microglia cell line. *European Journal of Neuroscience* 17, 813-821.

Gasser, A., Most, J., 1999. Generation of multinucleated giant cells in vitro by culture of human monocytes with Mycobacterium bovis BCG in combination with cytokine-containing supernatants. *Infection and Immunity* 67, 395-402.

Gaultier, A., Wu, X., Le Moan, N., Takimoto, S., Mukandala, G., Akassoglou, K., Campana, W.M., Gonias, S.L., 2009. Low-density lipoprotein receptor-related protein 1 is an essential receptor for myelin phagocytosis. *Journal of Cell Science* 122, 1155-1162.

Gautron, L., Laye, S., 2009. Neurobiology of inflammation-associated anorexia. *Frontiers in neuroscience* 3, 59-59.

Gaykema, R.P.A., Balachandran, M.K., Godbout, J.P., Johnson, R.W., Goehler, L.E., 2007a. Enhanced neuronal activation in central autonomic network nuclei in aged mice following acute peripheral immune challenge. *Autonomic Neuroscience-Basic & Clinical* 131, 137-142.

Gaykema, R.P.A., Chen, C.-C., Goehler, L.E., 2007b. Organization of immune-responsive medullary projections to the bed nucleus of the stria terminalis, central amygdala, and paraventricular nucleus of the hypothalamus: Evidence for parallel viscerosensory pathways in the rat brain. *Brain Research* 1130, 130-145.

Gaykema, R.P.A., Goehler, L.E., 2009. Lipopolysaccharide challenge-induced suppression of Fos in hypothalamic orexin neurons: Their potential role in sickness behavior. *Brain Behavior and Immunity* 23, 926-930.

Gaykema, R.P.A., Goehler, L.E., 2011. Ascending caudal medullary catecholamine pathways drive sickness-induced deficits in exploratory behavior: Brain substrates for fatigue? *Brain Behavior and Immunity* 25, 443-460.

Geijtenbeek, T.B.H., Gringhuis, S.I., 2009. Signalling through C-type lectin receptors: shaping immune responses. *Nature Reviews Immunology* 9, 465-479.

Gerber, J.S., Mosser, D.M., 2001. Reversing lipopolysaccharide toxicity by ligating the macrophage Fc gamma receptors. *Journal of Immunology* 166, 6861-6868.

Giannella, R.A., 1996. Salmonella. In: Baron, S. (Ed.), *Medical Microbiology*, 4th edition.

Gibb, W.R.G., Lees, A.J., 1988. The Relevance of the Lewy Body to the Pathogenesis of Idiopathic Parkinsons-Disease. *Journal of Neurology Neurosurgery and Psychiatry* 51, 745-752.

Gibbons, H.M., Dragunow, M., 2006. Microglia induce neural cell death via a proximity-dependent mechanism involving nitric oxide. *Brain Research* 1084, 1-15.

Ginhoux, F., Greter, M., Leboeuf, M., Nandi, S., See, P., Gokhan, S., Mehler, M.F., Conway, S.J., Ng, L.G., Stanley, E.R., Samokhvalov, I.M., Merad, M., 2010. Fate Mapping Analysis Reveals That Adult Microglia Derive from Primitive Macrophages. *Science* 330, 841-845.

Gitik, M., Liraz-Zaltsman, S., Oldenborg, P.-A., Reichert, F., Rotshenker, S., 2011a. Myelin down-regulates myelin phagocytosis by microglia and macrophages through interactions between CD47 on myelin and SIRP alpha (signal regulatory protein-alpha) on phagocytes. *Journal of Neuroinflammation* 8.

Gitik, M., Liraz-Zaltsman, S., Oldenborg, P.A., Reichert, F., Rotshenker, S., 2011b. Myelin down-regulates myelin phagocytosis by microglia and macrophages through interactions between CD47 on myelin and SIRP alpha (signal regulatory protein-alpha) on phagocytes. *Journal of Neuroinflammation* 8.

Gloire, G., Legrand-Poels, S., Piette, J., 2006. NF-kappa B activation by reactive oxygen species: Fifteen years later. *Biochemical Pharmacology* 72, 1493-1505.

Godbout, J.P., Berg, G.M., Krzyszton, C., Johnson, R.W., 2005a. alpha-Tocopherol attenuates NF kappa B activation and pro-inflammatory cytokine production in brain and improves recovery from lipopolysaccharide-induced sickness behavior. *Journal of Neuroimmunology* 169, 97-105.

Godbout, J.P., Chen, J., Abraham, J., Richwine, A.F., Berg, B.M., Kelley, K.W., Johnson, R.W., 2005b. Exaggerated neuroinflammation and sickness behavior in aged mice after activation of the peripheral innate immune system. *Faseb Journal* 19, 1329-1331.

Godbout, J.P., Moreau, M., Lestage, J., Chen, J., Sparkman, N.L., Connor, J.O., Castanon, N., Kelley, K.W., Dantzer, R., Johnson, R.W., 2008. Aging exacerbates depressive-like behavior in mice in response to activation of the peripheral innate immune system. *Neuropsychopharmacology* 33, 2341-2351.

Goehler, L.E., Busch, C.R., Tartaglia, N., Relton, J., Sisk, D., Maier, S.F., Watkins, L.R., 1995. Blockade of cytokine induced conditioned taste aversion by subdiaphragmatic vagotomy: further evidence for vagal mediation of immune-brain communication. *Neuroscience Letters* 185, 163-166.

Goehler, L.E., Gaykema, R.P.A., Opitz, N., Reddaway, R., Badr, N., Lyte, M., 2005. Activation in vagal afferents and central autonomic pathways: Early responses to intestinal infection with *Campylobacter jejuni*. *Brain Behavior and Immunity* 19, 334-344.

Goehler, L.E., Park, S.M., Opitz, N., Lyte, M., Gaykema, R.P.A., 2008. *Campylobacter jejuni* infection increases anxiety-like behavior in the holeboard: Possible anatomical substrates for viscerosensory modulation of exploratory behavior. *Brain Behavior and Immunity* 22, 354-366.

Goehler, L.E., Relton, J.K., Dripps, D., Kiechle, R., Tartaglia, N., Maier, S.F., Watkins, L.R., 1997. Vagal paraganglia bind biotinylated interleukin-1 receptor antagonist: A possible mechanism for immune-to-brain communication. *Brain Research Bulletin* 43, 357-364.

Golub, J.S., Tong, L., Ngyuen, T.B., Hume, C.R., Palmiter, R.D., Rubel, E.W., Stone, J.S., 2012. Hair Cell Replacement in Adult Mouse Utricles after Targeted

Ablation of Hair Cells with Diphtheria Toxin. *Journal of Neuroscience* 32, 15093-15105.

Gomez-Pina, V., Soares-Schanoski, A., Rodriguez-Rojas, A., del Fresno, C., Garcia, F., Vallejo-Cremades, M.T., Fernandez-Ruiz, I., Arnalich, F., Fuentes-Prior, P., Lopez-Collazo, E., 2007. Metalloproteinases shed TREM-1 ectodomain from lipopolysaccharide-stimulated human monocytes. *Journal of Immunology* 179, 4065-4073.

Gordon, S., 2003. Alternative activation of macrophages. *Nature Reviews Immunology* 3, 23-35.

Goto, M., 2008. Inflammaging (inflammation + aging): A driving force for human aging based on an evolutionarily antagonistic pleiotropy theory? *Biosci Trends* 2, 218-230.

Goulart, B.K., de Lima, M.N.M., de Farias, C.B., Reolon, G.K., Almeida, V.R., Quevedo, J., Kapczinski, F., Schroeder, N., Roesler, R., 2010. Ketamine impairs recognition memory consolidation and prevents learning-induced increase in hippocampal brain-derived neurotrophic factor levels. *Neuroscience* 167, 969-973.

Gower, R.M., Wu, H., Foster, G.A., Devaraj, S., Jialal, I., Ballantyne, C.M., Knowlton, A.A., Simon, S.I., 2011. CD11c/CD18 Expression Is Upregulated on Blood Monocytes During Hypertriglyceridemia and Enhances Adhesion to Vascular Cell Adhesion Molecule-1. *Arteriosclerosis Thrombosis and Vascular Biology* 31, 160-166.

Graber, D.J., Hickey, W.F., Harris, B.T., 2010. Progressive changes in microglia and macrophages in spinal cord and peripheral nerve in the transgenic rat model of amyotrophic lateral sclerosis. *Journal of Neuroinflammation* 7.

Gracia-Sancho, J., Villarreal, G., Zhang, Y.Z., Garcia-Cardena, G., 2010. Activation of SIRT1 by resveratrol induces KLF2 expression conferring an endothelial vasoprotective phenotype. *Cardiovascular Research* 85, 514-519.

Grant, A.J., Restif, O., McKinley, T.J., Sheppard, M., Maskell, D.J., Mastroeni, P., 2008. Modelling within-host spatiotemporal dynamics of invasive bacterial disease. *Plos Biology* 6, 757-770.

Grillo, M.A., Colombatto, S., 2008. Advanced glycation end-products (AGEs): involvement in aging and in neurodegenerative diseases. *Amino Acids* 35, 29-36.

Grimm, S., Ernst, L., Grötzinger, N., Höhn, A., Breusing, N., Reinheckel, T., Grune, T., 2010. Cathepsin D is one of the major enzymes involved in intracellular degradation of AGE-modified proteins. *Free Radical Research*, online.

Grossberg, A.J., Zhu, X., Leininger, G.M., Levasseur, P.R., Braun, T.P., Myers, M.G., Jr., Marks, D.L., 2011. Inflammation-Induced Lethargy Is Mediated by Suppression of Orexin Neuron Activity. *Journal of Neuroscience* 31, 11376-11386.

Guerreiro, R., Wojtas, A., Bras, J., Carrasquillo, M., Rogaeva, E., Majounie, E., Cruchaga, C., Sassi, C., Kauwe, J.S.K., Younkin, S., Hazrati, L., Collinge, J., Pocock, J., Lashley, T., Williams, J., Lambert, J.-C., Amouyel, P., Goate, A., Rademakers, R., Morgan, K., Powell, J., St George-Hyslop, P., Singleton, A., Hardy, J., Alzheimer Genetic Anal, G., 2013. TREM2 Variants in Alzheimer's Disease. *New England Journal of Medicine* 368, 117-127.

Guglielmotto, M., Aragno, M., Tamagno, E., Vercellinato, I., Visentin, S., Medana, C., Catalano, M.G., Smith, M.A., Perry, G., Danni, O., Boccuzzi, G., Tabaton, M., 2012. AGEs/RAGE complex upregulates BACE1 via NF-kappaB pathway activation. *Neurobiology of Aging* 33.

Guillemin, G.J., Brew, B.J., 2004. Microglia, macrophages, perivascular macrophages, and pericytes: a review of function and identification. *Journal of Leukocyte Biology* 75, 388-397.

Gur, R.C., Turetsky, B.I., Matsui, M., Yan, M., Bilker, W., Hughett, P., Gur, R.E., 1999. Sex differences in brain gray and white matter in healthy young adults: Correlations with cognitive performance. *Journal of Neuroscience* 19, 4065-4072.

Hall, M.N., 2008. mTOR-what does it do? *Transplant Proc* 40, S5-8.

Hallam, K.M., Li, Q., Ananthakrishnan, R., Kalea, A., Zou, Y., Vedantham, S., Schmidt, A.M., Yan, S.F., Ramasamy, R., 2010. Aldose Reductase and AGE-RAGE pathways: central roles in the pathogenesis of vascular dysfunction in aging rats. *Aging Cell* 9, 776-784.

Hamerman, J.A., Jarjoura, V.R., Humphrey, M.B., Nakamura, A.C., Seaman, W.E., Lanier, L.L., 2006. Cutting edge: Inhibition of TLR and FcR responses in macrophages by triggering receptor expressed on myeloid cells (TREM)-2 and DAP12. *Journal of Immunology* 177, 2051-2055.

Hamerman, J.A., Tchao, N.K., Lowell, C.A., Lanier, L.L., 2005. Enhanced Toll-like receptor responses in the absence of signaling adaptor DAP12. *Nature Immunology* 6, 579-586.

Han, M.H., Lundgren, D.H., Jaiswal, S., Chao, M., Graham, K.L., Garris, C.S., Axtell, R.C., Ho, P.P., Lock, C.B., Woodard, J.I., Brownell, S.E., Zoudilova, M., Hunt, J.F.V., Baranzini, S.E., Butcher, E.C., Raine, C.S., Sobel, R.A., Han, D.K., Weissman, I., Steinman, L., 2012. Janus-like opposing roles of CD47 in autoimmune brain inflammation in humans and mice. *Journal of Experimental Medicine* 209, 1325-1334.

Hansen, M., Chandra, A., Mitic, L.L., Onken, B., Driscoll, M., Kenyon, C., 2008. A role for autophagy in the extension of lifespan by dietary restriction in *C. elegans*. *Plos Genetics* 4.

Hansen, M.K., Nguyen, K.T., Fleshner, M., Goehler, L.E., Gaykema, R.P.A., Maier, S.F., Watkins, L.R., 2000a. Effects of vagotomy on serum endotoxin, cytokines, and corticosterone after intraperitoneal lipopolysaccharide. *American Journal of Physiology-Regulatory Integrative and Comparative Physiology* 278, R331-R336.

Hansen, M.K., Nguyen, K.T., Goehler, L.E., Gaykema, R.P.A., Fleshner, M., Maier, S.F., Watkins, L.R., 2000b. Effects of vagotomy on lipopolysaccharide-induced brain interleukin-1 beta protein in rats. *Autonomic Neuroscience-Basic & Clinical* 85, 119-126.

Harden, L.M., du Plessis, I., Poole, S., Laburn, H.P., 2008. Interleukin (IL)-6 and IL-1 beta act synergistically within the brain to induce sickness behavior and fever in rats. *Brain Behavior and Immunity* 22, 838-849.

Harrison, D.E., Strong, R., Sharp, Z.D., Nelson, J.F., Astle, C.M., Flurkey, K., Nadon, N.L., Wilkinson, J.E., Frenkel, K., Carter, C.S., Pahor, M., Javors, M.A., Fernandez, E., Miller, R.A., 2009. Rapamycin fed late in life extends lifespan in genetically heterogeneous mice. *Nature* 460, 392-U108.

Harrison, J.K., Jiang, Y., Chen, S.Z., Xia, Y.Y., Maciejewski, D., McNamara, R.K., Streit, W.J., Salafranca, M.N., Adhikari, S., Thompson, D.A., Botti, P., Bacon, K.B., Feng, L.L., 1998. Role for neuronally derived fractalkine in mediating interactions between neurons and CX3CR1-expressing microglia. *Proceedings of the National Academy of Sciences of the United States of America* 95, 10896-10901.

Hart, A.D., Wyttenbach, A., Perry, V.H., Teeling, J.L., 2012. Age related changes in microglial phenotype vary between CNS regions: Grey versus white matter differences. *Brain Behavior and Immunity* 26, 754-765.

Hart, B.L., 1988. Biological basis of the behavior of sick animals. *Neuroscience and Biobehavioral Reviews* 12, 123-137.

Hatherley, D., Cherwinski, H.M., Moshref, M., Barclay, A.N., 2005. Recombinant CD200 protein does not bind activating proteins closely related to CD200 receptor. *Journal of Immunology* 175, 2469-2474.

Hayashi, Y., Yoshida, M., Yamato, M., Ide, T., Wu, Z., Ochi-Shindou, M., Kanki, T., Kang, D.C., Sunagawa, K., Tsutsui, H., Nakanishi, H., 2008. Reverse of age-dependent memory impairment and mitochondrial DNA damage in microglia by an overexpression of human mitochondrial transcription factor A in mice. *Journal of Neuroscience* 28, 8624-8634.

Haynes, L., Maue, A.C., 2009. Effects of aging on T cell function. *Current Opinion in Immunology* 21, 414-417.

He, Y., Le, W.D., Appel, S.H., 2002. Role of Fc gamma receptors in nigral cell injury induced by Parkinson disease immunoglobulin injection into mouse substantia nigra. *Experimental Neurology* 176, 322-327.

Hefendehl, J.K., Neher, J.J., Sühs, R.B., Kohsaka, S., Skodras, A., Jucker, M., 2013. Homeostatic and injury-induced microglia behavior in the aging brain., *Aging Cell*.

Heijnen, I.A., Van de Winkel, J.G., 1995. A human Fc gamma RI/CD64 transgenic model for in vivo analysis of (bispecific) antibody therapeutics. *Journal of hematotherapy* 4, 351-356.

Hein, A.M., Stutzman, D.L., Bland, S.T., Barrientos, R.M., Watkins, L.R., Rudy, J.W., Maier, S.F., 2007. Prostaglandins are necessary and sufficient to induce contextual fear learning impairments after interleukin-1 beta injections into the dorsal hippocampus. *Neuroscience* 150, 754-763.

Henry, C.J., Huang, Y., Wynne, A., Hanke, M., Himler, J., Bailey, M.T., Sheridan, J.F., Godbout, J.P., 2008. Minocycline attenuates lipopolysaccharide (LPS)-induced neuroinflammation, sickness behavior, and anhedonia. *Journal of Neuroinflammation* 5.

Henry, C.J., Huang, Y., Wynne, A.M., Godbout, J.P., 2009. Peripheral lipopolysaccharide (LPS) challenge promotes microglial hyperactivity in aged mice that is associated with exaggerated induction of both pro-inflammatory IL-1 beta and anti-inflammatory IL-10 cytokines. *Brain Behavior and Immunity* 23, 309-317.

Herrero, C., Marques, L., Lloberas, J., Celada, A., 2001. IFN-gamma-dependent transcription of MHC class II IA is impaired in macrophages from aged mice. *Journal of Clinical Investigation* 107, 485-493.

Hess, J., Ladel, C., Miko, D., Kaufmann, S.H.E., 1996. Salmonella typhimurium aroA(-) infection in gene-targeted immunodeficient mice - Major role of CD4(+) TCR-alpha beta cells and IFN-gamma in bacterial clearance independent of intracellular location. *Journal of Immunology* 156, 3321-3326.

Hinkerohe, D., Smikalla, D., Haghikia, A., Heupel, K., Haase, C.G., Dermietzel, R., Faustmann, P.M., 2005. Effects of cytokines on microglial phenotypes and astroglial coupling in an inflammatory coculture model. *Glia* 52, 85-97.

Hinman, J.D., Duce, J.A., Siman, R.A., Hollander, W., Abraham, C.R., 2004. Activation of calpain-1 in myelin and microglia in the white matter of the aged rhesus monkey. *Journal of Neurochemistry* 89, 430-441.

Hinman, J.D., Peters, A., Cabral, H., Rosene, D.L., Hollander, W., Rasband, M.N., Abraham, C.R., 2006. Age-related molecular reorganization at the node of Ranvier. *Journal of Comparative Neurology* 495, 351-362.

Hodgkinson, C.P., Laxton, R.C., Patel, K., Ye, S., 2008. Advanced Glycation End-Product of Low Density Lipoprotein Activates the Toll-Like 4 Receptor Pathway

Implications for Diabetic Atherosclerosis. *Arteriosclerosis Thrombosis and Vascular Biology* 28, 2275-U2237.

Hoek, R.M., Ruuls, S.R., Murphy, C.A., Wright, G.J., Goddard, R., Zurawski, S.M., Blom, B., Homola, M.E., Streit, W.J., Brown, M.H., Barclay, A.N., Sedgwick, J.D., 2000. Down-regulation of the macrophage lineage through interaction with OX2 (CD200). *Science* 290, 1768-1771.

Hoffmann, W.H., Petit, G., Schulz-Key, H., Taylor, D.W., Bain, O., Le Goff, L., 2000. *Litomosoides sigmodontis* in mice: Reappraisal of an old model for filarial research. *Parasitology Today* 16, 387-389.

Hofmann, M.A., Drury, S., Fu, C.F., Qu, W., Taguchi, A., Lu, Y., Avila, C., Kambham, N., Bierhaus, A., Nawroth, P., Neurath, M.F., Slattery, T., Beach, D., McClary, J., Nagashima, M., Morser, J., Stern, D., Schmidt, A.M., 1999. RAGE mediates a novel proinflammatory axis: A central cell surface receptor for S100/calgranulin polypeptides. *Cell* 97, 889-901.

Hofstetter, H.H., Shive, C.L., Forsthuber, T.G., 2002. Pertussis toxin modulates the immune response to neuroantigens injected in incomplete Freund's adjuvant: Induction of Th1 cells and experimental autoimmune encephalomyelitis in the presence of high frequencies of Th2 cells. *Journal of Immunology* 169, 117-125.

Hoiseth, S.K., Stocker, B.A.D., 1981. Aromatic-dependent salmonella-typhimurium are non-virulent and effective as live vaccines. *Nature* 291, 238-239.

Holmes, C., Cunningham, C., Zotova, E., Woolford, J., Dean, C., Kerr, S., Culliford, D., Perry, V.H., 2009. Systemic inflammation and disease progression in Alzheimer disease. *Neurology* 73, 768-774.

Holmes, C., El-Okli, M., Williams, A.L., Cunningham, C., Wilcockson, D., Perry, V.H., 2003. Systemic infection, interleukin 1 beta, and cognitive decline in Alzheimer's disease. *Journal of Neurology Neurosurgery and Psychiatry* 74, 788-789.

Holness, C.L., Dasilva, R.P., Fawcett, J., Gordon, S., Simmons, D.L., 1993. Macrosialin, a mouse macrophage-restricted glycoprotein, is a member of the LAMP/LGP family. *Journal of Biological Chemistry* 268, 9661-9666.

Hopkins, S.J., 2007. Central nervous system recognition of peripheral inflammation: a neural, hormonal collaboration. *Acta Biomed* 78 Suppl 1, 231-247.

Howell, O.W., Palsler, A., Polito, A., Melrose, S., Zonta, B., Scheiermann, C., Vora, A.J., Brophy, P.J., Reynolds, R., 2006. Disruption of neurofascin localization reveals early changes preceding demyelination and remyelination in multiple sclerosis. *Brain* 129, 3173-3185.

Howell, O.W., Rundle, J.L., Garg, A., Komada, M., Brophy, P.J., Reynolds, R., 2010. Activated Microglia Mediate Axoglial Disruption That Contributes to Axonal Injury in Multiple Sclerosis. *Journal of Neuropathology and Experimental Neurology* 69, 1017-1033.

Howes, R.M., 2006. The free radical fantasy: a panoply of paradoxes. *Ann N Y Acad Sci* 1067, 22-26.

Huang, Y., Henry, C.J., Dantzer, R., Johnson, R.W., Godbout, J.P., 2008. Exaggerated sickness behavior and brain proinflammatory cytokine expression in aged mice in response to intracerebroventricular lipopolysaccharide. *Neurobiology of Aging* 29, 1744-1753.

Hudson, B.I., Kalea, A.Z., Arriero, M.D., Harja, E., Boulanger, E., D'Agati, V., Schmidt, A.M., 2008. Interaction of the RAGE Cytoplasmic Domain with Diaphanous-1 Is Required for Ligand-stimulated Cellular Migration through

Activation of Rac1 and Cdc42. *Journal of Biological Chemistry* 283, 34457-34468.

Huynh, H.K., Dorovinizis, K., 1993. Effects of interferon-gamma on primary cultures of human brain microvessel endothelial-cells. *American Journal of Pathology* 142, 1265-1278.

Jaiswal, S., Jamieson, C.H.M., Pang, W.W., Park, C.Y., Chao, M.P., Majeti, R., Traver, D., van Rooijen, N., Weissman, I.L., 2009. CD47 Is Upregulated on Circulating Hematopoietic Stem Cells and Leukemia Cells to Avoid Phagocytosis. *Cell* 138, 271-285.

Jansen, M., Reinhard, J.F., 1999. Interferon response heterogeneity: activation of a pro-inflammatory response by interferon alpha and beta. A possible basis for diverse responses to interferon beta in MS. *Journal of Leukocyte Biology* 65, 439-443.

Janssens, S., Beyaert, R., 2003. Functional diversity and regulation of different interleukin-1 receptor-associated kinase (IRAK) family members. *Molecular Cell* 11, 293-302.

Jiang, W.P., Swiggard, W.J., Heufler, C., Peng, M., Mirza, A., Steinman, R.M., Nussenzweig, M.C., 1995. The Receptor Dec-205 Expressed by Dendritic Cells and Thymic Epithelial-Cells Is Involved in Antigen-Processing. *Nature* 375, 151-155.

Johnson, J.D., Zimomra, Z.R., Stewart, L.T., 2013. Beta-adrenergic receptor activation primes microglia cytokine production. *Journal of Neuroimmunology* 254, 161-164.

Jurgens, H.A., Amancherla, K., Johnson, R.W., 2012. Influenza Infection Induces Neuroinflammation, Alters Hippocampal Neuron Morphology, and Impairs Cognition in Adult Mice. *Journal of Neuroscience* 32, 3958-3968.

Karperien, A., Ahammer, H., Jelinek, H.F., 2013. Quantitating the subtleties of microglial morphology with fractal analysis. *Frontiers in Cellular Neuroscience* 7.

Kaunzner, U., Miller, M., Gottfried-Blackmore, A., Gal-Toth, J., Felger, J., McEwen, B., Bulloch, K., 2012. Accumulation of resident and peripheral dendritic cells in the aging CNS. *Neurobiology of Aging* 33, 681-693.

Kelley, K.W., O'Connor, J.C., Lawson, M.A., Dantzer, R., Rodriguez-Zas, S.L., McCusker, R.H., 2013. Aging leads to prolonged duration of inflammation-induced depression-like behavior caused by *Bacillus Calmette-Guerin*. *Brain, Behavior, and Immunity* 32, 63-69.

Kennard, J.A., Woodruff-Pak, D.S., 2011. Age sensitivity of behavioral tests and brain substrates of normal aging in mice. *Frontiers in aging neuroscience* 3, 9.

Kent, S., Bluthé, R.M., Dantzer, R., Hardwick, A.J., Kelley, K.W., Rothwell, N.J., Vannice, J.L., 1992. Different Receptor Mechanisms Mediate the Pyrogenic and Behavioral-Effects of Interleukin-1. *Proceedings of the National Academy of Sciences of the United States of America* 89, 9117-9120.

Kettenmann, H., Hanisch, U.-K., Noda, M., Verkhratsky, A., 2011. Physiology of Microglia. *Physiological Reviews* 91, 461-553.

Kimball, A.W., 1954. Short-Cut Formulas for the Exact Partition of  $\chi^2$  in Contingency Tables. *Biometrics* 10, 452-458.

Knopman, D.S., Parisi, J.E., Salviati, A., Floriach-Robert, M., Boeve, B.F., Ivnik, R.J., Smith, G.E., Dickson, D.W., Johnson, K.A., Petersen, L.E., McDonald, W.C., Braak, H., Petersen, R.C., 2003. Neuropathology of cognitively normal elderly. *Journal of Neuropathology and Experimental Neurology* 62, 1087-1095.

Koebnick, H., Grode, L., David, J.R., Rohde, W., Rolph, M.S., Mittrucker, H.W., Kaufmann, S.H.E., 2002. Macrophage migration inhibitory factor (MIF) plays a pivotal role in immunity against *Salmonella typhimurium*. *Proceedings of the*

National Academy of Sciences of the United States of America 99, 13681-13686.

Koistinaho, M., Koistinaho, J., 2002. Role of p38 and p44/42 mitogen-activated protein kinases in microglia. *Glia* 40, 175-183.

Komatsu, M., Waguri, S., Chiba, T., Murata, S., Iwata, J., Tanida, I., Ueno, T., Koike, M., Uchiyama, Y., Kominami, E., Tanaka, K., 2006. Loss of autophagy in the central nervous system causes neurodegeneration in mice. *Nature* 441, 880-884.

Kong, X.N., Yan, H.X., Chen, L., Dong, L.W., Yang, W., Liu, Q., Yu, L.X., Huang, D.D., Liu, S.Q., Liu, H., Wu, M.C., Wang, H.Y., 2007. LPS-induced down-regulation of signal regulatory protein alpha contributes to innate immune activation in macrophages. *Journal of Experimental Medicine* 204, 2719-2731.

Koning, N., Swaab, D.F., Hoek, R.M., Huitinga, I., 2009. Distribution of the Immune Inhibitory Molecules CD200 and CD200R in the Normal Central Nervous System and Multiple Sclerosis Lesions Suggests Neuron-Glia and Glia-Glia Interactions. *Journal of Neuropathology and Experimental Neurology* 68, 159-167.

Konsman, J.P., Luheshi, G.N., Bluthé, R.M., Dantzer, R., 2000a. The vagus nerve mediates behavioural depression, but not fever, in response to peripheral immune signals; a functional anatomical analysis. *European Journal of Neuroscience* 12, 4434-4446.

Konsman, J.P., Tridon, V., Dantzer, R., 2000b. Diffusion and action of intracerebroventricularly injected interleukin-1 in the CNS. *Neuroscience* 101, 957-967.

Kriegstein, A., Alvarez-Buylla, A., 2009. The Glial Nature of Embryonic and Adult Neural Stem Cells. *Annual Review of Neuroscience* 32, 149-184.

Krstic, D., Madhusudan, A., Doehner, J., Vogel, P., Notter, T., Imhof, C., Manalastas, A., Hilfiker, M., Pfister, S., Schwerdel, C., Riether, C., Meyer, U., Knuesel, I., 2012. Systemic immune challenges trigger and drive Alzheimer-like neuropathology in mice. *Journal of Neuroinflammation* 9.

Kugler, S., Bocker, K., Heusipp, G., Greune, L., Kim, K.S., Schmidt, M.A., 2007. Pertussis toxin transiently affects barrier integrity, organelle organization and transmigration of monocytes in a human brain microvascular endothelial cell barrier model. *Cellular Microbiology* 9, 619-632.

Kullberg, S., Aldskogius, H., Ulfhake, B., 2001. Microglial activation, emergence of ED1-expressing cells and clusterin upregulation in the aging rat CNS, with special reference to the spinal cord. *Brain Research* 899, 169-186.

Kumar, H., Kawai, T., Akira, S., 2009a. Pathogen recognition in the innate immune response. *Biochemical Journal* 420, 1-16.

Kumar, H., Kawai, T., Akira, S., 2009b. Toll-like receptors and innate immunity. *Biochem Biophys Res Commun* 388, 621-625.

Kyuhou, S., Kato, N., Gemba, H., 2006. Emergence of endoplasmic reticulum stress and activated microglia in Purkinje cell degeneration mice. *Neuroscience Letters* 396, 91-96.

Lacroix, S., Rivest, S., 1998. Effect of acute systemic inflammatory response and cytokines on the transcription of the genes encoding cyclooxygenase enzymes (COX-1 and COX-2) in the rat brain. *Journal of Neurochemistry* 70, 452-466.

Laflamme, N., Rivest, S., 1999. Effects of systemic immunogenic insults and circulating proinflammatory cytokines on the transcription of the inhibitory factor kappa B alpha within specific cellular populations of the rat brain. *Journal of Neurochemistry* 73, 309-321.

Laflamme, N., Rivest, S., 2001. Toll-like receptor 4: the missing link of the cerebral innate immune response triggered by circulating gram-negative bacterial cell wall components. *Faseb Journal* 15, 155-163.

Laflamme, N., Soucy, G., Rivest, S., 2001. Circulating cell wall components derived from gram-negative, not gram-positive, bacteria cause a profound induction of the gene-encoding Toll-like receptor 2 in the CNS. *Journal of Neurochemistry* 79, 648-657.

Lanham S.A., Roberts C., Hollingworth T., Sreekumar R., Elahi M.M., Cagampang F.R., Hanson M.A., Oreffo R.O.C., 2010. Maternal high-fat diet: effects on offspring bone structure *Osteoporosis International* 21, 1703-1714.

Lawson, L.J., Perry, V.H., Dri, P., Gordon, S., 1990. Heterogeneity in the distribution and morphology of microglia in the normal adult-mouse brain. *Neuroscience* 39, 151-170.

Lawson, L.J., Perry, V.H., Gordon, S., 1992. Turnover of Resident Microglia in the Normal Adult-Mouse Brain. *Neuroscience* 48, 405-415.

Laye, S., Gheusi, G., Cremona, S., Combe, C., Kelley, K., Dantzer, R., Parnet, P., 2000. Endogenous brain IL-1 mediates LPS-induced anorexia and hypothalamic cytokine expression. *American Journal of Physiology-Regulatory Integrative and Comparative Physiology* 279, R93-R98.

Lebourg, E., Lints, F.A., 1984. A longitudinal study of the effects of age on spontaneous locomotor activity in *Drosophila melanogaster*. *Gerontology* 30, 79-86.

Lee, H.Y., Whiteside, M.B., Herkenham, M., 1998. Area postrema removal abolishes stimulatory effects of intravenous interleukin-1 beta on hypothalamic-pituitary-adrenal axis activity and c-fos mRNA in the hypothalamic paraventricular nucleus. *Brain Research Bulletin* 46, 495-503.

Lee, M., Cho, T., Jantaratnotai, N., Wang, Y.T., McGeer, E., McGeer, P.L., 2010. Depletion of GSH in glial cells induces neurotoxicity: relevance to aging and degenerative neurological diseases. *Faseb Journal* 24, 2533-2545.

Lenczowski, M.J.P., Bluthe, R.M., Roth, J., Rees, G.S., Rushforth, D.A., Van Dam, A.M., Tilders, F.J.H., Dantzer, R., Rothwell, N.J., Luheshi, G.N., 1999. Central administration of rat IL-6 induces HPA activation and fever but not sickness behavior in rats. *American Journal of Physiology-Regulatory Integrative and Comparative Physiology* 276, R652-R658.

Li, J.F., Schmidt, A.M., 1997. Characterization and functional analysis of the promoter of RAGE, the receptor for advanced glycation end products. *Journal of Biological Chemistry* 272, 16498-16506.

Li, L., Lu, J., Tay, S.S.W., Moochhala, S.M., He, B.P., 2007. The function of microglia, either neuroprotection or neurotoxicity, is determined by the equilibrium among factors released from activated microglia in vitro. *Brain Research* 1159, 8-17.

Li, Y., Daniel, M., Tollefsbol, T.O., 2011. Epigenetic regulation of caloric restriction in aging. *Bmc Medicine* 9.

Lin, H.H., Faunce, D.E., Stacey, M., Terajewicz, A., Nakamura, T., Zhang-Hoover, J., Kerley, M., Mucenski, M.L., Gordon, S., Stein-Streilein, J., 2005. The macrophage F4/80 receptor is required for the induction of antigen-specific efferent regulatory T cells in peripheral tolerance. *Journal of Experimental Medicine* 201, 1615-1625.

Lin, J.H., Lin, M.T., 1996. Inhibition of nitric oxide synthase or cyclo-oxygenase pathways in organum vasculosum laminae terminalis attenuates interleukin-1 beta fever in rabbits. *Neuroscience Letters* 208, 155-158.

Liu, Y., Hao, W., Letiembre, M., Walter, S., Kulanga, M., Neumann, H., Fassbender, K., 2006. Suppression of microglial inflammatory activity by

myelin phagocytosis: Role of p47-PHOX-mediated generation of reactive oxygen species. *Journal of Neuroscience* 26, 12904-12913.

Lo, W.F., Ong, H., Metcalf, E.S., Soloski, M.J., 1999. T cell responses to gram-negative intracellular bacterial pathogens: A role for CD8(+) T cells in immunity to *Salmonella* infection and the involvement of MHC class Ib molecules. *Journal of Immunology* 162, 5398-5406.

Loane, D.J., Deighan, B.F., Clarke, R.M., Griffin, R.J., Lynch, A.M., Lynch, M.A., 2009. Interleukin-4 mediates the neuroprotective effects of rosiglitazone in the aged brain. *Neurobiology of Aging* 30, 920-931.

Loftis, J.M., Hauser, P., 2004. The phenomenology and treatment of interferon-induced depression. *Journal of Affective Disorders* 82, 175-190.

Long, J.M., Kalehua, A.N., Muth, N.J., Hengemihle, J.M., Jucker, M., Calhoun, M.E., Ingram, D.K., Mouton, P.R., 1998. Stereological estimation of total microglia number in mouse hippocampus. *Journal of Neuroscience Methods* 84, 101-108.

Long, J.M., Mouton, P.R., Jucker, M., Ingram, D.K., 1999. What counts in brain aging? Design-based stereological analysis of cell number. *Journals of Gerontology Series a-Biological Sciences and Medical Sciences* 54, B407-B417.

Lu, B., Pang, P.T., Woo, N.H., 2005. The yin and yang of neurotrophin action. *Nature Reviews Neuroscience* 6, 603-614.

Lu, P.M., Gonzales, C., Chen, Y., Adedoyin, A., Hummel, M., Kennedy, J.D., Whiteside, G.T., 2009. CNS penetration of small molecules following local inflammation, widespread systemic inflammation or direct injury to the nervous system. *Life Sciences* 85, 450-456.

Luheshi, G.N., Stefferl, A., Turnbull, A.V., Dascombe, M.J., Brouwer, S., Hopkins, S.J., Rothwell, N.J., 1997. Febrile response to tissue inflammation involves both peripheral and brain IL-1 and TNF-alpha in the rat. *American Journal of Physiology-Regulatory Integrative and Comparative Physiology* 272, R862-R868.

Lunnon, K., Teeling, J.L., Tutt, A.L., Cragg, M.S., Glennie, M.J., Perry, V.H., 2011. Systemic Inflammation Modulates Fc Receptor Expression on Microglia during Chronic Neurodegeneration. *Journal of Immunology* 186, 7215-7224.

Luth, H.J., Ogunlade, V., Kuhla, B., Kientsch-Engel, R., Stahl, P., Webster, J., Arendt, T., Munch, G., 2005. Age- and stage-dependent accumulation of advanced glycation end products in intracellular deposits in normal and Alzheimer's disease brains. *Cerebral Cortex* 15, 211-220.

Lynch, E.D., Lee, M.K., Morrow, J.E., Welcsh, P.L., Leon, P.E., King, M.C., 1997. Nonsyndromic deafness DFNA1 associated with mutation of a human homolog of the *Drosophila* gene *diaphanous*. *Science* 278, 1315-1318.

Lyons, A., Lynch, A.M., Downer, E.J., Hanley, R., O'Sullivan, J.B., Smith, A., Lynch, M.A., 2009a. Fractalkine-induced activation of the phosphatidylinositol-3 kinase pathway attenuates microglial activation in vivo and in vitro. *Journal of Neurochemistry* 110, 1547-1556.

Lyons, A., McQuillan, K., Deighan, B.F., O'Reilly, J.-A., Downer, E.J., Murphy, A.C., Watson, M., Piazza, A., O'Connell, F., Griffin, R., Mills, K.H.G., Lynch, M.A., 2009b. Decreased neuronal CD200 expression in IL-4-deficient mice results in increased neuroinflammation in response to lipopolysaccharide. *Brain Behavior and Immunity* 23, 1020-1027.

Lyte, M., Li, W., Opitz, N., Gaykema, R.P.A., Goehler, L.E., 2006. Induction of anxiety-like behavior in mice during the initial stages of infection with the agent of murine colonic hyperplasia *Citrobacter rodentium*. *Physiology & behavior* 89, 350-357.

Ma, S.Y., Roytta, M., Collan, Y., Rinne, J.O., 1999. Unbiased morphometrical measurements show loss of pigmented nigral neurones with ageing. *Neuropathology and Applied Neurobiology* 25, 394-399.

Mahad, D.J., Ziabreva, I., Campbell, G., Lax, N., White, K., Hanson, P.S., Lassmann, H., Turnbull, D.M., 2009. Mitochondrial changes within axons in multiple sclerosis. *Brain* 132, 1161-1174.

Majed, H.H., Chandran, S., Niclou, S.P., Nicholas, R.S., Wilkins, A., Wing, M.G., Rhodes, K.E., Spillantini, M.G., Compston, A., 2006. A novel role for Sema3A in neuroprotection from injury mediated by activated microglia. *Journal of Neuroscience* 26, 1730-1738.

Makino, M., Kitano, Y., Komiyama, C., Hirohashi, M., Takasuna, K., 2000. Involvement of central opioid systems in human interferon-alpha induced immobility in the mouse forced swimming test. *British Journal of Pharmacology* 130, 1269-1274.

Mansour, A., Burke, S., Pavlic, R.J., Akil, H., Watson, S.J., 1996. Immunohistochemical localization of the cloned kappa(1), receptor in the rat CNS and pituitary. *Neuroscience* 71, 671-690.

Marner, L., Nyengaard, J.R., Tang, Y., Pakkenberg, B., 2003. Marked loss of myelinated nerve fibers in the human brain with age. *Journal of Comparative Neurology* 462, 144-152.

Martinez-Barricarte, R., Heurich, M., Valdes-Canedo, F., Vazquez-Martul, E., Torreira, E., Montes, T., Tortajada, A., Pinto, S., Lopez-Trascasa, M., Morgan, B.P., Llorca, O., Harris, C.L., Rodriguez de Cordoba, S., 2010. Human C3 mutation reveals a mechanism of dense deposit disease pathogenesis and provides insights into complement activation and regulation. *Journal of Clinical Investigation* 120, 3702-3712.

Martinowich, K., Cardinale, K.M., Schloesser, R.J., Hsu, M., Greig, N.H., Manji, H.K., 2012. Acetylcholinesterase inhibition ameliorates deficits in motivational drive. *Behavioral and Brain Functions* 8.

Marvel, F.A., Chen, C.C., Badr, N., Gaykema, R.P.A., Goehler, L.E., 2004. Reversible inactivation of the dorsal vagal complex blocks lipopolysaccharide-induced social withdrawal and c-Fos expression in central autonomic nuclei. *Brain Behavior and Immunity* 18, 123-134.

Mastroeni, P., Grant, A., Restif, O., Maskell, D., 2009. A dynamic view of the spread and intracellular distribution of *Salmonella enterica*. *Nature Reviews Microbiology* 7, 73-80.

Mastroeni, P., Harrison, J.A., Robinson, J.H., Clare, S., Khan, S., Maskell, D.J., Dougan, G., Hormaeche, C.E., 1998. Interleukin-12 is required for control of the growth of attenuated aromatic- compound-dependent salmonellae in BALB/c mice: Role of gamma interferon and macrophage activation. *Infection and Immunity* 66, 4767-4776.

Mastroeni, P., Villarrealramos, B., Hormaeche, C.E., 1992. Role of T-cells, TNF-alpha and IFN-gamma in recall of immunity to oral challenge with virulent salmonellae in mice vaccinated with live attenuated aro-salmonella vaccines. *Microbial Pathogenesis* 13, 477-491.

Matozaki, T., Murata, Y., Okazawa, H., Ohnishi, H., 2009. Functions and molecular mechanisms of the CD47-SIRP alpha signalling pathway. *Trends in Cell Biology* 19, 72-80.

Mayhan, W.G., 2002. Cellular mechanisms by which tumor necrosis factor-alpha produces disruption of the blood-brain barrier. *Brain Research* 927, 144-152.

Mazarati, A., Maroso, M., Iori, V., Vezzani, A., Carli, M., 2011. High-mobility group box-1 impairs memory in mice through both toll-like receptor 4 and

Receptor for Advanced Glycation End Products. *Experimental Neurology* 232, 143-148.

McGeer, P.L., Itagaki, S., Boyes, B.E., McGeer, E.G., 1988. Reactive Microglia Are Positive for Hla-Dr in the Substantia Nigra of Parkinsons and Alzheimers-Disease Brains. *Neurology* 38, 1285-1291.

McLinden, K., Kranjac, D., Deodati, L., Kahn, M., Chumley, M., Boehm, G., 2012. Age exacerbates sickness behavior following exposure to a viral mimetic. *Physiology & behavior* 105, 1219-1225.

McMurray, D.N., 1996. Mycobacteria and Nocardia. In: Baron, S. (Ed.), *Medical Microbiology*, 4th edition.

McQuaid, S., Cunnea, P., McMahan, J., Fitzgerald, U., 2009. The effects of blood-brain barrier disruption on glial cell function in multiple sclerosis. *Biochemical Society Transactions* 37, 329-331.

McSorley, S.J., Jenkins, M.K., 2000. Antibody is required for protection against virulent but not attenuated *Salmonella enterica* serovar typhimurium. *Infection and Immunity* 68, 3344-3348.

Medvedev, Z.A., 1990. An attempt at a rational classification of theories of ageing. *Biological Reviews of the Cambridge Philosophical Society* 65, 375-398.

Medvedik, O., Lamming, D.W., Kim, K.D., Sinclair, D.A., 2007. mTORC2 and mTORC1 link calorie restriction and TOR to sirtuin-mediated lifespan extension in *Saccharomyces cerevisiae*. *Plos Biology* 5, 2330-2341.

Mehr, R., Melamed, D., 2011. Reversing B cell aging. *Aging-Us* 3, 438-443.

Meuth, S.G., Simon, O.J., Gnim, A., Melzer, N., Herrmann, A.M., Spitzer, P., Landgraf, P., Wiendl, H., 2008. CNS inflammation and neuronal degeneration is aggravated by impaired CD200-CD200R-mediated macrophage silencing. *Journal of Neuroimmunology* 194, 62-69.

Mevorach, D., Mascarenhas, J.O., Gershov, D., Elkon, K.B., 1998. Complement-dependent clearance of apoptotic cells by human macrophages. *Journal of Experimental Medicine* 188, 2313-2320.

Michels, A.A., Robitaille, A.M., Buczynski-Ruchonnet, D., Hodroj, W., Reina, J.H., Hall, M.N., Hernandez, N., 2010. mTORC1 Directly Phosphorylates and Regulates Human MAF1. *Molecular and Cellular Biology* 30, 3749-3757.

Mihrshahi, R., Barclay, A.N., Brown, M.H., 2009. Essential Roles for Dok2 and RasGAP in CD200 Receptor-Mediated Regulation of Human Myeloid Cells. *Journal of Immunology* 183, 4879-4886.

Mildner, A., Schlevogt, B., Kierdorf, K., Boettcher, C., Erny, D., Kummer, M.P., Quinn, M., Brueck, W., Bechmann, I., Heneka, M.T., Priller, J., Prinz, M., 2011. Distinct and Non-Redundant Roles of Microglia and Myeloid Subsets in Mouse Models of Alzheimer's Disease. *Journal of Neuroscience* 31, 11159-11171.

Mildner, A., Schmidt, H., Nitsche, M., Merkler, D., Hanisch, U.K., Mack, M., Heikenwalder, M., Bruck, W., Priller, J., Prinz, M., 2007. Microglia in the adult brain arise from Ly-6C(hi)CCR2(+) monocytes only under defined host conditions. *Nature Neuroscience* 10, 1544-1553.

Miller, N.E., 1964. Some psychophysiological studies of motivation and of the behavioural effects of illness. *Bulletin of the British Psychological Society* 17, 1-20.

Mittelbronn, M., Dietz, K., Schluesener, H.J., Meyermann, R., 2001. Local distribution of microglia in the normal adult human central nervous system differs by up to one order of magnitude. *Acta Neuropathologica* 101, 249-255.

Mittrucker, H.W., Kaufmann, S.H.E., 2000. Immune response to infection with *Salmonella typhimurium* in mice. *Journal of Leukocyte Biology* 67, 457-463.

Mittrucker, H.W., Raupach, B., Kohler, A., Kaufmann, S.H.E., 2000. Cutting edge: Role of B lymphocytes in protective immunity against *Salmonella typhimurium* infection. *Journal of Immunology* 164, 1648-1652.

Mizuno, T., Kawanokuchi, J., Numata, K., Suzumura, A., 2003. Production and neuroprotective functions of fractalkine in the central nervous system. *Brain Research* 979, 65-70.

Morales, F.R., Boxer, P.A., Fung, S.J., Chase, M.H., 1987. Basic electrophysiological properties of spinal cord motoneurons during old age in the cat. *Journal of Neurophysiology* 58, 180-194.

Moreau, M., Andre, C., O'Connor, J.C., Dumich, S.A., Woods, J.A., Kelley, K.W., Dantzer, R., Lestage, J., Castanon, N., 2008. Inoculation of *Bacillus Calmette-Guerin* to mice induces an acute episode of sickness behavior followed by chronic depressive-like behavior. *Brain Behavior and Immunity* 22, 1087-1095.

Moreau, M., Lestage, J., Verrier, D., Mormede, C., Kelley, K.W., Dantzer, R., Castanon, N., 2005. Bacille Calmette-Guerin inoculation induces chronic activation of peripheral and brain indoleamine 2,3-dioxygenase in mice. *Journal of Infectious Diseases* 192, 537-544.

Morita, S., Miyata, S., 2012. Different vascular permeability between the sensory and secretory circumventricular organs of adult mouse brain. *Cell and Tissue Research* 349, 589-603.

Mott, R.T., Ait-Ghezala, G., Town, T., Mori, T., Vendrame, M., Zeng, J., Ehrhart, J., Mullan, M., Tan, J., 2004. Neuronal expression of CD22: Novel mechanism for inhibiting microglial proinflammatory cytokine production. *Glia* 46, 369-379.

Mouton, P., Kelley-Bell, B., Tweedie, D., Spangler, E., Perez, E., Carlson, O., Short, R., Decabo, R., Chang, J., Ingram, D., Li, Y., Greig, N., 2012. The effects of age and lipopolysaccharide (LPS)-mediated peripheral inflammation on numbers of central catecholaminergic neurons. *Neurobiology of Aging* 33.

Müller, T., Blum-Degen, D., Przuntek, H., Kuhn, W., 1998. Short communication Interleukin-6 levels in cerebrospinal fluid inversely correlate to severity of Parkinson's disease. *Acta Neurologica Scandinavica* 98, 142-144.

Munari, P.F., De Caro, R., Colletti, D., 1989. Anatomy of the optic nerve in elderly men. *Metabolic, pediatric, and systemic ophthalmology* (New York, N.Y. : 1985) 12, 13-16.

Naj, A.C., Jun, G., Beecham, G.W., Wang, L.-S., Vardarajan, B.N., Buross, J., Gallins, P.J., Buxbaum, J.D., Jarvik, G.P., Crane, P.K., Larson, E.B., Bird, T.D., Boeve, B.F., Graff-Radford, N.R., De Jager, P.L., Evans, D., Schneider, J.A., Carrasquillo, M.M., Ertekin-Taner, N., Younkin, S.G., Cruchaga, C., Kauwe, J.S.K., Nowotny, P., Kramer, P., Hardy, J., Huentelman, M.J., Myers, A.J., Barmada, M.M., Demirci, F.Y., Baldwin, C.T., Green, R.C., Rogaeve, E., St George-Hyslop, P., Arnold, S.E., Barber, R., Beach, T., Bigio, E.H., Bowen, J.D., Boxer, A., Burke, J.R., Cairns, N.J., Carlson, C.S., Carney, R.M., Carroll, S.L., Chui, H.C., Clark, D.G., Corneveaux, J., Cotman, C.W., Cummings, J.L., DeCarli, C., DeKosky, S.T., Diaz-Arrastia, R., Dick, M., Dickson, D.W., Ellis, W.G., Faber, K.M., Fallon, K.B., Farlow, M.R., Ferris, S., Frosch, M.P., Galasko, D.R., Ganguli, M., Gearing, M., Geschwind, D.H., Ghetti, B., Gilbert, J.R., Gilman, S., Giordani, B., Glass, J.D., Growdon, J.H., Hamilton, R.L., Harrell, L.E., Head, E., Honig, L.S., Hulette, C.M., Hyman, B.T., Jicha, G.A., Jin, L.-W., Johnson, N., Karlawish, J., Karydas, A., Kaye, J.A., Kim, R., Koo, E.H., Kowall, N.W., Lah, J.J., Levey, A.I., Lieberman, A.P., Lopez, O.L., Mack, W.J., Marson, D.C., Martiniuk, F., Mash, D.C., Masliah, E., McCormick, W.C., McCurry, S.M., McDavid, A.N., McKee, A.C., Mesulam, M., Miller, B.L., Miller, C.A., Miller, J.W., Parisi, J.E., Perl, D.P., Peskind, E., Petersen, R.C., Poon, W.W., Quinn, J.F., Rajbhandary, R.A., Raskind, M.,

Reisberg, B., Ringman, J.M., Roberson, E.D., Rosenberg, R.N., Sano, M., Schneider, L.S., Seeley, W., Shelanski, M.L., Slifer, M.A., Smith, C.D., Sonnen, J.A., Spina, S., Stern, R.A., Tanzi, R.E., Trojanowski, J.Q., Troncoso, J.C., Van Deerlin, V.M., Vinters, H.V., Vonsattel, J.P., Weintraub, S., Welsh-Bohmer, K.A., Williamson, J., Woltjer, R.L., Cantwell, L.B., Dombroski, B.A., Beekly, D., Lunetta, K.L., Martin, E.R., Kamboh, M.I., Saykin, A.J., Reiman, E.M., Bennett, D.A., Morris, J.C., Montine, T.J., Goate, A.M., Blacker, D., Tsuang, D.W., Hakonarson, H., Kukull, W.A., Foroud, T.M., Haines, J.L., Mayeux, R., Pericak-Vance, M.A., Farrer, L.A., Schellenberg, G.D., 2011. Common variants at MS4A4/MS4A6E, CD2AP, CD33 and EPHA1 are associated with late-onset Alzheimer's disease. *Nature Genetics* 43, 436-+.

Nakamura, K., Kaneko, T., Yamashita, Y., Hasegawa, H., Katoh, H., Negishi, M., 2000. Immunohistochemical localization of prostaglandin EP3 receptor in the rat nervous system. *Journal of Comparative Neurology* 421, 543-569.

Nauta, A.J., Trouw, L.A., Daha, M.R., Tijisma, O., Nieuwland, R., Schwaeble, W.J., Gingras, A.R., Mantovani, A., Hack, E.C., Roos, A., 2002. Direct binding of C1q to apoptotic cells and cell blebs induces complement activation. *European Journal of Immunology* 32, 1726-1736.

Neel, B.G., Gu, H.H., Pao, L., 2003. The 'Shp'ing news: SH2 domain-containing tyrosine phosphatases in cell signaling. *Trends in Biochemical Sciences* 28, 284-293.

Neher, J.J., Neniskyte, U., Zhao, J.-W., Bal-Price, A., Tolkovsky, A.M., Brown, G.C., 2011. Inhibition of Microglial Phagocytosis Is Sufficient To Prevent Inflammatory Neuronal Death. *Journal of Immunology* 186, 4973-4983.

Neumann, A., Schinzel, R., Palm, D., Riederer, P., Munch, G., 1999. High molecular weight hyaluronic acid inhibits advanced glycation endproduct-induced NF-kappa B activation and cytokine expression. *Febs Letters* 453, 283-287.

Neumann, H., Takahashi, K., 2007. Essential role of the microglial triggering receptor expressed on myeloid cells-2 (TREM2) for central nervous tissue immune homeostasis. *Journal of Neuroimmunology* 184, 92-99.

Nguyen, M.D., D'Aigle, T., Gowing, G.V., Julien, J.P., Rivest, S., 2004. Exacerbation of motor neuron disease by chronic stimulation of innate immunity in a mouse model of amyotrophic lateral sclerosis. *Journal of Neuroscience* 24, 1340-1349.

Nikic, I., Merkler, D., Sorbara, C., Brinkoetter, M., Kreutzfeldt, M., Bareyre, F.M., Brueck, W., Bishop, D., Misgeld, T., Kerschensteiner, M., 2011. A reversible form of axon damage in experimental autoimmune encephalomyelitis and multiple sclerosis. *Nature Medicine* 17, 495-U135.

Nimmerjahn, A., Kirchhoff, F., Helmchen, F., 2005. Resting microglial cells are highly dynamic surveillants of brain parenchyma in vivo. *Science* 308, 1314-1318.

Nimmerjahn, F., Ravetch, J.V., 2006. Fc gamma receptors: Old friends and new family members. *Immunity* 24, 19-28.

Nishimura, A., Ueda, S., Takeuchi, Y., Matsushita, H., Sawada, T., Kawata, M., 1998. Vulnerability to aging in the rat serotonergic system. *Acta Neuropathologica* 96, 581-595.

Nitti, M., Furfaro, A.L., Traverso, N., Odetti, P., Storace, D., Cottalasso, D., Pronzato, M.A., Marinari, U.M., Domenicotti, C., 2007. PKC delta and NADPH oxidase in AGE-induced neuronal death. *Neuroscience Letters* 416, 261-265.

Njie, E.G., Boelen, E., Stassen, F.R., Steinbusch, H.W., Borchelt, D.R., Streit, W.J., 2010. Ex vivo cultures of microglia from young and aged rodent brain reveal age-related changes in microglial function. *Neurobiology of Aging* 33.

O'Brien, A.D., Scher, I., Campbell, G.H., Macdermott, R.P., Formal, S.B., 1979. Susceptibility of cba-n mice to infection with salmonella-typhimurium - influence of the x-linked gene controlling lymphocyte-b function. *Journal of Immunology* 123, 720-724.

O'Connor, J.C., Andre, C., Wang, Y., Lawson, M.A., Szegedi, S.S., Lestage, J., Castanon, N., Kelley, K.W., Dantzer, R., 2009a. Interferon-gamma and Tumor Necrosis Factor-alpha Mediate the Upregulation of Indoleamine 2,3-Dioxygenase and the Induction of Depressive-Like Behavior in Mice in Response to Bacillus Calmette-Guerin. *Journal of Neuroscience* 29, 4200-4209.

O'Connor, J.C., Andre, C., Wang, Y.X., Lawson, M.A., Szegedi, S.S., Lestage, J., Castanon, N., Kelley, K.W., Dantzer, R., 2009b. Interferon-gamma and Tumor Necrosis Factor-alpha Mediate the Upregulation of Indoleamine 2,3-Dioxygenase and the Induction of Depressive-Like Behavior in Mice in Response to Bacillus Calmette-Guerin. *Journal of Neuroscience* 29, 4200-4209.

O'Connor, J.C., Lawson, M.A., Andre, C., Briley, E.M., Szegedi, S.S., Lestage, J., Castanon, N., Herkenham, M., Dantzer, R., Kelley, K.W., 2009c. Induction ofIDO by Bacille Calmette-Guerin Is Responsible for Development of Murine Depressive-Like Behavior. *Journal of Immunology* 182, 3202-3212.

O'Connor, J.C., Lawson, M.A., Andre, C., Moreau, M., Lestage, J., Castanon, N., Kelley, K.W., Dantzer, R., 2009d. Lipopolysaccharide-induced depressive-like behavior is mediated by indoleamine 2,3-dioxygenase activation in mice. *Molecular Psychiatry* 14, 511-522.

Ogura, K., Ogawa, M., Yoshida, M., 1994. Effects of aging on microglia in the normal rat brain - immunohistochemical observations. *Neuroreport* 5, 1224-1226.

Ohashi, K., Burkart, V., Flohe, S., Kolb, H., 2000. Heat shock protein 60 is a putative endogenous ligand of the toll-like receptor-4 complex. *Journal of Immunology* 164, 558-561.

Ohm, T.G., Busch, C., Bohl, J., 1997. Unbiased estimation of neuronal numbers in the human nucleus coeruleus during aging. *Neurobiology of Aging* 18, 393-399.

Oka, T., Oka, K., Scammell, T.E., Lee, C., Kelly, J.F., Nantel, F., Elmquist, J.K., Saper, C.B., 2000. Relationship of EP1-4 prostaglandin receptors with rat hypothalamic cell groups involved in lipopolysaccharide fever responses. *Journal of Comparative Neurology* 428, 20-32.

Okazawa, H., Motegi, S.I., Ohyama, N., Ohnishi, H., Tomizawa, T., Kaneko, Y., Oldenborg, P.A., Ishikawa, O., Matozaki, T., 2005. Negative regulation of phagocytosis in macrophages by the CD47-SHPS-1 system. *Journal of Immunology* 174, 2004-2011.

Oliveira, A.M.M., Hawk, J.D., Abel, T., Havekes, R., 2010. Post-training reversible inactivation of the hippocampus enhances novel object recognition memory. *Learn. Mem.* 17, 155-160.

Orr, P.T., Rubin, A.J., Fan, L., Kent, B.A., Frick, K.M., 2012. The progesterone-induced enhancement of object recognition memory consolidation involves activation of the extracellular signal-regulated kinase (ERK) and mammalian target of rapamycin (mTOR) pathways in the dorsal hippocampus. *Hormones and Behavior* 61, 487-495.

Pack, M., Trumpfheller, C., Thomas, D., Park, C.G., Granelli-Piperno, A., Muenz, C., Steinman, R.M., 2008. DEC-205/CD205(+) dendritic cells are abundant in the white pulp of the human spleen, including the border region between the red and white pulp. *Immunology* 123, 438-446.

Pakkenberg, B., Gundersen, H.J.G., 1997. Neocortical neuron number in humans: Effect of sex and age. *Journal of Comparative Neurology* 384, 312-320.

Palin, K., Cunningham, C., Forse, P., Perry, V.H., Platt, N., 2008. Systemic inflammation switches the inflammatory cytokine profile in CNS Wallerian degeneration. *Neurobiology of Disease* 30, 19-29.

Pangburn, M.K., Morrison, D.C., Schreiber, R.D., Mullereberhard, H.J., 1980. Activation of the alternative complement pathway: recognition of surface structures on activators by bound C3b. *Journal of Immunology* 124, 977-982.

Parajuli, B., Sonobe, Y., Kawanokuchi, J., Doi, Y., Noda, M., Takeuchi, H., Mizuno, T., Suzumura, A., 2012. GM-CSF increases LPS-induced production of proinflammatory mediators via upregulation of TLR4 and CD14 in murine microglia. *Journal of Neuroinflammation* 9.

Park, K.W., Baik, H.H., Jin, B.K., 2009. IL-13-Induced Oxidative Stress via Microglial NADPH Oxidase Contributes to Death of Hippocampal Neurons In Vivo. *Journal of Immunology* 183, 4666-4674.

Paturi, S., Gutta, A.K., Katta, A., Kakarla, S.K., Arvapalli, R.K., Gadde, M.K., Nalabotu, S.K., Rice, K.M., Wu, M.Z., Blough, E., 2010. Effects of aging and gender on muscle mass and regulation of Akt-mTOR-p70s6k related signaling in the F344BN rat model. *Mechanisms of Ageing and Development* 131, 202-209.

Paul, W.E., 2008. *Fundamental Immunology*.

Pawate, S., Shen, Q., Fan, F., Bhat, N.R., 2004. Redox regulation of glial inflammatory response to lipopolysaccharide and interferon gamma. *Journal of Neuroscience Research* 77, 540-551.

Pecchi, E., Dallaporta, M., Thirion, S., Salvat, C., Berenbaum, F., Jean, A., Troadec, J.D., 2006. Involvement of central microsomal prostaglandin E synthase-1 in IL-1 beta-induced anorexia. *Physiological Genomics* 25, 485-492.

Pelegri, C., Canudas, A.M., del Valle, J., Casadesus, G., Smith, M.A., Camins, A., Pallas, M., Vilaplana, J., 2007. Increased permeability of blood-brain barrier on the hippocampus of a murine model of senescence. *Mechanisms of Ageing and Development* 128, 522-528.

Perez-Perez, G.I., Blaser, M.J., 1996. *Campylobacter and Helicobacter*. In: Baron, S. (Ed.), *Medical Microbiology*, 4th edition.

Perry, V.H., Cunningham, C., Holmes, C., 2007. Systemic infections and inflammation affect chronic neurodegeneration. *Nature Reviews Immunology* 7, 161-167.

Perry, V.H., Matyszak, M.K., Fearn, S., 1993. Altered Antigen Expression of Microglia in the Aged Rodent Cns. *Glia* 7, 60-67.

Peruzzo, B., Pastor, F.E., Blazquez, J.L., Schobitz, K., Pelaez, B., Amat, P., Rodriguez, E.M., 2000. A second look at the barriers of the medial basal hypothalamus. *Experimental Brain Research* 132, 10-26.

Pesce, C., Reale, A., 1987. Aging and the nerve-cell population of the putamen - a morphometric study. *Clinical Neuropathology* 6, 16-18.

Peters, A., Sethares, C., 2013. Normal myelinated nerve fibres. The fine structure of the aging brain. Boston University School of Medicine.

Peters, A., Sethares, C., Moss, M.B., 2010. How the Primate Fornix Is Affected by Age. *Journal of Comparative Neurology* 518, 3962-3980.

Peterson, J.W., 1996. *Bacterial Pathogenesis*. In: Baron, S. (Ed.), *Medical Microbiology*, 4th Edition.

Phillips, L.M., Lampson, L.A., 1999. Site-specific control of T cell traffic in the brain: T cell entry to brainstem vs. hippocampus after local injection of IFN-gamma. *Journal of Neuroimmunology* 96, 218-227.

Phillips, L.M., Simon, P.J., Lampson, L.A., 1999. Site-specific immune regulation in the brain: Differential modulation of major histocompatibility complex (MHC) proteins in brainstem vs. hippocampus. *Journal of Comparative Neurology* 405, 322-333.

Piccio, L., Buonsanti, C., Cella, M., Tassi, I., Schmidt, R.E., Fenoglio, C., Rinker, J., Naismith, R.T., Panina-Bordignon, P., Passini, N., Galimberti, D., Scarpini, E., Colonna, M., Cross, A.H., 2008. Identification of soluble TREM-2 in the cerebrospinal fluid and its association with multiple sclerosis and CNS inflammation. *Brain* 131, 3081-3091.

Pickl, W.F., Majdic, O., Kohl, P., Stockl, J., Riedl, E., Scheinecker, C., Bello-Fernandez, C., Knapp, W., 1996. Molecular and functional characteristics of dendritic cells generated from highly purified CD14(+) peripheral blood monocytes. *Journal of Immunology* 157, 3850-3859.

Pitychoutis, P.M., Nakamura, K., Tsonis, P.A., Papadopoulou-Daifoti, Z., 2009. Neurochemical and behavioral alterations in an inflammatory model of depression: sex differences exposed. *Neuroscience* 159, 1216-1232.

Plowden, J., Renshaw-Hoelscher, M., Engleman, C., Katz, J., Sambhara, S., 2004. Innate immunity in aging: impact on macrophage function. *Aging Cell* 3, 161-167.

Pocock, J.M., Kettenmann, H., 2007. Neurotransmitter receptors on microglia. *Trends in Neurosciences* 30, 527-535.

Ponomarev, E.D., Maresz, K., Tan, Y., Dittel, B.N., 2007. CNS-Derived interleukin-4 is essential for the regulation of autoimmune inflammation and induces a state of alternative activation in microglial cells. *Journal of Neuroscience* 27, 10714-10721.

Popescu, B.O., Toescu, E.C., Popescu, L.M., Bajenaru, O., Muresanu, D.F., Schultzberg, M., Bogdanovic, N., 2009. Blood-brain barrier alterations in ageing and dementia. *Journal of the Neurological Sciences* 283, 99-106.

Püntener, U., Booth, S.G., Perry, V.H., Teeling, J.L., 2012. Long-term impact of systemic bacterial infection on the cerebral vasculature and microglia. *Journal of Neuroinflammation* 9.

Purves, D., Augustine, G., Fitzpatrick, D., Hall, W., LaMantia, A.S., McNamara, J., White, L., 2008. *Neuroscience, Fourth Edition*.

Qin, L.Y., Liu, Y.X., Wang, T.G., Wei, S.J., Block, M.L., Wilson, B., Liu, B., Hong, J.S., 2004. NADPH oxidase mediates lipopolysaccharide-induced neurotoxicity and proinflammatory gene expression in activated microglia. *Journal of Biological Chemistry* 279, 1415-1421.

Qin, L.Y., Wu, X.F., Block, M.L., Liu, Y.X., Bresse, G.R., Hong, J.S., Knapp, D.J., Crews, F.T., 2007. Systemic LPS causes chronic neuroinflammation and progressive neurodegeneration. *Glia* 55, 453-462.

Qin, Y.H., Dai, S.M., Tang, G.S., Zhang, J., Ren, D., Wang, Z.W., Shen, Q., 2009. HMGB1 Enhances the Proinflammatory Activity of Lipopolysaccharide by Promoting the Phosphorylation of MAPK p38 through Receptor for Advanced Glycation End Products. *Journal of Immunology* 183, 6244-6250.

Quan, D.N., Cooper, M.D., Potter, J.L., Roberts, M.H., Cheng, H., Jarvis, G.A., 2008. TREM-2 binds to lipooligosaccharides of *Neisseria gonorrhoeae* and is expressed on reproductive tract epithelial cells. *Mucosal Immunology* 1, 229-238.

Quan, N., 2008. Immune-to-brain signaling: How important are the blood-brain barrier-independent pathways? *Molecular Neurobiology* 37, 142-152.

Raghavendra, V., Tanga, R.Y., DeLeo, J.A., 2004. Complete Freund's adjuvant-induced peripheral inflammation evokes glial activation and proinflammatory

cytokine expression in the CNS. *European Journal of Neuroscience* 20, 467-473.

Ramirez-Icaza, G., Mohammed, K.A., Nasreen, N., Van Horn, R.D., Hardwick, J.A., Sanders, K.L., Tian, J., Ramirez-Icaza, C., Johnson, M.T., Antony, V.B., 2004. Th2 cytokines IL-4 and IL-13 downregulate paxillin expression in bronchial airway epithelial cells. *Journal of Clinical Immunology* 24, 426-434.

Rankine, E.L., Hughes, P.M., Botham, M.S., Perry, V.H., Felton, L.M., 2006. Brain cytokine synthesis induced by an intraparenchymal injection of LPS is reduced in MCP-1-deficient mice prior to leucocyte recruitment. *European Journal of Neuroscience* 24, 77-86.

Rapp, P.R., Gallagher, M., 1996. Preserved neuron number in the hippocampus of aged rats with spatial learning deficits. *Proceedings of the National Academy of Sciences of the United States of America* 93, 9926-9930.

Rasmussen, T., Schliemann, T., Sorensen, J.C., Zimmer, J., West, M.J., 1996. Memory impaired aged rats: No loss of principal hippocampal and subicular neurons. *Neurobiology of Aging* 17, 143-147.

Raucci, A., Cugusi, S., Antonelli, A., Barabino, S.M., Monti, L., Bierhaus, A., Reiss, K., Saftig, P., Bianchi, M.E., 2008. A soluble form of the receptor for advanced glycation endproducts (RAGE) is produced by proteolytic cleavage of the membrane-bound form by the sheddase a disintegrin and metalloprotease 10 (ADAM10). *Faseb Journal* 22, 3716-3727.

Rauch, S.D., Velazquez-Villasenor, L., Dimitri, P.S., Merchant, S.N., 2001. Decreasing hair cell counts in aging humans. In: Goebel, J., Highstein, S.M. (Eds.), *Vestibular Labyrinth in Health and Disease*, pp. 220-227.

Re, D.B., Przedborski, S., 2006. Fractalkine: moving from chemotaxis to neuroprotection. *Nature Neuroscience* 9, 859-861.

Re, F., Strominger, J.L., 2001. Toll-like receptor 2 (TLR2) and TLR4 differentially activate human dendritic cells. *Journal of Biological Chemistry* 276, 37692-37699.

Redford, E.J., Kapoor, R., Smith, K.J., 1997. Nitric oxide donors reversibly block axonal conduction: demyelinated axons are especially susceptible. *Brain* 120, 2149-2157.

Reed-Geaghan, E.G., Savage, J.C., Hise, A.G., Landreth, G.E., 2009. CD14 and Toll-Like Receptors 2 and 4 Are Required for Fibrillar A beta-Stimulated Microglial Activation. *Journal of Neuroscience* 29, 11982-11992.

Reichard, P., 1988. Interactions between deoxyribonucleotide and DNA-synthesis. *Annual Review of Biochemistry* 57, 349-374.

Reid, D.M., Montoya, M., Taylor, P.R., Borrow, P., Gordon, S., Brown, G.D., Wong, S.Y.C., 2004. Expression of the beta-glucan receptor, dectin-1, on murine leukocytes in situ correlates with its function in pathogen recognition and reveals potential roles in leukocyte interactions. *Journal of Leukocyte Biology* 76, 86-94.

Reimer, M.M., McQueen, J., Searcy, L., Scullion, G., Zonta, B., Desmazieres, A., Holland, P.R., Smith, J., Gliddon, C., Wood, E.R., Herzyk, P., Brophy, P.J., McCulloch, J., Horsburgh, K., 2011. Rapid Disruption of Axon-Glial Integrity in Response to Mild Cerebral Hypoperfusion. *Journal of Neuroscience* 31, 18185-18194.

Reiter, E., Jiang, Q., Christen, S., 2007. Anti-inflammatory properties of alpha- and gamma-tocopherol. *Molecular Aspects of Medicine* 28, 668-691.

Riedel, C.J., Muraszko, K.M., Youle, R.J., 1990. Diphtheria-toxin mutant selectively kills cerebellar purkinje neurons. *Proceedings of the National Academy of Sciences of the United States of America* 87, 5051-5055.

Riley, T.P., Neal-McKinney, J.M., Buelow, D.R., Konkol, M.E., Simasko, S.M., 2013. Capsaicin-sensitive vagal afferent neurons contribute to the detection of pathogenic bacterial colonization in the gut. *Journal of Neuroimmunology* 257, 36-45.

Rogers, J., Lubernard, J., Styren, S.D., Civin, W.H., 1988. Expression of immune system-associated antigens by cells of the human central nervous-system - relationship to the pathology of Alzheimers-disease. *Neurobiology of Aging* 9, 339-349.

Rogers, R.C., Hermann, G.E., 2012. Tumor Necrosis Factor Activation of Vagal Afferent Terminal Calcium Is Blocked by Cannabinoids. *Journal of Neuroscience* 32, 5237-5241.

Rottman, J.B., Ganley, K.P., Williams, K., Wu, L.J., Mackay, C.R., Ringler, D.J., 1997. Cellular localization of the chemokine receptor CCR5 - Correlation to cellular targets of HIV-1 infection. *American Journal of Pathology* 151, 1341-1351.

Rowe, C.C., Ng, S., Ackermann, U., Gong, S.J., Pike, K., Savage, G., Cowie, T.F., Dickinson, K.L., Maruff, P., Darby, D., Smith, C., Woodward, M., Merory, J., Tochon-Danguy, H., O'Keefe, G., Klunk, W.E., Mathis, C.A., Price, J.C., Masters, C.L., Villemagne, V.L., 2007. Imaging beta-amyloid burden in aging and dementia. *Neurology* 68, 1718-1725.

Salmon, A.B., Richardson, A., Perez, V.I., 2010. Update on the oxidative stress theory of aging: Does oxidative stress play a role in aging or healthy aging? *Free Radical Biology and Medicine* 48, 642-655.

Salzer, J.L., 2003. Polarized domains of myelinated axons. *Neuron* 40, 297-318.

Sandell, J.H., Peters, A., 2002. Effects of age on the glial cells in the rhesus monkey optic nerve. *Journal of Comparative Neurology* 445, 13-28.

Sandell, J.H., Peters, A., 2003. Disrupted myelin and axon loss in the anterior commissure of the aged rhesus monkey. *Journal of Comparative Neurology* 466, 14-30.

Sandler, N.G., Mentink-Kane, M.M., Cheever, A.W., Wynn, T.A., 2003. Global gene expression profiles during acute pathogen-induced pulmonary inflammation reveal divergent roles for Th1 and Th2 responses in tissue repair. *Journal of Immunology* 171, 3655-3667.

Santos, R.L., Zhang, S.P., Tsohis, R.M., Kingsley, R.A., Adams, L.G., Baumler, A.J., 2001. Animal models of Salmonella infections: enteritis versus typhoid fever. *Microbes and Infection* 3, 1335-1344.

Schaer, D.J., Boretti, F.S., Schoedon, G., Schaffner, A., 2002. Induction of the CD163-dependent haemoglobin uptake by macrophages as a novel anti-inflammatory action of glucocorticoids. *British Journal of Haematology* 119, 239-243.

Schindler, A.G., Li, S., Chavkin, C., 2010. Behavioral Stress May Increase the Rewarding Valence of Cocaine-Associated Cues Through a Dynorphin/kappa-Opioid Receptor-Mediated Mechanism without Affecting Associative Learning or Memory Retrieval Mechanisms. *Neuropsychopharmacology* 35, 1932-1942.

Schlesinger, L.S., Horwitz, M.A., 1991. Phagocytosis of Mycobacterium-Lepae by human monocyte derived macrophages is mediated by complement receptors CR-1 (CD35), CR3 (CD11b/CD18), and CR4 (CD11c/CD18) and IFN-gamma activation inhibits complement receptor function and phagocytosis of this bacterium. *Journal of Immunology* 147, 1983-1994.

Schluter, C., Duchrow, M., Wohlenberg, C., Becker, M.H.G., Key, G., Flad, H.D., Gerdes, J., 1993. The cell proliferation-associated antigen of antibody Ki-67 - a very large, ubiquitous nuclear-protein with numerous repeated elements,

representing a new kind of cell cycle-maintaining proteins. *Journal of Cell Biology* 123, 513-522.

Schmid, K., Haslbeck, M., Buchner, J., Somoza, V., 2008. Induction of heat shock proteins and the proteasome system by casein-N-epsilon-(carboxymethyl)lysine and N-epsilon-(carboxymethyl)lysine in Caco-2 cells. *Maillard Reaction: Recent Advances in Food and Biomedical Sciences* 1126, 257-261.

Schmitt, A., Bigl, K., Meiners, I., Schmitt, J., 2006. Induction of reactive oxygen species and cell survival in the presence of advanced glycation end products and similar structures. *Biochimica Et Biophysica Acta-Molecular Cell Research* 1763, 927-936.

Schmitz, F., Heit, A., Dreher, S., Eisenacher, K., Mages, J., Haas, T., Krug, A., Janssen, K.P., Kirschning, C.J., Wagner, H., 2008. Mammalian target of rapamycin (mTOR) orchestrates the defense program of innate immune cells. *European Journal of Immunology* 38, 2981-2992.

Schneider, C.A., Rasband, W.S., Eliceiri, K.W., 2012. NIH Image to ImageJ: 25 years of image analysis. *Nature Methods* 9, 671-675.

Schnell, L., Fearn, S., Klassen, H., Schwab, M.E., Perry, V.H., 1999a. Acute inflammatory responses to mechanical lesions in the CNS: differences between brain and spinal cord. *European Journal of Neuroscience* 11, 3648-3658.

Schnell, L., Fearn, S., Schwab, M.E., Perry, V.H., Anthony, D.C., 1999b. Cytokine-induced acute inflammation in the brain and spinal cord. *Journal of Neuropathology and Experimental Neurology* 58, 245-254.

Schroder, K., Sweet, M.J., Hume, D.A., 2006. Signal integration between IFN gamma and TLR signalling pathways in macrophages. *Immunobiology* 211, 511-524.

Schwab, R., Szabo, P., Manavalan, J.S., Weksler, M.E., Posnett, D.N., Pannetier, C., Kourilsky, P., Even, J., 1997. Expanded CD4(+) and CD8(+) T cell clones in elderly humans. *Journal of Immunology* 158, 4493-4499.

Schwacha, M.G., Meissler, J.J., Eisenstein, T.K., 1998. Salmonella typhimurium infection in mice induces nitric oxide-mediated immunosuppression through a natural killer cell-dependent pathway. *Infection and Immunity* 66, 5862-5866.

Sebastiani, G., Blais, V., Sancho, V., Vogel, S.N., Stevenson, M.M., Gros, P., Lapointe, J.M., Rivest, S., Malo, D., 2002. Host immune response to Salmonella enterica serovar typhimurium infection in mice derived from wild strains. *Infection and Immunity* 70, 1997-2009.

Seeger, W., Suttorp, N., Hellwig, A., Bhakdi, S., 1986. Noncytolytic terminal complement complexes may serve as calcium gates to elicit leukotriene B4 generation in human polymorphonuclear leukocytes. *Journal of Immunology* 137, 1286-1293.

Sekizawa, S.-I., Chen, C.-Y., Bechtold, A.G., Tabor, J.M., Bric, J.M., Pinkerton, K.E., Joad, J.P., Bonham, A.C., 2008. Extended secondhand tobacco smoke exposure induces plasticity in nucleus tractus solitarius second-order lung afferent neurons in young guinea pigs. *European Journal of Neuroscience* 28, 771-781.

Sekizawa, S.-i., Joad, J.P., Pinkerton, K.E., Bonham, A.C., 2010. Secondhand smoke exposure alters K plus channel function and intrinsic cell excitability in a subset of second-order airway neurons in the nucleus tractus solitarius of young guinea pigs. *European Journal of Neuroscience* 31, 673-684.

Serrats, J., Schiltz, J.C., Garcia-Bueno, B., van Rooijen, N., Reyes, T.M., Sawchenko, P.E., 2010. Dual Roles for Perivascular Macrophages in Immune-to-Brain Signaling. *Neuron* 65, 94-106.

Shah, V.B., Huang, Y., Keshwara, R., Ozment-Skelton, T., Williams, D.L., Keshwara, L., 2008. beta-Glucan activates microglia without inducing cytokine production in dectin-1-dependent manner. *Journal of Immunology* 180, 2777-2785.

Shan, S., Hong-Min, T., Yi, F., Jun-Peng, G., Yue, F., Yan-Hong, T., Yun-Ke, Y., Wen-Wei, L., Xiang-Yu, W., Jun, M., Guo-Hua, W., Ya-Ling, H., Hua-Wei, L., Ding-Fang, C., 2009. NEW evidences for fractalkine/CX3CL1 involved in substantia nigral microglial activation and behavioral changes in a rat model of Parkinson's disease. *Neurobiology of Aging* 32, 443-458.

Shavit, E., Beilin, O., Korczyn, A.D., Sylantiev, C., Aronovich, R., Drory, V.E., Gurwitz, D., Horresh, I., Bar-Shavit, R., Peles, E., Chapman, J., 2008. Thrombin receptor PAR-1 on myelin at the node of Ranvier: a new anatomy and physiology of conduction block. *Brain* 131, 1113-1122.

Sheffield, L.G., Berman, N.E.J., 1998. Microglial expression of MHC class II increases in normal aging of nonhuman primates. *Neurobiology of Aging* 19, 47-55.

Shepherd, M., Pomicter, A., Velazco, C., Henderson, S., Dupree, J., 2010. Paranodal reorganization results in the depletion of transverse bands in the aged central nervous system. *Neurobiology of Aging* 33.

Sherman, D.L., Tait, S., Melrose, S., Johnson, R., Zonta, B., Court, F.A., Macklin, W.B., Meek, S., Smith, A.J.H., Cottrell, D.F., Brophy, P.J., 2005. Neurofascins are required to establish axonal domains for saltatory conduction. *Neuron* 48, 737-742.

Shin, W.H., Lee, D.Y., Park, K.W., Kim, S.U., Yang, M.S., Joe, E.H., Jin, B.K., 2004. Microglia expressing interleukin-13 undergo cell death and contribute to neuronal survival in vivo. *Glia* 46, 142-152.

Sierra, A., Gottfried-Blackmore, A.C., McEwen, B.S., Bulloch, K., 2007. Microglia derived from aging mice exhibit an altered inflammatory profile. *Glia* 55, 412-424.

Simon, R., Heithoff, D.M., Mahan, M.J., Samuel, C.E., 2007. Comparison of tissue-selective proinflammatory gene induction in mice infected with wild-type, DNA adenine methylase-deficient, and flagellin-deficient *Salmonella enterica*. *Infection and Immunity* 75, 5627-5639.

Simonsen, A., Cumming, R.C., Brech, A., Isakson, P., Schubert, D.R., Finley, K.D., 2008. Promoting basal levels of autophagy in the nervous system enhances longevity and oxidant resistance in adult *Drosophila*. *Autophagy* 4, 176-184.

Simpson, J.E., Ince, P.G., Higham, C.E., Gelsthorpe, C.H., Fernando, M.S., Matthews, F., Forster, G., O'Brien, J.T., Barber, R., Kalaria, R.N., Brayne, C., Shaw, P.J., Stoeber, K., Williams, G.H., Lewis, C.E., Wharton, S.B., Neur, M.R.C.C.F.A., 2007. Microglial activation in white matter lesions and nonlesional white matter of ageing brains. *Neuropathology and Applied Neurobiology* 33, 670-683.

Sinclair, D.A., Oberdoerffer, P., 2009. The ageing epigenome: Damaged beyond repair? *Ageing Research Reviews* 8, 189-198.

Sjoberck, M., Dahlen, S., Englund, E., 1999. Neuronal loss in the brainstem and cerebellum part of the normal aging process? A morphometric study of the vermis cerebelli and inferior olivary nucleus. *Journals of Gerontology Series a-Biological Sciences and Medical Sciences* 54, B363-B368.

Skelly, D.T., Hennessy, E., Dansereau, M.A., Cunningham, C., 2013. A Systematic Analysis of the Peripheral and CNS Effects of Systemic LPS, IL-1B, TNF- $\alpha$  and IL-6 Challenges in C57BL/6 Mice. *Plos One* 8.

Sloane, J.A., Hollander, W., Moss, M.B., Rosene, D.L., Abraham, C.R., 1999. Increased microglial activation and protein nitration in white matter of the aging monkey. *Neurobiology of Aging* 20, 395-405.

Smiley, S.T., King, J.A., Hancock, W.W., 2001. Fibrinogen stimulates macrophage chemokine secretion through toll-like receptor 4. *Journal of Immunology* 167, 2887-2894.

Smith, A.P., 2012. Effects of the common cold on mood, psychomotor performance, the encoding of new information, speed of working memory and semantic processing. *Brain Behavior and Immunity* 26, 1072-1076.

Smith, A.P., 2013. Effects of upper respiratory tract illnesses and stress on alertness and reaction time. *Psychoneuroendocrinology* 38, 2003-2009.

Smith, R.E., Patel, V., Seatter, S.D., Deehan, M.R., Brown, M.H., Brooke, G.P., Goodridge, H.S., Howard, C.J., Rigley, K.P., Harnett, W., Harnett, M.M., 2003. A novel MyD-1 (SIRP-1 alpha) signaling pathway that inhibits LPS-induced TNF alpha production by monocytes. *Blood* 102, 2532-2540.

Soop, A., Sunden-Cullberg, J., Albert, J., Hallstrom, L., Treutiger, C.J., Sollevi, A., 2009. Adenosine infusion attenuates soluble RAGE in endotoxin-induced inflammation in human volunteers. *Acta Physiologica* 197, 47-53.

Soriano, S.G., Amaravadi, L.S., Wang, Y.F., Zhou, H., Yu, G.X., Tonra, J.R., Fairchild-Huntress, V., Fang, Q., Dunmore, J.H., Huszar, D., Pan, Y., 2002. Mice deficient in fractalkine are less susceptible to cerebral ischemia-reperfusion injury. *Journal of Neuroimmunology* 125, 59-65.

Starr, M.E., Evers, B.M., Saito, H., 2009. Age-Associated Increase in Cytokine Production During Systemic Inflammation: Adipose Tissue as a Major Source of IL-6. *Journals of Gerontology Series a-Biological Sciences and Medical Sciences* 64, 723-730.

Stefano, L., Racchetti, G., Bianco, F., Passini, N., Gupta, R.S., Bordignon, P.P., Meldolesi, J., 2009. The surface-exposed chaperone, Hsp60, is an agonist of the microglial TREM2 receptor. *Journal of Neurochemistry* 110, 284-294.

Stein, M., Keshav, S., Harris, N., Gordon, S., 1992. Interleukin-4 Potently Enhances Murine Macrophage Mannose Receptor Activity - a Marker of Alternative Immunological Macrophage Activation. *Journal of Experimental Medicine* 176, 287-292.

Stewart, C.R., Stuart, L.M., Wilkinson, K., van Gils, J.M., Deng, J.S., Halle, A., Rayner, K.J., Boyer, L., Zhong, R.Q., Frazier, W.A., Lacy-Hulbert, A., El Khoury, J., Golenbock, D.T., Moore, K.J., 2010. CD36 ligands promote sterile inflammation through assembly of a Toll-like receptor 4 and 6 heterodimer. *Nature Immunology* 11, 155-U175.

Stichel, C.C., Luebbert, H., 2007. Inflammatory processes in the aging mouse brain: Participation of dendritic cells and T-cells. *Neurobiology of Aging* 28, 1507-1521.

Stone, E.A., Lehmann, M.L., Lin, Y., Quartermain, D., 2006. Depressive behavior in mice due to immune stimulation is accompanied by reduced neural activity in brain regions involved in positively motivated behavior. *Biological Psychiatry* 60, 803-811.

Stone, T.W., 1993. Neuropharmacology of quinolinic and kynurenic acids. *Pharmacological Reviews* 45, 309-379.

Streit, W.J., 1996. The role of microglia in brain injury. *Neurotoxicology* 17, 671-678.

Sturrock, R.R., 1989. Changes in neuron number in the cerebellar cortex of the aging mouse. *Journal Fur Hirnforschung* 30, 499-503.

Sturrock, R.R., 1991. Stability of neuron number in the subthalamic and entopeduncular nuclei of the ageing mouse brain. *Journal of Anatomy* 179, 67-73.

Sturrock, R.R., 1992. Stability of neuron number in the lateral part of the nucleus of the solitary tract in the ageing mouse brain. *Annals of Anatomy-Anatomischer Anzeiger* 174, 335-336.

Sun, D., Newman, T.A., Perry, V.H., Weller, R.O., 2004. Cytokine-induced enhancement of autoimmune inflammation in the brain and spinal cord: implications for multiple sclerosis. *Neuropathology and Applied Neurobiology* 30, 374-384.

Sung, Y.M., Lee, T., Yoon, H., DiBattista, A.M., Song, J.M., Sohn, Y., Moffat, E.I., Turner, R.S., Jung, M., Kim, J., Hoe, H.-S., 2013. Mercaptoacetamide-based class II HDAC inhibitor lowers A beta levels and improves learning and memory in a mouse model of Alzheimer's disease. *Experimental Neurology* 239, 192-201.

Suuronen, T., Huuskonen, J., Pihlaja, R., Kyrylenko, S., Salminen, A., 2003. Regulation of microglial inflammatory response by histone deacetylase inhibitors. *Journal of Neurochemistry* 87, 407-416.

Suzumura, A., Tamaru, T., Yoshikawa, M., Takayanagi, T., 1999. Multinucleated giant cell formation by microglia: induction by interleukin (IL)-4 and IL-13. *Brain Research* 849, 239-243.

Swain, M.G., 2006. Fatigue in liver disease: Pathophysiology and clinical management. *Canadian Journal of Gastroenterology* 20, 181-188.

Swiergiel, A.H., Dunn, A.J., 1999. The roles of IL-1, IL-6, and TNF alpha in the feeding responses to endotoxin and influenza virus infection in mice. *Brain Behavior and Immunity* 13, 252-265.

Swiergiel, A.H., Dunn, A.J., 2002. Distinct roles for cyclooxygenases 1 and 2 in interleukin-1-induced behavioral changes. *Journal of Pharmacology and Experimental Therapeutics* 302, 1031-1036.

Swiergiel, A.H., Smagin, G.N., Johnson, L.J., Dunn, A.J., 1997. The role of cytokines in the behavioral responses to endotoxin and influenza virus infection in mice: effects of acute and chronic administration of the interleukin-1-receptor antagonist (IL-1ra). *Brain Research* 776, 96-104.

Szweda, P.A., Camouse, M., Lundberg, K.C., Oberley, T.D., Szweda, L.I., 2003. Aging, lipofuscin formation, and free radical-mediated inhibition of cellular proteolytic systems. *Ageing Research Reviews* 2, 383-405.

Tabet, N., Birks, J., Grimley Evans, J., 2000. Vitamin E for Alzheimer's disease. *Cochrane Database Syst Rev*, CD002854.

Tarozzo, G., Bortolazzi, S., Crochemore, C., Chen, S.C., Lira, A.S., Abrams, J.S., Beltramo, M., 2003. Fractalkine protein localization and gene expression in mouse brain. *Journal of Neuroscience Research* 73, 81-88.

Tateda, K., Matsumoto, T., Miyazaki, S., Yamaguchi, K., 1996. Lipopolysaccharide-induced lethality and cytokine production in aged mice. *Infection and Immunity* 64, 769-774.

Teeling, J.L., Carare, R.O., Glennie, M.J., Perry, V.H., 2012. Intracerebral immune complex formation induces inflammation in the brain that depends on Fc receptor interaction. *Acta Neuropathologica* 124, 479-490.

Teeling, J.L., Cunningham, C., Newman, T.A., Perry, V.H., 2010. The effect of non-steroidal anti-inflammatory agents on behavioural changes and cytokine production following systemic inflammation: Implications for a role of COX-1. *Brain Behavior and Immunity* 24, 409-419.

Teeling, J.L., Felton, L.M., Deacon, R.M.J., Cunningham, C., Rawlins, J.N.P., Perry, V.H., 2007. Sub-pyrogenic systemic inflammation impacts on brain and behavior, independent of cytokines. *Brain Behavior and Immunity* 21, 836-850.

Thangthaeng, N., Sumien, N., Forster, M.J., 2008. Dissociation of functional status from accrual of CML and RAGE in the aged mouse brain. *Experimental Gerontology* 43, 1077-1085.

Tian, S., Baracos, V.E., 1989. Prostaglandin-dependent muscle wasting during infection in the broiler chick (*Gallus domesticus*) and the laboratory rat (*Rattus norvegicus*). *Biochemical Journal* 263, 485-490.

Toguchi, M., Gonzalez, D., Furukawa, S., Inagaki, S., 2009. Involvement of Sema4D in the control of microglia activation. *Neurochemistry International* 55, 573-580.

ToliverKinsky, T., Papaconstantinou, J., PerezPolo, J.R., 1997. Age-associated alterations in hippocampal and basal forebrain nuclear factor kappa B activity. *Journal of Neuroscience Research* 48, 580-587.

Toth, M.L., Sigmund, T., Borsos, E., Barna, J., Erdelyi, P., Takacs-Vellai, K., Orosz, L., Kovacs, A.L., Csikos, G., Sass, M., Vellai, T., 2008. Longevity pathways converge on autophagy genes to regulate lifespan in *Caenorhabditis elegans*. *Autophagy* 4, 330-338.

Trapp, B.D., Peterson, J., Ransohoff, R.M., Rudick, R., Mork, S., Bo, L., 1998. Axonal transection in the lesions of multiple sclerosis. *New England Journal of Medicine* 338, 278-285.

Tribouillard-Tanvier, D., Striebel, J.F., Peterson, K.E., Chesebro, B., 2009. Analysis of Protein Levels of 24 Cytokines in Scrapie Agent-Infected Brain and Glial Cell Cultures from Mice Differing in Prion Protein Expression Levels. *Journal of Virology* 83, 11244-11253.

Trotter, J., Karram, K., Nishiyama, A., 2010. NG2 cells: Properties, progeny and origin. *Brain Research Reviews* 63, 72-82.

Tuijnman, W.B., Vanwichen, D.F., Schuurman, H.J., 1993. Tissue distribution of human-IgG Fc-receptors CD16, CD32 and CD64 - an immunohistochemical study. *Apmis* 101, 319-329.

Turnbull, I.R., Gilfillan, S., Cella, M., Aoshi, T., Miller, M., Piccio, L., Hernandez, M., Colonna, M., 2006. Cutting edge: TREM-2 attenuates macrophage activation. *Journal of Immunology* 177, 3520-3524.

Tyler, W.J., Alonso, M., Bramham, C.R., Pozzo-Miller, L.D., 2002. From acquisition to consolidation: On the role of brain-derived neurotrophic factor signaling in hippocampal-dependent learning. *Learn. Mem.* 9, 224-237.

Ushikubi, F., Segi, E., Sugimoto, Y., Murata, T., Matsuoka, T., Kobayashi, T., Hizaki, H., Tuboi, K., Katsuyama, M., Ichikawa, A., Tanaka, T., Yoshida, N., Narumiya, S., 1998. Impaired febrile response in mice lacking the prostaglandin E receptor subtype EP3. *Nature* 395, 281-284.

Valenzano, D.R., Terzibasi, E., Genade, T., Cattaneo, A., Domenici, L., Cellerino, A., 2006. Resveratrol prolongs lifespan and retards the onset of age-related markers in a short-lived vertebrate. *Current Biology* 16, 296-300.

Vallieres, L., Rivest, S., 1997. Regulation of the genes encoding interleukin-6, its receptor, and gp130 in the rat brain in response to the immune activator lipopolysaccharide and the proinflammatory cytokine interleukin-1 beta. *Journal of Neurochemistry* 69, 1668-1683.

van den Biggelaar, A.H.J., Huizinga, T.W.J., de Craen, A.J.M., Gussekloo, J., Heijmans, B.T., Frolich, M., Westendorp, R.G.J., 2004. Impaired innate immunity predicts frailty in old age. The Leiden 85-plus study. *Experimental Gerontology* 39, 1407-1414.

van Duin, D., Mohanty, S., Thomas, V., Ginter, S., Montgomery, R.R., Fikrig, E., Allore, H.G., Medzhitov, R., Shaw, A.C., 2007. Age-associated defect in human TLR-1/2 function. *Journal of Immunology* 178, 970-975.

Voll, R.E., Herrmann, M., Roth, E.A., Stach, C., Kalden, J.R., Girkontaite, I., 1997. Immunosuppressive effects of apoptotic cells. *Nature* 390, 350-351.

Vonvoigtlander, P.F., Lahti, R.A., Ludens, J.H., 1983. U-50,488: a selective and structurally novel non-Mu (kappa) opioid agonist. *Journal of Pharmacology and Experimental Therapeutics* 224, 7-12.

Wajant, H., Scheurich, P., 2011. TNFR1-induced activation of the classical NF-kappa B pathway. *Febs Journal* 278, 862-876.

Wake, H., Moorhouse, A.J., Jinno, S., Kohsaka, S., Nabekura, J., 2009. Resting Microglia Directly Monitor the Functional State of Synapses In Vivo and Determine the Fate of Ischemic Terminals. *Journal of Neuroscience* 29, 3974-3980.

Waller, R., Woodroffe, M.N., Francese, S., Heath, P.R., Wharton, S.B., Ince, P.G., Sharrack, B., Simpson, J.E., 2012. Isolation of enriched glial populations from post-mortem human CNS material by immuno-laser capture microdissection. *Journal of Neuroscience Methods* 208, 108-113.

Wang, S.-C., Oelze, B., Schumacher, A., 2008. Age-Specific Epigenetic Drift in Late-Onset Alzheimer's Disease. *Plos One* 3.

Wang, T.G., Qin, L., Liu, B., Liu, Y.X., Wilson, B., Eling, T.E., Langenbach, R., Taniura, S., Hong, J.S., 2004. Role of reactive oxygen species in LPS-induced production of prostaglandin E-2 in microglia. *Journal of Neurochemistry* 88, 939-947.

Wang, X.-J., Zhang, S., Yan, Z.-Q., Zhao, Y.-X., Zhou, H.-Y., Wang, Y., Lu, G.-Q., Zhang, J.-D., 2011. Impaired CD200-CD200R-mediated microglia silencing enhances midbrain dopaminergic neurodegeneration: Roles of aging, superoxide, NADPH oxidase, and p38 MAPK. *Free Radical Biology and Medicine* 50, 1094-1106.

Wang, X., Wang, B.R., Zhang, X.J., Xu, Z., Ding, Y.Q., Ju, G., 2002. Evidence for vagus nerve in maintenance of immune balance and transmission of immune information from gut to brain in STM-infected rats. *World Journal of Gastroenterology* 8, 540-545.

Watkins, L.R., Goehler, L.E., Relton, J.K., Tartaglia, N., Silbert, L., Martin, D., Maier, S.F., 1995. Blockade of interleukin-1 induced hyperthermia by subdiaphragmatic vagotomy - evidence for vagal mediation of immune brain communication. *Neuroscience Letters* 183, 27-31.

Wautier, M.P., Chappay, O., Corda, S., Stern, D.M., Schimidt, A.M., Wautier, J.L., 2001. Activation of NADPH oxidase by AGE links oxidant stress to altered gene expression via RAGE. *American Journal of Physiology-Endocrinology and Metabolism* 280, E685-E694.

Weichhart, T., Costantino, G., Poglitsch, M., Rosner, M., Zeyda, M., Stuhlmeier, K.M., Kolbe, T., Stulnig, T.M., Horl, W.H., Hengstschlager, M., Muller, M., Saemann, M.D., 2008. The TSC-mTOR Signaling Pathway Regulates the Innate Inflammatory Response. *Immunity* 29, 565-577.

Weinstein, J.R., Hong, S.Y., Kulman, J.D., Bishop, C., Kuniyoshi, J., Andersen, H., Ransom, B.R., Hanisch, U.K., Moller, T., 2005. Unraveling thrombin's true microglia-activating potential: markedly disparate profiles of pharmaceutical-grade and commercial-grade thrombin preparations. *Journal of Neurochemistry* 95, 1177-1187.

Wentworth, J.M., Naselli, G., Brovn, W.A., Doyle, L., Phipson, B., Smyth, G.K., Wabitsch, M., O'Brien, P.E., Harrison, L.C., 2010. Pro-Inflammatory CD11c(+)CD206(+) Adipose Tissue Macrophages Are Associated With Insulin Resistance in Human Obesity. *Diabetes* 59, 1648-1656.

West, M.J., 1993. Regionally specific loss of neurons in the aging human hippocampus. *Neurobiology of Aging* 14, 287-293.

Wieczorek, M., Swiergiel, A.H., Pournajafi-Nazarloo, H., Dunn, A.J., 2005. Physiological and behavioral responses to interleukin-1 beta and LPS in vagotomized mice. *Physiology & behavior* 85, 500-511.

Wilkins, A., Chandran, S., Compston, A., 2001. A role for oligodendrocyte-derived IGF-1 in trophic support of cortical neurons. *Glia* 36, 48-57.

Williams, A.E., Lawson, L.J., Perry, V.H., Fraser, H., 1994. Characterization of the microglial response in murine scrapie. *Neuropathology and Applied Neurobiology* 20, 47-55.

Williams, C.L., Teeling, J.L., Perry, V.H., Fleming, T.P., 2011. Mouse maternal systemic inflammation at the zygote stage causes blunted cytokine responsiveness in lipopolysaccharide-challenged adult offspring. *Bmc Biology* 9.

Williams, G.C., 1957. Pleiotropy, natural selection, and the evolution of senescence. *Evolution* 11, 398-411.

Willment, J.A., Lin, H.H., Reid, D.M., Taylor, P.R., Williams, D.L., Wong, S.Y.C., Gordon, S., Brown, G.D., 2003. Dectin-1 expression and function are enhanced on alternatively activated and GM-CSF-treated macrophages and are negatively regulated by IL-10, dexamethasone, and lipopolysaccharide. *Journal of Immunology* 171, 4569-4573.

Winkler, E.A., Bell, R.D., Zlokovic, B.V., 2011. Central nervous system pericytes in health and disease. *Nature Neuroscience* 14, 1398-1405.

Wohleb, E.S., Fenn, A.M., Pacenta, A.M., Powell, N.D., Sheridan, J.F., Godbout, J.P., 2012. Peripheral innate immune challenge exaggerated microglia activation, increased the number of inflammatory CNS macrophages, and prolonged social withdrawal in socially defeated mice. *Psychoneuroendocrinology* 37, 1491-1505.

Woodruff-Pak, D.S., 2006. Stereological estimation of Purkinje neuron number in C57BL/6 mice and its relation to associative learning. *Neuroscience* 141, 233-243.

Woodruff-Pak, D.S., Foy, M.R., Akopian, G.G., Lee, K.H., Zach, J., Nguyen, K.P.T., Comalli, D.M., Kennard, J.A., Agelan, A., Thompson, R.F., 2010. Differential effects and rates of normal aging in cerebellum and hippocampus. *Proceedings of the National Academy of Sciences of the United States of America* 107, 1624-1629.

Wright, G.J., Puklavec, M.J., Willis, A.C., Hoek, R.M., Sedgwick, J.D., Brown, M.H., Barclay, A.N., 2000. Lymphoid/neuronal cell surface OX2 glycoprotein recognizes a novel receptor on macrophages implicated in the control of their function. *Immunity* 13, 233-242.

Wynne, A.M., Henry, C.J., Huang, Y., Cleland, A., Godbout, J.P., 2010. Protracted downregulation of CX(3)CR1 on microglia of aged mice after lipopolysaccharide challenge. *Brain Behavior and Immunity* 24, 1190-1201.

Xu, Y.L., Toure, F., Qu, W., Lin, L.L., Song, F., Shen, X.P., Rosario, R., Garcia, J., Schmidt, A.M., Yan, S.F., 2010. Advanced Glycation End Product (AGE)-Receptor for AGE (RAGE) Signaling and Up-regulation of Egr-1 in Hypoxic Macrophages. *Journal of Biological Chemistry* 285, 23231-23238.

Xue, M., Hollenberg, M.D., Yong, V.W., 2006. Combination of thrombin and matrix metalloproteinase-9 exacerbates neurotoxicity in cell culture and intracerebral hemorrhage in mice. *Journal of Neuroscience* 26, 10281-10291.

Yang, M.S., Park, E.J., Sohn, S.Y., Kwon, H.J., Shin, W.H., Pyo, H.K., Jin, B.K., Choi, K.S., Jou, I., Joe, E.H., 2002. Interleukin-13 and-4 induce death of activated microglia. *Glia* 38, 273-280.

Yang, S.-B., Tien, A.-C., Boddupalli, G., Xu, A.W., Jan, Y.N., Jan, L.Y., 2012. Rapamycin Ameliorates Age-Dependent Obesity Associated with Increased mTOR Signaling in Hypothalamic POMC Neurons. *Neuron* 75, 425-436.

Yirmiya, R., Winocur, G., Goshen, I., 2002. Brain interleukin-1 is involved in spatial memory and passive avoidance conditioning. *Neurobiology of Learning and Memory* 78, 379-389.

Yong, T., Meininger, G.A., Linthicum, D.S., 1993. Enhancement of histamine-induced vascular leakage by pertussis toxin in SJL/J mice but not BALB/C mice. *Journal of Neuroimmunology* 45, 47-52.

Zeng, Y., Tan, M., Kohyama, J., Sneddon, M., Watson, J.B., Sun, Y.E., Xie, C.-W., 2011. Epigenetic Enhancement of BDNF Signaling Rescues Synaptic Plasticity in Aging. *Journal of Neuroscience* 31, 17800-17810.

Zhang G., Li J., Purkayastha S., Tang Y., Zhang H., Yin Y., Li B., Liu G., D., C., 2013. Hypothalamic programming of systemic ageing involving IKK- $\beta$ , NF- $\kappa$ B and GnRH. *Nature* 497, 211-216.

Zhang, J., Rivest, S., 1999. Distribution, regulation and colocalization of the genes encoding the EP2- and EP4-PGE(2) receptors in the rat brain and neuronal responses to systemic inflammation. *European Journal of Neuroscience* 11, 2651-2668.

Zhang, K., Sejnowski, T.J., 2000. A universal scaling law between gray matter and white matter of cerebral cortex. *Proceedings of the National Academy of Sciences of the United States of America* 97, 5621-5626.

Zhang, S.L., Cherwinski, H., Sedgwick, J.D., Phillips, J.H., 2004. Molecular mechanisms of CD200 inhibition of mast cell activation. *Journal of Immunology* 173, 6786-6793.

Zhang, W., Yang, S., Li, C., Chen, L., Tang, Y., 2009. Stereological Investigation of Age-Related Changes of Myelinated Fibers in the Rat Cortex. *Journal of Neuroscience Research* 87, 2872-2880.

Zhao, J., Brooks, D.M., Lurie, D.I., 2006. Lipopolysaccharide-activated SHP-1-deficient motheaten microglia release increased nitric oxide, TNF-alpha, and IL-1 beta. *Glia* 53, 304-312.

Zid, B.M., Rogers, A.N., Katewa, S.D., Vargas, M.A., Kolipinski, M.C., Lu, T.A., Benzer, S., Kapahi, P., 2009. 4E-BP Extends Lifespan upon Dietary Restriction by Enhancing Mitochondrial Activity in *Drosophila*. *Cell* 139, 149-160.

Zong, H.L., Madden, A., Ward, M., Mooney, M.H., Elliott, C.T., Stitt, A.W., 2010. Homodimerization Is Essential for the Receptor for Advanced Glycation End Products (RAGE)-mediated Signal Transduction. *Journal of Biological Chemistry* 285, 23135-23144.

Zujovic, V., Benavides, J., Vige, X., Carter, C., Taupin, V., 2000. Fractalkine modulates TNF-alpha secretion and neurotoxicity induced by microglial activation. *Glia* 29, 305-315.